BEHAVIOR OF ORGANIC CONTAMINANTS IN PERMAFROST-AFFECTED SOILS

Dissertation zur Erlangung des Doktorgrades an der Fakultät für Mathematik, Informatik und Naturwissenschaften
Fachbereich Geowissenschaften
der Universität Hamburg
vorgelegt von

Anne Zschocke

BAND 78
2015

ISBN: 0724 - 6382

Tag der Disputation: 24.06.2015

Folgende Gutachter empfehlen die Annahme der Dissertation:

Prof. Dr. Annette Eschenbach

Prof. Dr. Eva-Maria Pfeiffer

ACKNOWLEDGEMENT

First of all I want to thank Prof. A. Eschenbach, my first supervisor, for giving me the opportunity to conduct this scientific work and for organizing financial support, whenever needed. I am also grateful for fruitful discussion during all stages of this work and the helpful comments on the draft of this thesis.

I want to thank my second supervisor Prof. E.-M. Pfeiffer for guidance in the vast field of peculiarities of permafrost-affected soils and support in finishing the thesis.

Maike Schönborn, Maren Reese and Isa Behrendt shared my interest in the topic and worked on parts of the topic during their Diploma, Bachelor and Master thesis, respectively. Special thanks go to Isa for the excellent team work at the isotope laboratory in Klein Flottbek.

Volker Kleinschmidt for technical guidance, brain storming and the ability to invent anything out of nothing.

I could only take parts of the samples in Russia. The other samples were taken by Günther Stoof and E.-M. Pfeiffer, Tina, Julia and Seba. Thanks for your labor!

Furthermore I want to thank all technical and laboratory staff of the Institute of Soil Science, especially Andreas Behr.

Jo – the real scientist on frozen matters – for proofreading, support and understanding. Important input for the finishing touch of language and format came from my family in overseas, thanks Ali and Arnd!

I want to acknowledge the very cooperative scientific community, from which I got data, answers to my questions and else unavailable literature. Here I want to mention in particular Julia Boike for soil temperature data from Siberia, Kevin Biggar, Charles Collins and Wojciech Prus for providing important literature and information.

I appreciated to be part of the Institute of Soil Sciences and besides the already mentioned people I specially want to thank Inga, Tina, Marleen, Simon, Christoph, Lars, Jona, Seba, Fabian, Norman and Ingke for shared breaks, field work and knowledge.

Thanks go also to my family and friends, who supported the experiment of having a family and writing a doctoral thesis at once. Without Jules support in heavy seas I probably wouldn’t have finished this work.

And last but not least thanks go to Ole, Timon, Johann and Lukas that they stood this time and disclaimed one and the other evening without me!

Now it is done!

TABLE OF CONTENTS

SUMMARY

Soils and soil functions are a main resource for our existence on earth. But soils are under threat by degradation. Another resource that seems irreplaceable for human being on this planet is oil. Oil, as well as soil, is a non-renewable resource in relation to human life time. With decreasing reservoirs in the established oil production areas, remote oil resources, like in the Arctic, come into the focus of exploration activities (Bird et al., 2008). Exploration, transport and processing of oil inevitably cause accidental spills and continuous release of product and compounds into the soil on different levels. In general the reasons are technical inadequacy, human error or natural hazards (Siciliano et al., 2008). Furthermore increased human activity in Arctic regions also increases the entry of contaminants into the vulnerable environment.

Large parts of Arctic soils are perennially frozen and only small parts near the surface experience seasonal thaw. These permafrost-affected soils cover about one quarter of the landmass of the Northern Hemisphere (Zhang et al., 2000) and host about 13 % of the world's undiscovered oil and 30 % of the world's undiscovered gas resources (Bird et al., 2008). In contrast to soils of temperate regions the surface soil layers of Arctic regions undergo seasonally physical and chemical changes. These changes are predominantly caused by the freezing process and the phase transition from water to ice. They result in processes like cryosuction and subsequent frost heave, cryoturbation, gelifluction and finally they often cause the destruction of the usual horizontal layering in soils (French, 2007). Recently climate change with predicted increase of ambient air temperatures and precipitation rates in the Arctic is said to bring changes of the balanced system about (Bindoff et al., 2013).

Oil is always a mixture of several groups of compounds, with most of them being hydrophobic. Furthermore, oil enters soils often as a discrete phase, or so-called non-aqueous phase liquid (NAPL) and therefore competes with the soil solution for pore space. The freezing process has been shown to increase the number of NAPL ganglia present in oil contaminated soils and lead to a dispersion of the contaminant phase (Grechishchev et al., 2001; Niven & Singh, 2008). In permafrost-affected soils supra-permafrost water is impounded within the unfrozen active layer during summer. In a field study of an organic rich soil it was observed that the vertical contaminant migration was hindered, or at least delayed by the supra-permafrost water (Collins et al., 1993). This observation is supported by the findings of the present study at a diesel and lubricant oil spill in Northern Siberia. The analyzed contaminant groups of total petroleum hydrocarbons (TPHs) and polycyclic aromatic hydrocarbons (PAHs) showed almost similar distribution patterns with a local maximum just upon the supra-permafrost water table. Furthermore, a considerable partitioning of the single substances according to molecular weight within the investigated contaminant groups has been observed over soil depth. However, contaminants were detected with elevated contents compared to the Arctic background level over the whole sampling depth also beneath the supra-permafrost water table. The main factors influencing the migration and accumulation of the organic contaminants water content and freezing patterns included organic matter content, contaminant content and properties of the single substances, as well as soil texture. Thereby distinct water accumulation and migration patterns of permafrost-affected soils are assumed to control PAH and TPH migration, whereas the degree is determined by organic carbon content and the hydrophobic nature of the organic contaminants (log K_{OW}). The contaminant migration, induced by the freezing process, seems to enhance especially the mobility of 2- and 3-ring PAHs and therefore leads to a partitioning of the contaminant group.

For a better understanding of the impact of the freezing process and its accompanying phenomena on the PAH migration and distribution in contaminated soils, laboratory experiments were conducted. To ensure an adequate simulation of the freezing process in the vadose zone of the soil experimental approaches have been invented. A closed system setup has been developed for better determination of influencing parameters due to minimized boundary conditions. The best simulation of the freezing induced water migration was achieved by a two phase cooling approach. After equilibration of soil temperatures at 4°C, a phase of fast cooling at the beginning of the experiment brings the freezing front to the position of observation. A second cooling phase simulated the naturally occurring cooling rates in Arctic soils (Konrad & Seto, 1991) and employed cooling rates of 0°C to 0.006°C per day. These cooling rates initiated the freezing induced water migration and accumulation at the freezing front. Water contents at the freezing front increased up to saturation level. Formation of segregated ice and the impact of several freeze-thaw cycles may be simulated by an open system approach.

Laboratory experiments could show that freezing induced water migration may lead to PAH migration in silt loam. Observed effects were greater for the PAH anthracene, than for the PAH pyrene, because the former has a lower log K_{OW} value. It could be shown that the methanol-water extractable fraction of each PAH was the most mobile. This fraction is higher for 2- and 3-ring PAHs in soils than for higher molecular weight PAHs. Therefore the experiment could give an explanation for the partitioning of the group of PAHs with time over soil depth. Investigations on Antarctic soils with anthropogenic influence, an increase of the 3-ring PAH phenanthrene within the group of PAHs with depth could be observed (Curtosi et al., 2007). Also the sum parameter of PAHs increased with depth, reaching its maximum in the upper part of the transient layer that divides seasonally thawing ground (active layer) from perennial frozen ground (permafrost). The transient layer thaws on decadal or centennial scale (Shur et al., 2005) and is especially ice rich. In conjunction it can be hypothesized that lower molecular weight PAHs accumulate in the transient layer with several freeze-thaw cycles, while the lower molecular weight PAHs are enriched within the group of PAHs in the active layer during this process.

It has been shown in the literature that out of a solution of water and the hydrophilic organic contaminant 1-propanol almost pure ice is formed in clayey silt and a zone of increased contaminant concentration develops ahead the freezing front (Konrad & Seto, 1991). The formation of pure ice from sea water, a salty solution, is well known.

Experiments with salty soil solutions revealed that ice with lower salt contents than the solution only formed at freezing rates below 3°C per day (Konrad & McCammon, 1990). Furthermore the authors could show that up to 90 % of the salt was excluded from the forming ice at freezing rates of 0.1°C per day. On the other hand a concentrated salt solution formed ahead the freezing front. In this study it has been shown, that PAH, namely hydrophobic, organic substances, were redistributed after a one-directional freezing process and accumulated ahead the freezing front in oil contaminated soil materials at low freezing rates (< 0.006°C per day). This process was most obvious in sandy material. Additionally it has been observed that the methanol-water extractable fraction of the PAHs was the one involved in the migration and accumulation process. The ethyl acetate extractable fraction of the PAH, which is usually associated with the oil phase did not show any significant redistribution. Therefore it is assumed that the slow freezing process led to the formation of pure ice and induced the PAH migration, while it is not probable that the process of oil expulsion out of soil pores, due to freezing induced water migration and accumulation, as observed by Chuvilin et al. (2001) took place. As PAHs have very low water solubility, it is assumed that the methanol-water extractable fraction displays the part of the PAHs associated with dissolved organic matter (DOM) and / or dispersed NAPL droplets. Two reasons that the predicted process of oil expulsion out of soil pores did not take place, may be to the comparatively low oil content (0.5 % in the present study, 6.2 % in study of Chuvilin et al. (2001)) and the lower water contents of the experimental approach, simulating unsaturated conditions in contrast to saturated conditions in the study by Chuvilin et al. (2001).

It has been shown that the freezing process did hardly affect the availability of PAHs itself, but that the interaction with the sorbents of the PAHs is important. However, the processes described reveal, that the interaction of PAH, sorption partners and freezing processes lead to a redistribution of the contaminant and a partitioning. It has been shown that soil texture and temperature gradient within the unfrozen soil are controlling parameters. In conjunction with the literature it gets clear that water content and water saturation state of the soil determine the presence of organic contaminant migration processes. In soils with low water content (vadose zone) the formation of pure ice due to low freezing rates leads to organic contaminant migration, while at water saturated soil conditions the expulsion of an organic contaminant phase determines the migration process.

Since the complex chemical and physical processes taking place in permafrost-affected soils are still object of research, the investigation of their interrelation with the large group of organic contaminants is challenging. This challenge is increased due to the predicted impacts of climate change and the associated changes of the boundary conditions of permafrost-affected soils. This suggests that the study of the behavior of pollutants in permafrost-affected soils is only at the beginning, and the impact of climate change is an additional parameter.

ZUSAMMENFASSUNG

Böden sind unsere Lebensgrundlage. Trotzdem sind sie ständig durch Degradation in Form von Schadstoffeintrag oder Erosion bedroht. Eine weitere, scheinbar unersetzliche Hauptgrundlage des menschlichen Daseins ist Erdöl. Sowohl Erdöl als auch Böden sind auf humane Lebenszeiträume gesehen nicht regenerative Rohstoffe. Mit steigendem Rohölpreis rücken schwer zu explorierende Ölvorkommen, wie z.B. in der Arktis, in den Fokus von Explorationsfirmen (Bird et al., 2008). Mit Exploration, Transport und Verarbeitung dieses Öls gehen jedoch unvermeidliche Verschmutzungen der Umwelt, insbesondere der Böden, einher. Im Allgemeinen liegen die Gründe für solche Verschmutzungen sowohl in technischen und menschlichen Fehlern als auch in nicht vollständig beherrschbaren, natürlichen Ereignissen (Siciliano et al., 2008). Durch verstärkte menschliche Aktivität in arktischen Gebieten erhöht sich auch der Eintrag anderer (Schad-)stoffe in das empfindliche Ökosystem.

Ein Großteil der arktischen Böden ist dauerhaft gefroren und nur ein oberflächennaher Bereich taut saisonal auf. Diese Permafrost-beeinflussten Böden nehmen ungefähr ein Viertel der Landmasse der nördlichen Hemisphäre ein (Zhang et al., 2000). Und in diesem Gebiet befinden sich 13 % der geschätzten Erdölreserven sowie 30 % der geschätzten Gasreserven der Welt (Bird et al., 2008). Im Unterschied zu Böden gemäßigter Klimazonen unterliegen Permafrost-beeinflusste Böden jahreszeitlich bedingten physikalischen und chemischen Veränderungen. Diese Veränderungen werden hauptsächlich vom Gefrierprozess des Wassers zu Eis hervorgerufen und verursachen Prozesse wie die gefrierbedingte Saugspannung im Boden (cryosuction). Diese führt zu Wasserbewegungen im Boden und nachfolgend kann es zu gefrierbedingten Bodenbewegungen kommen (cryoturbation, gelifluction). Letztlich führen diese Prozesse oft zur Zerstörung der horizontalen Bodenstrukturen (French, 2007). Mit dem Klimawandel kommen weitere Veränderungen auf die arktischen Gebiete zu, die sich auch auf die beschriebenen Prozesse auswirken werden. Für die Arktis werden im aktuellen IPCC- Report sowohl steigende Temperaturen als auch erhöhte Niederschlagsraten vorausgesagt (Bindoff et al., 2013).

Erdöl ist eine Mischung aus vielen verschiedenen, meist organischen, chemischen Verbindungen. Die meisten von ihnen sind hydrophob. Wenn Erdöl in den Boden eindringt, bildet es deshalb meist eine eigene Phase in Form von Ganglia und einzelnen Tropfen, die als NAPL bezeichnet wird (engl. Abkürzung für **N**on-**A**queous **P**hase **L**iquid) und mit Wasser um den vorhandenen Porenraum konkurriert. In der Literatur wurde gezeigt, dass der Gefrierprozess im Boden die Anzahl der Ganglia erhöht und zu einer Dispersion des Öls im Boden führt (Grechishchev et al., 2001; Niven & Singh, 2008). In Permafrost beeinflussten Böden staut sich das Supra-Permafrost-Wasser im Sommer innerhalb der aufgetauten aktiven Schicht des Bodens auf dem dauerhaft gefrorenen Untergrund. Eine Feldstudie konnte zeigen, dass eine Dieselölphase über einen Zeitraum von 15 Jahren durch das Supra-

Permafrost-Wasser am tieferen Eindringen gehindert wurde (Collins et al., 1993). Diese Beobachtung wird durch die vorliegenden Untersuchungen eines Diesel- und Schmierölschadens in Nordsibirien in Teilen bestätigt. Die analysierten Schadstoffgruppen, MKW (engl. TPHs, Summenparameter der Mineralölkohlenwasserstoffe von C_{10} bis C_{40}) und PAK (engl. PAHs, Summenparameter der 16 von der EPA ausgewiesenen polyzyklischen aromatischen Kohlenwasserstoffe), zeigten lokale Konzentrationsmaxima unmittelbar über dem Supra-Permafrost-Wasserspiegel. Allerdings wurden die Schadstoffe in geringen Konzentrationen auch unterhalb des Supra-Permafrost Wasserspiegels über die gesamte Beprobungstiefe festgestellt. Im Verlauf des Bodenprofils wurde eine beträchtliche Änderung der Zusammensetzung beider Schadstoffgruppen in Abhängigkeit vom Molekulargewicht und der chemischen Struktur beobachtet. Als Haupteinflussfaktoren der Bewegung und Anreicherung der organischen Schadstoffe wurden Wassergehalt und Gefrierverlauf, Gehalt organischer Substanz im Boden, Schadstoffgehalt und Schadstoffeigenschaften sowie die Bodenart identifiziert. Demnach scheinen die spezifischen Wasserbewegungen und Wasseransammlungen in Permafrost-beeinflussten Böden die Verteilung von MKW und PAK zu bestimmen, während das Ausmaß der Verteilungsprozesse von der organischen Substanz und dem Gehalt und der Hydrophobie (log K_{OW}) der organischen Schadstoffe abhängt. Die durch den Gefrierprozess induzierte Schadstoffbewegung im Boden begünstigt die Mobilität von 2- und 3-Ring PAK und führt deshalb zu den beobachteten Änderungen der Zusammensetzung der Schadstoffgruppen über die Bodentiefe.

Um den Einfluss des Gefrierprozesses und seiner Begleitphänomene auf die PAK Verteilung in verunreinigten Böden besser verstehen zu können, wurden Laborversuche durchgeführt. Zur Simulation des Gefrierprozesses in der vadosen Zone des Bodens wurden zwei Versuchsaufbauten konzipiert. Es wurde ein geschlossenes Säulensystem gewählt, um die beeinflussenden Parameter durch festgesetzte Grenzbedingungen besser bestimmen zu können. Die beste Simulation des Gefrierprozesses und der dadurch hervorgerufenen Wasserbewegung im Boden wurde durch die Anwendung eines zweiphasigen Abkühlszenarios erreicht. Ausgehend von einer Bodentemperatur von 4°C bringt eine schnelle Abkühlphase am Anfang des Experiments die Gefrierfront in die Position der späteren Beobachtung. Eine zweite Kühlphase simulierte mit konstanter Kühlung, bzw. Kühlraten bis zu 0,006°C pro Tag die natürlicher Weise auftretenden Abkühlraten in arktischen Böden (Konrad & Seto, 1991). Durch die gefrierbedingte Wasserbewegung aus dem ungefrorenen Teil der Versuchssäule zur Gefrierfront erreichten die Wassergehalte Werte im Bereich der Wassersättigung des Bodens. Die Bildung von Segregationseis (Eislinsenbildung) und der Einfluss von mehreren Gefrier-Tau-Zyklen kann durch den Einsatz eines offenen Versuchsaufbaus mit unbegrenzter Wasserverfügbarkeit simuliert werden.

Die Laborexperimente konnten zeigen, dass die durch das Gefrieren hervorgerufene Wasserbewegung zur Verlagerung von PAK in schwach tonigem Schluff führen kann. Die beobachteten Effekte waren deutlicher für das 3-Ring PAK Anthracen als für das

4-Ring PAK Pyren, weil ersteres einen niedrigeren log K_{OW}-Wert hat. Es konnte gezeigt werden, dass die Methanol-Wasser extrahierbare Fraktion die größte Mobilität des jeweiligen PAKs besitzt. Diese Fraktion ist für 2- und 3-Ring PAK in Böden größer als für höher molekulare PAK, deshalb konnte es zur beobachteten Fraktionierung der Gruppe der PAK mit der Zeit über die Bodentiefe kommen. In einer Untersuchung anthropogen beeinflusster, antarktischer Böden wurde die Zunahme des Anteils des 3-Ring PAKs Phenanthren an der Gruppe der PAK mit zunehmender Bodentiefe beobachtet (Curtosi et al., 2007). Auch der Gesamtgehalt der PAK in den untersuchten Profilen nahm mit der Tiefe zu und erreichte sein Maximum im oberen Bereich der Übergangszone (engl. transient layer) zwischen saisonal tauendem (engl. active layer) und dauerhaft gefrorenem (engl. permafrost) Bodenbereich. Diese Beobachtungen und die Ergebnisse der vorliegenden Arbeit führen zu der Hypothese, dass sich mit der Zeit und mehreren Gefrier-Tau-Zyklen insbesondere die niedrigmolekularen PAK im Bereich der Übergangszone (die über Zeiträume von Dekaden bis zu Jahrhunderten gefroren sein kann) sammeln, während sich im Bereich der aktiven Schicht die höher molekularen PAK innerhalb der Schadstoffgruppe relativ anreichern.

In der Literatur wurde gezeigt, dass aus einer einphasigen Lösung von Wasser und dem organischen Schadstoff 1-Propanol in einem tonigen Schluff reines Eis gebildet wird. Vor der Gefrierfront bildete sich eine Zone erhöhter Schadstoffkonzentration (Konrad & Seto, 1991). Der Zusammenhang, dass aus einer Lösung reines Eis ausfriert, ist vom Meereis bekannt. Versuche mit einer salzigen Bodenlösung zeigten, dass nur bei Gefrierraten unterhalb 3°C pro Tag Eis mit niedrigeren Salzgehalten als in der Bodenlösung entsteht (Konrad & McCammon, 1990). Die Autoren zeigten außerdem, dass mit einer Abnahme der Gefrierraten bis 0,1°C pro Tag Eis mit bis zu 90 % reduziertem Salzgehalt gebildet wurde und sich eine konzentrierte Salzlösung vor der Gefrierfront bildete. Die Ergebnisse der vorliegenden Arbeit zeigen, dass PAK, also hydrophobe, organische Substanzen, durch einen einseitigen, langsamen Gefrierprozess (Gefrierraten < 0,006°C pro Tag) in ölverunreinigten Böden vor der Gefrierfront im ungefrorenen Bodenbereich angereichert werden. Dieser Prozess war am deutlichsten in sandigem Material. Außerdem wurde beobachtet, dass hauptsächlich die Methanol-Wasser-extrahierbare Fraktion der einzelnen PAK die Migration und die nachfolgende Akkumulation der Schadstoffe bestimmte. Die hauptsächlich mit dem Erdöl assoziierte, Ethylacetat-lösliche PAK Fraktion ist nicht signifikant an den beobachteten Migrationsprozessen beteiligt. Deshalb wird vermutet, dass der langsame Gefrierprozess die Bildung besonders reinen Eises induzierte und so zur Migration der PAK führte, während ein Prozess der Auspressung des Rohöls aus den Bodenporen durch das sich akkumulierende Wasser und die Eisbildung, wie von Chuvilin et al. (2001) beobachtet, nahezu ausgeschlossen werden kann. Aufgrund der geringen Wasserlöslichkeit der PAK wird vermutet, dass die Methanol-Wasser-lösliche PAK Fraktion den an gelöste, organische Substanz (DOM) und / oder an dispergierte Öltröpfchen gebundenen Anteil der vorhandenen PAK darstellt. Dass der anfangs vermutete Prozess der Auspressung des Rohöls aus den Bodenporen aufgrund des Gefrierprozesses, wahrscheinlich nicht stattgefunden hat, kann zum einen an der sehr viel niedrigeren Rohölkonzentration der hier durchgeführten Versuche liegen (0,5 % im Gegensatz zu 6,2 % bei Chuvilin et al. (2001)) und zum anderen an den niedrigeren Wassergehalten, die ungesättigte Bodenwasserverhältnisse simulierten, während Chuvilin et al. (2001) Böden im wassergesättigten Zustand untersuchten.

In den durchgeführten Versuchen wurde kaum ein Einfluss des Gefrierprozesses auf den Gesamtgehalt der extrahierbaren PAK festgestellt. Die beschriebenen Prozesse zeigen aber, dass das Zusammenspiel zwischen PAK-Sorptionspartnern und dem Gefrierprozess zur Umverteilung der Schadstoffe führt. Es wurde gezeigt, dass Bodenart und Temperaturgradient zwischen Gefrierfront und ungefrorenem Bodenteil die Haupteinflussgrößen der Schadstoffverteilungsprozesse sind. Im Zusammenhang mit der Literatur wurde deutlich, dass der Wassergehalt, bzw. die Wassersättigungsverhältnisse des Bodens, über das Auftreten der verschiedenen Migrationsprozesse bestimmen. In wasserungesättigten Böden ist die Bildung reinen Eises bei niedrigen Gefrierraten für die Verlagerung von organischen Schadstoffen verantwortlich, während in wassergesättigten Böden die Auspressung der Rohölphase die Schadstoffmigration bestimmt.

Es konnte gezeigt werden, dass der natürliche Gefrierprozess in der vadosen Zone des Bodens gut mit einem geschlossenen Säulensystem simuliert werden kann. Die Versuche zeigten, dass der Gefrierprozess und die einhergehenden Phänomene einen Einfluss auf die PAK Verteilung im Boden haben. Außerdem wurde die Bedeutung von Wassergehalt und Ablauf des Gefrierprozesses deutlich. Aufgrund der Untersuchungen und der Auswertung der Literatur wird die Hypothese aufgestellt, dass die vertikalen Verteilungsprozesse zu erhöhten Konzentrationen organischer Schadstoffe im Grenzbereich von Eislinsen und insbesondere im eisreichen Übergangshorizont führen. Allerdings sollten weitere Versuche durchgeführt werden, um diese Hypothese zu verifizieren.

Da die komplexen chemischen und physikalischen Prozesse in Permafrost Böden immer noch Forschungsgegenstand sind, ist die Untersuchung der großen, heterogenen Gruppe der organischen Schadstoffe im Zusammenhang mit diesen Böden eine Herausforderung. Diese Herausforderung wird durch den Einfluss des Klimawandels und den damit einher gehenden, veränderten Randbedingungen erhöht. Daraus lässt sich schließen, dass die Erforschung des Verhaltens von Schadstoffen in Permafrost beeinflussten Böden erst ganz am Anfang steht, in der der Einfluss des klimatischen Wandels eine zusätzliche Variable darstellt.

ABBREVIATIONS

dpm	decays per minute
dw	dry weight
DOM	dissolved organic matter
EPA	U.S. Environmental Protection Agency
IUSS	International Union of Soil Sciences
log K_{OW}	distribution coefficient for organics between octanol and water
log K_{OC}	sorption coefficient standardized on organic carbon content of the soil
n.a.	not analyzed
n.d.	not determined
NAPL	non-aqueous phase liquid (LNAPL=light non-aqueous phase liquid)
PAH	polycyclic aromatic hydrocarbon
PTFE	polytetrafluor ethylene (Teflon®)
PVDF	polyvinyliden fluoride
rmp	rounds per minute
TDR	time domain reflectometry
TPH	total petroleum hydrocarbon
WHC	water holding capacity
WRB	World Reference Base

Experiments

Ufb	silt loam with freezing from the bottom
Ufba	silt loam with freezing from the bottom and ^{14}C-anthracene
Ufbp	silt loam with freezing from the bottom and ^{14}C-pyrene
Uftao	silt loam with freezing from the top, ^{14}C-anthracene and oil
Uftpo	silt loam with freezing from the top, ^{14}C-pyrene and oil
Sftao	sand with freezing from the top, ^{14}C-anthracene and oil
Sftabo	sand with freezing from the top, anthracene, benzo[a]pyrene and oil
Pftabo	peat with freezing from the top, anthracene, benzo[a]pyrene and oil

LIST OF FIGURES

LIST OF TABLES

1. INTRODUCTION

Organic contaminants entering soils pose a threat to soil functions and properties (Valentín et al., 2013; White & Claxton, 2004; Yaron et al., 2012). In freezing soils, especially permafrost-affected soils, the freezing process leads to changes in soil's physical and chemical properties (Yershov, 1998). Soils represent a complex heterogeneous, multi-phase system, with a large interfacial area, which causes phenomena such as adsorption of water and chemicals, ion exchange and capillarity (Hillel, 2003). Therefore the interaction of freezing soils and organic contaminants is characterized by high complexity and a variety of processes, whose effects may accumulate or abate each other.

1.1.1 GENERAL INTRODUCTION

Soils are a non-renewable resource in terms of human time periods (Banwart, 2011; CEC, 2006). As they are a basis for life on earth their preservation is essential to our action on this planet. However, soil functions are threatened by anthropogenic actions. Environmental pollution is one factor that causes a restriction of soil functions, because soils usually act as a sink for contaminants (Blume et al., 2010).

Due to different soil development, landscape structure and resilience of ecosystems the fate of organic contaminants in cold region soils cannot be compared to the behavior of organic contaminants in soils of temperate regions (Snape et al., 2008). Firstly, biological transformation of chemicals and turnover takes place at much lower rates in cold environments (AMAP, 2002). Secondly, processes like volatilization and sorption are temperature dependent and thirdly, the soil water content in freezing soils is always a sensitive balance of liquid and frozen water. This balance mainly influences the physical conditions for distributions processes of chemicals and gives rise to water migration processes below 0°C.

Permafrost-affected soils are of interest, because nearly 24 % of the Northern Hemisphere is influenced by permafrost (Zhang et al., 2000). Permafrost-affected soils occur in high latitudes and high altitudes, because of past and present climatic conditions of these regions. Contrary to the term, permafrost affected soils are not characterized by permanency and this makes human activity in the cold regions of the earth difficult (Williams & Smith, 1991). The annual thawing and freezing surface soil layer varies in its thickness throughout the years. This in turn influences the water and ice content of the soil. In general, climatic conditions, soil type, vegetation and topography control the thermal state of permafrost-affected soils (Andersland & Ladanyi, 1994; French, 2007). As most permafrost is warmer than -5°C (Williams & Smith, 1991), only small changes in temperature can make big differences, when the phase transition from ice to water and vice versa takes place.

Despite the harsh conditions for human life in cold regions, resource exploration activities have increased. Figure 1.1 shows the undiscovered conventional oil and gas resources north of the arctic circle, which are estimated to account for 90 million barrels of oil and 1669 billion cubic feet of gas (Bird et al., 2008). These amounts approximately account for 13 % of world undiscovered oil and 30 % of world undiscovered gas resources, respectively. With the growing human demand for energy and exhausting oil fields elsewhere in the world, exploration activities in the Arctic are increasing. Large oil spills have already been reported in the Arctic, either by oil exploration companies (APSC, 2013) or by remote sensing data (White et al., 2000). Increasing exploration activities were already observed by Raisbeck and Mohtadi (1974), who stated that "any large scale development of these [*note: arctic oil resources*] will inevitably create new environmental problems. "Furthermore, Raisbeck and Mohtadi (1974) point out that the development of oil exploration facilities includes increased construction of roads, power lines, houses and sewage disposal facilities. In conjunction with this development the relative scarcity of potable water in the Arctic regions and its threat through contamination has to be taken into account.

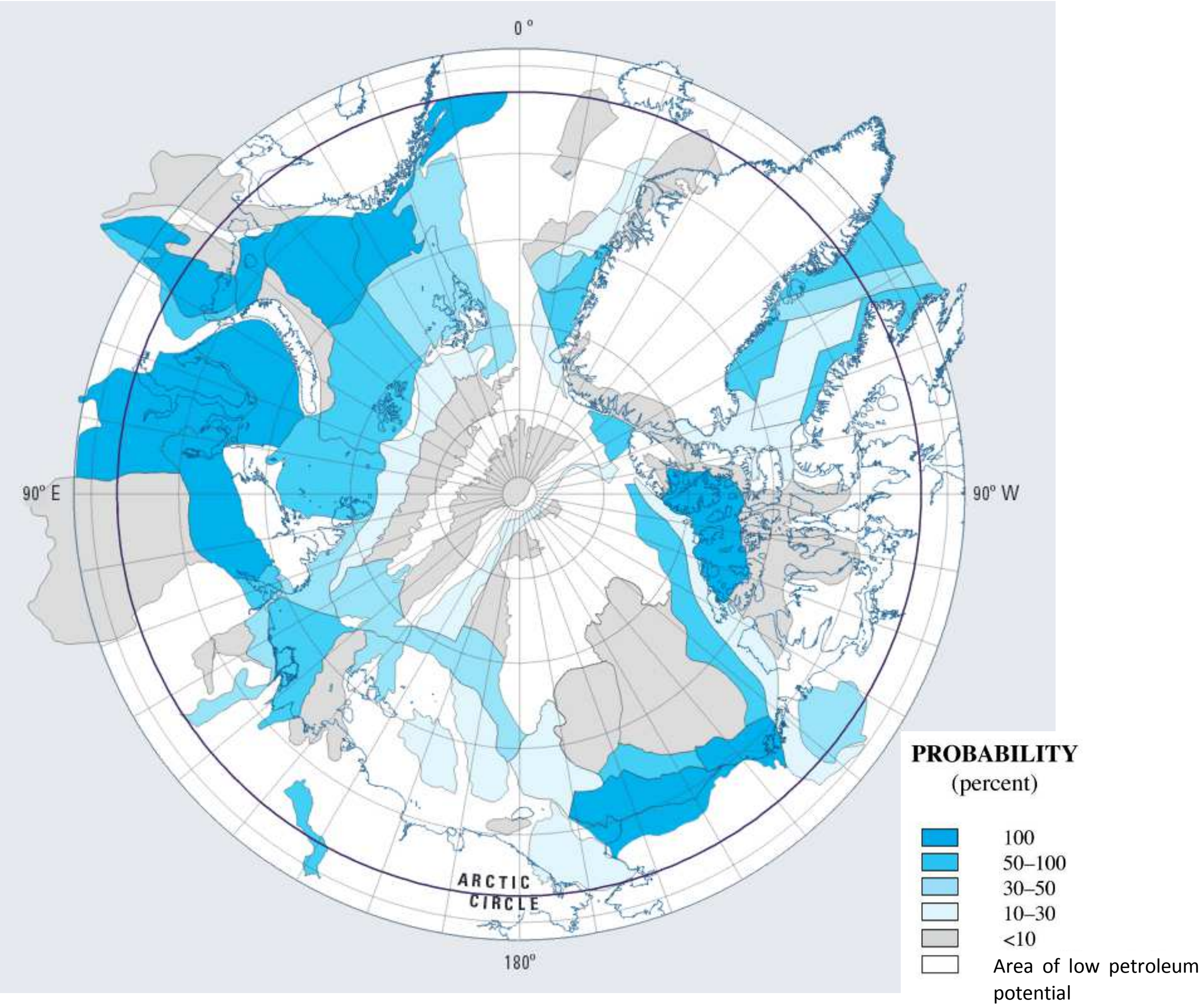

Figure 1.1 Probability map of Yet-To-Find oil or gas resources north of the Arctic Circle, assessed by the U.S. Geological Survey in 2008. Color-code displays probability of the presence of at least one undiscovered oil and/or gas field with recoverable resources greater than 50 million barrels of oil equivalent (MMBOE). Source: Bird et al. (2008)

Crude oil is a very complex mixture of many individual compounds, whose composition varies dependent on its origin. It can be classified according to its density. As density is a function of the composition of crude oil, some main structural groups have been determined for classification, such as paraffins and aromatics. For the quantification of oil products in soils a sum parameter of petroleum hydrocarbons with certain chain length can be determined (total petroleum hydrocarbons, TPHs). A subgroup of the aromatics is polycyclic aromatic hydrocarbons (PAHs). For risk assessment the sum of 16 single PAHs, determined by the U.S. environmental protection agency due to their persistence and toxicity, is given as measure for PAH contamination (16 EPA PAHs).

The main causes of soil contamination with oil in form of spills may be limited to human error and sabotage, unreliable constructions, failed infrastructure or natural hazards (Siciliano et al., 2008; Yershov, 1998). PAHs also enter soils via atmospheric transport after being released from natural and industrial incomplete combustion processes. Therefore they are ubiquitous in soils (Curtosi et al., 2007; Howsam & Jones, 1998; Nam et al., 2009). PAHs are a widespread contaminant group with a well-known negative impact on soil functions, which also threatens human health because of its carcinogenic and mutagenic potential (Tsibart & Gennadiev, 2013; White & Claxton, 2004). For temperate regions the fate of organic contaminants in soils, and especially of TPHs and PAHs, has been subject to numerous studies (Caravaca & Roldán, 2003; Fine et al., 1997; Jarsjö et al., 1994; Schwille, 1984; Tsibart & Gennadiev, 2013; Zhang et al., 2008). It has been shown that processes like sorption, volatilization, transport and transformation are mainly determined by the soil and contaminant properties, as well as microbial degradation. The main soil properties controlling the interaction of the soil with organic contaminants are organic carbon content, grain size distribution, water content, soil density and temperature (Hillel, 2003). Porosity and permeability of the soil are closely connected to the mentioned properties. Complexity of the interaction of soils and organic contaminants is increased, as the latter usually appear in groups of compounds with different properties. A main aspect of the determination and fate of organic contaminants is the physical phase in which they are present. TPHs usually occur as non-aqueous phase liquids (NAPLs). The main properties determining the migration behavior of NAPLs in soils are their viscosity, density and quantity. PAHs enter soils either associated to TPHs within the NAPL or associated to other chemical compounds. Their further fate in soils depends amongst others on chemical structure, water solubility and volatility, which may vary a lot between different PAHs. It is obvious that the interaction of soils and organic contaminants of these two heterogeneous groups is characterized by numerous parameters which influence the behavior of the latter in different ways.

The subsurface behavior of spilled crude oil and its products is an ongoing research area (Iwakun et al., 2010), which has also been studied at in-situ spill sites in permafrost-affected areas (Balks et al., 2002; Johnson et al., 1980; McCarthy et al., 2004; Revill et al., 2007). Interaction of organic contaminants and permafrost-affected soils influence the soil properties on all scales. Increases of active layer thickness and subsidence of oil contaminated permafrost-affected soils have been observed (Aislabie et al., 2004; Collins et al., 1993). The inner soil structure may be changed due to the formation of alternate layers of ice and oil, consolidation of the soil as a whole or the formation of aggregates and micro-fissures may occur (Barnes & Wolfe, 2008; Grechishchev et al., 2001; White & Williams, 1999). NAPL ganglia that form in soils are fragmented due to several freeze-thaw cycles and their entrapment on complete freezing is not fully understood yet (Grechishchev et al., 2001; Singh & Niven, 2013). The behavior of PAHs in permafrost-affected soils has been studied at some sites in Antarctica near research stations (Aislabie et al., 1999; Curtosi et al., 2007; Prus et al., 2015). It was found that the contaminants are present at very low levels, and contents increase with increasing soil depth. PAHs were even found in the perennial frozen ground, but the processes that led to this distribution are not clear yet (Curtosi et al., 2007).

The process of freezing induces particular soil water, heat and particle migration processes, which may also influence the migration behavior of organic contaminants. To understand the processes and their driving factors, laboratory experiments were conducted. Thus it has been shown that soluble organic contaminants were excluded from the formation of segregated ice (Konrad & Seto, 1991; Tumeo & Davidson, 1993). Some authors could show the exclusion of oil ahead a freezing front for distinct soil textures and in glass beads, respectively (Barnes et al., 2004; Chuvilin et al., 2001; Niven & Singh, 2008). Other studies could not reveal the effect of oil exclusion ahead a freezing front (Biggar & Neufeld, 1996), or even observed an upward movement of oil at the beginning of the freezing process and during ice thaw (Iwakun et al., 2010). Varying results may be partly explained by the differing experimental procedures, which were seldom nature-orientated (Biggar & Neufeld, 1996; Chuvilin et al., 2001; Henry, 2007). That fact revealed the need for an experimental apparatus and experimental procedures, which are able to simulate natural freezing conditions, but are also adequate for the quantification of organic contaminants.

In addition to the already very complex relation between soils, organic contaminants and the particular climatic conditions of Arctic and Antarctic regions, climate change induces thermal (ACIA, 2004; Boike et al., 2013; Hinzman et al., 2005; Lange, 2015) , hydrological (Jorgenson et al., 2010; Schindler & Smol, 2006; Woo, 2012) and ecological changes (Knoblauch et al., 2013; Kutzbach et al., 2014; Serreze et al., 2000) in these areas and the soils. That means soil properties and freezing and thawing processes in the surface soil layer are very likely to change. Jorgenson et al. (2010) identified the interaction of different biophysical factors to create either negative feedbacks (vegetation succession) or positive feedbacks (thaw settlement and water impoundment) on climate warming, which result in preservation or thaw of present perennial frozen ground. Furthermore, climate warming may accelerate rates of atmospheric contaminant transport and induce the melting of accumulated, contaminated snow and ice, and is therefore also responsible for increased threatening from contamination to the vulnerable cold environment (ACIA, 2004; Siciliano et al., 2008). Therefore it is most probable that identified factors and processes concerning organic contaminant behavior in permafrost-affected soils will alter due to changing climate conditions.

1.2 AIMS AND OBJECTIVES

It is not clear if the freezing process enhances transport or retardation of TPHs and PAHs in soils, and if its influence is more pronounced than other influencing factors which control the organic contaminant behavior in soils of temperate regions. The assessment of future contaminations with organic contaminants in permafrost-affected soils is complicated by climate change and its influence on the factors controlling the contaminants behavior in the soils. One of the most important questions in this context is the evolution of the hydraulic connectivity between surface waters, supra-permafrost waters and groundwater (Ireson et al., 2013; Walvoord & Striegl, 2007; Walvoord et al., 2012), because it is not known if these connections may be pathways for contaminant transport (Fourie & Shur, 2008). For metals which may be released out of peat due to permafrost thaw the problem of contamination of surface waters and riverine systems has already been described (Stepanova et al., 2015).

Previous laboratory studies concerning the influence of the freezing process on organic contaminant behavior in soils focused either on water soluble organic contaminants (Konrad & Seto, 1991) or NAPLs (Chuvilin et al., 2001; Iwakun et al., 2010; Singh & Niven, 2013). The present work focuses on the impact of the freezing process on PAHs and TPHs. To decode single processes in the multifactor-system of PAHs, soil and other organic contaminants, laboratory experiments with set boundary conditions were conducted. For an adequate simulation of the natural occurring processes it is important to adjust the setup according to their natural properties.

The experimental approach should allow the variation of single factors to investigate their influence on the contaminant's behavior in the freezing soil. These requirements gave the first aim of the present study:

1. The development of an experimental setup that allows the simulation of natural freezing processes with the accompanying water migration and accumulation phenomena in soils contaminated with PAHs and TPHs.

In conjunction with the influence of the freezing process on the distribution of PAHs in abundant arctic soil materials the following research questions arise:

2. Is the distribution of PAHs with different chemical structure and properties in freezing soils influenced by freezing induced water migration?
3. Are PAHs expulsed with a NAPL present ahead a freezing front? Does soil texture have an influence on this process?
4. Does the freezing process influence the availability of PAHs in the soil?

To assess the impact of the investigated processes in the natural soil system, which shows the result of all factors influencing each other, soil contaminated with diesel in a permafrost-affected area in Northern Siberia was assessed. With respect to the findings of Chuvilin et al. (2001); Collins et al. (1993) and Johnson et al. (1980) the following questions arose:

5. Does supra-permafrost water table influence the migration behavior of PAHs and TPHs?
6. What are the main factors influencing the TPH and PAH distribution within the investigated soil and in general?
7. Do TPHs and PAHs show similar distribution patterns and does partitioning between single substances of the two groups take place?

2. THEORETICAL BACKGROUND

The following text gives definitions, theoretical background and the state of the art on permafrost-affected soils, freezing process, organic contaminant behavior in soils and their interaction. The main focus lies on the chemicals water, polycyclic aromatic hydrocarbons (PAHs) and light non-aqueous phase liquids (LNAPLs), such as crude oil. The importance of water is based on its phase transition to ice at temperatures around 0°C and the process of freezing induced water migration that may take place. The latter is one of the most important processes controlling physicochemical processes specific for permafrost-affected soils (Yershov, 1998).

2.1 PERMAFROST-AFFECTED SOILS

The definition of permafrost-affected soils is based on the thermal state. The temperature of the ground has to remain at or below 0°C for two or more consecutive years (French, 2007; Yershov, 1998). That does not necessarily mean that the ground is completely frozen, because there is still active, unfrozen water in the system. Therefore French (2007) uses the term cryotic. Soil freezing is related to the phase transition from water to ice. The process of freezing depends on soil moisture content and composition of the soil solution. It may take place at several degrees below 0°C and over a range of degrees Celsius. The reason for this phenomenon is the dependence of the partitioning between liquid water and ice on certain factors. Besides the temperature these are mineral composition, specific surface areas of the particles and the presence of solutes (Andersland & Ladanyi, 1994). Depending on these factors considerable amounts of liquid water may coexist with ice in soils at temperatures below 0°C. These unfrozen water contents in a freezing or partially frozen fine-grained soil cause hydraulic gradients that may be large enough to induce the migration of pore water from unfrozen to partially frozen soil via unfrozen water films (Blanchard & Fremond, 1982). This process is called cryosuction and will be presented in more detail in chapter 2.2. The water that migrated due to cryosuction freezes when it reaches the freezing front (Williams & Smith, 1991), or if it was liquid water movement within frozen soil, close to the freezing front in a zone of low hydraulic conductivity (Konrad & Morgenstern, 1980). That may lead to moisture contents (sum of ice and liquid water) of frozen soils, which exceed the value of soil moisture capacity to a great extend (Yershov, 1998). If the freezing front rests for a certain time at the same position, a discrete ice layer (or ice lens) forms (Penner, 1972). This segregated ice can range in thickness from hairline to more than 10 m, and thus cause considerable frost heave processes (Williams & Smith, 1991). Commonly segregated ice occurs in alternating layers of ice and soil, the ice layers may then be referred to as ice lenses. The potential of a water saturated soil to experience segregation ice formation mainly depends on soil type and porosity, rate of cooling and pressure in the phases of soil water (Konrad, 1989).

Besides the moisture content, density and porosity are the most relevant physical soil properties of permafrost-affected soils (French, 2007; Yershov, 1998). The density of frozen soils varies generally between 0,62 and 2 g cm^{-1}, depending on soil material and ice content (Yershov, 1998). The latter has also a great influence on the porosity. Generally ice-rich soils have low bulk densities and high porosities. Yershov (1998) gives porosity data for fine grained permafrost-affected soils of 60 % to 90 %, while porosities of their unfrozen equivalents are only between 20 % and 40 %.

Permeability is strongly influenced by the ice content, because the void spaces, filled with ice, lead to the consolidation of the soil. Therefore permafrost generally acts like an aquiclude or at least like an aquitard (Woo, 2012). The permeability of wet soils is much less when they are frozen, because water freezes firstly in large pores, decreasing hydraulic conductivity. Sandy, dry, frozen soils have similar hydraulic conductivities like their unfrozen equivalents (Andersland & Ladanyi, 1994). This effect is most pronounced in coarse grained soils. Permeability for frozen gravelly sands decreases linearly with an increasing pore ice content (Wiggert et al., 1997). Therefore Walvoord et al. (2012) defined permafrost in an hydrological point of view as "... *ground containing perennial ice or perennial frozen geologic substrate that impedes the flow of water*." The soil ice content also controls the washout capacity for aggregates and elementary particles in freezing and thawing soils (Yershov, 1998).

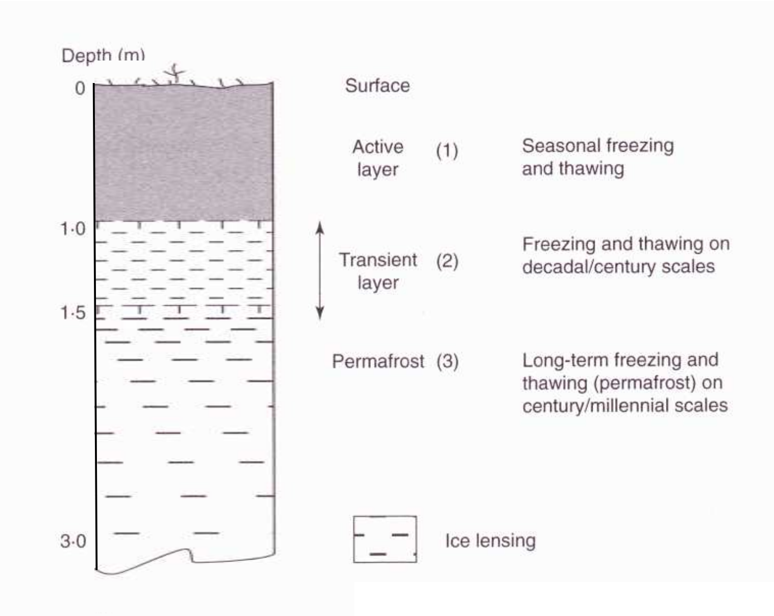

Figure 2.1 **Scheme of a permafrost affected soil adapted from French (2007)**

Due to seasonal changes in atmospheric temperatures the surface layer of permafrost-affected soils melts during the summer months. It is called active layer (see Figure 2.1). Active layer thickness is between 15 cm and 200 cm, depending on ambient temperatures, geomorphology, vegetation, snow cover, soil composition, water content and drainage (French, 2007; Shur et al., 2005). Some of these factors mainly influence the surface albedo. The surface albedo in turn is the main parameter for the heat energy fluxes into the soil, which mainly control the seasonal thaw depth. When permafrost behaves like an aquiclude below the active layer, the melt water cannot run off, which leads to water stagnation within the active layer (Jones et al., 2010). Authors like Ireson et al. (2013) and Woo (2012) use the term groundwater for these supra-permafrost waters. However, as this saturated soil zone is mainly recharged by snow melt waters and may not be present throughout the whole year the term supra-permafrost water will be used in the present study for water saturated zones in the active layer. The water saturated conditions are accompanied by reduced conditions. Another characteristic generated by the low temperatures in arctic climate is the decreased biological activity, which leads to the accumulation of partially decomposed remains of flora and fauna in the topsoil, often creating a thick O horizon (Jones et al., 2010).

The active layer is separated from the perennial frozen ground by the transient layer. Within this layer the permafrost table (frontier between active layer and permafrost) is situated. That means depending on the aforementioned factors for the active layer depth the transient layer may thaw. This thawing typically takes place on decadal to centennial scale (Fourie & Shur, 2008; Shur et al., 2005). The transient layer is characterized by high ice and water content, respectively. In some cases the seasonally frozen active layer and perennial frozen permafrost are separated by an unfrozen layer, which is called talik.

Before the active layer refreezes in autumn a period of constant temperatures at about zero degrees Celsius characterizes the soil thermal regime. The effect is caused by the release of energy from the chemical phase transition from water to ice, which accounts for 334 J g^{-1} (Williams & Smith, 1991; Yershov, 1998). The released latent heat slows down the freezing process in the soil, resulting in the described steady thermal state of the soil, which may last for hours up to several weeks. This effect is called zero curtain effect and depends mainly on total water content, snowcover and ambient air temperatures (Washburn, 1979).

In Figure 2.2 zero curtain effect has been observed at a site in the wet polygonal tundra of Northern Siberia between 8th of October and 1rst of December 2007. It can be seen that temperatures at 33 cm soil depth and below stay around 0°C for a much longer time, than the temperatures in the upper part of the soil. This indicates that the water table lies between 21 cm and 33 cm soil depth, because the higher water content of the saturated zone in the active layer leads to a higher release of latent heat and therefore the prolongation of the zero curtain effect.

A second important aspect of permafrost-affected arctic soils is that the refreezing process of the active layer in autumn takes place from two sides, the soil surface and to a smaller extend from the permafrost surface. Boike et al. (2013) observed refreezing times of a polygonal rim over 10 years. The start of freeze-back was determined when temperatures in all thawed layers had fallen to 0°C and the end of the refreezing process was determined by the TDR signal reaching and remaining at its minimum (Boike et al., 2013). The refreezing times varied in the range from 35 to 65 days, depending on ambient temperatures and snow cover. Moisture contents did not vary much over the years (Boike, 2014). The advancing freezing fronts from the surface and the bottom induce a pressure on the saturated part of the active layer, which may lead to thixotropic effects (Sloan & van Everdingen, 1988). That means the upward seepage force of the water exceeds a critical value at which there is no grain-to-grain pressure anymore. The physical result is that the soil acts like a fluid. This effect may also be reached, if pressure is exerted on a thawed active layer with supra-permafrost water (Woo, 2012).

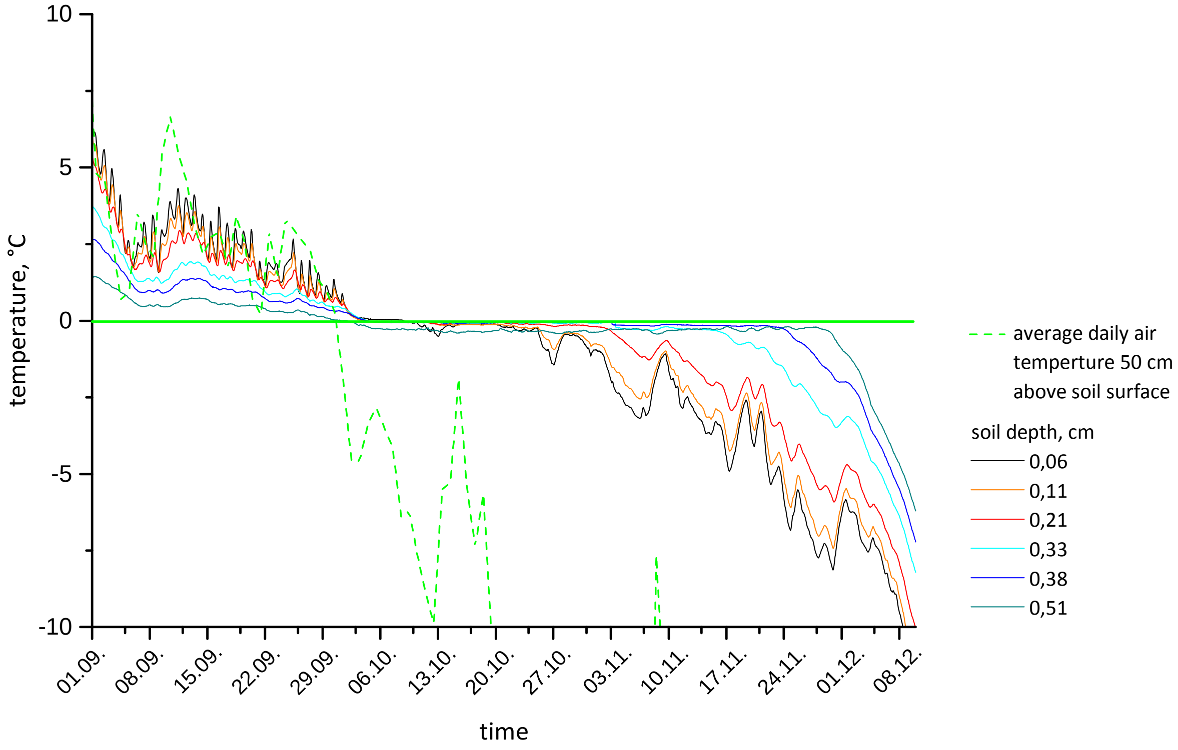

Figure 2.2 Soil temperatures in different depth of a polygonal rim on Samoylov island (Northern Siberia) from 2007, bold green line marks 0°C, figure arranged with data from Julia Boike.

Due to the mentioned factors frost penetration rates in the soil vary. In Canadian soils average frost penetration rates are 1 – 5 cm day^{-1} and the temperature gradients within permafrost-affected soils usually do not exceed 10°C (Konrad & Seto, 1991). The resulting cooling rates range from 0.05°C day^{-1} to 0.5°C day^{-1}. The cooling rate within a freezing soil is a main factor determining the dimension of segregated ice formation.

The temperatures of the active layer in winter depend mainly on snow cover and snow thickness. Thawing is a one-sided process from the soil surface (French, 2007). The seasonal water recharge pattern is strongly correlated to the thermal state of the active layer and the snow accumulation pattern. With the snow melt the water table in the active layer rises and reaches its maximum in spring (Ireson et al., 2013). During the summer month the water table falls, because water is lost through root uptake and evapotranspiration until September. Sometimes single rain events may induce a slight rise of the water table within the summer month. In winter the water migration and distribution is driven by the freezing process and sublimation at the soil surface. Ireson et al. (2013) suggested that the degree of hydraulic isolation between the supra-permafrost water and water within or below permafrost is the principal hydrologic effect in permafrost-affected soils.

Besides the described processes a great variation of other processes is observed in the active layer, such as cryoturbation, frost heave, frost sorting, gelifluction and frost crack formation (French, 2007; Zubrzycki et al., 2014). Cyropedogenic processes within the transient layer and permafrost are cryogenic weathering, ice segregation and accumulation (Zubrzycki et al., 2014). All these processes lead to a destruction of the usual horizontal layering in the soil (Jones et al., 2010).

With regard to physical and chemical soil properties and microbial activity there is no consensus yet to what extent they are influenced by freeze-thaw cycles, nor if observed effects accumulate or dissipate with the number of cycles (Henry, 2007). Studies on the hydraulic conductivity and the influence of freeze-thaw cycles on this soil property are an example for the given uncertainties. It has been shown that freeze-thaw cycles may induce the compaction of a soil, meanwhile increasing its hydraulic conductivity (Qi et al., 2006). The responsible factors for the increase in hydraulic conductivity are the formation of micro fissures due to the freezing process and the large pore spaces that are left, when ice has been thawed (Qi et al., 2006). Besides the grain size distribution and the density of the soil the main factors controlling the changes in hydraulic conductivity due to freeze-thaw cycles are water content and pressure. For silty sand relevant increase in hydraulic conductivity was observed for medium water contents, whereas hardly any change could be seen for water content near saturation level (Viklander & Eigenbrod, 2000). For a glacial clay Othman and Benson (1993) could show that overburden pressures of 10 kPa could already prevent an increase in hydraulic conductivity, because the freezing induced cracks are closed. However generally it is observed that freeze-thaw cycles leave a residual void ratio, which leads to a convergence in hydraulic conductivity of dense soils and loosely packed soils (Viklander & Eigenbrod, 2000). The latter having a decreased hydraulic conductivity, whereas the hydraulic conductivity for dense soils increases. In general the relationship between hydraulic permeability and soil density in conjunction with freeze-thaw cycles is not fully understood yet.

In the Arctic a broad variety of soil types developed upon different geological parent materials. The following classifications are based on the World Reference Base for Soil Resources 2014 (WRB) (IUSS Working Group WRB, 2014). The WRB is used due to its international utilization, its applicability in the field and due to the fact that organic contaminants are not committed to a certain area. North of the Arctic Circle Cryosols (WRB) dominate. To the south Histosols, Gleysols and Podzols belong to the main soil types encountered. In the West Siberian Basin, the world's second largest petroleum basin, Podzols and Histosols are encountered. To the south of the basin Albeluvisols replace the Podzols and to the north Cryosols constitute the main soil type. (Jones et al., 2010)

As described above the thermal state of permafrost-affected soils depends on several factors, like ambient air temperatures, snow cover and vegetation. All factors mentioned change due to climate change and further changes are predicted (Hartmann et al., 2013). In the Arctic the mean annual temperature rose by 1.7°C in the last 50 years. As most permafrost is warmer than -5°C many scientists predict increasing active layer thicknesses with increasing air temperatures (Hinzman et al., 2005; Jorgenson et al., 2010; Serreze et al., 2000). However, Boike et al. (2013) did not observe increasing active layer thicknesses in the Siberian Arctic within the last 15 years. They state that it is not clear whether there is actually no increase in active layer thickness, or if thaw settlement masks an increasing active layer thickness. Jorgenson et al. (2010) assess the resilience and vulnerability of permafrost to climate change and came to the conclusion that the complex interaction of biophysical factors may protect permafrost from thawing or enhance its thawing in conjunction with climate change scenarios. As enhancing factors they give thaw settlement and water impoundment, whereas the vegetation succession which is predicted to go along with climate warming protected permafrost thaw in the model.

2.2 FREEZING PROCESS

The freezing of water to ice under standard conditions takes place at 0°C. This freezing temperature is lowered by increasing pressure and solutes. However to initiate the phase transition from water to ice a crystal nucleus is needed, otherwise pure water freezes far below 0°C. The formation of ice is attended by an expansion in volume from water to ice of approximately 9 %.

2.2.1 FREEZING PROCESS IN NATURAL SOILS

The freezing process of a soil solution is given in Figure 2.3. At the beginning the solution is cooled down, due to losses of heat energy. The temperature of the soil solution falls below 0°C, due to the presence of solutes and soil texture. The temperature can even fall below the equilibrium freezing point, which is called "supercooling". With the first ice crystal forming on a nuclei, which may be aggregations of water molecules or soil particles, an abrupt interruption in the cooling process can be observed (Kozlowski, 2009). This effect is caused by the phase transition from water to ice and the along going release of latent heat (see chapter 2.1). During thawing the effect is vice versa, but not as pronounced. If no void pore spaces are available, as in water or ice saturated soils, high pressures such as 13 MPa (Blume et al., 2010) or as 65.8 MPa maximum under ideal conditions (Singh & Niven, 2013) may be generated. The freezing point depression shown in is based on different factors, with the most important being capillarity and adsorption, which affect the decreasing amount of liquid water by lowering its free energy and thus its freezing point. This effect is amplified with decreasing grain size. Sparrman et al. (2004) could show that the liquid water content in a soil at -4.7°C increases with an increasing amount of humus material. Kozlowski (2009) could show that the equilibrium freezing point can also be expressed as a function of water content and plasticity limit. A lower water content is related to a lower equilibrium freezing point then a higher water content, but in turn the freezing rate in the soil with the lower water content is higher (Grechishchev et al., 2001; Horn et al., 2014). The presence of dissolved substances plays a minor role, approximately accounting for 0.1°C of freezing point depression (Konrad & Seto, 1991; Williams & Smith, 1991).

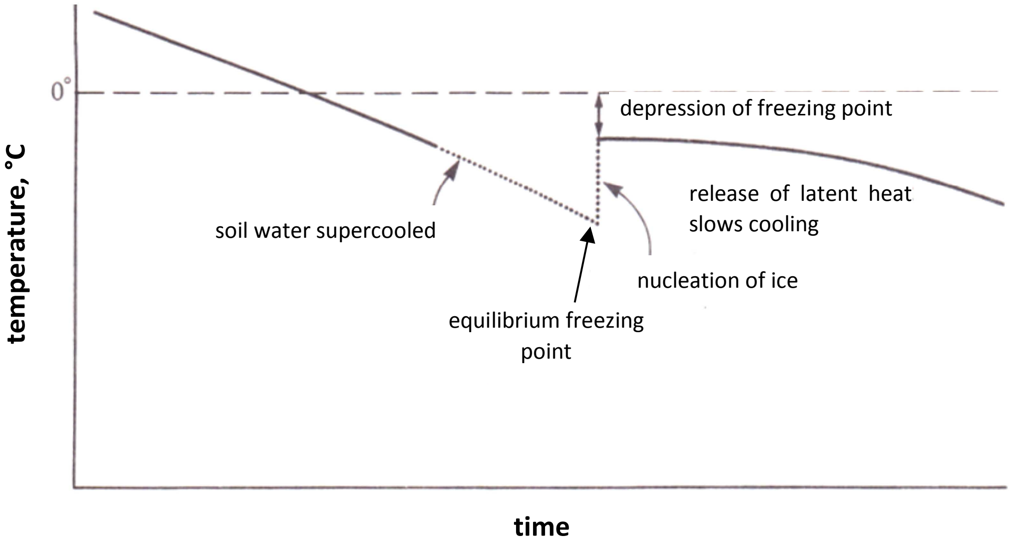

Figure 2.3 **Freezing process of soil solution taken from Williams and Smith (1991)**

To summarize free water in soil pores freezes at negative temperatures close to 0°C, whereas film waters in fine grained soils freeze within a wide range of negative temperatures (Andersland & Ladanyi, 1994; Yershov, 1998). Williams and Smith showed the big differences in this unfrozen water content between different soil materials (see Figure 2.4).

Tice et al. (1976) developed the following equation to calculate the unfrozen water content w_u of a soil at temperatures below 0°C from experimental data, neglecting the vapor phase:

$$w_u = \alpha * \Delta T^{\beta} \quad \textbf{Equation 1}$$

with α and β being characteristic soil parameters and ΔT being the absolute value of the temperature in degrees Celsius below freezing.

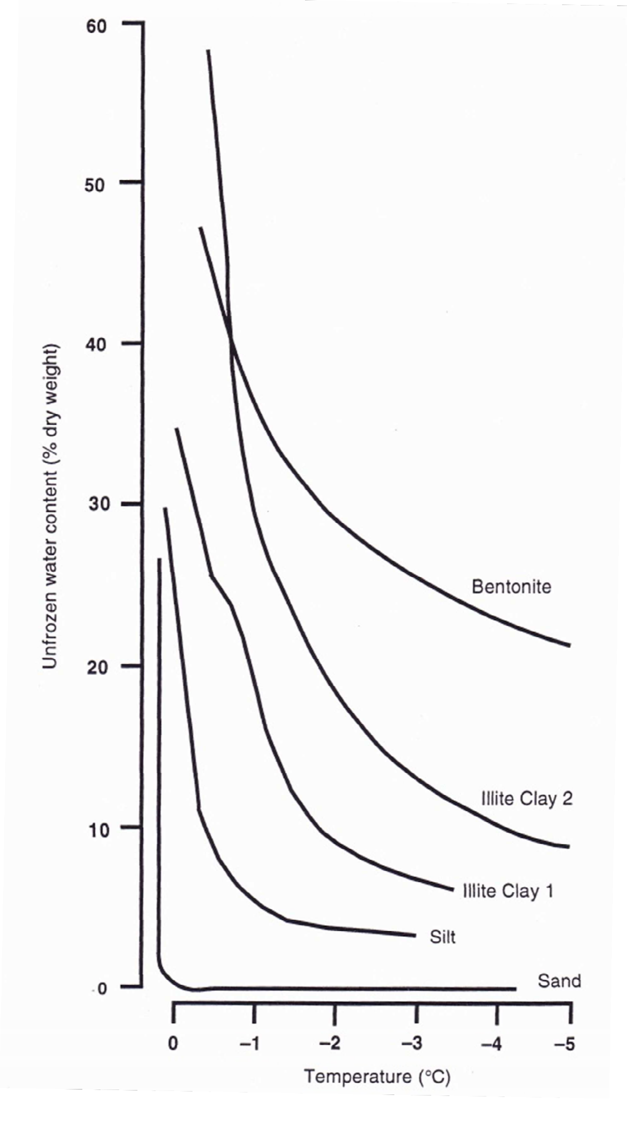

Figure 2.4 **Amount of unfrozen water at temperatures below 0°C in various soils taken from Williams and Smith (1991)**

The parameters α and β can be calculated from the water contents at N = 25 and N = 100, with N being the number of blows with a Casagrande cup required to close the standard groove in the liquid limit test. The latter is usually used to give the Atterberg limits.

The empirical relation between the determined water contents and unfrozen water content is:

$$\boldsymbol{w_{u,\Delta T=1} = 0,346 * w_{N=25} - 3,01} \qquad \textbf{Equation 2}$$

$$\boldsymbol{w_{u,\Delta T=2} = 0,338 * w_{N=100} - 3,72} \qquad \textbf{Equation 3}$$

The parameters α and β can be determined by solving equations 2 and 3, using the derived water contents together with equation 1 in the form:

$$\boldsymbol{log\, w_u = log\, \alpha + \beta\, log\Delta T}$$

Williams (1976) showed that at -1°C up to 40 % of the soil water content may remain unfrozen. When temperatures decrease the liquid part of the soil water is reduced in favor of ice, which captures more and more space. This process is accompanied by continuous lowering of the free energy of the remaining liquid water, which results in further freezing point depression. The remaining liquid water can migrate through the soil due to cryosuction. The cryosuction causes the so called Marangoni convection of soil water towards the freezing front (Flerchinger et al., 2005), which in turn is responsible for heat transport within the cooling soil (Harlan, 1973). This relationship can be explained as a temperature-pressure relationship, which is mathematically described by the Clausius-Clapeyron equation, if the transport takes place through film waters and equilibrium is assumed (Kurylyk & Watanabe, 2013). The latter is only given, if freezing rates do not exceed 0.1°C hour^{-1}. Then the freezing front is not advancing and ice lenses are growing within the frozen fringe (see Figure 2.5).

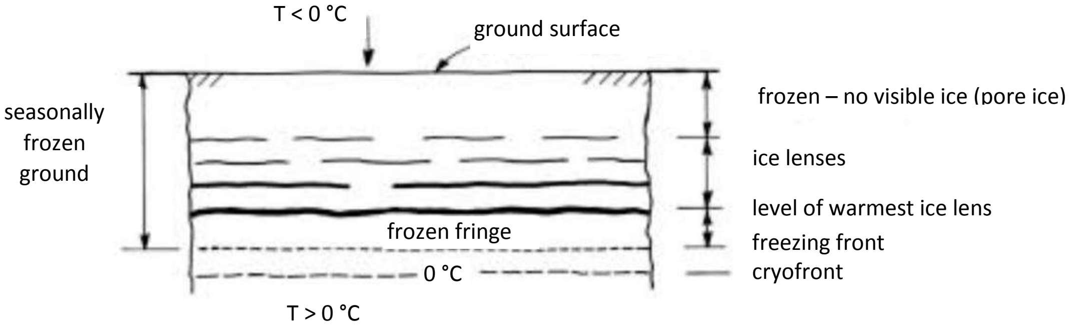

Figure 2.5 Diagram of frozen fringe, freezing front and cryofront during the freezing of a fine-grained, frost-susceptible soil, taken from Konrad and Morgenstern (1983)

This process goes on as long as enough water is migrating towards the ice. When less water arrives at the growing ice lens the latent heat energy of the phase transition from water to ice is not sufficient to impede the freezing front propagation. This in turn, stops the ice lens formation. Konrad (1989) defined the rate of cooling in the frozen fringe as product of temperature gradient within the frozen fringe and the rate of freezing front advance. That means the temperature gradients commonly found in natural soils, can lead to enormous suction gradients due to soil characteristics and freezing conditions, accounting for approximately 1.2 MPa m^{-1} for a temperature gradient of 1°C m^{-1} and may reach pore pressures up to 10 MPa (Williams & Smith, 1991).

However a thermal gradient induces water and vapor movement towards the cooler side, even at temperatures above 0°C (Hillel, 2005; Horn et al., 2014). Harlan (1973) employed a mathematical model and found that soil texture and initial moisture content are main factors influencing this water migration. He states furthermore that for soils with a zone of water saturation the water migration from the water table towards a constant freezing front would increase with increasing grain size, resulting in a water table recession. Fine grained soils as well as low initial water contents restrict the soil water redistribution process to areas close to the freezing front. As coarse grained soils have a lower water holding capacity and hardly any unfrozen water in the frozen state, it is not clear yet, in which textures the process is most pronounced (see Figure 2.4).

In water saturated soils a second process may be induced by the freezing process. The soil solution can be expelled from the soil pores ahead the advancing freezing front (McRoberts & Morgenstern, 1975; Nakano, 1999). Singh and Niven (2013) calculated the freezing induced pressure in a water saturated sandstone, which would allow expulsion of pore water to be 0.42 MPa. Thermal and hydraulic gradient are driving forces for this process, however the soil properties, namely the grain size distribution is the most important. McRoberts and Morgenstern (1975) could show that the water expulsion process in sandy soils takes place under different conditions, whereas for fine grained soils the process only occurs at higher overburden pressures. Summing up the shape of thermal and hydraulic gradient controls the freezing rate and the velocity of the proceeding freezing/thawing front (Flerchinger et al., 2005). The resulting water migration processes and the soil properties determine the type of ice formation and possible expulsion processes.

Not only the water is migrating in a freezing soil, but all dissolved substances as well. Konrad and Seto (1991) observed that dissolved solutes tend to be rejected at varying degrees from the growing ice. After thawing higher concentrations of the soluble substances were found where ice lenses had been formed. They explain this rejection due to the heat energy release of the phase transition from water to ice and the formation of the crystal ice structure. Yershov (1998) explains formation of ice with little or no inclusions with the precipitation of dissolved substances due to exceeded solubility product in the remaining soil solution. The water migration causes considerable dehydration in the unfrozen soil close to the freezing front (Harlan, 1973). Aggregation of soil particles takes place. Pores inside of aggregates become smaller, whereas volume and number of inter-aggregate pores grow. The latter take shape of elongated slits. (Yershov, 1998)

If freezing takes place without water migration, due to high freezing rate, low moisture content or specific grain size distribution the present soil water freezes first in the largest pores. As water is not migrating considerable crystallization pressures evolve and soil aggregates are condensed. Hence liquid water is squeezed out of the aggregates into large inter-aggregate pores where it crystallizes and leads to the destruction of inter-aggregate structure. With the ongoing freezing process thermal weathering of sand and coarse silt fraction can take place as well. On the other hand with increasing concentration of ions in still unfrozen water coagulation of soil particles, especially clay minerals can occur, generating silt-size micro-aggregates. (Yershov, 1998)

The freezing process and freeze-thaw cycles with the accompanying processes described above cause irreversible modifications of soil physical properties (Oztas & Fayetorbay, 2003; Qi et al., 2008) and microbial activity (Schadt et al., 2003) in permafrost-affected soil. Nevertheless Williams and Smith (1991) state that for many practical purposes the effects of variations between different soils and their properties are more important than the influence of freezing. The periodic freezing and thawing of the active layer leads under certain circumstances to patterned ground phenomena (French, 2007). This can include migration of small particles from the surface to depth and an opposite movement of coarse particles. Henry (2007) states that neither overall impact of freeze-thaw cycles is clear, nor if the effects in soils accumulate or attenuate with increasing number of cycles.

2.2.2 SIMULATION OF THE FREEZING PROCESS IN LABORATORY EXPERIMENTS

Contaminated soils exist in permafrost-affected Arctic and Antarctic landscapes (Aislabie et al., 1999; Braddock & McCarthy, 1996; Gennadiev & Pikovskii, 2007; McCarthy et al., 2004). Investigations at contaminated sites often emphasize on contaminant content distribution and its behavior with time. The interactions of contaminants and soils are diverse and a great number of processes that influence each other take place. If processes and their influencing parameters are understood, natural occurring phenomena may be interpreted. The impact of changing outside influences, like changing climatic conditions, may be better deducible and possible trends may be forecasted. To get an understanding of single processes it can be helpful to conduct laboratory experiments, as the influencing parameters may be set and varied according to the research issue. Furthermore availability and accessibility of samples and sites, as well as cost effectiveness play a role in the decision for the adequate method to answer the pending research questions.

Laboratory experiments employing soil columns were firstly used to investigate hydrological issues. Lewis and Sjoestrom (2010) distinguished soil column experiments by construction method (packed, undisturbed monolith) and the adjusted soil water content (saturated, unsaturated). They see the advantage of packed soil columns compared to undisturbed soil monoliths in the homogeneity within the columns, which results in better reproducibility and the reduction of sidewall flow. But they also point out that these advantages are gained on the expense of realism, because soil pore structure is not considered. In general chemical and physical properties of the soil used must be rigorously reported for the purposes of allowing reproducibility (Lewis & Sjoestrom, 2010).

That means for the present work that wants to investigate the influence of freezing on organic contaminants in soils, thermal properties and chemical reaction of the column setup have to be taken into account. Until recent several studies using laboratory column experiments to investigate the influence of freezing on organic contaminant behavior in soils have been conducted (Biggar & Neufeld, 1996; Chuvilin et al., 2001; Grechishchev et al., 2001; Konrad & Seto, 1991; Niven & Singh, 2008). Substantially they all wanted to investigate the impact of freezing or freeze-thaw cycles on the behavior and properties of soils contaminated with an organic contaminant. It is obvious that most of the experiments employed constant input cooling temperatures, which resulted in very high freezing rates at the beginning of the experiments and end up at a freezing rate of 0°C, creating a quasi-stationary freezing front at a certain microcosm depth. The main properties concerning the simulation of the freezing process are given in Table 2.1.

Laboratory studies are always a simplification of complex natural relationships, therefore boundary conditions should be carefully chosen. Furthermore the following recommendations are given in the literature for the conduction of laboratory column experiments and especially in conjunction with the simulation of a natural occurring freezing process and contaminants:

- Reproducibility of results should be displayed (Biggar & Neufeld, 1996).
- For column specimen side wall flow should be minimized/avoided (Biggar & Neufeld, 1996; Lewis & Sjoestrom, 2010).
- For large, unsaturated soil columns Bergström (2000) suggest a diameter : length ratio of 1 : 4.
- For experiments with organic contaminants a chemically resistant material for column construction should be used (Wehrer & Totsche, 2005).
- To detect phase transition of water to ice TDR probes should be used additionally to temperature probes (Müller-Lupp, 2002).
- Lowest temperature reached in the soil microcosms should be in the range of naturally observed temperatures (Henry, 2007).
- The use of cooling rates according to natural occurring cooling rates (Biggar & Neufeld, 1996; Henry, 2007).
- To observe rejection of solved organic contaminants from the forming ice threshold rates of cooling of 2.95 ± 0.25°C day^{-1} (Konrad & McCammon, 1990) and 4 ± 1°C day $^{-1}$ (Konrad & Seto, 1991) should not be exceeded. For cooling rates smaller than 0.1°C day^{-1} Konrad and McCammon (1990) state that 90 % of the solutes are rejected from forming ice.
- Water balance should be according to natural occurring conditions (Henry, 2007; Konrad & Seto, 1991).

Table 2.1 **Properties of laboratory freezing experiments on contaminant behavior in porous media from different studies. Abbreviations: d = diameter of a cylinder, L = length, H = heigths, W = width, wc = water content, tdc =two-dimensional cell**

reference	column dimension, cm material	freezing scenario	freezing rate °C day^{-1} experiment duration	organic contaminant used concentration	soil texture according to IUSS Working Group WRB (2014) water content	objective
Biggar and Neufeld (1996)	d: 17.5 H: 45.0 (30 soil core) plexiglas, stainless steel	freeze- thaw from the top, constant cooling from the bottom (-3.5°C), lower 22.5 cm constantly frozen	10 to 40 2, 6 and 8 freeze-thaw cycles	diesel fuel, in the upper 7.5 cm 8-12 % plus 116 ml diesel fuel on top in frozen state	sandy loam wc: 20 % dw (saturated conditions)	influence of freeze-thaw cycles on LNAPL distribution in the active layer upon a frozen, saturated soil zone
Chuvilin et al. (2001)	L: 4 H: 16 W: 4 plexiglas	freezing from the top, approx. half of the column	- 24 hours	crude oil 6.2 %	sand wc: 16 % silt loam (clay 4 %) wc: 21.5 % silt loam (clay 25 %) wc: 44 % saturated conditions	effect of unidirectional freezing process on oil distribution in soil
Grechishchev et al. (2001)	d: 7 H: 10 fiber glas	constant freezing from the top (-5±1°C) constant heating from the bottom (+3±1°C)	- 240 to 480 hours	crude oil from Zapadnoy (Siberia) 4 % and 14 %	silt loam wc: 21.5 %	impact of unidirectional freezing process on properties of oil polluted soil
Konrad and Seto (1991)	d: ? H: 7.9 to 114.2 not given	constant freezing from the bottom -4.7° C to -7.5°C in different experiments	- 93 to 238 hours	1-propanol 0.79 to 30.0 g L^{-1}	silt loam water saturated, open system conditions	effect of unidirectional freezing on water migration and organic contaminant behavior
Niven and Singh (2008)	L: 2.1 H: 1.0 W: 0.05 tdc	freeze-thaw from the bottom	- 1 to 10 freeze-thaw cycles	dodecane 21 to 26 %	glass beads water saturated	impact of freeze-thaw cycles on LNAPL below water table

2.3 ORGANIC CONTAMINANTS IN SOILS

The term contaminant is used in the present study for substances in soils that pose a significant risk to soil functions, biota and man, due to their persistence, bioavailability and harmful nature (BBodSchG, 1998; Berkowitz et al., 2008; Valentín et al., 2013). The structure of organic contaminants is built up of various carbon atoms. Most relevant groups of organic contaminants in permafrost-affected soils result from oil exploration activities. The main constituents of crude oil are alkanes, cycloalkanes and aromatics. The present study focuses on total petroleum hydrocarbons (TPHs) as main compound of crude oil and polycyclic aromatic hydrocarbons (PAHs), which belong to the aromatics and may also enter the soil through atmospheric transport and deposition. The term TPH is used here for the sum parameter of the content of hydrocarbons with chain length between C_{10} and C_{40}, which are determined by extraction and GC-FID analysis. PAHs contain two or more fused benzene rings. Detailed information about structure and properties of PAH and TPH is given in chapters 2.3.1and 2.3.2. The contaminants enter the soil in different physical phases (see Table 2.2). Crude oil belongs to the LNAPLs (Light Non-aqueous Phase Liquids), due to its density below 1 g cm^{-3}. That means TPHs and PAHs may enter the soil as an additional phase in the system of soil vapor, soil solution and particles. TPHs as main compound make up the LNAPL, whereas PAHs may be associated to the other organic compounds of the LNAPL. Furthermore PAHs may also enter soils adsorbed to other particles, mainly via atmospheric deposition.

The partitioning and fate of contaminants in soils is controlled by the physicochemical properties of soils and contaminants themselves. As both, organic contaminants and soils, are mostly complex mixtures not only their properties vary in a great range, but also their interaction. Processes of contaminant retention and transport take place, as well as microbiological interaction.

Table 2.2 Organic contaminants entering the soil can be divided into five broad categories on the basis of their physical phase (Berkowitz et al., 2008; Eschenbach et al., 1998; Fetter, 1999; Singh & Niven, 2013)

	Phase	Interaction with three soil compartments	Examples of contaminants
1	dissolved	soluble in water	1-propanol
2	non aqueous phase liquids (NAPLs) LNAPL DNAPL	immiscible in water lighter than 1 g cm^{-3} denser than 1 g cm^{-3}	 hydrocarbon fuels chlorinated hydrocarb.
3	vapor	volatilized into soil vapor	naphthalene
4	adsorbed and chemical bound	bound to soil matrix due to adsorption	different PAHs
5	solid	distinct solid phase	phenol, cresols, soot

Retention of crude oil and its compounds is controlled by sorption, entrapment and an aging effect with time (Fetter, 1999; Tang et al., 2012). PAHs can also be adsorbed, reach nanopores by diffusion processes and together with microbial activity form bound residues (Eschenbach et al., 2001; Northcott & Jones, 2001).

Main factors that determine the adsorption of TPHs and PAHs to the soil compartments are polarity of the chemicals and the influence of soil organic matter (Valentín et al., 2013). Polarity may be described by the octanol-water coefficient (log K_{OW}), which gives the term hydrophobic for log K_{OW} values greater than four. For soils with organic carbon contents ≥ 0.1 % and a low clay to organic carbon relation sorption behavior of TPHs and PAHs can be described by log K_{OC} (Blume et al., 2010). K_{OC} values are a measure of the partitioning of the chemicals between organic soil substance and soil solution, which can differ between soils or soil fractions by up to one order of magnitude (Marschner et al., 2005; Skark et al., 2011). To describe the sorption affinity of organic chemicals different authors see an advantage of using the log K_{OW} instead of log K_{OC} values, because of the heterogeneity of organic compounds in soils (Grathwohl, 2007). For TPHs entrapment in thin soil pores is an important retention factor (Singh & Niven, 2013), whereas for PAHs sorption and entrapment at sub-particle and molecular level is most important (Bauw et al., 1991).

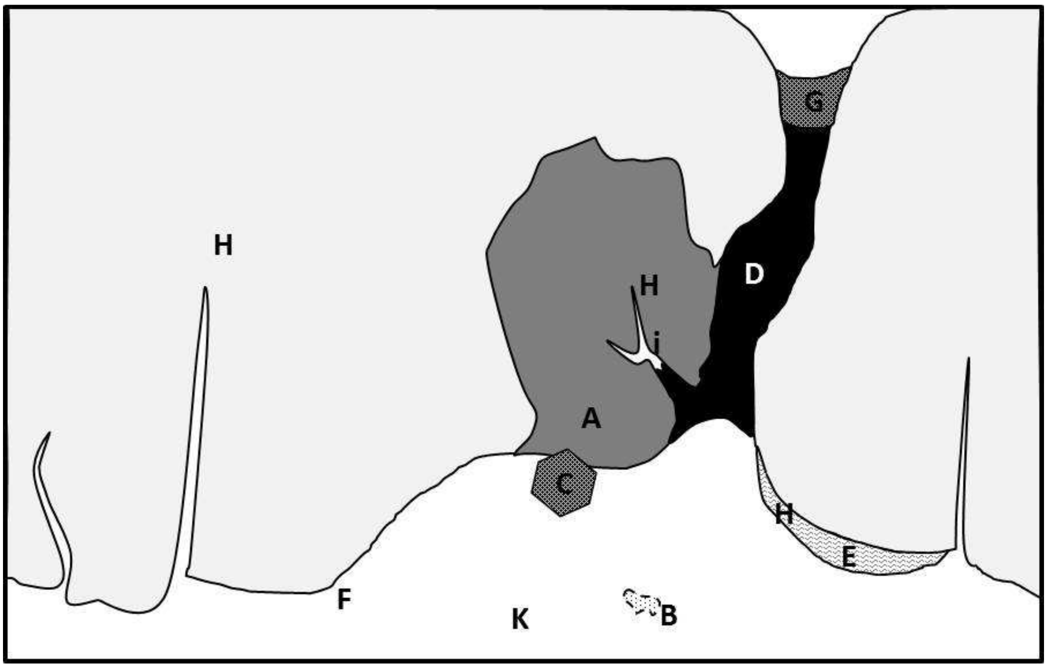

Figure 2.6 Conceptual model of chemical and physical geosorbent domains, A=different forms of organic matter, B=dissolved organic matter (DOM), C=combustion residue (e.g. soot), D=NAPL, E=clay particles and/or iron oxide coatings, F=moist mineral surfaces, G=weathered/aged NAPL, H=micro-pores (not visible in this model), i=meso-pores, K=soil solution (solution processes). Adapted from Luthy et al. (1997) and Bergknut (2006).

The velocity for fast adsorption processes ranges from minutes to days and is usually the basis of the determination of distribution coefficients (Pignatello & Xing, 1995). Domains for fast adsorption would be some organic matter (A), DOM (B), NAPL (D) and moist mineral surfaces (E, F) (see Figure 2.6). Slow sorption takes place in conjunction with organic combustion residues (C) and micropores (H). In many studies it could be shown that the extractability of contaminants from soils decreases with increasing contact time (Eschenbach et al., 1998; Pignatello & Xing, 1995; Zhao et al., 2013). The activation energy for fast adsorption processes is lower (0 - 50 kJ mol^{-1} Delle Site (2001)) than for slow adsorption (60 - 70 kJ mol^{-1} Cornelissen et al. (1997)). The interpretation is that slow adsorption processes follow diffusion processes (Hulscher & Cornelissen, 1996).

In general sorption is a temperature dependent process (Yaron et al., 2012). Most sorption processes are exothermic, therefore the adsorption of components to soil compartments decreases with increasing temperature. On the other hand water solubility increases with increasing temperature, but with respect to organic contaminants the impact on the adsorption processes is more pronounced (Delle Site, 2001). Over all it has to be taken into account that most studies investigated temperature effects above 0°C. That means an important process concerning the fate of TPHs and PAHs is not fully understood with respect to freezing soils.

Furthermore it has to be taken into account that TPH and PAH content may decrease with time, due to microbial degradation, solution and volatilization processes (Bergknut, 2006; Chang et al., 2013; Luthy et al., 1997; Rike et al., 2005). Microbial transformation and degradation determines the transport and distribution behavior of total petroleum hydrocarbons and PAHs in a considerable way (Chang et al., 2013; Gan et al., 2009; Valentín et al., 2013). Especially the potential risk of PAH for the environment and humans increases with incomplete degradation, because a lot of PAH metabolites are carcinogenic. Therefore Atlas and Bragg (2009) state that PAHs may not be degraded at all, in a sense of complete mineralization or transformation to simple organic compounds (Das & Chandran, 2010). The microbial degradation of organic contaminants in soils depends on water solubility of the contaminants and on the conditions for microbial growth, like availability of water and duration of the growing season (Gennadiev & Pikovskii, 2007).

The aforementioned processes may lead to the formation of non-extractable residues of PAHs or their metabolites. That means they cannot be extracted with solvent extractions from the soil matrix. They can be divided into four groups according to the adsorption process of the organic compound (see Figure 2.7). Organic compounds strongly adsorbed to the soil matrix may partially be determined by matrix destroying procedures, employing high temperatures and / or pressures. Figure 2.7 illustrates the different sites for adsorption, binding and physical retention as well as the main interaction processes taking place in soils.

To what extend the sorption to dissolved organic matter (DOM) and the soluble contamination phases are contributing to the migration processes of PAHs in soils is not clear yet (Busche & Hirner, 1997; Kögel-Knabner & Totsche, 1998; Raber et al., 1998). Concerning the properties of PAHs (Table 2.3) and TPHs (Table 3.1) solution and volatilization processes play a minor role for their fate in soils (Madsen, 2003).

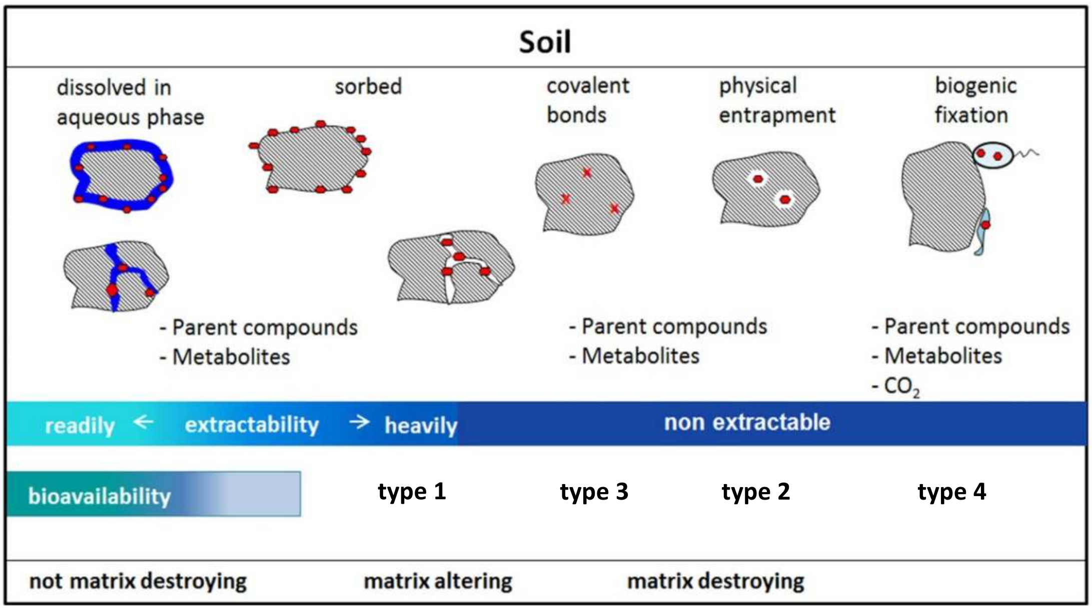

Figure 2.7 Model of possible binding forms of PAHs and differentiation of PAHs in soils according to their extractability, adapted from Eschenbach and Oing (2013).

Gennadiev and Pikovskii (2007) stated on the other hand that up to 20 % of the total content of an oil spill may be removed from the soil due to volatilization. However, they also admit that this process is temperature dependent and is mainly related to the light hydrocarbon fractions.

2.3.1 POLYCYCLIC AROMATIC HYDROCARBONS

Several hundred different PAH compounds are known. Following the precise definition benzene rings contain only carbon and hydrogen atoms. However, PAHs are usually extended to substituted PAHs, derivatives and hetero-atoms as well. The US Environmental Protection Agency listed 16 of these compounds as environmental priority pollutants. They are selected to cover different levels of toxicity, potential carcinogenicity and a wide range of physicochemical properties. Their most relevant properties concerning their interaction with the environment are listed in Table 2.3. Due to their persistence and toxicity PAHs and their behaviour in the environment are of special concern. Certain PAHs have carcinogenic and mutagenic potencies, but they require activation to electrophilic metabolites to exert their mutagenic and carcinogenic effects (Desler et al., 2009; White & Claxton, 2004; Xue & Warshawsky, 2005). Furthermore molecular structure with a bay or fjord region and the number of rings has been shown to influence carcinogenicity (Desler et al., 2009; Karttunen et al., 2010). The 5-ring PAH benzo[a]pyrene has been intensively studied and may be used to estimate total PAH concentrations. Sims and Overcash (1983) give natural background levels for benzo[a]pyrene between 5 – 10 µg kg^{-1}. For arctic soils, considered as most remote soils the amounts are even lower 0.8 – 4.3 µg kg^{-1} (Knoche et al., 1995).

The main properties determining the fate of PAHs in soils are their low water solubility, their hydrophobicity, given with high log K_{OW} values (see Table 2.3) and linked with these the low degradability. In this context the content, composition and structure of the soil organic material is an important factor for the fate of PAHs in soils (Maliszewska-Kordybach, 2005; Tsibart & Gennadiev, 2013). In general the low molecular weight PAHs, containing two or three fused rings, are more volatile and water soluble and can migrate as true solutions (Tsibart & Gennadiev, 2013). The high molecular weight PAHs, which contain four or more rings, can only migrate together with sorbing particles in most cases. There are exceptions from this generalisation for adjacent substances in the table. An example is the water solubility of pyrene compared with the one of anthracene. The 4-ring PAH pyrene has a three times higher water solubility and a four times higher fugacity ratio than anthracene, which is a 3-ring PAH.

The high organic carbon partitioning coefficients determine the adsorption of PAHs to soil organic matter (Karickhoff, 1981; Wilcke, 2000). This statement is supported by studies that showed considerably higher PAH contents in organic top soil layers of forests compared to mineral soils of similar sites (Krauss et al., 2000; Matzner et al., 1981). Distribution between two phases and surface adsorption phenomena are determined as responsible processes for the interaction of PAHs and soil organic matter (McCarthy & Zachara, 1989; Pignatello & Xing, 1995; Yang et al., 2001).

The phenomenon that PAHs are less extractable from soil with increasing contact time can be attributed to slow sorption processes, physical entrapment and mineralization and formation of metabolites (see Figure 2.6) (Eschenbach, 1995; Eschenbach & Oing, 2013; Mahro & Kästner, 1993). The formation of atomic bonds is a contentious issue (Marschner et al., 2005). Extractability is also influenced by the organic carbon content of the soil. It has been shown that higher total organic carbon contents (TOC) in natural soils and sterilized natural soils correspond with lower extractability of ^{14}C-pyrene (Šmídová et al., 2012). Furthermore the particle size influences sorption capacities for PAHs. Hwang et al. (2003) identified particles with diameters less than 50 µm (fine silt fraction and smaller) that contain organic material to be the predominant sorption sites for PAHs in soils. Other authors confirm the relation between PAH concentration in the soil and the silt fraction and give four explanations for this relationship (Krauss & Wilcke, 2002; Müller et al., 2000; Pernot et al., 2013; Zhang et al., 2008; Zhe et al., 2012):

- first, a high affinity of PAHs to silt sized soil organic matter (SOM)
- second, the presence of highly reactive mineral matter (clay minerals and iron oxides) within this grain size fraction
- third, the most important way for PAHs into soils is atmospheric transport, which is limited to small grain sizes
- fourth, PAHs in macro-porous fractions are better available for degradation and naphthalene is more easily volatilized

Studies on the partitioning of the low molecular weight PAHs to different particle sizes showed contrary results. While Curtosi et al. (2007) found an enrichment in low molecular weight PAHs in the silt fraction in Antarctic soils (enriched in the deeper soil), Müller et al. (2000) found them decreasing from coarse to fine fraction in tropical, urban surface soils. Müller et al. (2000) explained this observation with the degradation or volatilization of the more volatile PAHs during soil organic matter degradation and associate this finding with increasing soil organic matter alteration with decreasing particle size. Bauw et al. (1991) identified big organic molecules and sub-micron particles as the main carriers for PAHs through the soil and therefore support the hypothesis that PAHs preferably adsorb to small particle sizes.

Table 2.3 Selected properties of the 16 US-EPA PAHs (Bojes & Pope, 2007; Eschenbach, 1995; Mackay & Callcott, 1998; Peters et al., 1997) and n- Hexane and n-Decane (Wabbels & Teutsch, 2008)

Name	No. of rings	Molecular weight, g mol^{-1}	Fugacity ratio, at 25°C	log K_{OW}	Log K_{OC}	Solubility in water, mg L^{-1}
Naphthalene	2	128.17	0.283	3.37	3.37	31
Acenaphthylene	3	152.20	0.22	4.00	3.40	16.1
Acenaphthene	3	154.21	0.198	3.92	3.8	3.8
Fluorene	3	166.22	0.126	4.18	3.9	1.9
Phenanthrene	3	178.23	0.177	4.57	4.08	1.1
Anthracene	3	178.23	0.0129	4.54	4.32	0.045
Pyrene	4	202.26	0.0506	5.18	4.79	0.132
Fluoranthene	4	202.26	0.141	5.22	4.3	0.26
Benzo[a]anthracene	4	228.29	0.04	5.91	4.8	0.011
Chrysene	4	228.29	0.0097	5.91	4.9	0.0015
Benzo[*b*]fluoranthene	5	252.32	0.039	5.80	6.2	0.0015
Benzo[*k*]fluoranthene	5	252.32	0.013	6.00	5.6	0.0008
Benzo[*a*]pyrene	5	252.32	0.0328	5.91	6.65	0.0038
Dibenzo[a,h]anthracene	5	278.35	0.00403	6.75	5.97	0.0005
Benz[g,i,h]perylene	6	276.34	0.003	6.50	6.20	0.00026
Indeno[1,2,3-cd]pyrene	6	276.34	0.04	6.50	6.2	0.062
n-Hexane	-	86.2	-	4.11	-	12.7
n-Decane	-	142.3	-	-	-	0.038

Sorption of hydrophobic compounds to polar, mineral surfaces is impeded by water (Chiou, 2002), but clay minerals can be considered as good sorbents for organic compounds (Birkel, 2000). Combined effects of the organic matter and clay minerals at low soil organic carbon contents have been observed (Hwang et al., 2003). However in competition with organic matter the sorption to mineral particles has hardly any relevance (Delle Site, 2001).

Both, sorption to soil organic matter and small sized soil particles lead to PAH fixation in soils. The presence of dissolved organic matter (DOM) increases the apparent solubility of PAHs (Busche & Hirner, 1997; McCarthy & Zachara, 1989). It is not finally resolved, if this also increases PAHs mobility in soil. Kögel-Knabner and Totsche

(1998) explained PAH retention by co-sorption and cumulative sorption processes of aggregates of DOM and PAHs to the particulate matter of the soil and therefore a decreasing effect on PAHs mobility. The affinity of certain PAHs to dissolved organic matter (DOM) can vary more than one order of magnitude due to the source of DOM (Marschner, 1998; Raber et al., 1998).

In hydrocarbon contaminated soils, the oil phase is probably the principle medium for adsorption of PAHs, as the partitioning coefficients in Table 2.4 reveal. That means that also migration behavior of PAHs is controlled by the oil phase present in the contaminated soil (Walter et al., 2000; Zemanek et al., 1997). Zhe et al. (2012) observed that PAH distribution in the bottom soil layers of an alluvial sandy soil contaminated with oil in eastern China was mainly influenced by the total petroleum hydrocarbon distribution, whereas in the top soil layer the additional input of PAHs through the atmosphere determined their concentrations and distribution.

Table 2.4 Comparison of partitioning coefficients for single PAHs between water and soil organic carbon (log K_{OC}), creosote (log K_{CREOW}) and diesel oil (log K_{DW}), respectively. Data measured either at 20°C or 23°C. Adapted from Eschenbach (1995), (source of data: log K_{OC}, see Table 2.3; log K_{creow} (Lane & Loehr, 1992); log K_{dw} (Lee et al., 1992).

PAH	log K_{OC}	log K_{CREOW}	log K_{DW}
naphthalene	3.37	3.8 – 3.9	3.7
acenaphthene	3.8	-	4.53
fluorine	3.9	5.0 – 5.1	4.48
phenanthrene	4.08	-	4.69
fluoranthene	4.3	6.2	5.29
anthracene	4.32	5.7 – 6.1	5.27
pyrene	4.79	6.3	-
benzo[a]anthracene	4.8	6.21	-
chrysene	4.9	6.4	-

Microbial transformation of PAHs is a further important process that determines the fate of the contaminants in soils. Due to their aforementioned hydrophobicity and low water solubility they are potentially unavailable for bacteria, as the latter only degrade dissolved chemicals (Johnsen et al., 2005). However, biological transformation has often been described (Eschenbach, 1995; Johnsen & Karlson, 2007; Ting et al., 2011). Its rate depends on the chemical structure of the single PAH to be degraded and transformed, microbial population, pH, temperature, acclimation and accessibility of nutrients (Haritash & Kaushik, 2009). Biological degradation of PAHs is a main driver of the formation of bound, or non-extractable residues (neR) (see Figure 2.6) (Eschenbach et al., 1998). On the other hand it may lead to the formation of metabolites which have mutagenic and carcinogenic effects on organisms.

2.3.2 PETROLEUM HYDROCARBONS

Petroleum hydrocarbons are a broad family of compounds and the main constituents of crude oil. The latter itself covers a broad group of chemical mixtures. Crude oils can be classified by their density, sulfur content and geographic origin. Further properties for their description are viscosity, pour point and fraction of waxes. As mentioned in chapter 0 petroleum hydrocarbons enter the soil as light non-aqueous phase liquid (LNAPL). Hydrocarbons are distributed between the three soil phases with time. The responsible processes are sorption, volatilization, dissolution, transformation and transport (Fine et al., 1997; Zhu & Sykes, 2000). Viscosity and density of residual LNAPLs mainly change due to volatilization of light hydrocarbon fractions (< C_{11}) (Fine et al., 1997; Jarsjö et al., 1994). Therefore migration and retention processes of the petroleum product are changed with time.

The mobility of LNAPLs in soils basically depends on mineral and organic matter content, texture, moisture content and the LNAPLs properties itself (Fine et al., 1997; Yaron et al., 2012). The soil properties determine the capillary force, which in turn controls LNAPL migration. In soils with a great variance in pore size Wilson et al.(1990) showed that the LNAPL migrated through the larger pore spaces, whereas water was bypassed to the smaller pores. However Berkowitz et al.(2008) state that the downward migration of contaminants within soils is highly non-uniform and strongly influenced by preferential pathways.

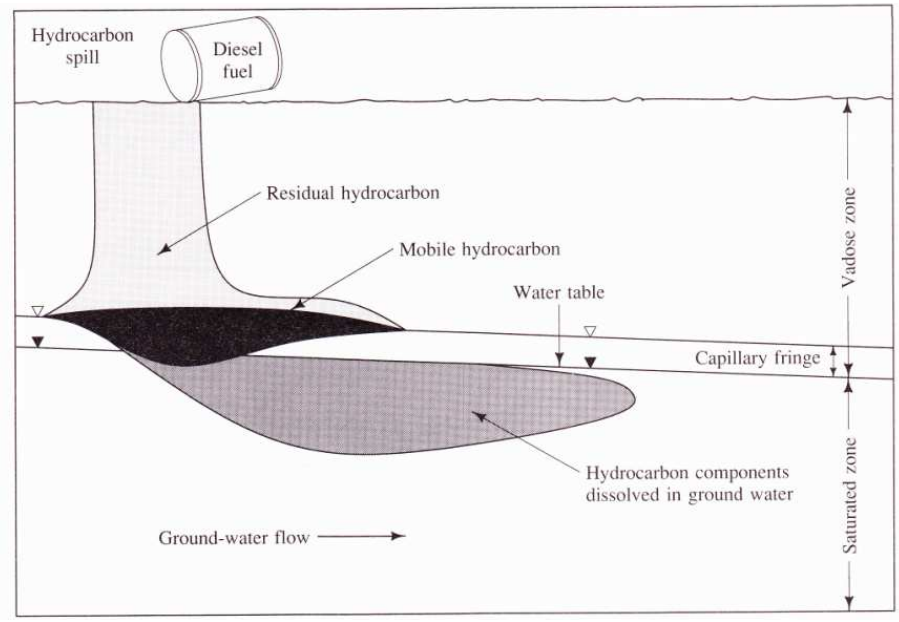

Figure 2.8 **Subsurface distribution of an LNAPL spill taken from Fetter (1999)**

After an oil spill total petroleum hydrocarbons will follow the gravitational force downwards within the soil profile (Fetter, 1999; Schwille, 1984; Walter et al., 2000). When it reaches the capillary fringe it starts to accumulate there (see Figure 2.8). Due to the additional load of LNAPL on water of the capillary fringe, the latter can be thinned or even disappear, resulting in a direct contact of flowing ground water and

LNAPL (Abdul, 1988; Schwille, 1984). Due to their low density LNAPL form an “oil table” on the groundwater, which can partially migrate with the slope of the water table (Fetter, 1999). LNAPLs and water compete for soil pore space. The relative permeability for the two depends on their saturation level in the soil. In most cases water is the wetting fluid on the soil minerals and the LNAPL is the wetting fluid on organic matter and soil gas (Barnes & Biggar, 2008; Fetter, 1999). Water can only replace LNAPLs until their residual saturation is reached and LNAPLs can only migrate at saturation levels above their residual saturation (Brost & deVaull, 2000; Schwille, 1984). The residual saturation of LNAPLs ranges from 9 – 50% of the total pore volume in soils (Schwille, 1984; Wilson et al., 1990). In the vadose zone the authors found an average residual saturation of 9.1 % ± 2.2 %, which is very low, and explained it with the differences in interfacial tension between the organic liquid and water and air, respectively. Migration also depends on viscosity and pour point, which in turn depend on temperature and are specific for each crude oil.

The main processes controlling the retention to further percolation of the LNAPLs in soil are their entrapment in soil capillaries and pores and their sorption to particle surfaces, respectively. The degree of entrapment and sorption in turn is controlled by the properties of the petroleum hydrocarbons, the properties of the soil solid phase and the moisture content. The presence of clays in coarse grained soils for example, can affect entrapment of LNAPLs. If the clays swell, they can close pore spaces, which leads to increased LNAPL by-passing (Matmon & Hayden, 2003). Fine et al.(1997) state that with the decrease of soil moisture content the transport of petroleum hydrocarbon vapor phase increases, as well as its retention by entrapment or sorption by the mineral soil. With increasing moisture content on the other hand, the retention of petroleum hydrocarbons decreases.

The considerable amounts of immobile LNAPLs, which stay in the soil as residual saturation, are a continuous source of hydrocarbon compounds, which partition to infiltrating water and gas, leaving a residual LNAPL with relatively increasing number of high molecular weight compounds (Tang et al., 2012; Wilson et al., 1990). Yaron et al. (2012) state that such fractionation leads to a changed porosity of the soil, as heavy petroleum residues form discontinuous blobs within large pores. Furthermore these heavy components are not readily degraded by organisms, therefore changes in porosity can be regarded irreversible. Due to changed porosity, water migration behavior in the soil is influenced as well.

As stated before, organic contaminant phases are subject to microbial transformation and degradation processes in soils. Most compounds of oil and oil products are biodegradable under anoxic conditions (Vogt & Richnow, 2014). If this effect is used or even enhanced by the manipulation of the environmental conditions, contaminated sites may be remediated in-situ. The procedure is called natural attenuation and enhanced natural attenuation, respectively. The susceptibility of oil compounds to microbial degradation decreases from linear alkanes to branched alkanes and small aromatics.

2.4 BEHAVIOUR AND IMPACT OF ORGANIC CONTAMINANTS IN PERMAFROST-AFFECTED SOILS

Climate is a main factor of soil formation. In high latitudes and high altitudes climate is dominated by low temperatures and soils are often underlain by permafrost (see chapter2.1). Increasing exploration activities in Arctic regions on permafrost-affected soils also cause an increase in oil spillages (Raisbeck & Mohtadi, 1974). Additionally, processing and transport of resources and an increasing number of workers living in the Arctic bring an increased environmental hazard about. However the behavior of contaminants entering permafrost-affected soils is not fully understood yet. The state of the art concerning the relationship between organic contaminants and freezing soils and their interaction will be presented in this chapter.

Impact of contaminants on permafrost affected soils and their interaction

Organic contaminants in permafrost-affected soils have an impact on active layer thickness, biological activity and chemical and physical properties of the soil. The main impact on the chemical properties of the soil is the additional carbon which is introduced with organic contaminants, especially crude oil, into the soil (Aislabie et al., 2004). This leads to higher total organic carbon content. How DOC levels are influenced is not clear yet. Aislabie et al. (2004) observed a lowered pH at contaminated sites in comparison to pristine sites. They attributed this phenomenon on the microbial interaction with the present oil phase. Another main impact was observed in conjunction with the liquid water content in the frozen soil. In a laboratory test the liquid water content in a sandy loam quadrupled between -2°C and -10°C compared to an uncontaminated control (Siciliano et al., 2008). Investigated in-situ contaminations of a clay loam still showed an increase in liquid water content of 50 % compared to the uncontaminated control. Liquid water content in frozen soils in conjunction with cryosuction processes induces frost heave processes. However, it is not clear yet, how the increase in liquid water content due to oil contamination affects frost heave processes. In laboratory experiments Grechishchev et al. (2001) observed a reduction of ice segregation and frost heave in oil contaminated silt. The freezing point of the contaminated soil was only marginally influenced. For silt and the water miscible organic contaminant 1-propanol, which can be used as a freezing point depressant similar observations were made (Konrad & Seto, 1991). Laboratory tests showed that already 1 g L^{-1} 1-propanol reduces the segregation potential about two thirds compared to the uncontaminated control. For higher contaminant concentrations the segregation potential was even lower. The authors also observed less frost heave as consequence of the low segregation potentials. The freezing point was lowered by 1-propanol about 0.03°C (Konrad & Seto, 1991).

Permafrost-affected soils develop particular soil structures (see chapter 2.1). The entry of organic contaminants into these soils may lead to considerable structural changes of the soil on all scales. At low contents of organic contaminants in soils (0.05 – 0.2 % per weight unit) contaminant molecules are able to replace water molecules in the structure of clay minerals, if the soil is subject of freeze-thaw cycles (White & Coutard, 1999). This process leads to aggregate and inter-aggregate pore formation, which in turn causes a higher water conductivity (White & Williams, 1999). Available pore spaces are also an important factor for biodegradation. Chang et al. (2013) found that biodegradation performance in a clayey soil was much more effective, if an extensive pore network, provided by macro aggregates, was available for degrading bacteria. They investigated total petroleum hydrocarbon contents slightly above 1000 mg kg^{-1} dw. White and Williams (1999) observed on the other hand that for such high total petroleum hydrocarbon contamination levels the soil consolidates in its entirety with a considerable reduction of permeability.

When contaminants, such as crude oil, get in contact with the soil surface they change the color of the soil to darker colors and black. That decreases the albedo of the soil surface, which leads to increased surface soil temperatures (Balks et al., 2002). Higher soil temperatures in turn may induce deeper thaw and therefore increase active layer depth. Disturbed or destroyed vegetation cover may also lead to increased thaw penetration into the soil (Shur et al., 2005). Deeper thawing of the ground triggers differential thaw settlement at the surface and influences all processes taking place in the active and transient layers. Oil contaminated soils subjected to freeze-thaw cycles may develop an alternate formation of ice and LNAPL layers in the soil, which decreases the strength of the soil and my lead to slope instability (Grechishchev et al., 2001).

The question, if permafrost acts as a barrier for contaminants and other substances has been discussed often. For petroleum hydrocarbons it is not a reliable boundary (Fourie & Shur, 2008), as LNAPLs have been found in perennial frozen ground (McCarthy et al., 2004). Other investigation came to the conclusion that petroleum hydrocarbon migration into permafrost-affected soils is site specific, as it was observed in perennial frozen ground only at some sites (Biggar et al., 1998). In general Rike et al. (2003) postulated that permafrost constricts the downward migration of organic contaminants. Gennadiev and Pikovskii (2007) described permafrost as a barrier that restricts vertical migration of organic pollutants. They furthermore classify the soils of the West Siberian lowland and the Lena river delta as “soils with minimum potential tolerance towards pollution with hydrocarbons”, because microbial activity is very low and dispersion of the contaminants is impeded by permafrost.

Microbial degradation of organic contaminants in permafrost-affected soils has been proved to take place (Braddock et al., 1997; Margesin et al., 2003; Rike et al., 2003), even though low temperatures, low moisture contents and freeze-thaw cycles provide a challenging environment for microorganisms (Aislabie et al., 2004; Rike et al., 2008). In conjunction with total petroleum hydrocarbons petroleum-degrading microorganisms seem to be always present in freezing soils (Braddock et al., 1997; Filler et al., 2009; Margesin et al., 2003), but it is not known how much time is required for them to establish (Balks et al., 2002). The persistence of petroleum hydrocarbons in permafrost affected soils over decades, implies that biodegradation rates must be very slow (Aislabie et al., 2004). That hypothesis is supported by the investigation of chromatograms by Prus et al. (2015) who hardly found any changes in the structure of n-alkanes, steranes and alkyl PAHs, even though the chemicals rested for considerable times at Antarctic environments. On the other hand Whelan et al. (2015) observed losses up to of 25 % of initial TPH concentration in biopiles (enhanced natural attenuation technique) in Antarctica.

Distribution of organic contaminants in freezing soils

Additionally to the main factors and processes influencing the behavior and distribution of organic contaminants in soils (see chapter 2.3) aggregate state of the soil solution and freezing speed are of great importance in freezing soils (Barnes & Filler, 2003; Chuvilin, 1999; Curtosi et al., 2007; Grechishchev et al., 2001). When the soil solution freezes the remaining liquid water content is a main driver for all sorts of distribution and interaction processes in the soil (see chapter 2.2.1). It is influenced by the grain size distribution and the connected capillarity of the soil material.

As explained in chapter 2.3.2 water and contaminant phase compete for the pore space, therefore their contents control their relative permeability. However, the relationship between organic contaminant phase and water is more complex in permafrost affected soils. The unfrozen water in a frozen soil can act as a conduit for the diffusion of contaminant into the soil (Biggar et al., 1998). For organic contaminants with low water solubility this may only be a marginally effect. But laboratory tests with loamy sand with different organic carbon contents revealed that fuel penetration rates into the soil decreased with increasing ice content, whereas the fuel penetration rate was not influenced by the moisture content in unfrozen soils (McCauley et al., 2002). This process can be explained by the ice closing the migration routes for the petroleum hydrocarbons. But lateral movement is enhanced, especially on coarse grained soils. In turn LNAPLs may control the infiltration of melt water into the soil. In coarse grained soils, contaminated with LNAPLs the capillary retention is increased so that more water stays in the soil pores. This effect in conjunction with freezing may either reduce LNAPL migration, because pore spaces are closed, or enhance it, due to the creation of preferential pathways (Barnes & Wolfe, 2008).

The freezing speed is of great importance concerning water distribution and ice forming processes in freezing soils (see chapter2.2.1). Konrad and McCammon (1990) suggested that a rejection of solute takes place during ice formation for cooling rates smaller than 2.95 ± 0.25°C day^{-1}. They identify this cooling rate as the threshold rate of cooling, which still would permit significant solute rejection. The authors showed that more than 90% of the solutes were excluded from the forming ice, when cooling rates were less than 0.1°C day^{-1}. Thus a nearly contaminant free ice lens may grow at a quasi-stationary frost front. For the miscible organic contaminant 1-propanol the solute exclusion form the forming ice was observed until a cooling rate of 4 ± 1°C (Konrad & Seto, 1991) (see Figure 2.9). The authors quantified the 1-propanol concentration ahead a freezing front, penetrating 20 mm day^{-1}, to be 130 times higher than the initial contaminant concentration in silty soils and 34 times higher than the initial 1-Propanol concentration in sandy soils.Konrad and Seto (1991) and Tumeo and Davidson (1993) could also show that 1-propanol and phenol, respectively, migrated with the water towards the freezing front.

For soluble inorganic contaminants Ostroumov et al. (2001) also found that redistribution of solved elements takes place during ice segregation. They specified the accumulation zone to be at the interface between the growing ice lens and the mineral soil layer.

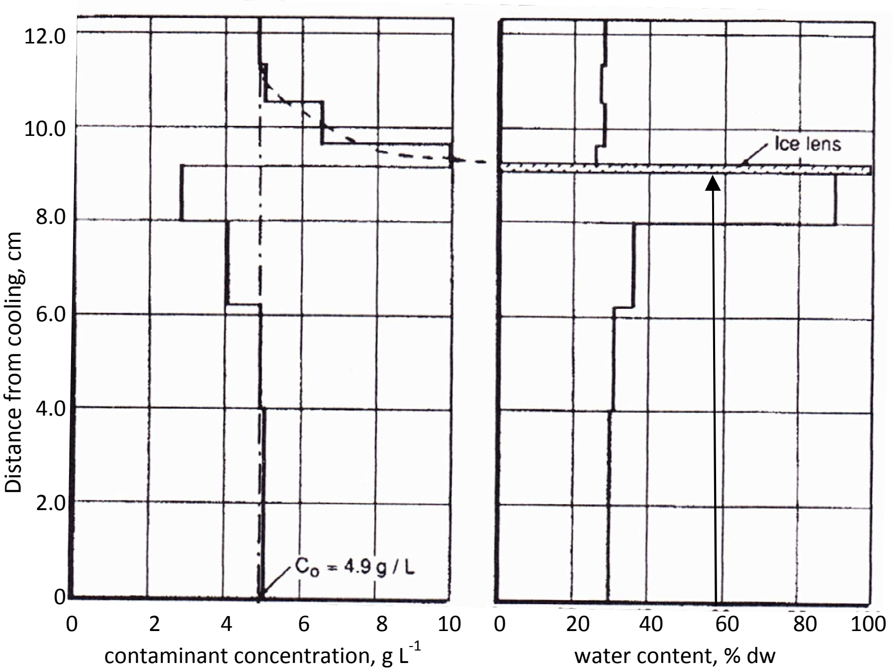

Figure 2.9 Development of a zone with increased contaminant content and a contaminant free ice-lens due to solute migration and rejection processes, which are based on very low freezing rates, taken from Konrad and Seto (1991)

In freezing soils the process of volatilization is most important for low molecular weight compounds with high fugacity ratios (Whelan et al., 2015). For the light fuel Kerosene volatilization in freezing affected soils was greatest in sand and lowest in peat (Jarsjö et al., 1994). Even though the temperature had an effect on Kerosene retention capacity of the soil, the impact of organic carbon content was most important.

PAHs

The behavior and distribution of PAHs in permafrost-affected soils has been subject to only a few studies, but is an upcoming topic of interest, especially in the vast areas of Siberia with still unexplored resources.

The influence of and freeze-thaw cycles on high PAH contents (100 µg g^{-1}) in soils has been studied in laboratory batch tests (Zhao et al., 2009; Zhao et al., 2013). The overall impact of freeze-thaw cycles is diverse, as extraction efficiency of PAHs can increase due to the lowered diffusion rates at low temperatures or decrease as glassy adsorption domains swell and get more accessible. The authors stated that phenanthrene and pyrene extraction efficiency from soils generally increased after experiencing freeze-thaw cycles. However, the extractability of the investigated PAHs was greatly dependent on physical and chemical properties of the investigated soil (Zhao et al., 2009).

Near Jubany station at Potter peninsula (Antarctica) Curtosi et al. (2007) investigated PAH content profiles at different sites. Even though soils are not significantly contaminated the authors observed some interesting PAH distribution phenomena in the Antarctic soils (see Figure 2.10). The most striking observation is that PAH contents increase with soil depth. Aislabie et al. (1999) reported increasing PAH contents with depth within the first 30 cm of different Antarctic soils, too. Soil texture data from Potter Peninsula show increased clay and silt contents from 20 to 100 cm soil depth compared to the upper 20 cm of the soil (Godagnone, 1997). This distribution may be due to selective downward transport of fine particles due to freeze-thaw cycles. In conjunction with these data it is hypothesized that PAHs are associated to the fine particle fraction of the soil, and therefore also transported to greater soil depth (Curtosi et al., 2007).

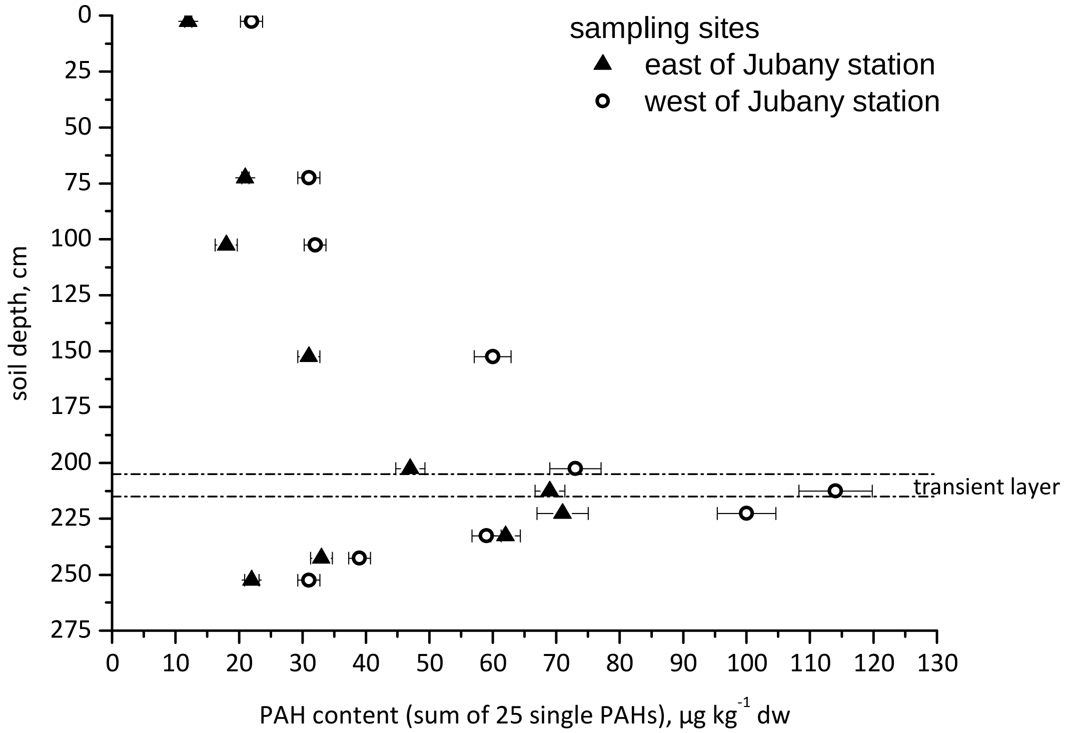

Figure 2.10 Distribution of PAHs (Sum parameter of 25 PAHs) in the active layer and upper permafrostfrom two sampling sites near Jubany station, Antarctica. Adapted from Curtosi et al. (2007).

Furthermore the dominance of 2- and 3-ring PAHs in subsurface soils is reported, compared to surface soil layers, where a range of PAHs, including high molecular weight PAHs, has been found (Curtosi et al., 2007). This selective transport of low molecular weight PAHs is explained by higher water solubility and lower log K_{OW}

values. High molecular weight PAHs are mainly associated to soot and black carbon (see Figure 2.6), which have low density and very low water solubility and therefore are rather washed out by surface run off than by downward migration of water (Cornelissen et al., 2005).

Additionally, Curtosi et al. (2007) determined the maximum PAH content of two profiles east and west of Jubany station beneath the permafrost table in the perennial frozen ground (see Figure 2.10). PAH content decreases steeply within the frozen soil. From the PAHs distribution Curtosi et al. (2007) derived the statement that permafrost at Potter Cove acts as a semi-permeable barrier for PAHs originating from low-temperature combustion. With respect to climate warming and predicted increase of precipitation and permafrost thaw the authors predict gradually mobilization of PAHs.

TPHs

Total petroleum hydrocarbons in permafrost-affected soils are more intensively investigated than PAHs, but the overall impact of freezing and thawing processes in permafrost-affected soils on the distribution and fate of TPHs is not fully understood yet. TPHs enter the soil commonly as an accidental spill at a defined site. In permafrost affected regions the time of spill and the accompanying soil conditions matter, when oil distribution in and on soil is considered. Johnson et al. (1980) observed in an in-situ experiment in Alaska that crude oil spilled on a frozen, snow covered soil in winter affected a larger surface area of the soil (75,2 m^2) than a spill that occurred during summer (30 m^2) (see Figure 2.11). The oil flowed on the frozen ground and during spring thaw on the saturated soil. However, the total area affected by the summer spill was with 303 m^2 about twice as large as the total area affected by the winter spill (188 m^2). The subsurface movement of the oil in both spills mainly happened in the organic layers of the soil O_2 and A_1 soil horizons (see Figure 2.12). Collins et al. (1993) explain this migration behavior of the oil with supra-permafrost water, which saturates the mineral soil horizons below the organic soil layers throughout the summer thaw season. They found TPHs at the same depth in the organic soil layers 15 years after the experimental spill occurred. Exceptions were sampling sites, where the mineral layer started at 20 cm soil depth. The total affected areas were only slightly increased in these 15 years, by 1.6 % at the winter spill site and by 0.7 % at the summer spill site (see Figure 2.11). This movement could be the result of single extreme events, like rainstorms or snowmelts (Collins et al., 1993; Hutchinson & Freedman, 1978). The thaw depth of the active layer was significantly increased and the original ground surface subsided in the surface oil blackened areas, that means mainly on the winter spill site (Collins et al., 1993). The authors describe these effects with the changed heat flux of the ground. As influencing factors of the heat flux they determine decreased albedo of surface blackened areas, increased solar radiation income due to death of tree canopy, alteration of thermal diffusivity of the oil contaminated soil compared to the natural soil and the compaction of the dead insulating moss layer.

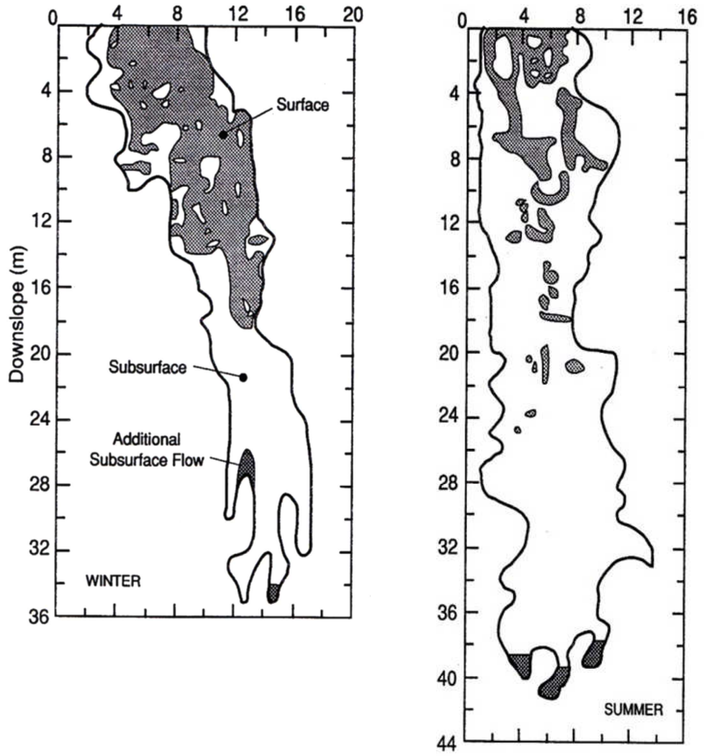

Figure 2.11 Affected area of 7560 l oil with a temperature of 57°C spilled during a single event in a) summer and b) winter in 1976 (mapped 1978). Grey areas display surface soil areas and line delimits subsurface soil area, where petroleum hydrocarbons were encountered in 1978. Black marks additional subsurface areas, where petroleum hydrocarbons were encountered in 1991. Figure taken from Collins et al. (1993).

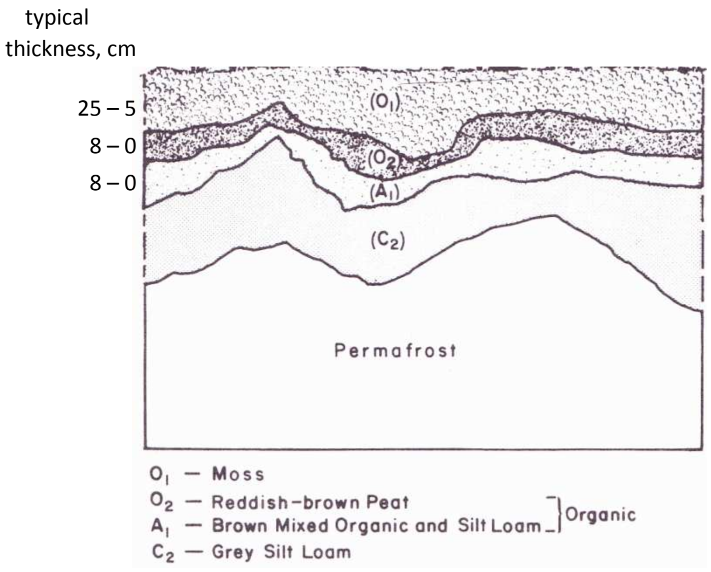

Figure 2.12 Scheme of the soil profile at the experimental sites in the Caribou-Poker Creek watershed with typical thickness of the soil layers found in the lower slopes of the watershed, soil was classified as histic, pergelic Cryaquept. Figure taken from Johnson et al. (1980).

Laboratory studies verified the observation of the enhanced lateral movement and restricted infiltration into the ground of petroleum hydrocarbons on soils with high ice saturations (75 – 100 %) (Barnes & Wolfe, 2008; Chuvilin et al., 2001; Wiggert et al., 1997). Together with the formation of ice clusters (relatively ice rich areas, next to areas with ice depletion) and micro fissures vertical movement of LNAPLs may be enhanced as well (Barnes & Wolfe, 2008). It was also found that the lateral movement of the oil increased with the start of thaw, due to decreased viscosity of the LNAPL and the infiltrating melt water, which saturated the pores upon the still frozen ground, thus preventing the LNAPLs infiltration (Johnson et al., 1980). McCarthy et al. (2004) determined free-phase hydrocarbons within the perennial frozen ground near Barrow (Alaska), which provided evidence that permafrost is not an impermeable barrier for organic contaminants, such as oil and its compounds.

Several authors observed the formation of micro fissures in the forming ice and the freezing media, which increased with decreasing temperature and may act as preferential path ways for LNAPLs (Biggar et al., 1998; Chuvilin & Miklyaeva, 2003; Iwakun et al., 2010).

The behavior of TPHs in permafrost-affected soils is mainly determined by water and ice contents. High ice contents in surface soils may increase LNAPL penetration into the ground due to formation of preferential flow path ways, or restrict it, due to formation of dead end pores (Barnes & Wolfe, 2008; Biggar & Neufeld, 1996; Iwakun et al., 2010). The impact of grain size distribution is very important upon this issue. However, even pure ice without fissures has been shown to be permeable for fuel (Jepsen et al., 2006). The presence of supra-permafrost water restricts vertical migration of LNAPLs in permafrost-affected soils.

Laboratory experiments to investigate the behavior of petroleum hydrocarbons in conjunction with the freezing process

For LNAPLs, with the analysis of total petroleum hydrocarbons, several authors conducted laboratory test, to examine the influence of the freezing process on their distribution in soil (Barnes et al., 2004; Biggar & Neufeld, 1996; Chuvilin et al., 2001; Iwakun et al., 2010). All studies were conducted at or near water saturation level.

To investigate the influence of the freezing process on LNAPL distribution in different soil types, Chuvilin et al. (2001) carried out laboratory experiments with oil contaminated soil materials and unidirectional freezing process. The oil used for contamination is described as a “paraffin and naphthene-paraffin” mixture with a hardening temperature (pour point) at +2°C and a density of 0.8692 g cm^{-3} at 20°C. The columns were frozen from the top and freezing lasted 24 hours at a fixed input cooling temperature. In silt loam with low and high clay content water migration towards the freezing front could be observed (see Figure 2.13 b and c). In the sandy soil material only an unspecific increase of water content accounting for 1 % dw just beneath the freezing front was observed (see Figure 2.13 a). However, in the sandy soil material the oil content displayed a clear decrease in the frozen part and an increase in the unfrozen part of the column from initially 6.2 % to 7.2 % after the experiment.

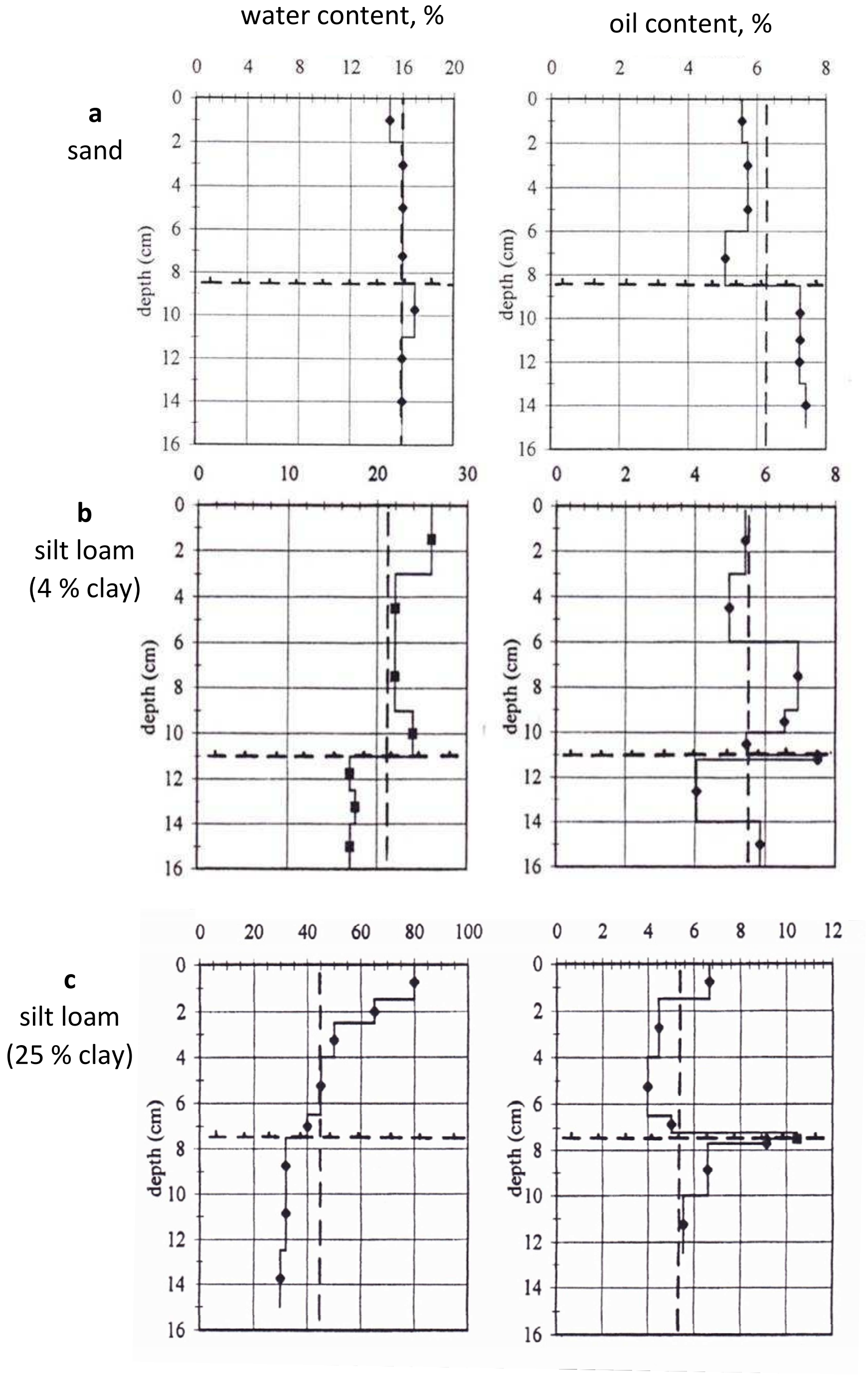

Figure 2.13 Results for water distribution and petroleum hydrocarbon distribution after 24 hours freezing from the top with a constant temperature in three different materials, a = sand, b = silt loam (4 % clay), c = silt loam (25 % clay), taken from Chuvilin et al. (2001).

For clay rich silt loam there was also a decrease in oil content in the frozen part of the column, except the uppermost soil layer and a steep increase in a restricted area at the freezing front. Further downwards, in the unfrozen part of the column the oil contents decreased and reached the level of the starting conditions 1.3 cm beneath the freezing front (see Figure 2.13 c). The oil distribution in silt loam with low clay content showed a steep increase just beneath the freezing front, but overall distribution does not show a distinct pattern (see Figure 2.13b). The increase of the oil content in the sandy soil material was explained with an expulsion of the LNAPL ahead the freezing front. This process takes place, because the oil is the non-wetting fluid in the system and occupies the large pore spaces, rather than the small ones. Due to stronger matrix potential the equilibrium freezing point of water in smaller pores is lower than in larger pores, therefore the phase transition from water to ice starts in the larger pore spaces. The oil is expulsed from the soil pores due to the volume increase during pore ice formation and expanding ice nuclei during segregation ice formation, respectively (Barnes et al., 2004). Furthermore Chuvilin et al. (2001) state that with decreasing temperature gradient (and therefore decreasing freezing rate) the expulsion efficiency for the oil increased.

Biggar and Neufeld (1996) wanted to prove the hypothesis of TPH exclusion ahead a freezing front in conjunction with the simulation of an active layer above a perennial frozen part of the soil. They hypothesized that due to the influence of freezing and freeze-thaw cycles the contaminants would concentrate in a zone distinctly above the permanently frozen soil material, because freezing in the active layer occurs from the soil surface and from the permafrost table upwards (see chapter 2.1). In their laboratory setup to prove their hypotheses they kept 20 cm of the 30 cm high, cylindrical soil columns permanently frozen throughout the experiment. The upper part of the soil column was contaminated with 8 % diesel fuel and after the first freeze-thaw cycle additionally 116 ml of diesel fuel were put on top of the soil.

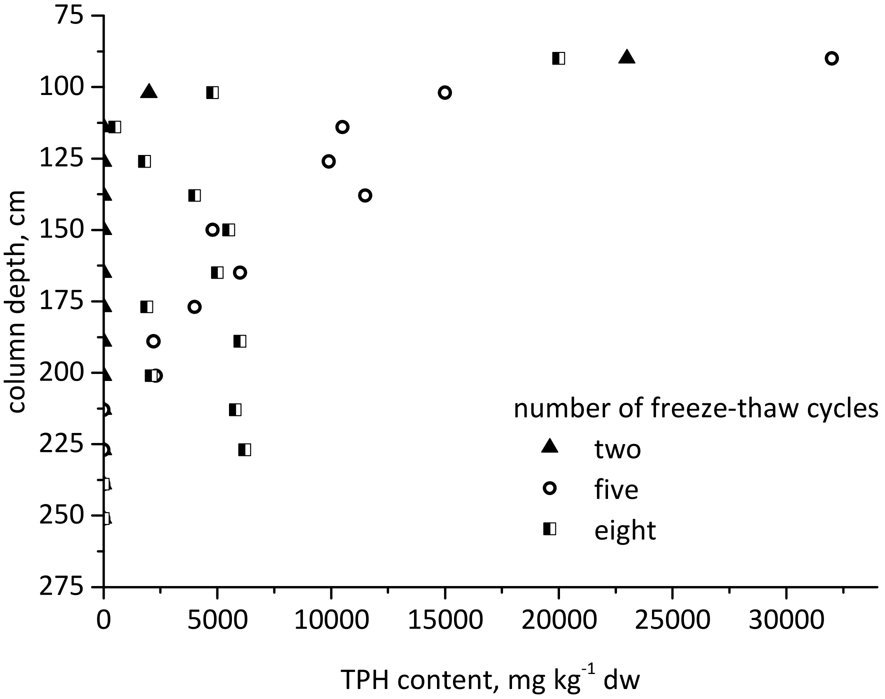

Figure 2.14 Petroleum hydrocarbon content in mg kg^{-1} dw in the center of experimental columns after two, five and eight freeze-thaw cycles, adapted from Biggar and Neufeld (1996)

In Figure 2.14 the total petroleum hydrocarbon content in µ g^{-1} in the center of the experimental columns after two, five and eight freeze-thaw cycles, respectively, can be seen. The results reveal the petroleum hydrocarbon progression into the soil with increasing number of freeze-thaw cycles. The intermittent peaks and valleys in the profiles for five and eight cycles are explained by the authors with variability in the soil matrix and contaminant exclusion processes forward the up and downward proceeding freezing front. The improvements the authors suggested for the experimental setup, which would allow a better interpretation of the results are given in chapter 2.2.2.

Later studies by Iwakun et al. (2010) with glass beads could reinforce the observations of the development of micro-fissures and their function as pathway for petroleum hydrocarbons. Additionally the authors observed an upward mobilization of LNAPLs at the commencement of freezing and during thawing. They attributed the process to cryosuction towards the freezing front and pressure relief during ice thaw, respectively. The buoyant nature of LNAPLs (density < 1 g cm^{-3}) supports the upward mobilization processes. The influence of the cryosuction points the importance of thermal and hydraulic gradients out once more (Flerchinger et al., 2005), that means in turn experimental setup and procedure are of great importance, if processes should simulate naturally occurring processes.

In non-frozen soils LNAPLs are not mobile if the residual content is not exceeded (see chapter 2.3.2). In a two dimensional experiment with glass beads, water and dodecane (alkane with 12 C-atoms) it has been shown that the LNAPLs moved ahead the freezing front and ganglia were fragmented (Niven & Singh, 2008). The authors explained these processes with the pressure evolving from volumetric expansion during ice formation. The freezing induced pressure in this situation is higher than the pressure, which holds ganglia in position (Singh & Niven, 2013). Several freeze-thaw cycles resulted in a substantial remobilization of LNAPL and the formation of numerous small sized ganglia. However it is questionable if LNAPLs in three dimensional porous media exhibit similar changes due to freeze-thaw cycles and the pressures created by pore ice and growing ice lenses exaggerate adsorption and capillary forces. These uncertainties emphasize on the importance of soil properties, which determine the mentioned retention forces. Singh and Niven (2013) pointed out that also parameters like the fluids viscosity and density, the presence of a gaseous phase and freezing front propagation are worth further investigations. The freezing process can also lead to a weathering process of the oil, which goes along with increased density and viscosity of the LNAPL (see chapter 2.3.2). This in turn enhances its downward pull potential, but also decreases its mobility (Luthy et al., 1997; Wilson et al., 1990). As the viscosity of petroleum products is generally high at low temperatures and the pour point (see Table 3.1) can be reached, the mobility of the contaminant phase is limited. That means LNAPL mobility in soil increases with decreasing pour point which leads to higher LNAPL contents in deeper part of the soil (Chuvilin et al., 2001).

3. MATERIALS AND METHODS

In order to achieve the objectives set in chapter 1.2 it was important to choose the boundary conditions of the experiments close to natural occurring conditions. That required the careful selection and adjustment of soil materials and properties, experimental equipment and methods. As the invention of the experimental setup and procedure to simulate a natural occurring freezing process was part of the objectives detailed descriptions of soil materials and methods are given in chapters 4 and 5.

3.1 MATERIALS

3.1.1 SOIL AND SOIL MATERIALS

Two representative soils of the most abundant soil types in western Siberia were described and classified (see chapter 4.1 and Table A.4). On that basis the soil materials to conduct the laboratory experiments were chosen. They originate from different stages of the saalian glacial period (Ehlers, 1987). Soil material was air dried and sieved < 2 mm before used in experiments.

The assessment of an in-situ oil spill in Northern Siberia based on disturbed and undisturbed samples taken in the years 2009 and 2011. Further description of the site is given in chapter 4.3. Main soil properties are given in Table A.5. Samples were transported and stored before analysis at -18°C.

3.1.2 CHEMICALS

Two main groups of chemicals used to conduct the present studies may be distinguished. The first group of chemicals was needed to conduct the laboratory experiments. In the experimental procedures crude oil and different single PAHs were applied with varying contents (see Table 3.5). Due to its sensitivity with low standard error of the analysis radioactive labeled PAHs were used to investigate the influence of freezing on the distribution of PAHs. They are specified in Table 3.3.

Crude oil is always a complex mixture of compounds and may be distinguished by its composition. The oils used for this investigations are from North Sea oil fields and were obtained from Royal Dutch Shell plc, named Ekofisk and Gryphon. Their main properties are given in Table 3.1 in comparison to diesel and n-Hexan. Ekofisk is a paraffin-based oil, whereas Gryphon is a naphthene-based oil (see Figure A.4 and A.5). To adjust the water content in the experiments water with pH 7.3 and an ionic strength of 0.009 S · m^{-1} was used. To adjust the water content in the experiments water with pH 7.3 and an ionic strength of 0.009 S · m^{-1} was used.

Table 3.1 Physical and chemical properties of diesel, Ekofisk (paraffin-based crude oil, Royal Dutch Shell plc), Gryphon (naphthene-based crude oil, Royal Dutch Shell plc) and n-Hexane. n.d. = not determined
the pour point for diesel varies upon composition and n-Hexan is liquid until its melting point at -95°C

Name	Density g cm^{-3}	Viscosity m^2 s^{-1}	Pour point °C
Diesel (C_{10} – C_{22})	0.820….0.845 (15 °C)	1.640….3.803 (40°C)	-
Ekofisk	0.830 (20°C)	n.d.	-27
Gryphon	0.932 (20°C)	n.d.	-3
n-Hexane (C_6)	0.66	0.485 (20°C)	-

The chemicals needed to conduct extraction and analysis procedures are given in Table 3.2.

Table 3.2 Chemicals used for extraction and analysis

Chemical	CAS number	Supplier	Specification, Grade
Acetone, ACS	67-64-1	Merck KGaA, Darmstadt, Germany	
Kalibrierstandards BAM K008 BAM K009	 - -	Bundesanstalt für Materialforschung und –prüfung, Berlin, Germany	mass fraction C_{10} – C_{40}, g g^{-1} 0.936 0.995
CarboSorb		Perkin Elmer corp., Waltham, USA	
Dichloromethane, puriss.	75-09-2	Fluka, Sigma Aldrich C. LLC, St.Louis, USA	
Ethyl acetate	141-78-6	J.T.Baker, Avantor performance materials, Deventer, Netherlands	≥ 99.6 %
Florisil	1343-88-0	J.T.Baker, Avantor performance materials, Deventer, Netherlands	60 – 100 mesh

Chemical	CAS number	Supplier	Specification, Grade
Hexane, picograde	110-54-3	Promochem LGC Standards GmbH, Wesel, Germany	
Hydrochloric acid	7647-01-0	Chemsolute, Th.Geyer GmbH & Co. KG, Hamburg, Germany	35% - 38% p.a.
Methanol, p.a.	67-56-1	Merck KGaA, Darmstadt, Germany	
Pico Fluor		Perkin Elmer corp., Waltham, USA	
Quartz wadding	65997-17-3	Merck KGaA, Darmstadt, Germany	20 - 160 kg m^{-3}
Quartz sand	60676-86-0	Supelco, Sigma Aldrich C. LLC, St.Louis, USA	
Sodium sulfate	7757-82-6	Merck KGaA, Darmstadt, Germany	≥ 99 %
Sulfuric acid	7664-93-9	Merck KGaA, Darmstadt, Germany	0.5 mol L^{-1}

Table 3.3 Characteristics of radio chemicals

name	specific activity, mCi $mmol^{-1}$	Radio chemical purity %	Supplier	Stock solution with ethyl acetate ml	Manu facturing date
[1,2,3,4,4A,9A-^{14}C]-anthracene	53.4	98.6	Campro Scientific, Veenendaal, Netherlands	10	18.08.2011
[4,5,9,10-^{14}C]-pyrene	58.8	99.4		10	31.03.2011
[4,5,9,10-^{14}C]-pyrene	58.8	99.6		10	07.09.2011

3.2 METHODS

3.2.1 STANDARD SOIL ANALYSIS

To characterize the soil materials and the natural Siberian soils basic soil analysis were conducted. They are summarized in Table 3.4. The methods were used according to the references.

Table 3.4 Methods used to characterize the basic soil properties

Parameter	Description	References
gravimetric water content	weighing and drying of 10 – 20 g of field moist soil at 105°C until constant weight (approx. 24 h); approx. 2 g in conjunction with ^{14}C-labeled experimental material; Water content is given in % dry weight (dw)	(DIN11465, 1996; Horn et al., 2014)
maximum water holding capacity	a filter hopper is filled with 30 g of air dried soil and saturated with water; after 1 h collected water is applied again to the soil; afterwards soil is left to stand for 24 h protected from evaporation, before water content is analyzed gravimetrically	(Eschenbach et al., 1995)
pH	preparation of two soil suspensions by addition of aqua dist. and 0.01 $CaCl_2$, respectively, with a ratio of 1:2.5 (soil:water); measurement with pH-electrode (WTW Sentix®, Weilheim, Germany) after 1 hour with repeated stirring of the suspension	(Blume et al., 2010; DIN10390, 2005)
C/N ratio	0.7 g of fine ground, dried sample is combusted at 900°C with oxygen; release gases are separated and dried; CO is oxidized to CO_2 and NO_x is reduced to N_2. measurement by thermal conductivity with vario MAX, Elementar Analysensysteme GmbH, Hanau, Germany	(DIN10694, 1995; DIN13878, 1998)
particle size distribution	combined sieving and pipette procedure, using a Sedimat (UGT, Müncheberg, Germany)	(DIN11277, 1998)
exchangeable cations and cation exchange capacity (CEC)	exchangeable cations are removed with a surplus of ammonium (5g of air dried soil, five extractions with 25 ml 1 M NH_4Cl each) and are quantified by atomic absorption spectroscopy (AAS)	(DIN11260, 2011)
pore space	undisturbed soil samples are put into a low pressure apparatus at different pressures, after each step the samples are weighted	(DIN11274, 1998)
density	calculation from weight data of defined volume	
Atterberg limits	determination of the Atterberg limits (consistency limits) of a soil with a Casagrande cup	(Spagnoli, 2012)

3.2.2 ARTIFICIAL CONTAMINATION

The basic requirement for experiments with artificially contaminated soils and soil materials is the homogeneity of the produced mixture. For all experiments moisture content and contaminant level were adjusted using a stainless steel agitating machine (KM 020 Titanium Major, Kenwood Limited, U.K.) according to Eschenbach (1995). Firstly, the water content was adjusted to 60 % of the water holding capacity (WHC) of the material. According to (Ross, 1989) water contents of less than 50 % WHC have a negative influence on the microbial activity in the soil. Higher water contents have no significant impact on microbiology (Inubushi et al., 1991). Furthermore water contents in permafrost affected soils are considered to be high during the summer (thaw) season. The wetted soil material was homogenized.

For a homogeneous application the PAHs were mixed with solvents (for particular concentrations see Table 3.5). For the experiments with ^{14}C-labeled substances 100 ml ethyl acetate were used to solve the labeled and unlabeled PAHs. If crude oil had to be applied, too, the PAH solution was mixed with the oil before application to the soil. For experiments with non-labeled contaminants ethyl acetate and dichloromethane were used to solve the PAHs to be applied and crude oil was added separately. The application of the contaminant solutions to the moist soil material was conducted with a 5 ml Hamilton syringe for material amounts up to 1.7 kg and with a titration burette for bigger amounts. Meanwhile the moist soil material was stirred by the agitating machine (see Figure 3.1).

Figure 3.1 Application of contaminants to the moist soil material using an agitating machine and a 5 ml Hamilton syringe to apply the contaminant solution

These techniques allowed for dripping rates between 1 - 2 ml per minute and 3 – 5 ml per minute, respectively. After adding all of the contaminant solution the jar and syringe were flushed with ethyl acetate and the soil mixture was stirred for another hour to let the solvent evaporate, support homogeneous distribution of the contaminants and to allow sorption of the contaminants to particles and dissolved materials (Eschenbach, 1995). For some experiments the contaminated soil material was left for incubation for 14 days with stirring in between (see Table 3.5). Due to evaporation it was necessary to add certain amounts of water just before filling the experimental columns, to reach the target water content.

Homogeneity was tested with the analysis of six to eight parallel soil samples while packing the columns with the material. The coefficient of variation for labeled experiments ranged from 1.20 to 4.35. For materials with incubation before experiment variation coefficients increased during the incubation time from 4.35 to 4.75 for anthracene and from 12.78 to 20.45 for benzo[a]pyrene. Coefficients of variation for the PAHs in peat were considerably higher, but had decreased after incubation. For anthracene the variation coefficient decreased from 55.88 to 33.53 and for benzo[a]pyrene it decreased from 60.16 to 57.90. These data already show the interaction of soil and contaminant properties and reveal the advantage of using ^{14}C-labeled chemicals compared to non-labeled chemicals

3.2.3 EXPERIMENTAL SETUP AND PROCEDURE

To verify the hypotheses that the freezing process with its accompanying phenomena influences the behavior of different PAHs in soils experiments with ^{14}C-labeled PAHs were conducted. The use of radio-labeled chemicals has several advantages compared to the use of non-labeled chemicals, such as higher sensitivity, lower coefficients of variation and less time consuming extraction procedure and analysis. To keep down amounts of isotopes needed, but still meet all other requirements the choice fell for columns with a volume of 390 cm^3 (see Figure 3.2). Hereinafter this setup is referred to as **setup 1**. A second setup, referred to as **setup 2** with columns with a volume of 2775 cm^3 and a height of 40 cm was invented for experiments with non-labeled PAHs (see Figure 3.3). These dimensions were chosen to resemble the thickness of an active layer and use the advantageous diameter to length ratio of 1:4 (Bergström, 2000).

Experimental setup

The experiments with **setup 1** consisted of three parallel run columns (A – C) and a reference column, which rested at 4°C for the duration of the experiment and was not subjected to freezing. All columns remained closed for the duration of the particular experiment. The experimental columns were insulated with 20 mm Styrodur® (BASF, Ludwigshafen, Germany), an extruded polystyrol (XPS) usually used for the insulation of houses with a thermal conductivity of 0.033 W (m · K)$^{-1}$ at 0°C. Outside another 35 mm thick insulating layer of the more flexible insulation material Armaflex® (Armacell, Capellen, Grand-Duchy of Luxembourg), a synthetic rubber based foam with a thermal conductivity of 0.038 W (m · K)$^{-1}$ at 0°C was mounted. Armaflex® is often used in conjunction with cooling devices and is also available in the form of tubes with different diameters.

During the experiments temperature und volumetric water content in the experimental columns were measured. Except for experiment *Ufba* (see Table 3.5) temperature measurement was conducted with resistance thermometers, type Pt-100 with 2-wire connection, 6 mm diameter and 50 mm length (TC-Mess- und Regeltechnik GmbH, Mönchengladbach, Germany). At 3 cm column depth the temperature probes only extended 1 cm into the soil column (Figure 3.2). The other part of each probe ran through the column material (PVDF) and the insulation layers of Styrdodur® and Armaflex®. For experiment *Ufba* temperature was measured with platinum resistance thermometers, type PT 100 with 4-wire connection and 5 mm diameter (Driesen+Kern GmbH, Bad Brahmstedt, Germany). Probes at 3 cm column depth were 20 mm long and the probes at 6.5 cm column depth had a length of 50 mm. All temperature measurements were logged every 5 minutes using a Delta-T logger (Delta-T Devices Ltd., Cambridge, U.K.). The two types of thermometers differ in their precision, because in the measurement with the 2-wire probes the resistivity of the cable from the probe to the logger is not compensated, and increases with cable length and temperature. The 4-wire probes compensate the error of the temperature measurement that is introduced by the cable. However, the error that is caused by the mere heat conductivity of the cable from outside into the probe cannot be compensated by the two of them. For both probes a precision of ± 0.3°C is given, but it can be stated, that the 4-wire probes are close to that value and the precision of the 2-wire probes may vary considerably from this value according to cable length and material and temperatures involved.

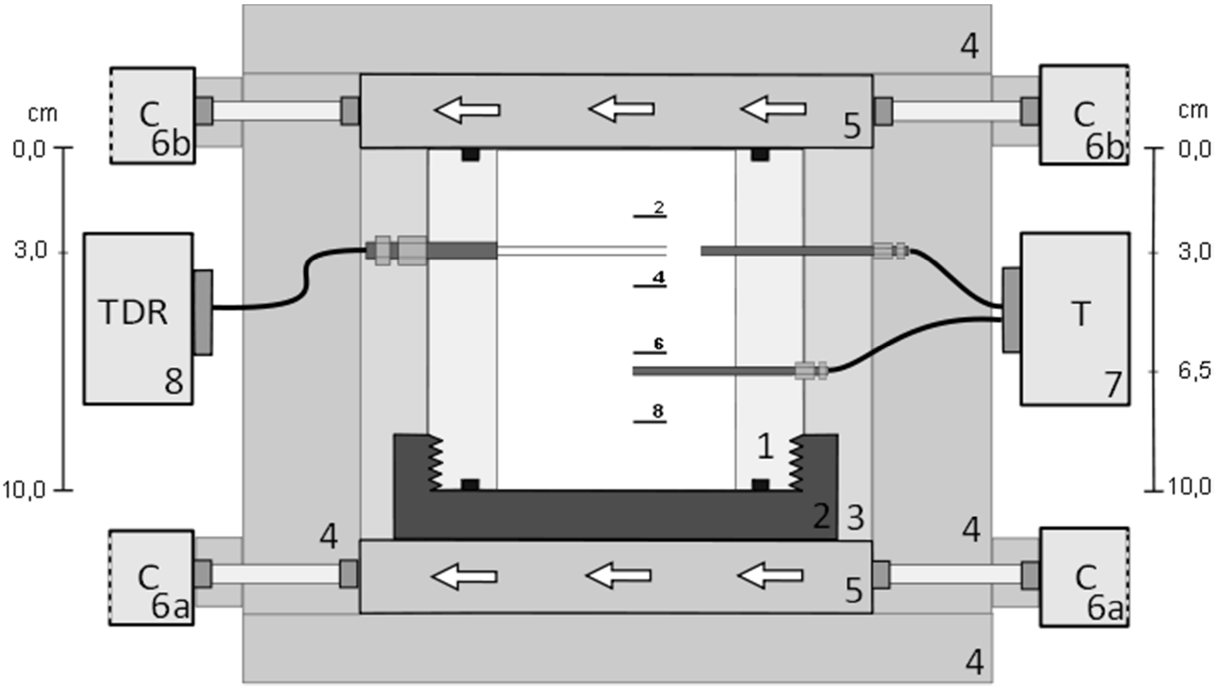

Figure 3.2 Sketch of experimental setup 1 (inner volume 390 cm^3), 1= PVDF cylinder, 2= stainless steel lid, 3= Styrodur® insulation, 4= Armaflex® insulation, 5=cooling head (hollow aluminum), 6a= cooling machine for experimental approach with freezing from the bottom, 6b= cooling machine for experimental approach with freezing from the top, 7= Delta-T logger with coupled temperature probes, 8= multiplexer with coupled TDR probe

The volumetric water content was measured with TDR-probes, type LP/ms with 50 mm length (Easy Test, Institute of Agrophysics, Lublin, Poland). Data were logged every 5 minutes with a multiplexer. The main reason to install the TDR probes was to determine the equilibrium freezing point of the soil during the experiment. The TDR probes are able to measure the presence of liquid water, as a result of the different dielectric constants of water (ε_r = 80.36 at 20°C), ice (ε_r = 3.2) and other soil compartments such as soil particles and air (ε_r < 5). Therefore the phase transition from water to ice is displayed by a steep decrease of the TDR signal.

In experimental **setup 2** temperatures were measured with the platinum resistance thermometers, type PT 100 from Driesen+Kern GmbH (Bad Brahmstedt, Germany) at seven different column depth (see Figure 3.3).

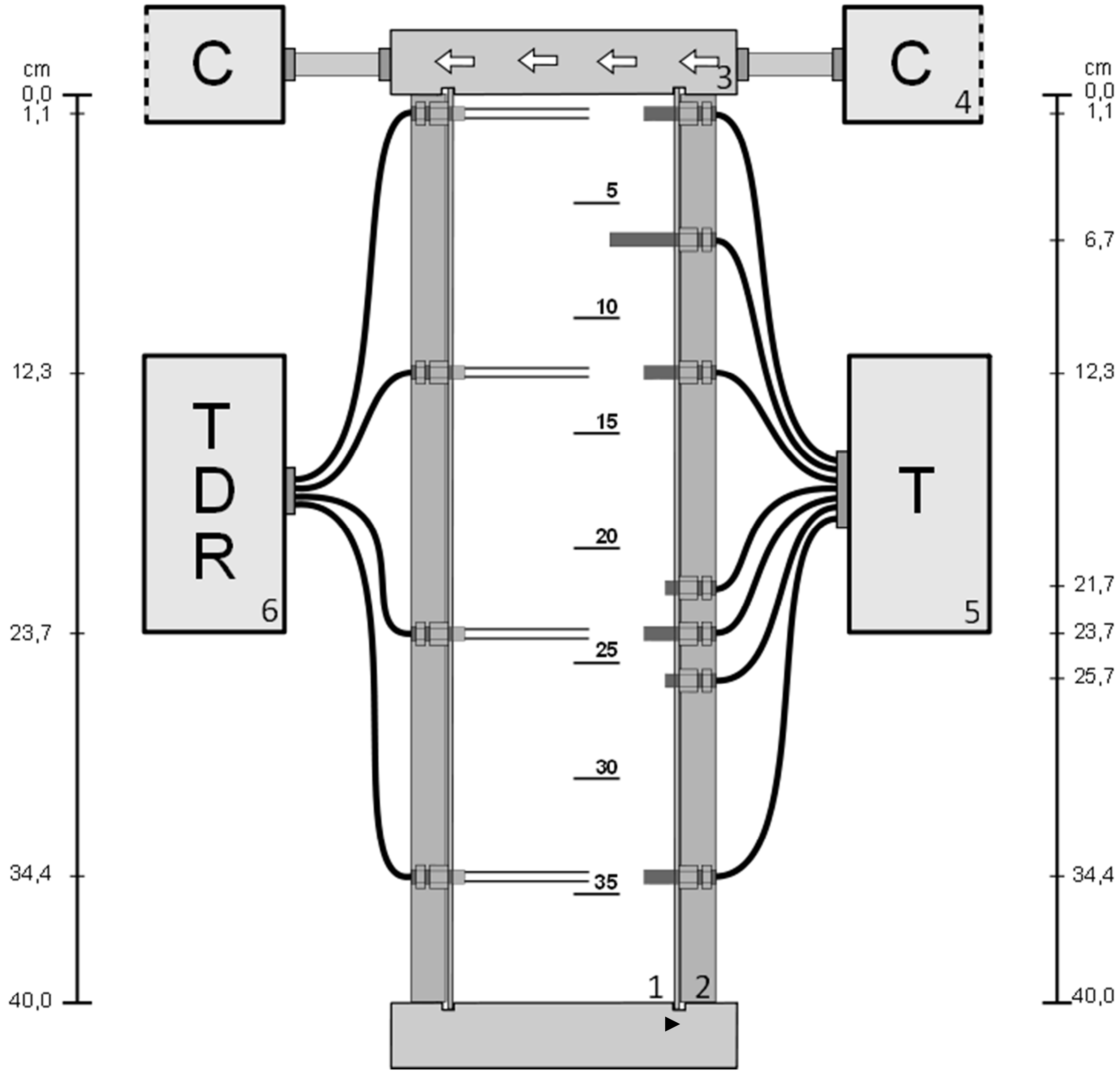

Figure 3.3 **Sketch of experimental setup 2 (inner volume 2775 cm^3), 1=Plexiglas cylinder, 2=polyethylene insulation, 3= cooling head (hollow aluminum), 4= cooling machine to regulate flow and temperature of the cooling liquid, 5= Delta-T logger with coupled temperatures probes, 6= multiplexer with coupled TDR probes**

They extended with different lengths into the column (see Figure 3.2). The feezing process and water migration could be observed with 4 TDR probes. The columns were insulated with 13 mm thick polyethylene cellular plastic (Thermaflex Isolatie bv, Waalwijk, Netherlands) with a thermal conductivity of 0.040 W (m · K)$^{-1}$ at 40°C.

Setup 1 – Preparation and experimental procedure

The filling of the experimental columns was conducted with the contaminated, homogenized and therefore disturbed soil material. This procedure should ensure homogeneous conditions inside the columns without sidewall flow or sidewall lag and gain (Lewis & Sjoestrom, 2010; Schoen et al., 1999). As it is very important to achieve homogeneous and reproducible conditions (Bromly et al., 2007), the packing procedure is described below.

All four columns were packed with the same procedure from bottom to top and with a given density and moisture content of the soil material (see Table 3.5). To reach a homogenous and reproducible packing, the weight of soil to be packed in each part was determined by

$$\boldsymbol{m_{dw} = V * \rho_s + w} \qquad \textbf{Equation 4}$$

m_{dw} = moist soil material in an increment of the column with the height h, g
V = volume of given column increment, cm^3
ρ_s = oven-dry density of the soil, g cm^{-3}
w = water content, g

Material was filled in the columns in one centimeter steps of the column heights. After packing one layer with the calculated amount of soil, the surface was scraped before the addition of the soil material of the next layer, to prevent layering within the column (Funderburg et al., 1979). An exception of this procedure was made for the boundary between contaminated and non-contaminated areas. This boundary was additionally marked with three spots of quartz sand (approx. 1g in total) on the column walls. The lower part of the columns consisted of homogenized, non-contaminated material (see 3.2.2) with the same water content as the contaminated material. If freezing started from the top, the upper 5 cm of the columns were filled with contaminated soil material and for experiments with freezing from the bottom, the upper 2 cm were filled with contaminated material. The three prepared experimental columns were equipped with temperature and TDR probes, insulated with Styrodur© (2 cm thick) and Armaflex© (3.5 cm thick) and placed into the experimental setup. Room temperature was logged near the columns, too. The reference column was placed into a climate chamber at 4°C.

The freezing process during the experiment was operated with a cooling system (Julabo F32.HE, Julabo Labortechnik GmbH, Seelbach, Germany) with insulated tubes (Armaflex® pipe insulation, 1.3 cm), which were connected to the head and the bottom, respectively. The arriving cooling liquid was split with a three-way valve to cool the three columns parallel. Tube lengths between valve and each column were equal. Additionally it was possible to regulate the flow of the cooling liquid to each column with another valve. The experimental programs to cool the column material down are given in Figure 5.1.

At the end of each experiment the columns were taken off the system consecutively. The first step was to take the insulation off and leave the column to thaw at the walls at room temperature (with cooling device on former cooling end). The thawing lasted between 30 and 45 minutes. Afterwards the soil core could be pressed out with a punch with the non-contaminated material coming out first. For sandy material no thawing time was needed. Initially freezing front, total lengths and contamination boundary of the soil core were determined (see Figure 3.4). Then frozen and unfrozen parts were divided. The latter was sampled at room temperature with a long knife into 0.3 cm to 2.5 cm thick slices. The frozen part was sampled in an air conditioned room at 8°C with a hand saw.

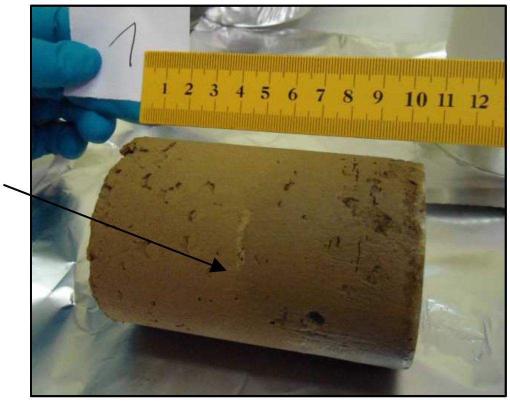

Figure 3.4 Determining freezing front, total lengths and contamination boundary of the soil core before sampling, arrow shows quartz sand mark

Samples were immediately stored in brown jars with PTFE coated caps at -18°C until analysis. Rost et al. (2002) showed that concentrations of 3- to 5-ring PAHs in contaminated soil samples changed within 6 weeks at a storage temperature of 4°C, while samples stored at -20°C did not show changes in PAHs concentrations.

Setup 2 – Preparation and experimental procedure

The homogenized, contaminated soil material for experiments with setup 2 were incubated for 14 days at 18°C with occasional stirring, before it was packed into the two experimental columns (A and B) and the reference column. Packing was performed following the same procedure as described for setup 1, except the thickness of the filled-in layers was 5 cm instead of 1 cm. Furthermore columns were entirely filled with contaminated material. Details for each experiment can be taken from Table 3.5. To evaluate the influence of the incubation time, material was sampled directly after contamination and as described before, during column preparation. The experimental columns were equipped with temperature and TDR measurement devices (see Figure 3.3). Together with the reference column they were then placed into a climate chamber at 4°C. After 24 hours for equilibration of the soil material to this temperature, the experimental columns were insulated and freezing procedure was started, using a separate cooling system for each column (Julabo F32.HE, Julabo Labortechnik GmbH, Seelbach, Germany). Both machines were programmed using the same temperature and time steps for cooling. At the end of each experiment the columns were taken of the climate chamber consecutively. The Plexiglas® allowed the identification of the freezing front right after taking of the insulation material. After 10 to 20 minutes at room temperature the soil core was slowly pressed of the cylinder and immediately cut into 5 cm thick slices with an electric saber saw (GSA 900 PE, Bosch, Stuttgart, Germany) or with a long knife, depending on whether the material was frozen or not. The outer centimeter of the round sample slices was discarded, to avoid an influence of the Plexiglas® on the contaminant concentration in the sample. Sample storage was conducted as described before.

Table 3.5 gives an overview over the experiments conducted and their main boundary conditions. Each experiment got a code for better understanding in the text. The codes were formed after the following scheme:

First letter – material description

S	Sand
P	*Peat*
U	Silt

Second part – description of experimental procedure

fb	freezing from the bottom
ft	freezing from the top

Third part – contaminants present in the soil material

a	anthracene
b	benzo[a]pyrene
p	pyrene
o	crude oil

Table 3.5 Contamination levels, ^{14}C activities and other boundary conditions of the experiments

code	Experimental approach	set up	Column height, cm	Density, g cm^{-3}	Water content, % dw	PAH content, mg kg^{-1} dw	Oil content, % dw	Oil density, g cm^{-3}	^{14}C-activity, dpm g^{-1} dw	Duration, h	Notes
Ufb	silt, single freezing from the bottom	1	10	1,51	-	-	-	-	-	96	without stainless steel lid
Ufba	silt, single freezing from the bottom	1	10	1,51	26.6	50 anthracene	-	-	22099.5±687.0 ^{14}C-anthracene	113	
Ufbp	silt, single freezing from the bottom	1	10	1.52	26.1	50 pyrene	-	0.830	24220.0± 184.4 ^{14}C-pyrene	160	
Uftao	silt, single freezing from the top	1	10	1.51	26.2	50 anthracene	0.5	0.830	23002.3 ±422.3 ^{14}C-anthracene	160	
Uftpo	silt, single freezing from the top	1	10	1.51	29.2	50 pyrene	0.5	0.830	11743.3 ± 171.1 ^{14}C-pyrene	159	
Sftao	sand, single freezing from the top	1	10	1.62	9.4	50 anthracene	0.5	0.830	7714.2 ± 119.9 ^{14}C-anthracene	138	
Sftabo	sand, single freezing from the top	2	40	1.75	13.6	258 ant 13 BaP	5	0.932	-	144	14 days pre-incubation of contaminants in soil material
Pftabo	peat, single freezing from the top	2	40	0,17	480	223 ant 11,16 BaP	5	0.932	-	168	14 days pre-incubation of contaminants in soil material

3.2.4 EXTRACTION, MEASUREMENT AND ANALYSIS OF ^{14}C-LABELED CONTAMINANTS

Methods for extraction, measurement and analysis were used according to cited references. Samples from field were transported and stored in frozen stage until sampling. Sampling and consecutive sample storage was conducted as described in chapter 3.2.3 for the samples of laboratory experiments. Before analysis samples were thawed and subsequently homogenized by stirring. Three independent subsamples were taken from each sample, analyzed and the result corrected by the blank value of the analyses.

The determined ^{14}C-activity is assumed to result from the ^{14}C-labeled PAHs used in the experiments, because values far exceed natural background levels and other ^{14}C-labeled chemicals were not used in the experiments. However, as only the radioactivity has been determined, the presentation and discussion of the results will always deal with ^{14}C-activity and not use the terms ^{14}C-anthracene or ^{14}C-pyrene with respect to certain analyzed values.

Total content

To determine the total content of ^{14}C in a sample, three times 1 g of an independent moist sample were weighted in a porcelain crucible and burned under an oxygen stream with a combustion unit (see Figure 3.5).

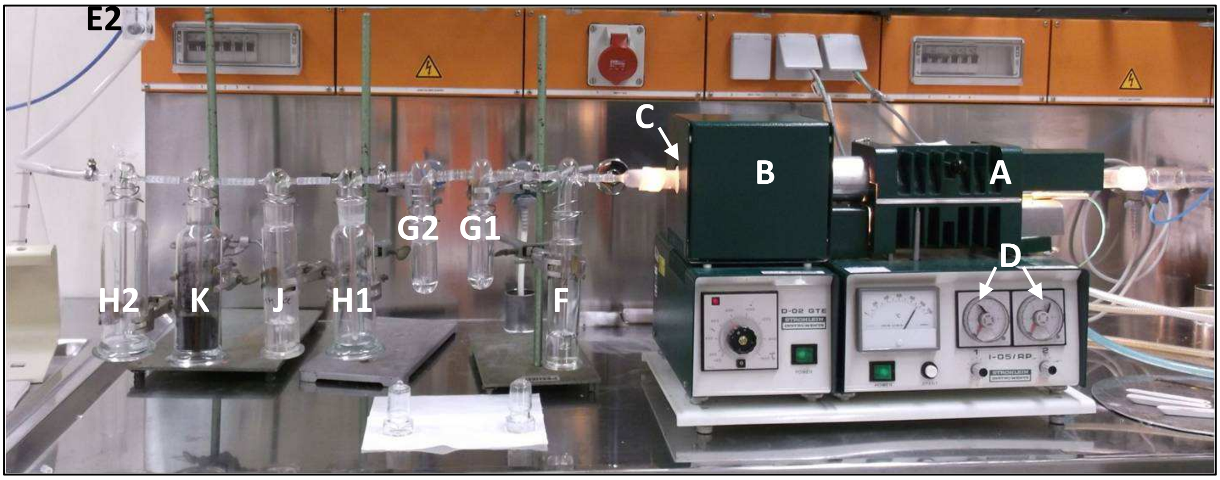

Figure 3.5 Combustion apparatus to determine total ^{14}C-activity, Ströhlein Instruments, Kaarst, Germany.
A: first oven "I-05/RP" with a maximum temperature of 1100°C B: second oven "D-02 GTE" constantly running at 900°C, C: CuO catalyst, D: timer, E: flow meter (E1 in flow, not shown, E2 out flow), F: washing flask (H2SO4), G1 and G2: flasks with sorption agent (Carbo-Sorb, 2-methoxyethylamine), H1 and H2: empty security washing flasks, J: washing flask (1M HCl), K: washing flask with activated carbon

The combustion process started with 150 – 190°C for four minutes to evaporate the water and was followed by combustion at approx. 1000 °C for 6 minutes. The second oven ran constantly at 900°C (Eschenbach, 1995). The $^{14}CO_2$ originating from the combustion process was sorbed to a sorbing chemical (Carbo-Sorb) in two consecutive flasks (G1 and G2 in Figure 3.5). Afterwards the Carbo-Sorb was transferred to 20 ml scintillation vials and flasks were flushed with 16 ml scintillation cocktail (Pico-Fluor) in four steps, which was also transferred to the scintillation vials. The content of both flasks was counted separately, because ^{14}C-levels at background level in the second flask proved the completeness of the $^{14}CO_2$ sorption in the first flask and that no ^{14}C-activity was lost and set free.

The threshold of measurement is at 37 dpm g^{-1} dw. The approximation of the detection limit is 111 dpm g^{-1} dw. Recovery rates were determined with 100 % ± 4 % by the combustion of a solution of ^{14}C-glucose. The variation coefficient for contaminated silt loam was four, usually less than one and sometimes eight. For sand the coefficient of variation was less than two for contaminated samples. Coefficients of variation for uncontaminated samples were with ten to 30 much higher, because their values ranged below the detection limit. Attention has to be paid to condensed water within the closed apparatus after the oven. If there is water before G_1 CO_2 will be solved to a certain extend and therefore not be captured in the counting afterwards. Tests showed that 1 – 2 % of the activity of the burned sample is sorbed by the water. Therefore glassware directly after the oven was dried, if condensed water occurred.

Sequential extraction with different solvents

To determine the extractability for different solvents a sequential extraction procedure, based on the method of Eschenbach et al. (1994), was conducted. It consisted of four steps with three different solvents without matrix alteration. That means all four types of fixation that involve strong matrix interaction of the organic contaminants are found in the soil, after the four extractions. For some samples only three steps were conducted sequentially. In these cases the water extraction was conducted afterwards with new sample material. In summed results the amount of water extractable ^{14}C-activity was subtracted from the methanol-water extractable amount. The procedure for each extraction step was the same.

Before sampling the samples were allowed to thaw overnight. After homogenization three times 3 g of moist soil sample were weighted into 9 ml centrifuge tubes (10 cm long, made at University of Hamburg) with screw cap and septum. Then 3 ml of solvent were put to each tube with a 5 ml pipette (Eppendorf AG, Hamburg, Germany). After stirring each sample with a Vortex mixing machine (Reax top, Heidolph Instruments GmbH & Co. KG, Schwabach, Germany) twelve samples were put into an ultrasonic bath (Sonorex, Bandelin, Berlin, Germany) for 30 min. To separate the extract from the soil particles the samples were centrifuged for 20 min. at 2500 rpm with a 3K10 centrifuge (Sigma Laborzentrifugen GmbH, Osterode am Harz, Germany). It was important to slow down the centrifuge slowly to prevent breaking of the sample tubes. The supernatant was taken off with a 5 ml syringe (Hamilton Bonaduz AG, Bonaduz, Switzerland). Volume was determined by metering and then the extract was stored in 4 ml amber tubes. For analysis 500 µl of the solution were mixed with 4 ml Pico-Fluor in 5 ml scintillation vials. The coefficients of variation for the sand and the silt were < 2.8 and < 4.5, respectively. If a further extraction step followed the tube with the solid sample rest was weighted and then mixed with the next solvent. The solvents to determine the extractable fractions were used in the following order:

1. water: for the water soluble and dissolved ^{14}C-fraction
2. methanol-water mixture (50 vol% : 50 vol%): for the weakly sorbed and readily extractable ^{14}C-fraction
3. first ethyl acetate: ^{14}C-fraction that may be desorbed without matrix alteration
4. second ethyl acetate: to guarantee the exhausting extraction with ethylacetate

Analysis of ^{14}C-activity

The measurement of ^{14}C-activities from soil materials and extracts was done with a Wallac 1409 β-scintillation counter (Wallac, Tuku, Finland) using a Xylen based, fluorescent scintillation cocktail (Picofluor). The technique is based on detection of emitted light at wave length of 340 to 400 nm. When this light strikes the photocathode, electrons are released and reinforced, so that the electrical impulse can be measured. This impulse is proportional to the energy of the radioactive decay of the present ^{14}C. The unit is counts per minute (cpm). Due to radiation losses, it is not possible to count 100 % of the emitted light (Cooper, 1981). Therefore cpm are corrected with an internal calculation of the counter to decays per minute (dpm). Furthermore quenching effects, due to color of solution or interactions of chemicals used, may lead to underestimation of ^{14}C-activity. The internal correction works with individual measurements, which may be saved and used by the counter. The measurements were computed using 1414 WinSpectralTM on a windows workstation. The parameters set for the measurement for the present studies are given in Table A.1.

3.2.5 EXTRACTION, MEASUREMENT AND ANALYSIS OF NON-LABELED CONTAMINANTS

Extraction and analysis of 16 EPA-PAHs

Non-labeled PAHs were extracted with n-Hexane using a Soxhlet apparatus. The extracts were analyzed with a gas-phase chromatograph with mass spectrometer (GC-MS). The procedure was carried out based on DIN ISO DIN18287 (2006).

In preparation for extraction soil samples were thawed and homogenized. Peat samples were air dried additionally. After homogenization 8.0 g (± 0.1 g) of moist soil sample was weighted and dried with sodium sulfate. Then it was filled into a cellulose extraction thimble, covered with quartz wadding and put into the Soxhlet apparatus. Together with the solvent a deuterated PAH internal standard solution was added to each sample. Afterwards the heating was started. The extraction ran for two hours. Before analysis extracts were diluted 1:10 due to the high oil contents of the soil samples. For extracts from sand n-Hexane was used for dilution. For peat samples Dichloromethane was used. An additional cleaning step from hydrocarbons other than PAHs was not included, as pre-test had shown no significant improvement of PAH analyses. The parameters for the GC-MS analysis are given in Table A.3. The detection limit of the single PAHs is below 1.0 µg kg^{-1} dw. However, in the presence of high contents of other organic compounds, such as organic carbon and petroleum hydrocarbons, respectively, certain PAHs may be masked, resulting if much higher detection limits. Zemanek et al. (1997) recorded large variations of PAH recovery rates from oil matrices, which ranged from 50 % to 180 %.

Extraction and analysis of total petroleum hydrocarbons

On the basis of DIN EN ISO 16703 (2011-09) for determination of total petroleum hydrocarbon content, soil samples were extracted by an acetone hexane mixture and extracts were analyzed with GC-FID. After baseline correction based on blind and standard values a sum parameter between C_{10} and C_{40} was determined from chromatograms.

In preparation for extraction soil samples were thawed and homogenized thoughtfully. An amount of 3.0 g ($\underline{+}$ 0.1g) of field moist soil were weighted in 50 ml flasks. For extraction 20 ml of n-hexane marked with decane (C_{10}), eicosane (C_{20}) and tetracontane (C_{40}) and 20 ml of acetone were added. The mixture was agitated for 60 minutes in a horizontal shaker at 150 rot min^{-1}. The hexane phase with the solved petroleum hydrocarbons was separated from the rest by adding distilled water, shaking and taking the buoyant phase of with a one-way glass pipette. This procedure was repeated. Afterwards the extract was cleaned up by column filtration. Columns were filled with quartz wadding, 2 g Florisil® (magnesium silicate gel) and 2 g sodium sulfate. Extract was put on column until 10 ml extract for analysis were obtained. From this sample three aliquots were filled in 1.5 ml crimp neck vials for analysis with gas chromatograph and flame ionization detector (GC-FID, Shimadzu 2010, type FID and AOC20i, Shimadzu Deutschland GmbH, Duisburg, Germany). Parameters for analysis are given in Table A.2.

High standard errors for some means may partially be explained by the fact that no direct injection on column was possible. For quantification of contaminated samples from northern Siberia the BAM standard was used.

3.2.6 STATISTICS

As normal distribution of data is a basic assumption for many statistical tests, data were tested with the Shapiro-Wilk test and Kolmogorov-Smirnov test for normal distribution before employing any other statistical test. Laboratory analysis was usually performed with three replicates. Outliers were determined by Dixon’s Q test and deleted, if they could be identified as result of analysis procedure. Mean value and standard error were determined. If only two analyses were available the median was taken and no error bar is displayed in graphs. To test statistical significance of the difference in contaminant concentration and water content compared each with the starting conditions student’s T-Test with Levene’s test of variance were performed. For not normally distributed data the Mann-Whitney-U-test was performed. For linear fittings Pearson’s r was calculated. All tests were performed at $p < 0.05$. Means of samples with ^{14}C-activities around the detection limit were not compared.

For statistical approach the programs OriginPro 9.1G (OriginLab Corporation, Northampton, USA) and SPSS 16.1 (IBM Corp., Armonk, USA) were used.

4. CHARACTERIZATION OF SOIL SAMPLES UNDER INVESTIGATION

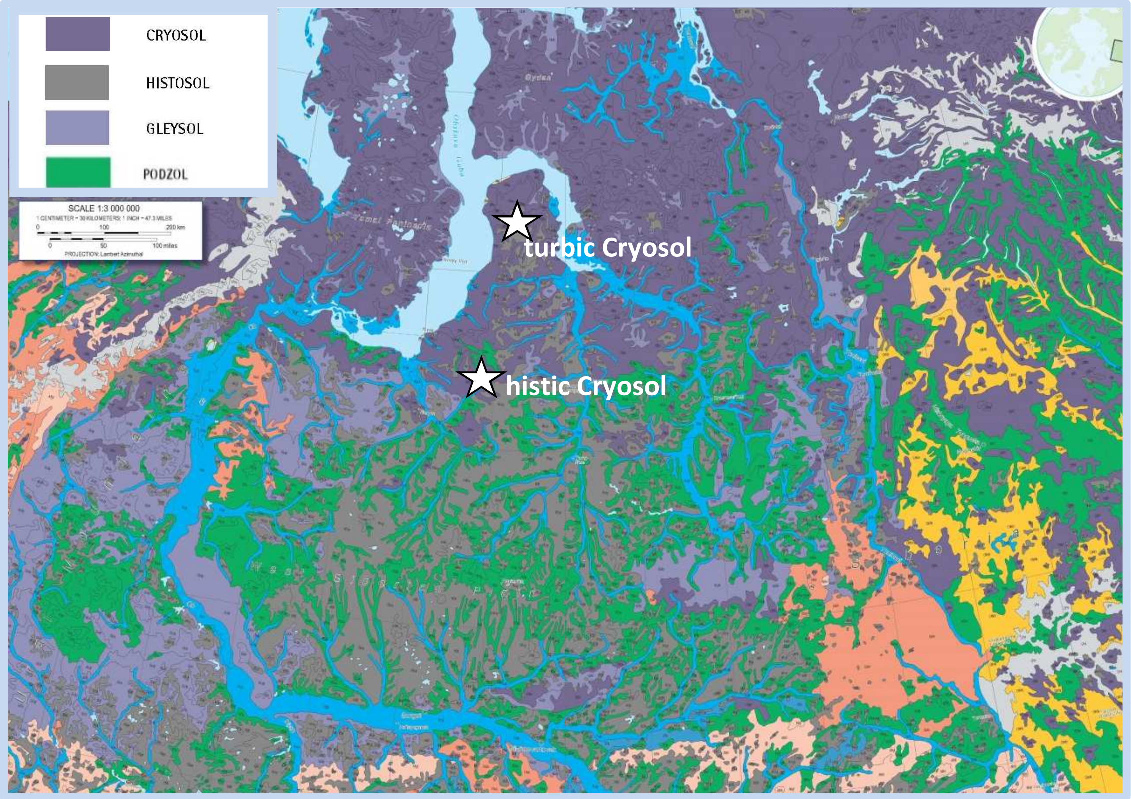

Figure 4.1 Distribution of abundant soil types in central western Siberia (West Siberian Basin) according to World Reference Base (Jones et al., 2010)

In the Arctic a broad variety of soil types developed upon different geological parent materials. North of the Arctic Circle cryosols (WRB) dominate. To the south Histosols, Gleysols and Podzols belong to the main soil types. This distribution pattern can also be found in western Siberia (see Figure 4.1). The determining geological structure in this region is the West Siberian Basin. With an area of 1.6 Mio km^2 it is the world's second largest petroleum basin and its most important gas province (see Figure 1.1). High pumping rates and challenging climatic conditions lead to considerable amounts of spilled petroleum hydrocarbons.

As the class Cryosol (IUSS Working Group WRB, 2014) determines the soils with influence of permafrost and freezing and comprises all sorts of parent material, two main soil subtypes abundant in western Siberia were chosen as examples, a trubic and a histic Cryosol.

4.1 PROPERTIES OF TWO CRYOSOLS FROM WESTERN SIBERIA

The turbic Cryosol used as reference has been found at a hummocky Tundra site north of the Arctic Circle with typical vegetation with *Betula nana*, *Salix polarica*, *Ledum palustre*, *Carex sp.* and *Sphagnum sp.* as most abundant species (see mark in

Figure 4.1). It was sampled at the beginning of august over the whole active layer thickness of 79 cm ± 10 cm (see Figure 4.2 a).

Figure 4.2 a Turbic Cryosol (reductaquic)N 68°17’42,4’’ E 075°49’43,9’’
Figure 4.2 b upper 40 cm of the profile with inter-aggregate pores (elongated slits)

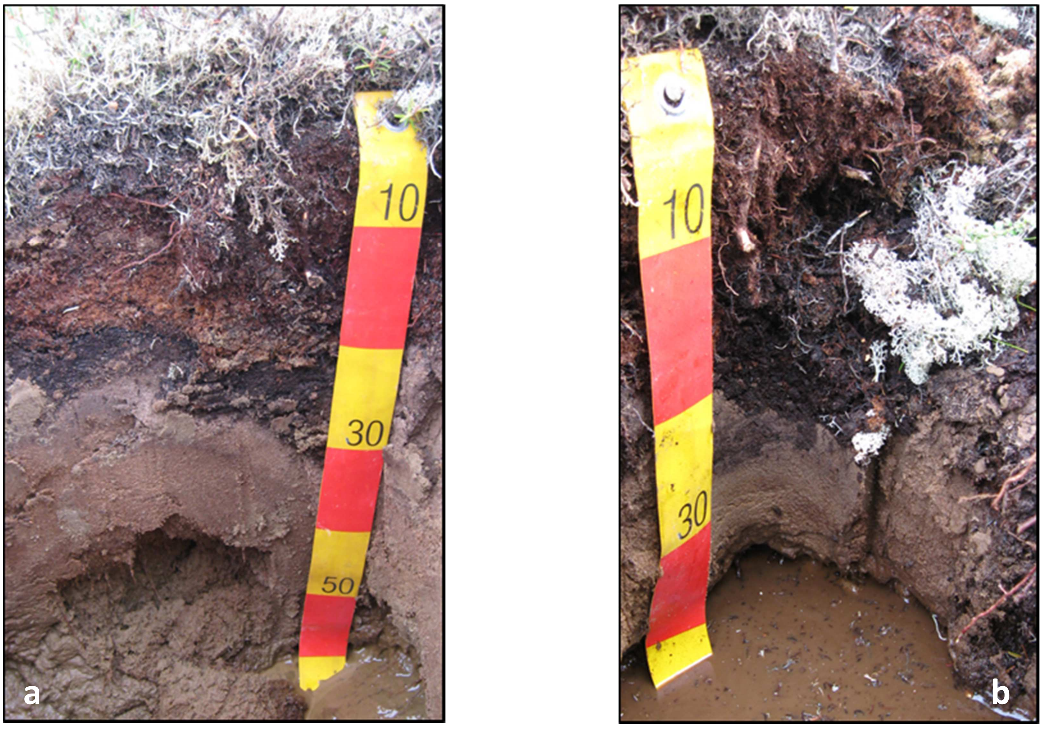

Figure 4.3 a Histic Cryosol (arenic, thixotropic)N 65°58’50,5’’ E 075°47’26,1’’
Figure 4.3 b upper 40 cm of the soil profile with water level

The carbon content below the organic surface soil layer is only at 1 % (see Table A.4). The soil has hydromorphic and cryometamorphic features, such as greyish color, bands of iron oxides and large inter-aggregate pores. A close-up of the first 40 cm reveals relictic soil ice structures between 30 cm and 40 cm, and less well pronounced around 20 cm (see Figure 4.2 b). The latter is also displayed in a lower bulk density of the horizon, compared to the other horizons of the profile (see Table A.4). According to Yershov (1998) such elongated slits are a result of dehydration due to freezing induced water migration.

The histic Cryosol was found at a hummocky Tundra site with some patches heave within a large thermokarst depression. Most abundant vegetation species were *Betula nana*, *Ledum palustre* and *Cetraria islandica*. The active layer had a thickness of 70 cm and the supra-permafrost water table was determined at 42 cm. As the site is close to a talik (approx. 500 m) and no reductaquic horizon could be determined, it is not clear, how permanent the perennial frozen ground is at the site. The soil is a good example for a permafrost-affected arenic substrate on which several peat layers developed (for details see Table A.4).

4.2 PROPERTIES OF SOIL MATERIALS USED IN LABORATORY EXPERIMENT

To determine single parameters that influence a process, it is important to keep others constant, for example soil texture and carbon content. Furthermore, to get statistically relevant results, it is important to run several parallels. Depending on the size of the experimental setup this approach may be very material consuming. As the availability of Siberian soil material is restricted, three reference materials with approximate soil properties were chosen to conduct the experiments (see Table 4.1 and Table A.4).

Table 4.1 Main properties of soil materials used in experiments

name/texture	clay	silt	sand	C_{org}	density in laboratory experiments
silt loam	10.84	79.73	9.43	1.36	1.51
sand	5.61	2.43	92.0	0.16	1.62…1.75
peat	n.d.	n.d.	n.d.	53.1	0.17

As equivalent for the silty loam of the turbic Cryosol a silty loam of an Ultisol from loam upon sandy loam was chosen. The soil material was found south of Hamburg (N 53°25’37.6’’ E 009°55’17.8’’) upon saalian depositions. The main soil properties texture, carbon content and bulk density were approximately equivalent to the properties found in situ in the turbic Cryosol. Clay content was 8 % lower and carbon content 0.3 % higher in the soil material near Hamburg (for further details see Table

A.4). As water is one of the main influencing factors concerning the freezing process in soils, details concerning the interaction of the used soil materials and water are given in Table A.5.

Furthermore the liquid water content for the soil material at temperatures below 0°C was predicted with the procedure from Tice et al. (1976) followed by Equation 1 (see Figure 4.4). Compared to measured values from Yershov (1998) the predicted liquid water contents are similar to those of a sandy clay-silt (light, silty). Yershov (1998) could also show that a wider range of present pores sizes led to higher liquid water contents at lower temperatures, but if the maximum of pore diameters is larger than 10 µm, the liquid water content at temperatures below -4°C already converges to zero. That relation has also been shown by Williams and Smith (1991), see Figure 2.4. The maximum of pore diameters for the used silt loam is around 10 µm, but the range of present pore sizes is not wide.

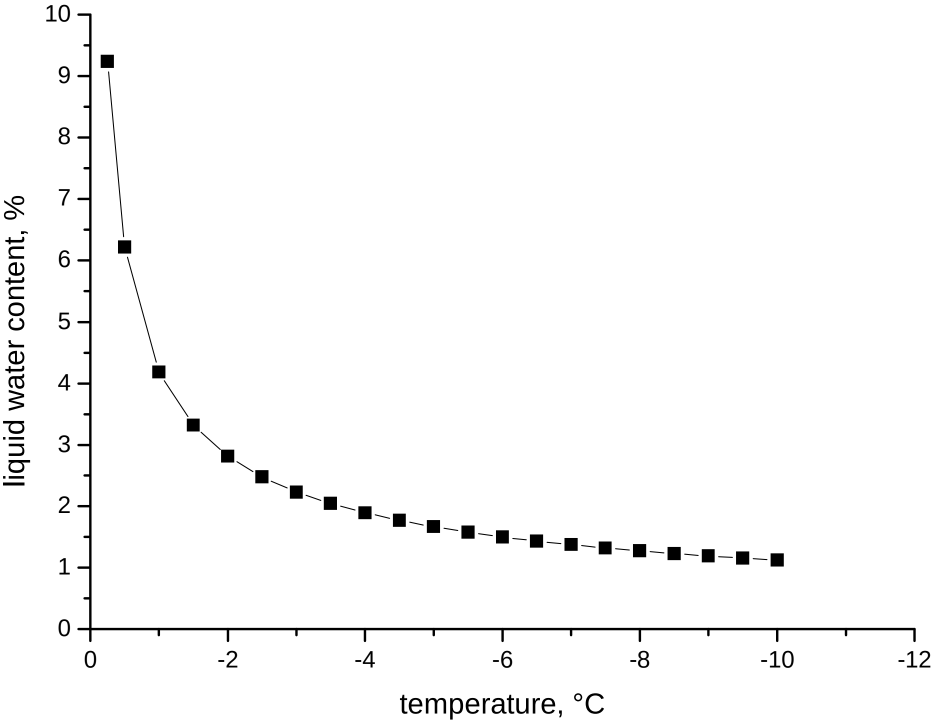

Figure 4.4 Predicted amount of water remaining unfrozen at soil temperatures below 0°C in the silt loam from the south of Hamburg, calculated with the equation $w_u=\alpha*\theta^\beta$ from Tice et al. (1976)

The equivalent for the arenic substrate of the histic Cryosol was a glacial melt water sand. For this material the liquid water content at temperatures below 0°C is close to zero, because most pores are narrow macro-pores, where the water freezes first (see chapter 2.1.1 and Figure 2.4). As the liquid limit test is only applicable to plastic soil materials, it was not possible to predict the unfrozen water content at temperatures below 0°C with the procedure from Tice et al. (1976) for the sandy material. The material was found south of Hamburg near the location of the silt loam, at saalian deposits (N 53°25’37.6’’ E 009°55’17.8’’). Its other main properties are approximate to the sandy soil horizons of the profiles from western and northern Siberia, with significant difference in sand content (see Table A.4). Higher silt and clay contents in the Siberian soils can be attributed to soil forming processes, and particularly freezing processes.

The peat material used in the laboratory experiments was found north of Hamburg at a peat bog (N 53°44’6.5’’ E 009°51’10.7’’). Details are also given in Table A.4. It is a well decomposed peat, whose properties may be compared to the ones of the second horizon of the West Siberian histic Cryosol. A main difference of peat compared to sand is the bulk density of the material (see Table 4.1) and heat conductivity. The heat conductivity of dry sand is 1.8 W $m^{-1} \cdot K^{-1}$, whereas it is only 0.5 W $m^{-1} \cdot K^{-1}$ for peat (Bachmann et al., 2001). These values may vary by 0.5 W $m^{-1} \cdot K^{-1}$ depending on the water content.

4.3 PROPERTIES OF SOIL AT IN-SITU SPILL SITE IN NORTHERN SIBERIA

The in-situ spill in northern Siberia is located at a degraded polygonal rim of a low centre polygon within a wet polygonal tundra landscape (N 72°22’25’’, E 126°29’38’’, Figure 4.5a). Vegetation is dominated by mosses and carex (*Hylocomium sp., Aulacomium sp.*, *Dryas octopetala* and *Carex aquatilis*). Climate is characterized by low mean annual air temperatures and a mean annual precipitation of 190 mm. The winter season lasts nine months, from the end of September to the end of May (Wagner et al., 2003).

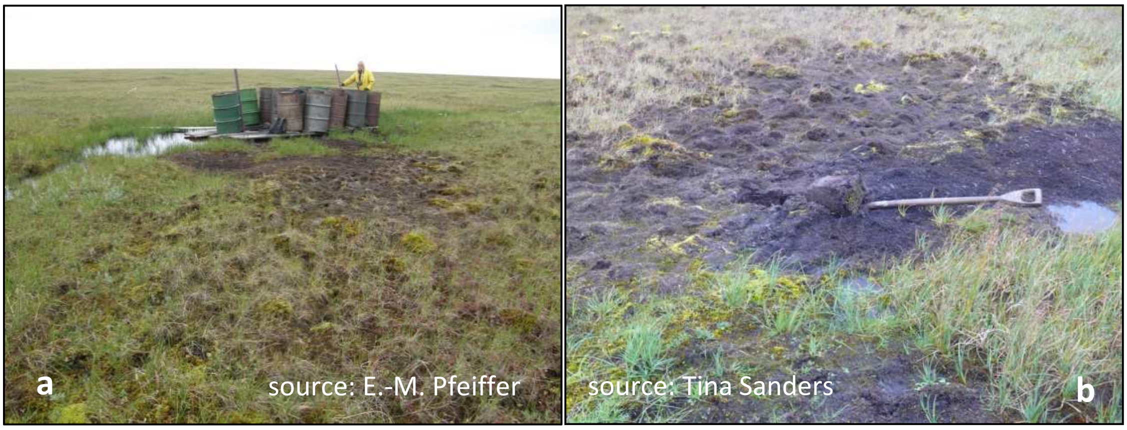

Figure 4.5 a **Landscape and vegetation at Diesel spill site in Northern Siberia**
Figure 4.5 b **Close-up of contaminated soil with disturbed sample for soil analysis**

The soil is classified as a turbic, histic Cryosol according to WRB (cryic Historthel, according to soil taxonomy). The soil profile can be distinguished into three main soil layers, which are all dominated by peat (Table A.4). The site had been used for meteorological measurement devices, which needed power produced by a generator. The contamination with diesel and lubricating oil resulted from a leakage of the generator, which ran from 2003 to 2006. The contamination was discovered, when the generator was dismounted. When samples for analysis were taken in 2009 and 2011, diesel was still visible at the soil surface (see Figure 4.5b). The active layer depth varied between 2007 and 2011 between 62 cm and 34 cm. In the years of sampling the ground water table was encountered in 19 cm and 19.5 cm soil depth, respectively.

5. INVENTION OF COLUMN EXPERIMENTS TO SIMULATE FREEZING PROCESSES IN THE LABORATORY

To decode single processes laboratory experiments have great importance because with set boundary conditions the variables of the system can be minimized allowing for the understanding of the influence of single parameters. Other reasons to decide for laboratory experiments rather than field investigations may also be availability of samples and cost effectiveness.

The aim was to develop an experimental setup, which is able to simulate natural occurring freezing processes in permafrost-affected soils in conjunction with organic contaminants. That means special attention has to be paid to selection of materials used, according to thermal properties and chemical reaction. Furthermore experimental approaches that simulate the freezing process in conjunction with the freezing induced water migration had to be developed, because the transferability of the laboratory results depends on the proper simulation of the natural occurring phenomena.

5.1 CONSTRUCTION OF LABORATORY COLUMNS

Firstly the column material should have a low thermal conductivity, allowing for the simulation of a unidirectional freezing process with a horizontal freezing front within the soil material. The column material should be inert to chemicals, as organic contaminants are subject of the investigations. Thirdly, the compressive resistance of the material is important when freezing experiments are conducted, because significant pressure emerges of the phase transition from water to ice in closed systems (see chapter 2.2.1) and the tightness of the soil columns is ensured by the contact pressure of the upper and lower cooling head (see Figure 3.3).

As low thermal conductivity was the leading characteristic the materials given in Table 5.1 were preselected. Stainless steel, which is often used for experiments dealing with organic contaminants is not listed, due to its high thermal conductivity ($15\ W \cdot (K \cdot m)^{-1}$). The chemical resistance of the given materials can be seen in the amount of adsorbed water and the description of chemical resistance given by the manufacturer. Plexiglas® is not consistent against organic compounds nor against the uptake of water (Evonik, 2014; Weihermüller et al., 2007). Therefore it is not well suited for experiments employing organic chemicals. The third precondition, the compressive resistance, is better for PVDF than for PTFE, additionally the latter has the characteristic to react with cold flow at pressure. This might influence the tightness of the system. Therefore PVDF is the material which meets the requirements best. As result of the material comparison it was chosen for the construction of the experimental columns.

The parameters to determine the dimensions of the soil columns are the needed amount of sampling material for analysis together with the possibility to sample in small distances, secondly the minimization of side wall effects and thirdly enough space to place probes for temperature and moisture control. Besides working with contaminants it is always the aim to contaminate only the essential amount of soil material. For the understanding of the processes concerning the contaminant migration in the soil columns a bench scale setup with 10 cm high cylindrical columns is sufficient. Studies on both, the influence of freezing (Chuvilin et al., 2001; Konrad & Seto, 1991), as well as studies of the behavior of contaminants in soils (Wehrer & Totsche, 2005; Weigand et al., 1999) were carried out with columns of this magnitude. The length of the installed TDR-probes is 5 cm and a space of about 1 cm should be left between the probe and other sensors or electrical disturbances. At the same heights a temperature probe should be installed to control the temperature course within the column. Bearing this and the aforementioned parameters in mind, the inner diameter of the columns was set to be 7 cm. This diameter leaves 1 cm within the soil column to measure the temperature without disturbing the TDR measurement.

For the investigations on the scale of a natural active layer, columns with the dimensions of 40 cm height and 9.4 cm width, which corresponds approximately to a diameter to lengths ratio of 1 : 4, were determined to be the best choice. Only PVDF could not be delivered in these dimensions. As the first assumption for the choice of material was the low thermal conductivity and due to its cost effectiveness Plexiglas® was chosen for these microcosms. With respect to the bad chemical resistance, sampling included rejection of the outer cm of the round sample slices (see chapter 3.2.3.)

Table 5.1 Column material characteristics (Ensinger, 2011; Ensinger, 2012; Evonik, 2014)

Parameter			**Column Material**		
	unit	conditions	Plexiglas® Acrylic polymer	PTFE Polytetrafluor - ethylene	PVDF Polyvinyliden fluoride
density	$g \cdot cm^{-3}$		1.19	2.15	1.78
compressive resistance	MPa	1% de-formation	110	5	16
thermal conductivity	$W \cdot K^{-1} \cdot m^{-1}$		0.19	0.20	0.25
absorption of water	%	24h at 23°C	2.1	< 0.01	<0.01
chemical resistance		as per the manu-facturer	not consistent against organic compounds	very good	very good

Another basic requirement for the conduction of freezing experiments is the proper insulation of the experimental setup, to minimize thermal losses at the margins of the system and to ensure a unidirectional freezing process. In this context the kinetic state of the ambient air is important, because it significantly influences the heat flux. Müller-Lupp (2002) showed that with increasing ambient air movement the effect of an insulation increases.

During preliminary test it has been seen that a combination of Styrodur® and Armaflex® (for material details see chapter 3.2.3) proofed to be a good insulation for setup 1. The experiments were conducted at approximately 20°C room temperature in a laboratory with an air circulation at an exchange rate of eight times the room volume per hour. Experiments with setup 2 were conducted in a climate chamber running at 4°C. The experimental columns of setup 2 were insulated with a layer of 13 mm thick polyethylene cellular plastic.

In both experimental setups the freezing process could be simulated. It was possible to freeze the whole soil columns of experimental setup 1, filled with different soil materials with certain water contents, if needed. In experimental setup 2 the maximum freezing depths that could be achieved by setting the input cooling temperature on a maximum of -24°C was 24 cm for sand with a water content of 12.9 % dw and 13 cm for peat with a water content of 570 % dw. Later tests revealed that an improvement of the insulation, using 35 mm thick Armaflex® could decrease the heat flux of the ambient air into the experimental columns resulting in greater freezing depth.

5.2 SIMULATION OF FREEZING PROCESS IN LABORATORY COLUMNS

After constructing the experimental setup the freezing programs to simulate naturally occurring freezing conditions in permafrost-affected soils were developed. For this purpose temperature profiles from the wet polygonal tundra in Northern Siberia were analyzed (see Figure 2.2). Boike et al. (2013) showed that the refreezing process in the polygonal tundra is a quite slow process, lasting three to eight weeks in a polygonal rim, depending on soil depth. During the zero curtain effect the cooling rates of the soil are close to 0°C. The measurements of Boike (Figure 2.2) show cooling rates up to 3.1°C day^{-1}, after the zero curtain effect had passed. In the Canadian Arctic similar refreezing times have been observed and freezing rates of the soil of 0.05°C day^{-1} to 0.5°C day^{-1} were reported (Konrad & Seto, 1991).

The main factors determining temperature and water content profiles in the laboratory experiments are input temperature, soil material, water content and insulation. The water content is set to a certain amount, as the column setups used were closed systems. That means the amount of water available for freezing induced redistribution processes is restricted within the system. The zero curtain effect controlled by the dimensions of the soil system affected by permafrost, its mostly high water saturation level and the air temperatures. For the simulation of these specific conditions can only be gained by low cooling rates.

To determine a certain position of the freezing front and assure low freezing rates the thermal state within the experimental columns was monitored with temperature probes. To control the phase transition from water to ice, additional TDR measurements were conducted (see chapter 2.2.2 and 3.2.3). One of the main influencing parameters, controlling the naturally occurring freezing process in soils is the ambient air temperature. This parameter was simulated by temperature and flow of the cooling liquid through the head and bottom of the columns, respectively. Other parameters influencing the freezing process in Arctic landscapes, like snow cover and vegetation were not simulated in the experiments. As soil moisture content influences the freezing rate, it was fixed at 60 % of the maximum water holding capacity as a boundary condition (details given in Table 3.5 and chapter 3.2.3). To induce low freezing rates and in almost all cases a static freezing front at the end of each experimental approach the cooling programs in Figure 5.1 were invented.

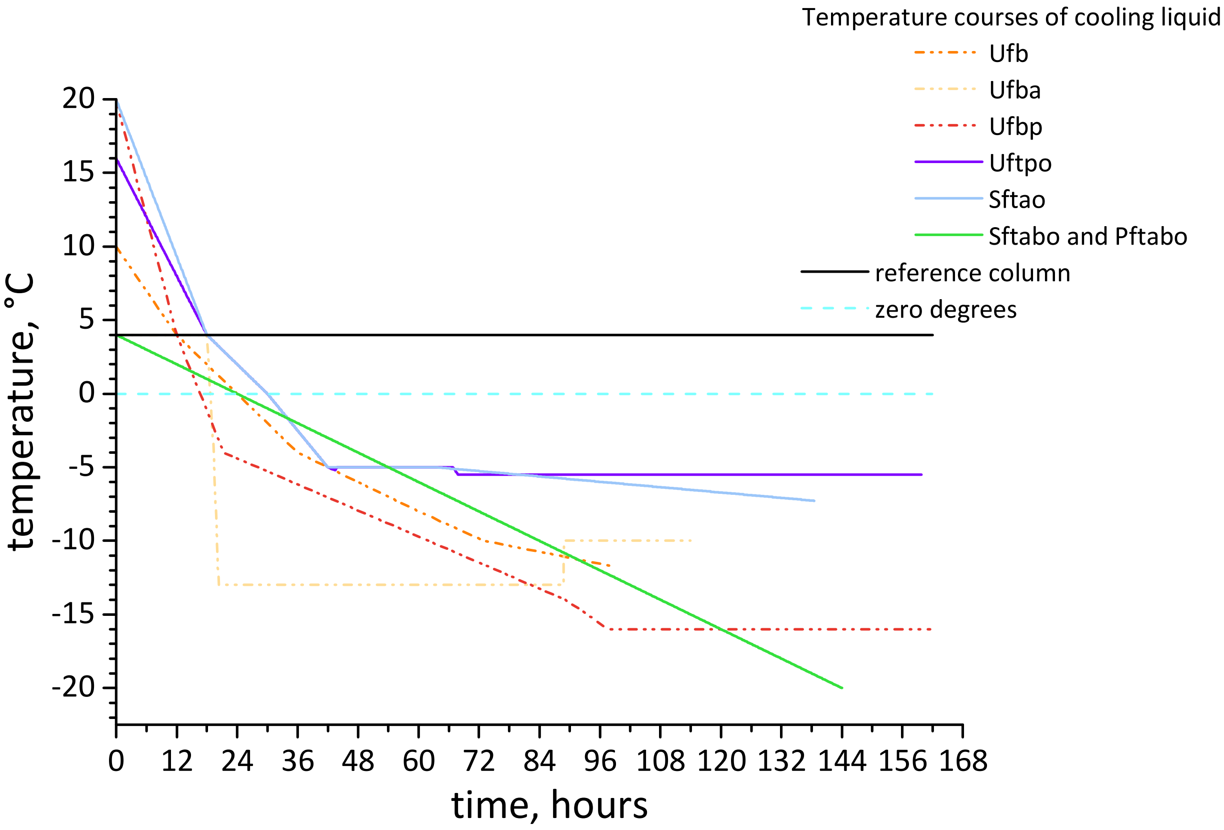

Figure 5.1 Cooling programs and duration of different experimental approaches for setup 1, with freezing from the bottom (dotted lines) and freezing from the top (continuous blue coloured lines) and setup 2 with freezing from the top (green line). Constant line at 4°C displays temperature of the reference column. See Table 3.5 for codes given in legend.

The differences of the temperature courses were obligatory due to different experimental setups and different soil materials used. The three experiments with freezing from the bottom used with setup 1 employed the lowest input temperatures, because about two thirds of the columns were frozen and the stainless steel lid was between input temperature and soil (see Figure 3.2) All experimental approaches used in conjunction with setup 1 started off with a phase of fast cooling, followed by smaller cooling rates or even static state input temperatures. The effects of the different experimental approaches will be shown and discussed in chapters 6 to 9.

Experimental approaches with bench scale laboratory columns (setup 1)

Figure 5.3 displays the water distribution after the experiment with silt and freezing from the bottom (*Ufb*). It can be seen that the continuously slow freezing from the bottom resulted in a water migration towards the freezing front, because the frozen columns show significantly different water distributions compared to the reference column. The maximum water content within all three frozen columns lay between 7.1 cm and 8.5 cm column depth and accounted for 137 % to 158 % of the initial water content. The freezing front marked a step from water contents below the starting conditions in the unfrozen zone to water contents above the starting conditions in the frozen part of the soil columns. Nevertheless the temperature differences around the freezing front were not as pronounced as between the soil layers in in the lower part of the columns. The water contents in the unfrozen column part range around half of the water content at the beginning of the experiment (starting conditions 25.8 % dw) with the lowest value being 7.2 % dw, found in the top layer of column B. This value is slightly above the wilting point of the silt loam. The results revealed that the freezing process in the closed laboratory column system had to be modified, to account for the differing boundary conditions of the laboratory system compared to the natural soil. This aspect had been taken into account for further experiments. Furthermore a stainless steel lid was invented at the bottom of the system, because two of the three experimental columns in the experiment with silt and freezing from the bottom (*Ufb*) showed water outlets at the bottom.

The input temperature from the cooling machine and the resulting temperatures in the soil cores differed, due to different thermal conductivities and heat energy losses along the way from the machine to the experimental columns. Figure 5.2 shows the temperature profiles in three different soil columns of experiment *Ufb*, at a depth of 9 cm. In this case setup 1 was used in a preliminary form without the screwed stainless steel lid at the bottom. The columns were cooled from the bottom. The soil core had direct contact with the cooled bottom plate, which resulted in maximum temperature differences between input temperature and soil temperatures in experimental columns of 2.3°C, 5.7°C and 3.2°C, respectively. The inclinations for each cooling step with constant cooling rate could be described by linear equations. Only the last cooling step, which started 72 hours after the beginning of the experiment and had with 2°C per day the smallest cooling rate within this experiment, did not result in a linear decrease of the soil temperatures in the experimental columns, but temperatures were approximately constant. This behavior increased the temperature difference between input temperature from cooling machine and soil temperatures.

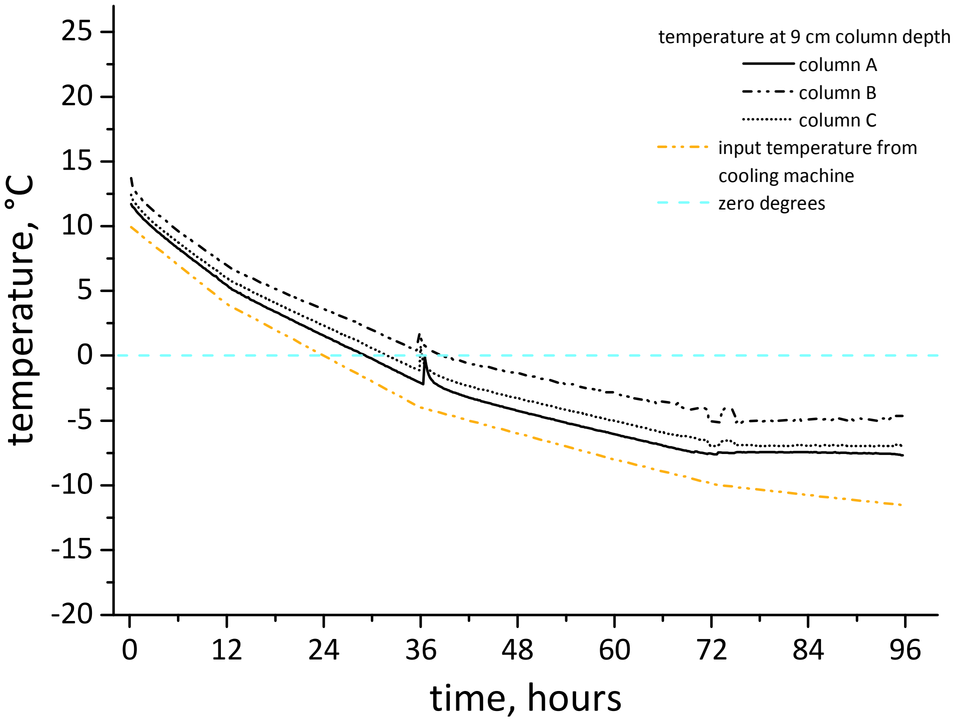

Figure 5.2 Temperature profiles for three parallel run experimental columns at a depth of 9 cm for the experiment with silt loam and freezing from the bottom (***Ufb***) without stainless steel lid at the bottom.

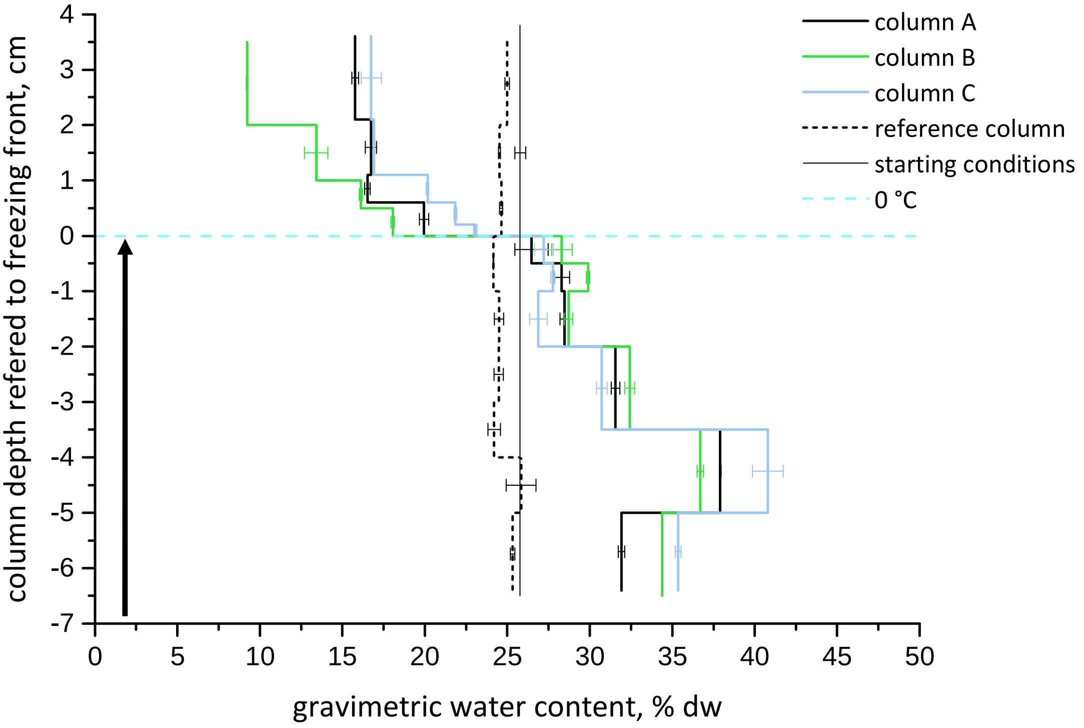

Figure 5.3 Gravimetric water content distribution for experiment with silt loam and slow freezing from the bottom (***Ufb***) in three experimental columns standardized on freezing front and the reference column with results in comparable heights. Standard error reflects n=3. Arrow marks freezing directionin the experimental columns.

The peaks after 36 hours and the irregularities after 74 hours were caused by checking the sensors and the insulation. Temperature profiles of the three experimental columns showed differences up to 2.8°C. This observation could be explained by different distances from the cooling machine to the experimental columns and therefore different cooling liquid tube length.

The temperature and TDR measurement profiles in the experimental approach used for the experiment with silt loam, freezing from the bottom and ^{14}C-pyrene (*Ufbp*) are displayed in Figure 5.4. Setup 1 was used, which included the stainless steel lid at the bottom of the columns. This provided the system with an impermeable boundary which does not interact with organic chemicals. The lid resulted in cooling energy losses, which resulted in maximum temperature differences between the input temperature from the cooling machine and the temperatures measured in the soil columns at 6.5 cm depth up to 9.8°C (see Figure 5.4).

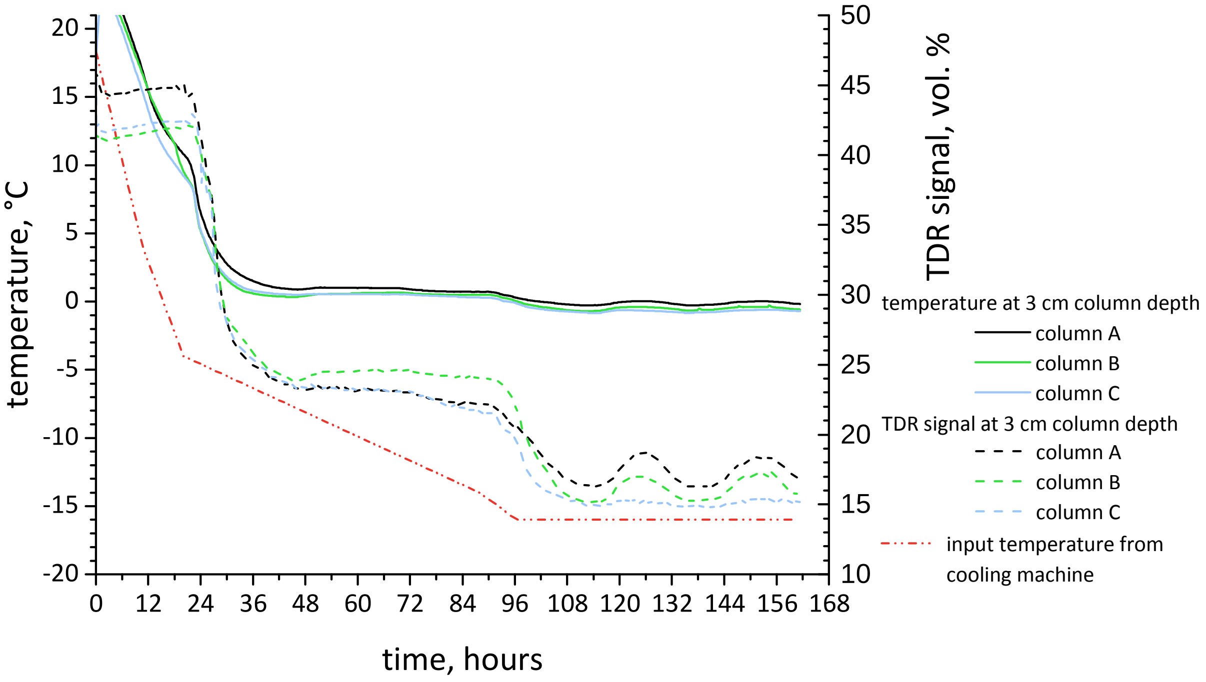

Figure 5.4 TDR (dashed lines) and temperature (lines) profiles for the three experimental at 3 cm column depth for the experiment with silt loam, freezing from the bottom and pyrene (*Ufbp*), dotted-dashed line displays input temperature from cooling machine.

The cooling in experiment *Ufbp* from the machine started with a cooling rate of 32°C day^{-1} and was slowed down to 20°C day^{-1} after 12 hours. Due to the stainless steel lid between cooling plate and soil these cooling rates result in maximum cooling rates of the soil of 25°C day^{-1} and approximately 10°C day^{-1}, respectively. About 22 hours after the start of the experiment the input cooling rate was slowed down to 3.54°C day^{-1}. The measured soil temperatures started to fall steeply and cooling rates increased. After approximately five hours they equilibrated with the incoming cooling energy. After 36 hours of the experiment they reached a relatively constant temperature level with cooling rates < 1°C per day, even though the incoming cooling energy still increased. The drop of the TDR signal after 96 hours duration of the experiment is the result of freezing front propagation and the freezing of the area around the temperature and TDR probe. This effect has been induced by an eight hours lasting, increased cooling rate of 5.5°C day^{-1}. During the last 64 hours of the experiment with steady input cooling temperatures the TDR profiles oscillated considerably. Temperature profiles showed the same effect, oscillating between 0.28°C and 0.04°C. The room temperature showed differences up to 0.6°C during the same time.

The water content distribution that resulted from the presented experimental procedure is shown in Figure 6.2. The aim of the modification of the temperature program to cause highest water contents within the soil columns just beneath the freezing front in the frozen parts of the columns has been reached in column A. In the other two experimental columns maximum water contents were found 1 cm and 2 cm beneath the freezing front within the frozen parts of the columns. That means in order to simulate the freezing process with the freezing induced water migration it is necessary to apply fairly high cooling rates at the beginning of the experiment.

The introduced freezing scenarios applied freezing from the bottom of the experimental columns. Soil materials were not contaminated with an organic contaminant phase. In the following freezing scenarios from the top with a LNAPL present will be shown.

In Figure 5.5 temperature profiles and TDR profiles of the experiment with silt loam, freezing from the top, ^{14}C-pyrene and paraffin-based crude oil Ekofisk (*Uftpo*) are displayed. It started with a fast cooling period with cooling rates of 16°C day^{-1} for the first 18 hours, followed by 10°C day^{-1} for the following 24 hours. The input temperature from the cooling machine was set on -5°C with a cooling rate of 0°C day^{-1} 42 hours after the start of the experiment. The temperatures in the experimental columns decreased continuously from the start. Five and two hours after the cooling rate had been set on 0°C the temperatures of column A and B rose for 40 minutes by 0.27°C and 0.15°C, respectively. Further drop in temperature until the constant temperatures of the second half of the experiment may be described by an exponential decay function. The pattern of the temperature profile in column C differed from the other experimental columns. Together with the cooling rate of 0°C the temperature profile of column C stabilized at about 2.5°C. Only with a decrease of input cooling temperature from -5°C to -5.5°C, 67 hours after the experiment started, and a manual regulation of the cooling liquid flow through the cooling head of the column, the temperatures showed a similar pattern as in columns A and B. However, the absolute temperature differences were higher than in the other columns. Firstly temperature decreased by 0.46°C, afterwards it decreased over a period of two hours by 0.55°C, which was followed by the final temperature decrease in form of an exponential decay. The observed temperature courses resemble the pattern of the freezing process in soils, displayed in Figure 2.2. Firstly temperatures decrease below 0°C, with the first ice crystal forming a short temperature increase goes along, which marks the start of the phase transition from water to ice. It is caused by the latent heat that is released during the phase transition process (see chapter 2.2.1).

However, absolute temperature plotted for the small temperature peaks at 3 cm column depth were 3.46°C, 3.51°C and 2.84°C for columns A-C, respectively.

Measured TDR signals of the three experimental columns started off at different levels, with values of 46 vol%, 44 vol% and 52 vol%, respectively. The course of the TDR signal during the first half of the experiment was quite turbulent in column C. However, all TDR signal courses showed a steep decrease at the time the slight temperature increases were observed. That pattern is described in chapter 2.2.2 and is very likely the proof of the phase transition from water to ice and not a result of water migration processes. However, the TDR signal in column A does not decrease as far as the TDR signals from the other two experimental columns. Within the last 40 hours of the experiment the TDR signal even increases again.

The reason for the observation of the phenomena of the freezing process at absolute temperatures above 0°C can be explained in conjunction with final freezing front and the position of the probes. The final freezing front in columns A-C, resulting from the constant temperatures in the second half of the experiment was found in 3.0 cm, 3.1 cm and 3.1 cm column depth, respectively. That means the temperature and TDR probe in column A were situated directly at the freezing front, whereas the probes in columns B and C were within the frozen part of the columns. That observation provides evidence that the temperatures measured in column B and C during the second half of the experiment must have been below 0°C.

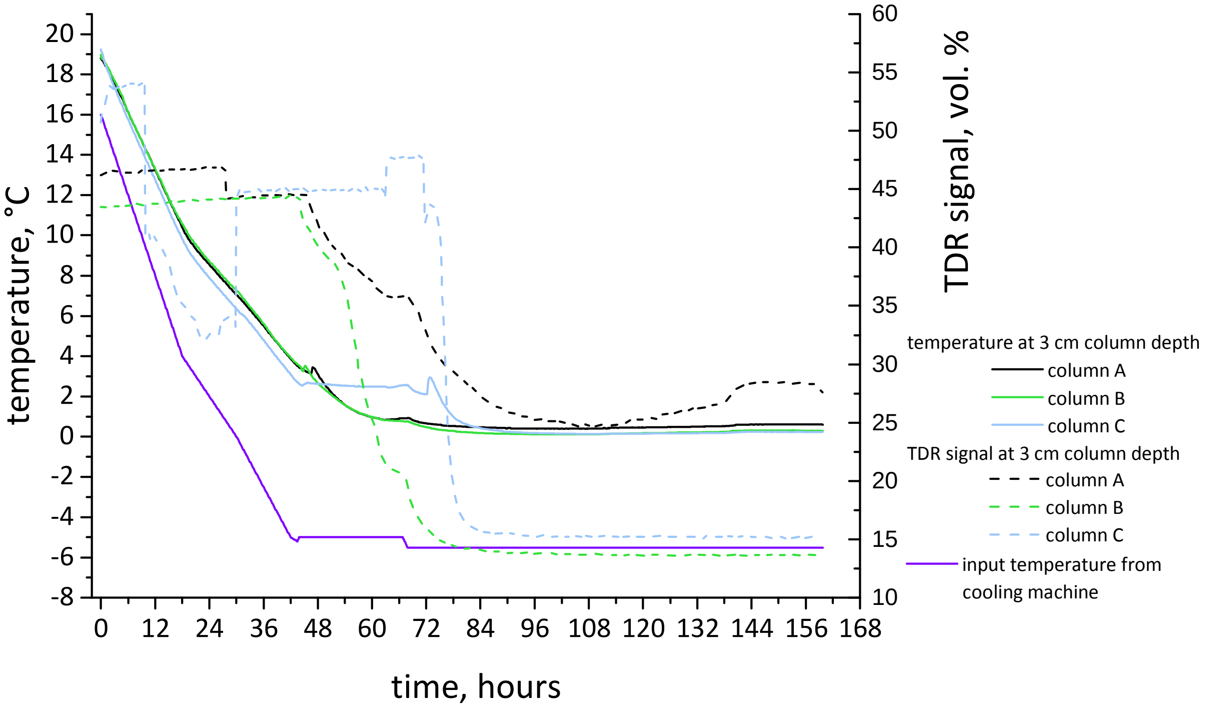

Figure 5.5 **TDR (dashed lines) and temperature (lines) profiles for the three experimental columns at 3 cm column depth for the experiment with silt loam, freezing from the top, ^{14}C-pyrene and paraffin-based crude oil Ekofisk (*Uftpo*), dark grey line displays input temperature from cooling machine.**

Measured temperature values from 88 to 160 hours experiment duration were between 0.11°C and 0.29°C in columns B and C. That means the measurement error was at least 0.30°C. For column A temperatures during the second half of the experiment ranged between 0.49°C and 0.61°C

The water distribution within the experimental columns obtained from this experimental procedure are shown in Figure 7.1 and described there. Main results were that freezing induced water migration has been observed, as well as the formation of segregation ice. The latter could only be proved for columns B and C.

In Figure 5.6 temperature profiles and TDR signals for all three experimental columns and input temperature from cooling machine for the experiment with sand, freezing from the top, ^{14}C-anthracen and paraffin-based crude oil Ekofisk (*Sftao*) are shown. The cooling started off with a rate of 16°C day^{-1}, was then slightly slowed down and brought to 0°C 40 hours after the experiment had started. With this event temperatures in columns A and B decrease steeper than before, whereas temperatures in column C seemed to equilibrate. The divergence of the temperature profiles was stopped with a manual adjustment of the cooling liquid flux through the cooling head of column C, 48 hours after the experiment had started. The event in change of input cooling rate 40 hours after the experiment started is also reflected in the TDR signals displayed as dashed lines in Figure 5.6.

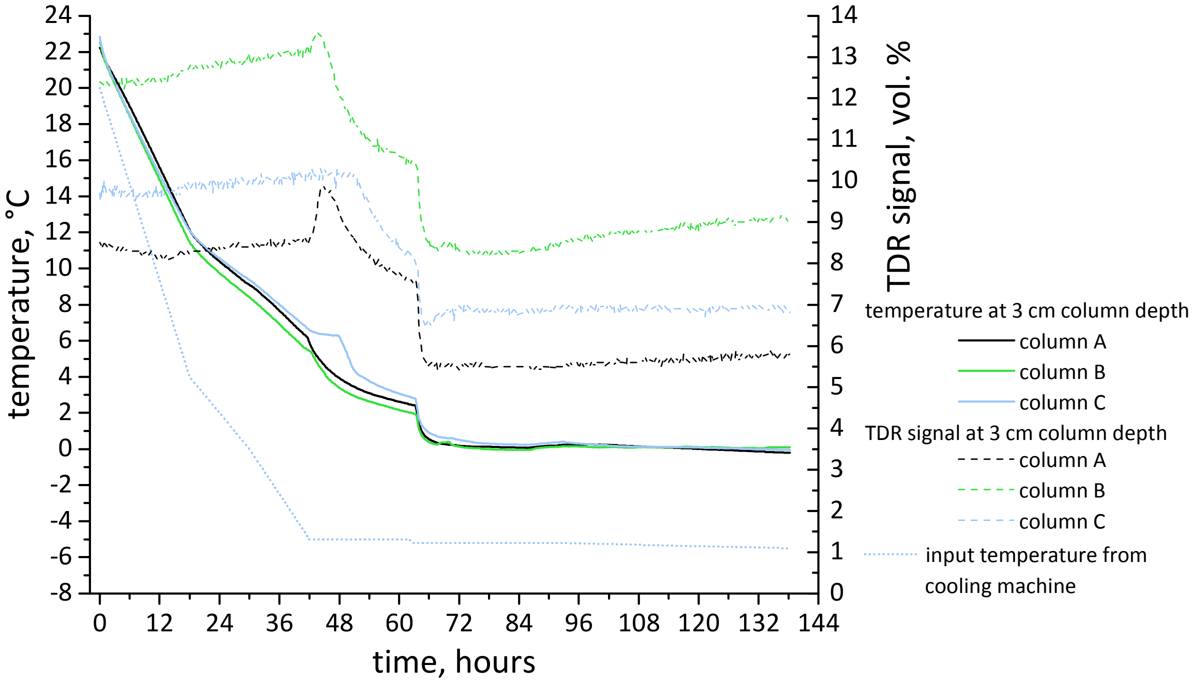

Figure 5.6 TDR (dashed lines) and temperature (lines) profiles for the three experimental columns at 3 cm column depth for the experiment with sand, freezing from the top, ^{14}C-anthracen and paraffin-based crude oil Ekofisk (*Sftao*), dotted line displays input temperature from cooling machine.

In columns A and B a distinct increase of the TDR signal was observed, before values started to fall. That indicates that water contents increased in 3 cm column depth. In column C the increase was not as pronounced as in the other two columns, but together with the adjustment of cooling liquid flux and the along going temperature drop 48 hours after the experiment started, TDR signals decrease steeply, like it was observed before for the other two experimental columns. As temperature and TDR measurements revealed that the freezing front had not reached 3 cm column depth 63 hours after the experiment started, the input temperature was brought from -5.0°C to -5.2°C within half an hour. This led to steep decreases in temperatures, starting at values of 2.41°C, 1.80 C and 2.83°C in the three columns A-C and nearly vertical decreases of the TDR signals in all experimental columns. Thirty hours later the cooling rate was adjusted from 0°C day^{-1} to 0.15°C day^{-1}. This led to slightly decreasing temperatures and slightly increasing TDR signals in the experimental columns. The temperatures in the experimental columns A and C measured slightly negative temperatures (-0.21°C and -0.05°C, respectively) by the end of the experiment.

The detected freezing fronts at the end of the experiment at 4.0 cm and 3.9 cm column depth revealed that the soil at 3 cm column depth, the position of the probes, must have been frozen before. This observation supports the statement that the temperature probes systematically measured too high temperatures values. The TDR signals start off at different water contents with values for column A-C of 8.45 vol%, 12.40 vol% and 9.60 vol%, respectively. At the end of the experiment the relation of the differences was almost the same.

A comparison of the presented freezing scenarios and the resulting temperature and water distribution patterns within the experimental columns reveal the following results:

- Constantly low freezing rates, as used in experiment *Ufb* (1.17 °C day^{-1} decreasing to 0.08°C day^{-1}) led to maximum water contents in the lowest column part. Differences in water content beneath and above the freezing front were significant, but not very pronounced.
- The temperature probes used showed a systematic measurement error of at least 0.3°C. However, the freezing process, observed by the nearly vertical decrease in TDR signals in experiment Sftao, was initiated at 2.41°C, 1.80°C and 2.83°C within the three experimental columns A-C, respectively. Therefore the measurement error more likely had a value of approximately 2°C.
- The experimental approach used for the experiment *Ufbp,* could induce the formation of segregation ice, but there was still a lot of water frozen in the lower parts of the columns, which was not available any more for the formation of segregation ice at the freezing front.
- The phase transition from water to ice could be observed best in column C of the experiment *Uftpo*, because temperatures had equilibrated just above 0°C (actual temperature, not measured temperature), before they fell below 0°C and rose again upon the first ice formation. The TDR signal emphasized this process, because it firstly increased, and then dropped nearly vertically after the described peak of the temperature.
- The process of ice segregation might be disturbed, if the freezing front is situated directly at the depth of the temperature probes, like it was observed in column A of experiment *Uftpo*.

- The freezing process used with the experiment *Sftao* showed the formation of segregation ice best, as maximum water contents within the experimental columns were found just above the freezing front in the frozen part of the columns and reached saturation level in column C.

Experimental approach with large laboratory columns (setup 2)

The columns of setup 2 were 40 cm high and had an inner diameter of 9.4 cm (see Figure 3.3). The freezing scenario was determined by an input cooling rate of 4°C day^{-1} (see Table 5.2). Temperatures were measured with 4-wire temperature probes of the type pt 100 and the soil materials used were sand and peat (see chapter 3.2.3).

The temperature and TDR profiles in three different depths of experimental column A of the experiment with sand, freezing from the top, anthracene, benzo[a]pyrene and the naphthene-based crude oil Gryphon (*Sftabo*) are shown in Figure 5.7. Within the first six hours of the experiment the soil temperatures in the columns equilibrated. Afterwards they were nearly constant on levels between 2°C and 4°C, according to column depth, for 18 hours. When the input temperature started to be negative, the temperatures in the different column depths started to fall. From that point on the cooling input resulted in linear decreasing soil temperatures which were fitted to the linear equations given in Table 5.2 for the specific column depths. It can be seen that all gradients were smaller than the gradient of the equation of the input temperature, with the smallest being the one for the temperature decrease as 23.7 cm column depth. Furthermore the average cooling rates are within the range that would theoretically allow for water migration and solute rejection processes during ice formation of 2.95 ± 0.25°C day^{-1} and 4 ± 1°C day $^{-1}$ suggested by Konrad and McCammon (1990) and Konrad and Seto (1991), respectively. The freezing front proceeded during the whole time of the experiment.

Table 5.2 Cooling of a 40 cm high soil column filled with sand and frozen from the top, linear adjustment for the area between 24 and 144 hours of the experiment.

column depth, cm	linear fit for temperature decrease and equation for cooling machine	Person's r for linear fit	average cooling rate, °C day^{-1}	temperature after 144 hours, °C
1.1	$y = -0.1026x + 4.11$	-0.9994	2.47	-10.74
12.3	$\boldsymbol{y = -0.0525 + 4.55}$	-0.9993	0.67	-3.11
23.7	$y = -0.0266x + 4.31$	-0.9982	0.53	0.82
Cooling machine	$y = -0.1666x + 4.00$		4.00	-20.00

Average cooling rates within the soil columns decreased with depth (see Table 5.2). The soil column at 1.1 cm column depth was frozen 43 hours after the experiment had started. A detail of the temperature and TDR profile at 1.1 cm column depth displays the freezing process, as described in chapter 2.2.1 with freezing point depression and super cooling below 0°C and a short temperature rise as the first ice nuclei forms, very well (see Figure 5.8).

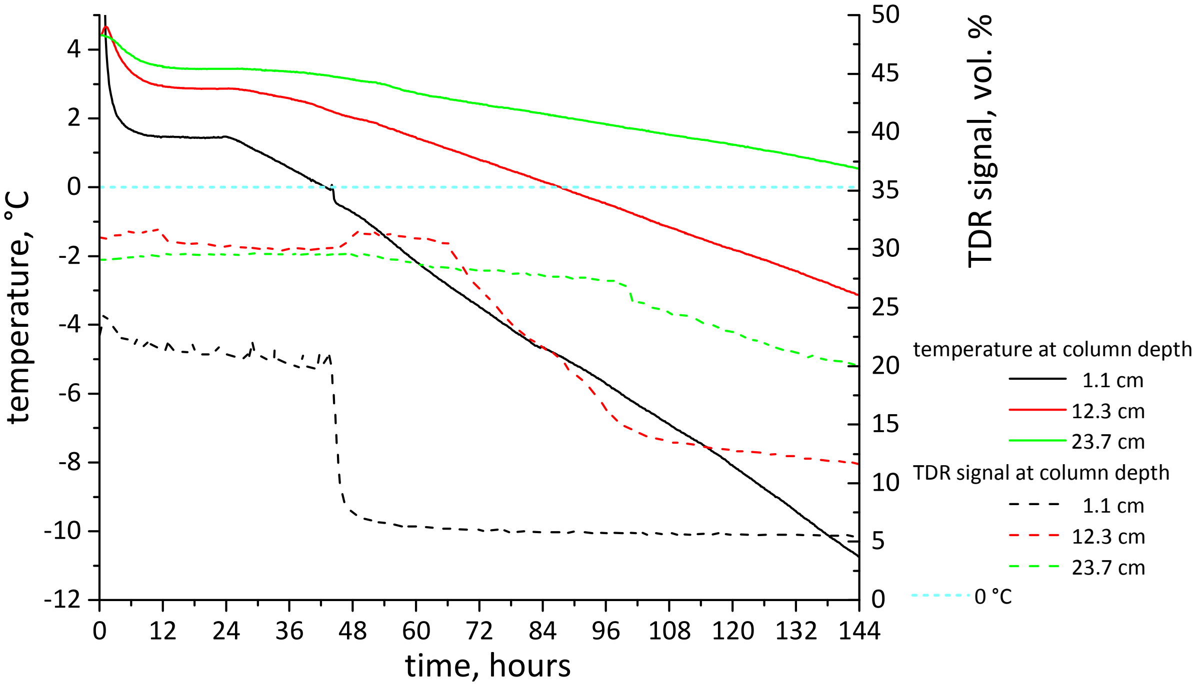

Figure 5.7 Temperature and TDR profiles in three different depths of experimental column A for the experiment Sftabo conducted with setup 2 (40 cm high columns), lines display temperature profiles and dashed lines display profiles of TDR signals at 1.1 cm (black), 12.3 cm (dark grey) and 23.7 cm (light grey) column depth.

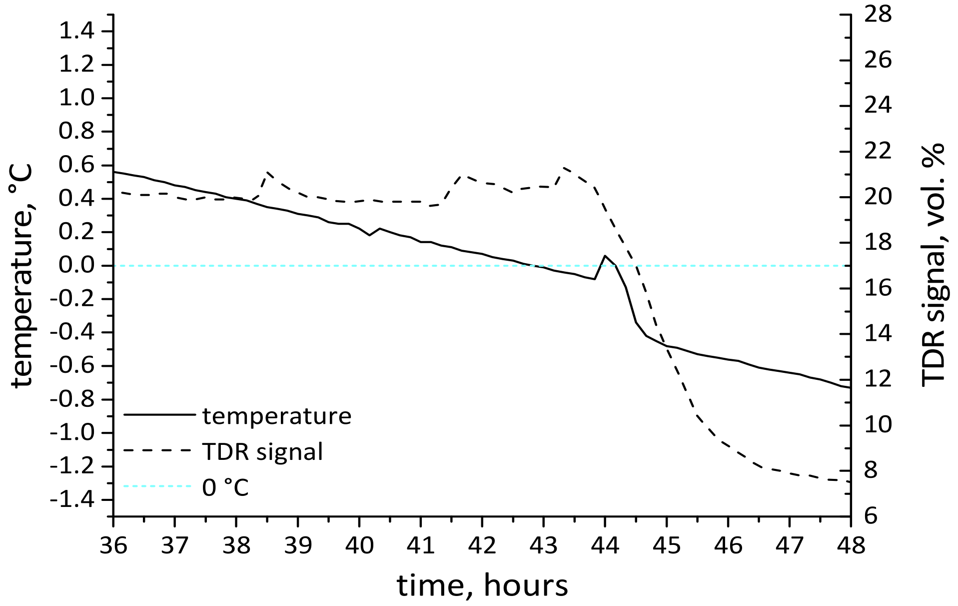

Figure 5.8 Detail of temperature and TDR profile at 1.1 cm column depth for experiment *Sftabo*, line displays temperature profile and dashed line displays TDR profile. Zero degrees are marked with the grey dashed line.

The temperatures decreased below 0°C for 60 minutes and reached -0.08°C. After that temperatures increased by 0.14°C. The duration of this temperature increase is determined by the 10-minutes measurement interval to be between 20 and 40 minutes. TDR signal started to decrease slightly, as temperatures fell below 0°C. However, the almost vertical drop of the TDR signal was initiated with the observed temperature peak that marked the ice formation. Temperature and TDR profile in 12.3 cm column depth did neither show the distinct freezing pattern when temperatures fell below 0°C, nor the nearly vertical decrease of the TDR signal, which would be expected around this event. At 23.7 cm column depth the soil remained unfrozen throughout the whole time of the experiment. The final freezing front was detected at 18 cm column depth. Temperature and TDR profiles of the experimental column B were similar to those presented here.

The water distribution resulting from the presented experimental procedure is shown in Figure 7.12. The constant input freezing rate which resulted in linearly decreasing temperatures within the experimental columns induced maximum differences in water content of only 3.2 % dw. The freezing induced water migration process might be seen as a trend, because water contents in the experimental columns below the freezing front were significantly lower than water contents above the freezing front. Compared to the experimental approach used with experiment *Sftao*, which had a phase of steady state temperatures, followed by cooling rates of 0,006°C day^{-1}, the freezing scenario with continuously forwarding freezing front, could only induce minor redistribution of water.

In Figure 5.9 the temperature und TDR profiles in three different depth for column A of the experiment with peat, freezing from the top, anthracene, benzo[a]pyrene and the naphthene-based crude oil Gryphon (Pftabo) are displayed. Cooling rates were generally a little bit smaller than in the experiment with sand, as can be taken from Table 5.3 and Table 5.2. The experiment ran longer than the experiment *Sftabo* and the final input cooling temperature was -24°C. It can be seen that the temperature at 1.1 cm column depth reached 0°C after 43 hours and 40 minutes. Figure 5.10 shows the temperature and TDR profile at 1.1 cm column depth in detail between 42 and 64 hours experiment duration. A similar pattern of both profiles compared to the profiles at 1.1 cm column depth in experiment *Sftabo* was observed, but duration was different. The temperature decreased for 11 hours and 50 minutes from 0°C down to -1.03°C. The following abrupt temperature increase accounted for 1.30°C and lasted as long as the temperature increase during the freezing event observed in experiment *Sftabo*, namely between 20 and 40 minutes. At 12.3 cm column depth temperature fell below 0°C after 126 hours and 50 minutes experiment duration. The course of the temperature profile did not show any distinct fluctuations, as described for 1.1 cm column depth. However, TDR signal showed a steep decrease short before temperature fell below °C and a vertical increase, as temperature fell below 0°C. At 3 hours and 10 minutes after this event, the TDR signal decreases vertically beneath a value of 20 vol%. This behavior indicates the phase transition from water to ice. The peat remained unfrozen throughout the whole experiment in 23.7 cm column depth. Temperatures after 144 hours experiment duration, which equals the duration of experiment Sftabo were nearly the same for both experiments at 1.1 cm column depth, but differed significantly in 12.3 cm and 23.7 cm column depth. The final freezing front, determined during sampling was situated at 13 cm column depth in the experiment with peat. The pattern of temperature and TDR signal profiles in the experimental column B were similar to those presented here. Data on water content distribution at the end of the freezing experiment are not available.

Table 5.3 Cooling of a 40 cm high soil column filled with peat and frozen from the top, linear adjustment for the area between 45 and 160 hours of the experiment. For 12.3 cm column depth linear fit was applied only between 100 to 160 hours in order to reach a Person's r greater than -0.99.

column depth, cm	linear fit for temperature decrease and equation for cooling machine	Person's r for linear fit	average cooling rate, °C day^{-1}	temp. after 144 hours, °C	temp. after 168 hours, °C
1.1	$y = -0.1069x + 4{,}95$	-0.9996	2.42	-10.52	-13.13
12.3	$y = -0.0790x + 4{,}83$	-0.9966	0.39	-1.6	-3.36
21.7	$y = -0.0117x + 3.92$	-0.9943	0.25	2.20	1.83

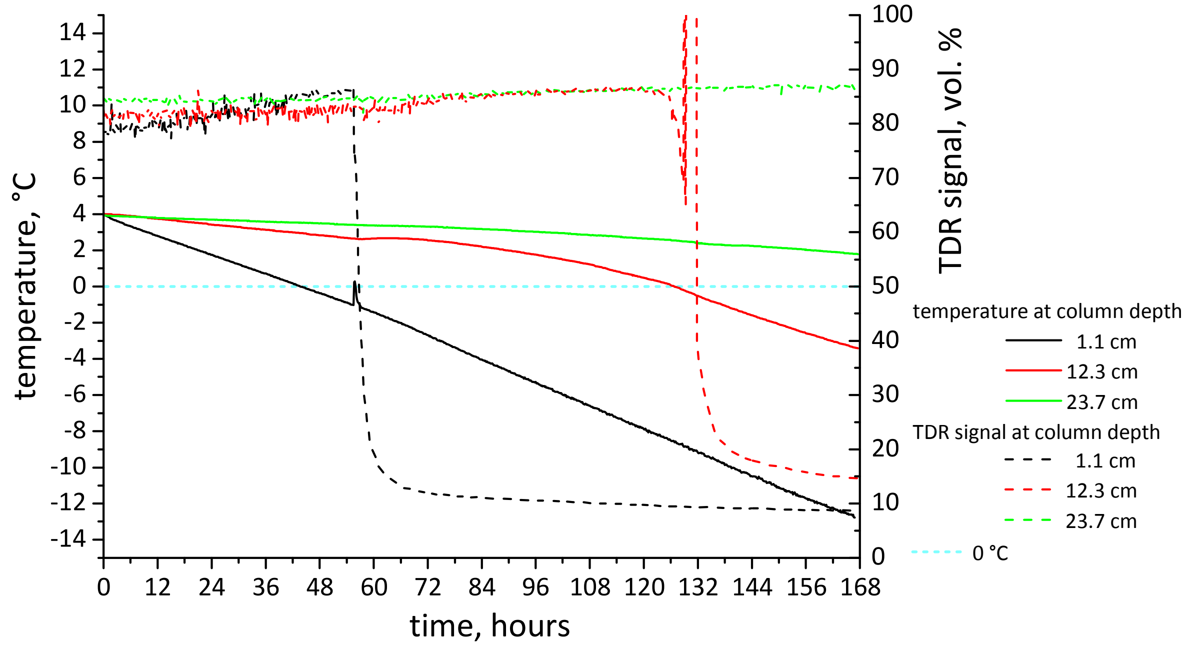

Figure 5.9 Temperature and TDR profiles in three different depths of experimental column A for the experiment with peat, freezing from the top, anthracene, benzo[a]pyrene and the naphthene-based crude oil Gryophon (Pftabo), conducted with setup 2 (40 cm high columns), lines display temperature profiles and dashed lines display profiles of TDR signals at 1.1 cm (black), 12.3 cm (g) and 23.7 cm (light grey) column depth.

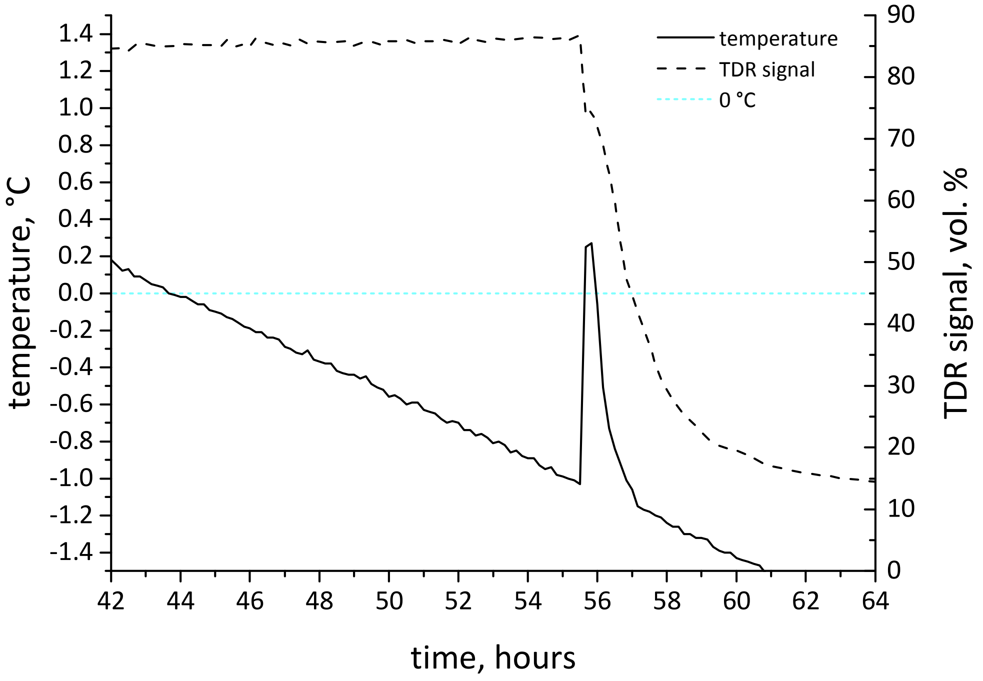

Figure 5.10 Detail of temperature and TDR profile at 1.1 cm column depth for experiment *Pftabo*

The findings according to the aim to simulate a naturally occurring freezing process using homogeneous, 40 cm high soil columns are as follows:

- One-dimensional freezing of the soil columns using naturally occurring freezing rates was achieved up to 18 cm for sand and 13 cm for peat.
- Cooling rates in peat were 0.05°C to 0.28°C lower than in sand. The time lag for the temperature in the uppermost soil layer to fall below 0°C between sand and peat only accounted for 40 minutes. But the time needed to reach the equilibrium freezing point differed considerably between the two materials and was twelve times longer in peat than in sand.
- The equilibrium freezing point for sand with 12.9 % dw water content was at -0.08°C, for peat with a water content of 480 % dw it was at -1.03°C.
- The process of latent heat release caused a temperature increase within the soil of 0.14°C in sand and 1.30°C in peat. The duration of the process until temperatures started to fall again was in both materials 20 to 40 minutes.
- The freezing process with equilibrium freezing point and the phase transition process of water had been shown clearly in the uppermost part of the soil columns for both materials. In deeper soil layers the process could only partially be displayed by the temperature and TDR measurements.
- Even though freezing had been simulated well, the resulting water distribution in the sand reveals that the process could only induce minor water migration processes. A distinct increase in water content within the frozen zone at the final freezing front was not observed.

6. RESULTS ON THE INFLUENCE OF THE FREEZING PROCESS ON PAH DISTRIBUTION IN SOILS

If temperatures in soils fall below the equilibrium freezing point and ice formation is initiated considerable water redistribution processes within the soil may take place (see chapter 2.2). To now, it is not known how these redistribution processes influence the behavior of hydrophobic organic compounds in the soil. To investigate the interaction of freezing process and contaminant behavior experimental setup 1 (see chapter 3.2.3) was used to conduct laboratory experiments. As the freezing induced water movement in soils is most pronounced in silty soils (see chapter 2.2) the silt loam described in chapter 4.2 was chosen to conduct the experiments. As the present studies focus on PAHs, two compounds with different properties were chosen, the 3-ring PAH anthracene and the 4-ring PAH pyrene (see Table 2.3). Especially their differences in hydrophobicity (log K_{ow}) and water solubility suggest differing results concerning their behavior in conjunction with freezing induced water migration processes in the soil. As the interaction of water and hydrophobic compounds is generally limited, effects may be small. Therefore the decision fell for the use of ^{14}C-labeled PAHs, because their chemical analysis is far more sensitive and involves much lower standard errors than the analysis of non-labeled chemicals (see chapter 3.2.4). Furthermore it is possible to get a complete mass balance of the chemicals used and therefore also the fraction of bound residues may be determined (Eschenbach, 1995). Adjustment of water content, contaminant content and column preparation were conducted as described in chapter 3.2. For the experiments 8.2 cm of the columns were filled with uncontaminated material and 2.0 cm were filled with material contaminated with ^{14}C-anthracene and ^{14}C-pyrene, respectively (see Table 3.5). The freezing process was initiated from the bottom to induce a water migration process from the contaminated part of the soil columns towards the stable freezing front of the last cooling period. The position of the stable freezing front should be at 3 cm column depth. Therefore approx. 1 cm uncontaminated soil lay between the contaminated soil and the freezing front. The duration of the experiment with ^{14}C-anthracene (*Ufba*) was 113 h with a steady state temperature period at the end of the experiment of 92 hours. The experiment with ^{14}C-pyrene (*Ufbp*) lasted 160 hours with a steady state period of 64 hours at the end (see Figure 5.1).

6.1 FREEZING PROCESS AND WATER DISTRIBUTION

The experimental setup and procedure for the experiment with silt loam, contaminated with anthracene and ^{14}C-anthracene in the upper 2 cm of the experimental columns and freezing from the bottom (*Ufba*) resulted in the water distribution shown in Figure 6.1. The starting conditions of the material were 26.23 % dw and 26.66 % dw in the contaminated and the uncontaminated soil material, respectively. The water contents of the reference column, which rested at 4°C for the duration of the experiment, ranges around these values. In the lower part of the reference column the water content differs up to 2.3 % dw from the initial water content, which is significantly (see Table A.6). The water contents in the experimental columns differed significantly from the starting conditions except for one soil layer in column A and two soil layers in column C. Maximum water contents were encountered at the bottom of the columns, within the frozen soil. The value of column B is the highest and lay one quarter above the starting conditions. Just above the freezing front water contents of all experimental columns were reduced compared to the frozen soil layer just beneath the freezing front. In the upper three centimeters of the experimental columns water contents were about one quarter lower than at the beginning of the experiment.

The water distribution patterns shown in Figure 6.1 may be explained by the temperature courses within the experimental columns (see Figure A.1).

The aim to simulate freezing induced water migration within the experimental columns has been reached, because water contents in the upper and lower parts of the experimental columns differ significantly from the water contents within the reference column and maximum water contents were encountered within the frozen parts of the columns. However, the formation of segregated ice in soil layers just beneath the freezing front, which would be determined by particularly high water contents in these layers, was not pronounced.

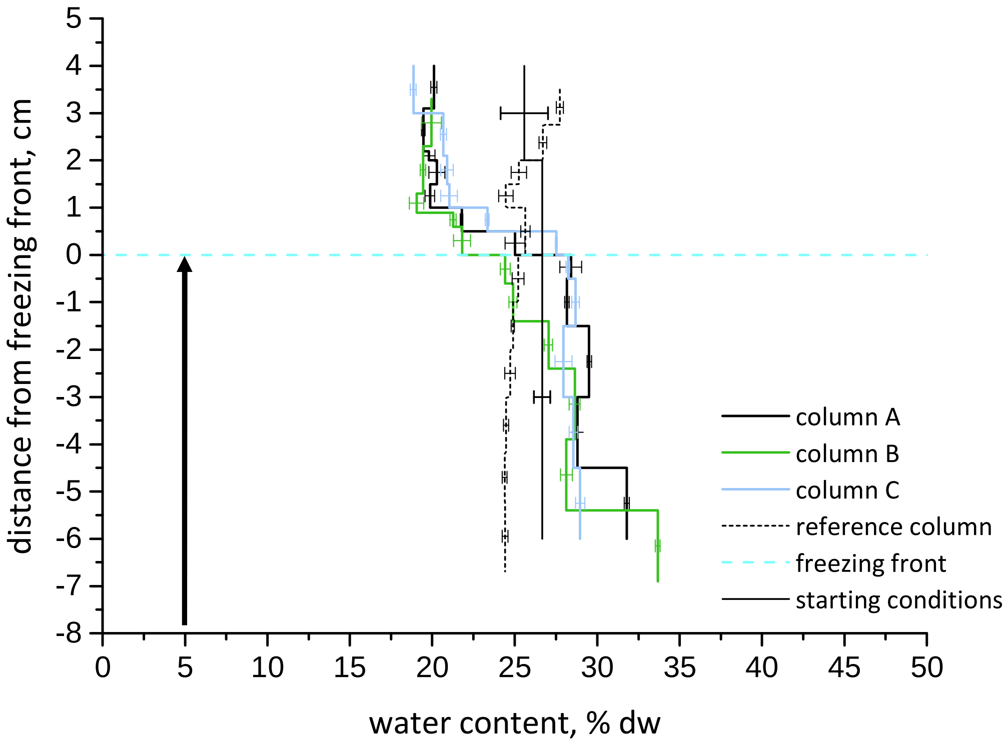

Figure 6.1 **Gravimetric water content distribution for experiment with silt loam, freezing from the bottom and ^{14}C-anthracene (*Ufba*), standard error reflects n=3, arrow marks freezing direction.**

In contrast the water contents in the experimental columns of the experiment with silt loam contaminated with ^{14}C-pyrene and freezing from the bottom (*Ufbp*) reached their maxima in the middle of the soil columns, just beneath (column A) or close to (columns B and C) the freezing front, within the frozen column parts. Minimum water contents were measured in the uppermost layer of all experimental columns.

Furthermore the water contents in the unfrozen parts of the columns were significantly lower than the water contents at the beginning of the experiment, except one sample in column B and one in column C. In the frozen part all experimental columns show high water contents ranging around 30 % dw, which was significantly more than at the beginning of the experiment.

Like for experiment *Ufba* the freezing induced water migration could be simulated, because nearly all water contents in the frozen and the unfrozen parts of the columns differed significantly from the starting conditions.

The maximum water content of column A just beneath the freezing front is an indicator for the process of segregated ice formation. According to the water distributions it can be stated that the freezing scenario of experiment *Ufbp* is more suitable to simulate the processes of freezing induced water migration and segregated ice formation in an experimental setup in the laboratory than the one used in experiment *Ufba*.

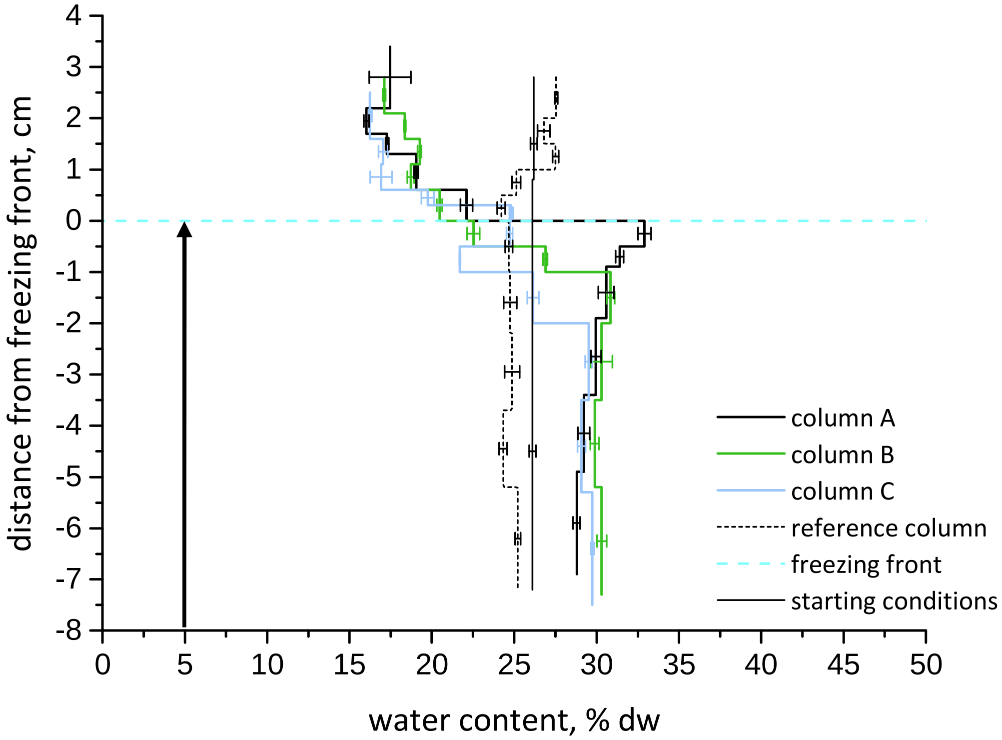

Figure 6.2 Gravimetric water content distribution for experiment with silt loam, freezing from the bottom and ^{14}C-pyrene (*Ufbp*), standard error reflects n≥3, arrow marks freezing direction.

6.2 DISTRIBUTION OF ^{14}C-ANTHRACENE AND ^{14}C-PYRENE

The distribution of the ^{14}C-anthracene activity in the three experimental columns A – C of the experiment with silt loam, freezing from the bottom and ^{14}C-anthracene compared with results from the reference column and the starting conditions is shown in Figure 6.3 . It can be seen that the ^{14}C-activity in the reference column decreased from the top towards the contamination boundary. Just above the contamination boundary ^{14}C-activity decreased in a huge step from 20600 dpm g^{-1} dw to 5800 dpm g^{-1} dw. An explanation for this decrease may be the sampling procedure. As the whole reference column was not frozen and water contents are quite high, the stability of the soil core itself is not very high. Therefore it may suffer deformation during the pushing out of the PVDF column. Additionally the pressure of the knife, slicing the samples, led to deformation of the soil core and therefore also to a deformation of the contamination boundary. As the ^{14}C-activity is given per gram dry weight, it is assumed that the lowest contaminated sample includes parts of the uncontaminated soil layer from beneath. The experimental columns all had their maximum ^{14}C-activity in the uppermost sampling layer. For columns A and B these data did not differ significantly from the starting conditions (see Table A.6). But for column C the maximum ^{14}C-activity was significantly lower than at the beginning of the experiment. For the second sampled layer, which represented the last sample within the contaminated part of each column, ^{14}C-activities for columns A and C were around 15300 dpm g^{-1} dw and for column B 17656 dpm g^{-1} dw. These ^{14}C-activities were significantly lower compared to the initial ^{14}C-activity. But as well as for the reference column it can be assumed that the samples might have been “diluted” by uncontaminated material from beneath the contamination boundary.

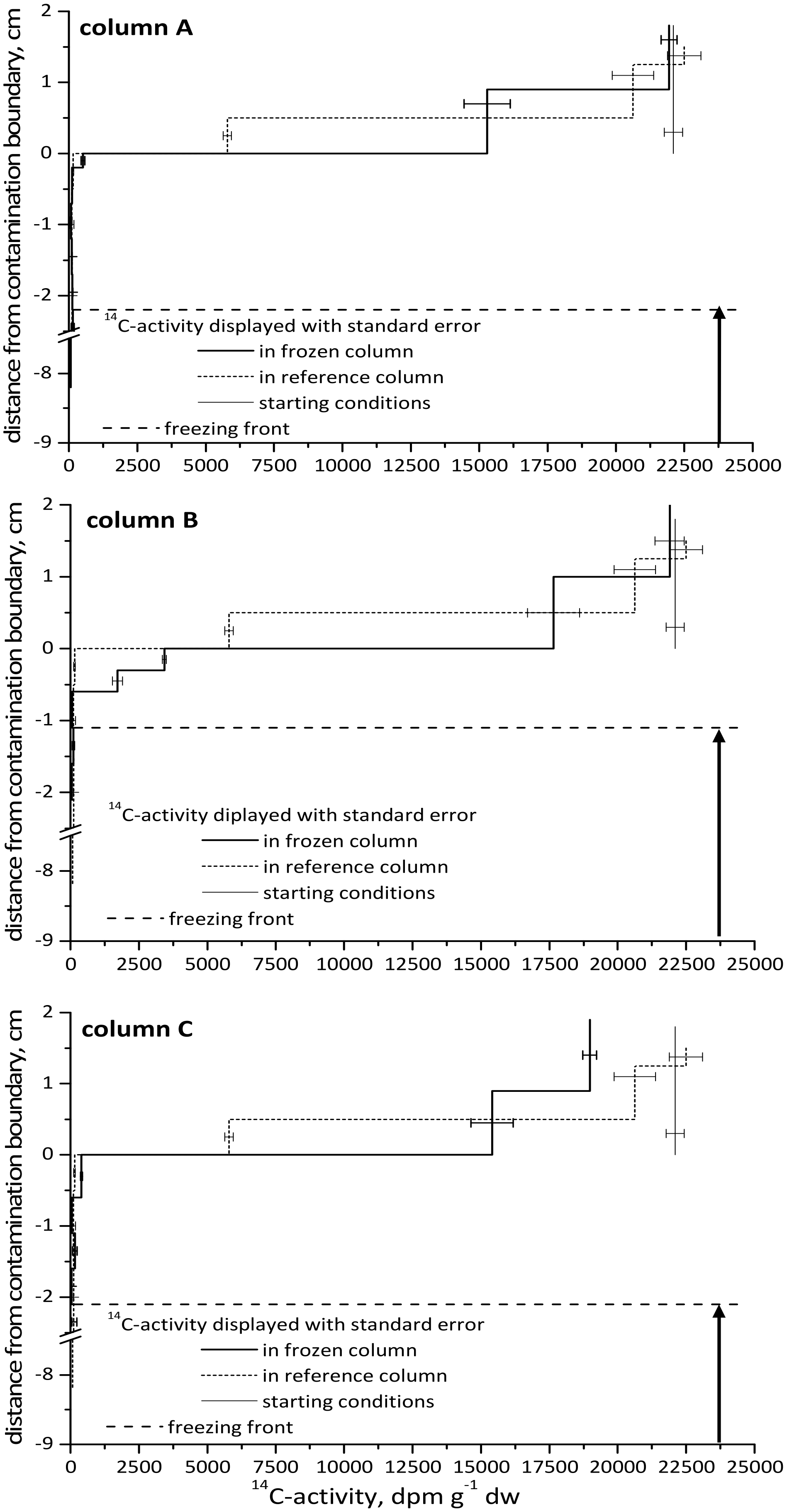

Figure 6.3 **Distribution of ^{14}C-activity in the three experimental columns (A-C) of the experiment *Ufba*, standard error reflects n≥3, arrow marks freezing direction.**

That the dilution effect was not as pronounced as in the reference column, absolute activities lay about 10000 dpm g^{-1} dw and 12000 dpm g^{-1} dw above the ones found in the reference column, can be explained by the sample thickness and lower water contents in these parts of the experimental columns (see Table A.6). Samples thicknesses were 0.9 cm in columns A and C, 1.0 cm in column B and 0.5 cm in the reference column. The ^{14}C-anthracene activity beneath the contamination boundary in columns A and C was 515 dpm g^{-1} dw and 403 dpm g^{-1} dw, respectively. These values corresponded to approximately four times of the mean ^{14}C-activity (116 dpm g^{-1} dw) in the frozen, uncontaminated part of the experimental columns. Column B showed a significant increase in ^{14}C-activity below the initial contamination boundary compared to ^{14}C-activity of the material at the beginning of the experiment (11.1 dpm g^{-1} dw), as well as compared to the detection limit of the scintillation counter (111 dpm g^{-1} dw). The first two samples beneath the contamination boundary with a thickness of 0.3 cm each, had ^{14}C-activities of 3428 dpm g^{-1} dw and 1711 dpm g^{-1} dw, respectively. These amounts represented ten to 30 times the ^{14}C-activity of the mean of the frozen, uncontaminated parts of the experimental columns. The differences in ^{14}C-activities between the three experimental columns may be explained by the position of the freezing front and the water distributions throughout the soil columns. For columns A and C the distance between freezing front and contamination boundary was 2.2 cm and 1.5 cm, respectively. In column B the freezing front was encountered 1.3 cm beneath the contamination boundary. The water contents in the soil layers of column B, which were described in chapter 6.1 decreased more smoothly over the column profile and did not show a pronounced step at the freezing front, like columns A and C did. In summary it can be said, that significantly higher ^{14}C-activities were encountered beneath the contamination boundary in the uncontaminated parts of the experimental columns. These account for 2.3 % and 1.8 % of the initial ^{14}C-activity of the contaminated material in columns A and C, respectively. In column B the encountered ^{14}C-activity in the 0.3 cm thick layer beneath the contamination boundary accounted for 15.5 % of the initial ^{14}C-activity of the contaminated material. In the following 0.3 cm still 7.7 % of the initial ^{14}C-activity was encountered. However, it is not clear how much of the ^{14}C-activity measured in the uncontaminated part of the soil columns may be the result of material mixing during the sampling procedure, like it had been observed for the ^{14}C-activity in the reference column.

The distribution of the ^{14}C-activities in the experiment with silt loam, freezing from the bottom and ^{14}C-pyrene (*Ufbp*) is shown in Figure 6.4. The ^{14}C-activity within the upper contaminated part of the reference column did not vary significantly from the starting conditions (see Table A.7). However, in the lowermost sample in the contaminated part of the reference column ^{14}C-activity only reached 91 % of the initial ^{14}C-activity. The ^{14}C-activity beneath the contamination boundary was with 3393 dpm g^{-1} dw significantly higher than the ^{14}C-activity of the material at the beginning of the experiment. That was different compared to the experiment with ^{14}C-anthracene (*Ufba*), where no significant ^{14}C-activity could be encountered in the uncontaminated part of the reference column. The experimental columns B and C showed a similar behavior, with the results of column B having the same course as the ones of the reference column. The ^{14}C-activity above the contamination boundary in columns B and C was 21808 dpm g^{-1} dw and 18154 dpm g^{-1} dw, respectively, which was significantly less ^{14}C-activity compared to the ^{14}C-activity of the material at the beginning of the experiment . Beneath the contamination boundary ^{14}C-activites still reached 3704 dpm g^{-1} dw in column B and 3588 dpm g^{-1} dw in column C. Further down in the soil profiles values did not exceed 40 dpm g^{-1} dw. The ^{14}C-activities in column A decreased continuously from the top towards the contamination boundary and further downwards. All values in the contaminated part and the soil layer directly beneath the contamination boundary varied significantly from the initial ^{14}C-activity. However, the value just below the contamination boundary was with 830 dpm g^{-1} dw much lower than in columns B and C. Within the deeper parts of column A ^{14}C-activities did not exceed 70 dpm g^{-1} dw.

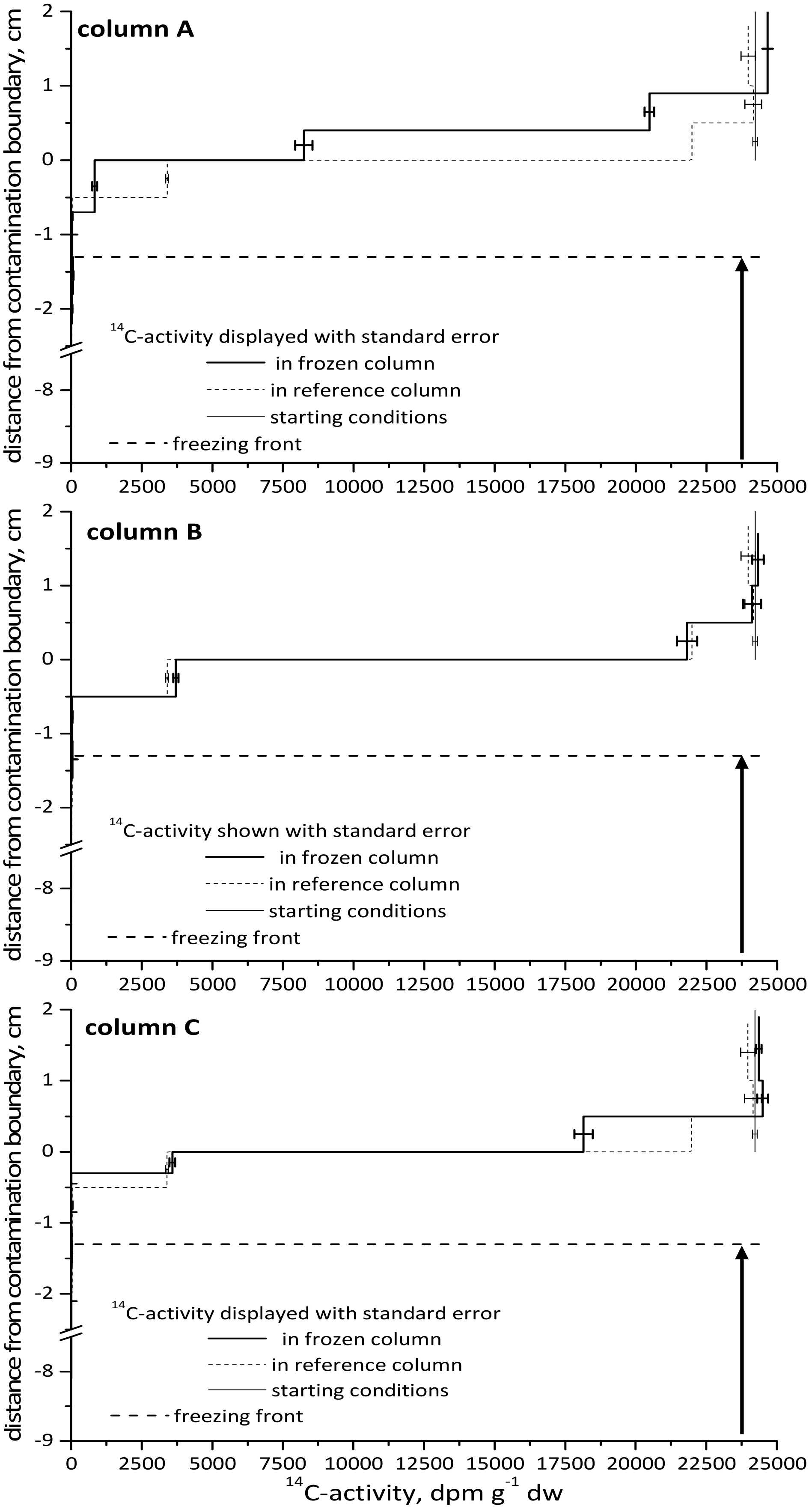

Figure 6.4 Distribution of ^{14}C-activity in the three experimental columns (A-C) of experiment *Ufbp*. Standard error reflects n ≥ 3, arrow indicates freezing direction.

The experiment with ^{14}C-pyrene did not reveal any significant ^{14}C-activity redistribution in the experimental columns compared to the values encountered in the reference column. This statement is mainly the result of the ^{14}C-activity distribution found in the reference column, which in turn may be strongly influenced by the sampling procedure. On the other hand these results put the results encountered in column B of the experiment with ^{14}C-anthracene (*Ufba*) into perspective, as the values of ^{14}C-activity measured below the contamination boundary in experiment *Ufba* only vary by 276 dpm g^{-1} dw and 160 dpm g^{-1} dw from the ones in experiment *Ufbp*.

6.3 EXTRACTABILITY OF ^{14}C-ANTHRACENE AND ^{14}C-PYRENE FROM THE SOIL

PAHs that enter soils adsorb to different compartments of the soils (see chapter 0). As adsorbents and processes vary, also availability of PAHs varies in a great range. This may be displayed by sequential extractions, which use different solvents. The sequential extraction method used for experiments Ufba and Ufbp displays three fractions:

1. methanol-water extractable (grey)
2. ethyl acetate, first extraction step (dark grey)
3. ethyl acetate, second extraction step (black)

More details of the procedure are given in chapter 3.2.4. Solvent extractions without matrix destroying procedures do not extract non-extractable residues. The amount of the latter may be calculated by the subtraction of total extraction yield from total ^{14}C-activity in soil sample. As it is a sequential extraction results are displayed as stacked bars, given with standard error for $n \geq 3$. The thickness of the bars is not in relation to the thickness of the sampled soil layer, which can be taken from Table A.6 and Table A.7. If there wasn't enough material for three replicates the median has been determined and results were displayed without error bar. Following, the results of the extractions of the samples from the experiments with ^{14}C-anthracene (*Ufba*) and ^{14}C-pyrene (*Ufbp*) with silt loam and freezing from the bottom are displayed. All figures show the extracted ^{14}C-activity of the upper soil layers of each experimental column (A-C), the reference column and one stacked bar displays the mean extraction yields of the material at the beginning of the experiments. The parts of the soil columns, which were contaminated at the beginning of the experiment are marked with a black and white rectangle at the left hand side of the diagram. Total ^{14}C-activities determined by combustion are given as dots with the according standard error.

Extractability of ^{14}C-anthracene from silt loam after indirect influence of a freezing process

The results of the sequential extractions for experiment *Ufba* can be seen in Figure 6.5. The extraction yields of all three extraction steps from the uppermost samples of the soil cores (uppermost bar of each column) were equivalent to the extraction yields gained from the contaminated soil material from the beginning of the experiment (see Table A.13). Variations between these samples were within the range of the homogeneity of the contaminated material used (see chapter 3.2.2). These results confirm the comparability of the parallel run columns and the reference column, because they display that all started off under the same conditions. Total extraction yields in second soil layer from the top were lower, as total ^{14}C-activities determined by combustion were lower, too. However, total extraction yield of the soil material from the second soil layer of the reference column was about 20 % higher than the mean of the experimental columns. The total extraction yields of the experimental columns differ by 6 %, which is close to the variation of the method. For further interpretation the sample thickness has also to be taken into account (see Table A.6). It is only 0.8 cm for the second soil layer in the reference column and 0.9 for second soil layers in columns A and C and 1.0 cm for the corresponding soil layer in column B. That means the thicker soil samples from the experimental columns include lower soil parts of the columns, which might be depleted. Therefore total extraction yields for the whole soil layer were lower. Non-extractable residues were not encountered in the contaminated parts of the experimental columns. They could be seen in by a distance between the end of the stacked bar and the dot for the total ^{14}C-activity. However, it can be seen, that results must include methodological errors, because in some cases total extraction yield exceeds total ^{14}C-activity. The total extraction yields in the formerly uncontaminated parts of the columns were lower than the total amounts of ^{14}C-activity analyzed by combustion, except for the third soil layer in column B (see Table A.6 and Table A.13). That would generally be an indication for non-extractable residues, whose amounts could be calculated by subtraction of total extraction yields from total ^{14}C-actvitiy. However, absolute values were considerably low, accounting for approximately 200 dpm g^{-1} dw, exept for the value of the fourth soil sample in column B (B2), which accounted for 1363 dpm g^{-1} dw. But with respect to the differences between total extracted amount and total ^{14}C-activity in the soil layer above, this result has to be interpreted with care.

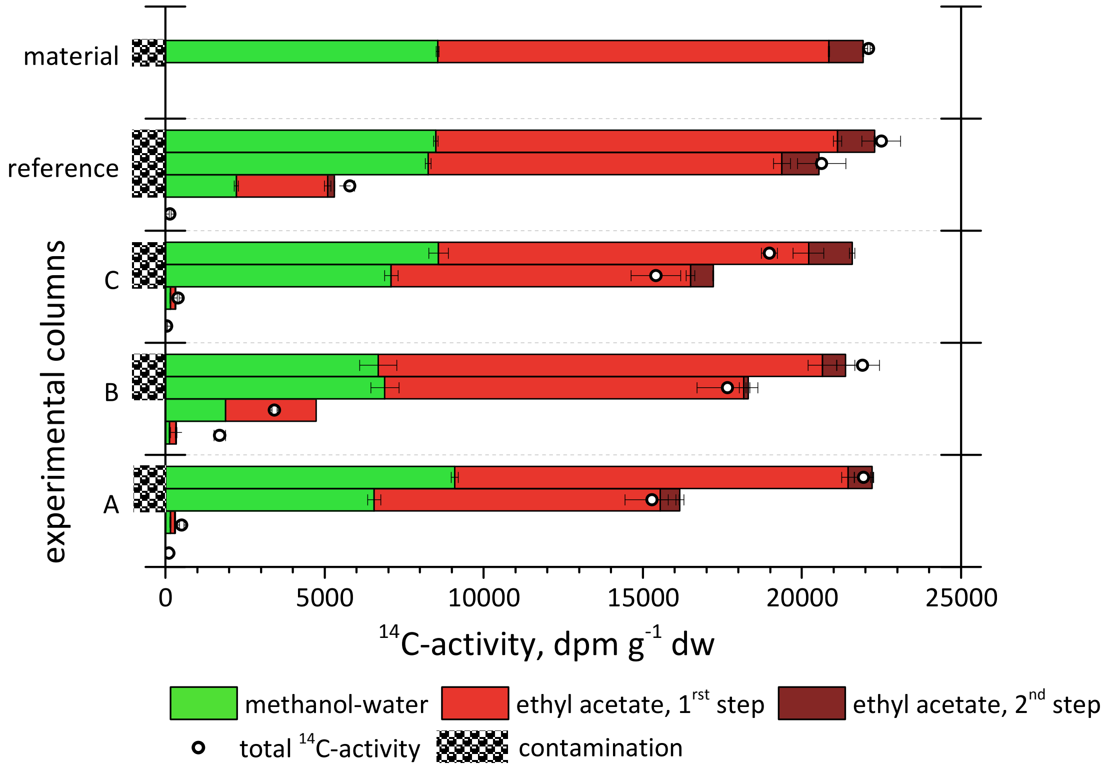

Figure 6.5 **Summed ^{14}C-activity extraction yields of upper three and four layers of the columns and material from the beginning of the experiment *Ufba*, methanol-water extraction (green) and two consecutive extractions with ethyl acetate (red and brown) were conducted sequentially. Dots display total ^{14}C-activity. Standard error reflects n≥3. Black and white rectangle marks contaminated column parts at the beginning of the experiment.**

To compare the relation of PAH extractability within the different soil layers, it is useful to present the results as percentage of the total amount extracted (see Figure 6.6). The y-axis has the same structure as used in Figure 6.5. It can be seen that the methanol-water extractable ^{14}C-activity (grey) is about 10 % higher in the lowest, formerly uncontaminated soil layers in column A and C, which have a very low total content. The values differ significantly from the value of the starting conditions of the soil material. For column B no significant difference compared to the methanol-water extractable fraction of the soil material from the beginning was observed. In all, the amount of the methanol-water extractable ^{14}C-activity (grey) makes up approximately 40 % of the total extracted ^{14}C-activity in the contaminated soil layers.

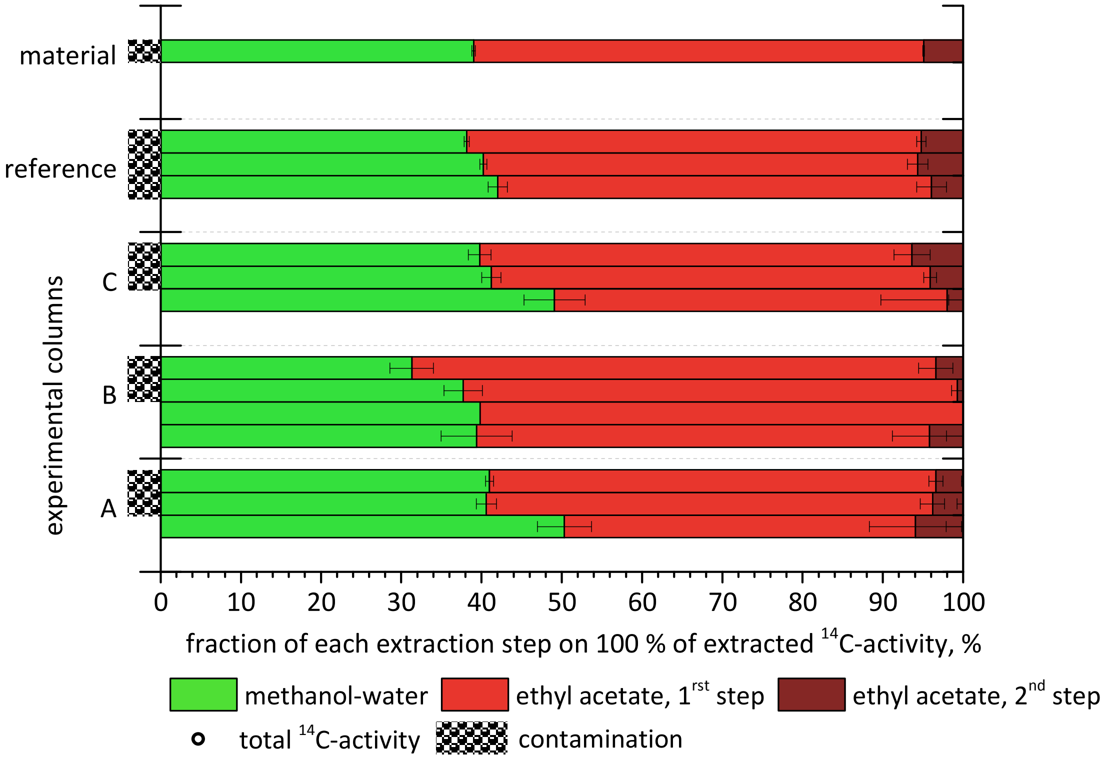

Figure 6.6 **Fractions of the three sequential extractions for the *Ufba* on the sum of extracted ^{14}C-activity, methanol-water extraction (green) and two consecutive extractions with ethyl acetate (red and brown) were conducted sequentially. Standard error reflects n≥3. Black and white rectangles on the left mark contaminated column parts at the beginning of the experiment.**

Extractability of ^{14}C-pyrene from silt loam after indirect influence of a freezing process

The results for the experiment with silt loam, freezing from the bottom and ^{14}C-pyrene (*Ufbp*) are displayed in Figure 6.7 and Figure A.2. Different from experiment *Ufba*, three samples were taken in the contaminated parts of the columns, therefore sample thicknesses were smaller. In all columns the total extracted amounts decreased slightly from the top layers towards the contamination boundary (see Table A.7). The first sample beneath the contamination boundary in the former uncontaminated parts of the columns showed contamination with ^{14}C-activitiy. Values in columns B and C were 3704.6 dpm g^{-1} dw and 3588.5 dpm g^{-1} dw, respectively. The ^{14}C-activity in the correspondent layer of the reference column was with 3393.2 dpm g^{-1} dw only slightly lower. In column A the ^{14}C-activities of the third and the fourth soil layer were considerably lower than the ones encountered in the other columns. Different from experiment *Ufba* non-extractable residues could be determined in almost all soil layers. However, to a small extend of only 1.0 % to 8.4 % in the contaminated parts of the columns. These amounts did not differ significantly from the amount analyzed for the soil material at the beginning of the experiment of

4.8 %. In the reference column non-extractable residues made up 0.6 % to 3.6 % of the total ^{14}C-activity in the contaminated part of the column.

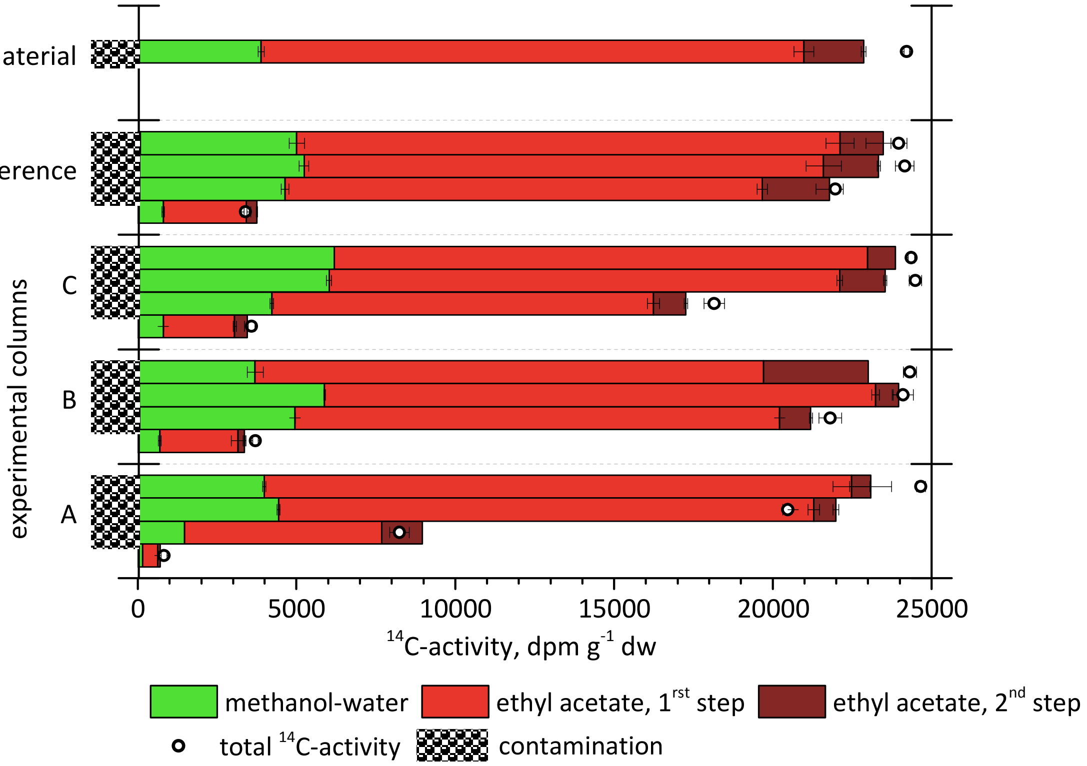

Figure 6.7 **Summed ^{14}C-activity extraction yields of upper four layers of the columns and material from the beginning of the experiment *Ufbp*, methanol-water extraction (green) and two consecutive extractions with ethyl acetate (red and brown) were conducted sequentially. Dots display total ^{14}C-activity. Standard error reflects n≥3. Black and white rectangles on the left mark contaminated column parts at the beginning of the experiment.**

The comparison of the extraction yield displayed on 100 % of extracted ^{14}C-activity did not reveal considerable differences between columns or contaminated and former uncontaminated parts (see Figure A.2). Compared to experiment *Ufba* with ^{14}C-anthracene the extraction yield for the methanol-water extractable fraction was much lower. It accounted only for about 20 % of the total extraction yield of the ^{14}C-activity in experiment *Ufbp*, whereas it accounted for 40 % up to 50 % of the total extracted ^{14}C-activity in experiment *Ufba*. As the total amounts of ^{14}C-pyrene did not clearly show an influence of the freezing induced water migration on the ^{14}C-pyrene distribution within the experimental columns, the sequential extraction also did not display great variations.

On the basis of the presented results the question, if the fate of PAHs in silt loam is influenced by freezing induced water migration processes cannot finally be answered. Although trends were observed, methodological weaknesses of the sampling procedure leave doubts on the interpretation of the results.

7. RESULTS ON THE BEHAVIOR OF PAH ASSOCIATED WITH PETROLEUM HYDROCARBONS IN FREEZING SOILS

On contaminated sites crude oil, as a light non-aqueous phase liquid (LNAPL) enters the soil as a fourth phase in the system bulk soil, soil water and soil vapor. This fourth phase influences chemical and physical reactions within the whole system as shown in chapter 2.3.2 (Walter et al., 2000). Due to its chemical structure it may act as sorbent for hydrophobic chemicals. The adsorption processes taking place among this group of chemicals are assumed to be fast (Luthy et al., 1997). PAHs are generally characterized as hydrophobic. Hydrophobicity increases among the single substances of this group with increasing log K_{oc} (see chapter 2.3.1). The competition between soil organic matter and present oil phase as sorption sites for PAHs has been studied by Walter et al. (2000). They found that adsorption of PAHs on soil organic matter significantly decreased in the presence of low-viscous oil, whereas extremely viscous oils had only slight effects on the partitioning of the PAHs. The distribution coefficients in Table 2.4 support these findings. It is therefore hypothesized that PAHs will partially adsorb to the medium viscous, paraffin-based crude oil Ekofisk, if it is present in the soil. The impact of the higher viscous, naphthene-based crude oil Gryphon is hypothesized to be smaller. These relations imply that the migration behavior of the PAHs will be governed to different extends by the behavior of the two NAPLs in the soil. In conjunction with the freezing process in soils in turn the distribution of the NAPL within the soil will be determined by the ice formation and the volume increase that comes along with it (see chapter 2.4). Furthermore the impact of different soil materials on the interacting processes is of interest. Therefore experiments on the fate of PAHs in combination with different crude oil phases were conducted to analyze the impact of the freezing processes on the distribution of PAHs in soils.

7.1 RESULTS OF EXPERIMENTS WITH ^{14}C-LABELED PAHs

To answer the question, if PAHs are expulsed ahead a freezing front if a medium viscous crude oil is present, experiments with two different soil materials, silt loam and sand were conducted. The 10 cm high columns of setup 1 were filled with uncontaminated material in the lower 5.2 cm and with contaminated material in the upper 5 cm. A mixture of the paraffin-based crude oil Ekofisk, a PAH and a ^{14}C-labeled PAH were used to contaminate the soil materials (detailed data in Table 3.5). For the experiments all three columns were cooled from the top downwards. The freezing front was always situated within the contaminated part of each column. Therefore already small changes in contaminant content can be detected. Initial bulk density varied due to the different grain sizes of the materials used. Water content was regulated to 60 % maximum water holding capacity, which resulted in absolute water contents of 29.2 % g^{-1} dw for silt loam and 9.4 % g^{-1} dw for sand.

7.1.1 FREEZING PROCESS AND WATER DISTRIBUTION

For the experimental approach used with silt loam, freezing from the top, ^{14}C-pyrene and the crude oil Ekofisk (*Uftpo*) it can be seen that the water distribution in the experimental columns differs distinctly for almost all soil layers from the starting conditions (see Figure 7.1,

Table A.10). Water contents within the reference column did not differ significantly from the water contents at the beginning of the experiment. Water content maxima for experimental columns (A-C) were found in the top soil layer of each column. Water contents within the frozen zone were significantly higher than the starting conditions, whereas water contents in the unfrozen part of the columns were nearly all significantly below the initial water content of the soil material. These water distribution patterns provide evidence of freezing induced water migration processes within the experimental columns caused by the used freezing scenario (see Figure 5.5). In the top layer column A had the highest water content with 48.30 % dw. The water content of the surface soil layer in column B was with 47.43 % dw only 0.87 % g^{-1} dw lower than that of column A. Both water contents slightly exceeded the maximum water holding capacity of the soil material (47.23 % dw). The maximum water content in column C was with 40.73 % g^{-1} dw significantly lower. It corresponded to 85 % of the value in column A. This difference may be explained by the variation of the temperature profiles (see Figure 5.5). In column C freezing front reached its final position about 20 hours later than in the other two columns.

In the middle of the columns, in the frozen soil layer next to the freezing front, water content increased in columns B and C by 6.29 % dw and 4.48 % dw, respectively. As temperatures in the second half of the experiment stayed constant, it may be assumed that the freezing fronts encountered at the end of the experiments were in this position during the whole second half of the experimental duration. Therefore the increases in water content adjacent to the freezing front are evidence for cryosuction and the formation of segregation ice. In column A water contents decreased continuously from the top down until 2 cm below the freezing front in the unfrozen column part, where the minimum water content was found. The difference, especially between the water content distribution pattern in columns A and B cannot be explained by temperature differences, because the temperatures in the two columns ran parallel. But the comparison of the TDR profiles displayed in Figure 5.5 revealed that water contents at 3 cm column depth were significantly different between column A and columns B and C in the second half of the experiment.

The absolute minimum water content reached was found between 2.6 cm and 3.6 cm below the freezing front in the unfrozen part of column B with a value of 20.8 % g^{-1} dw. Minimum water content for column C lay between the other two columns for both, depth and content. In the unfrozen parts of the experimental columns, water contents varied less than 2 % g^{-1} dw, except for the bottom soil layer. While water contents in columns A and C increased slightly (1 %) compared to the soil layer above, water content in column B decreased. This led to a difference in water content between column B and C of 5.67 % dw.

The fact that the lowest water content was not found at the bottom of the soil columns, which represented the warmest part of the columns, may be explained by the decreasing influence of cryosuction with increasing distance from the freezing front. Soil water with distances of 3 to 3.5 cm of the freezing front and farther, were not mobilized as strongly as the soil water within the first 3 cm next to the freezing front.

In column A the water content in the soil layer just beneath the contamination boundary (between -2 cm and -2.3 cm in Figure 7.1) was about 2 % g^{-1} dw higher than in the soil layers beneath and above it. A possible explanation for this increase might be that water movement towards the freezing front was partially impeded by the oil phase present. Therefore water content increase just below the contaminated area. However, as this pattern was not observed in the other two columns, the effect seems not to be very pronounced.

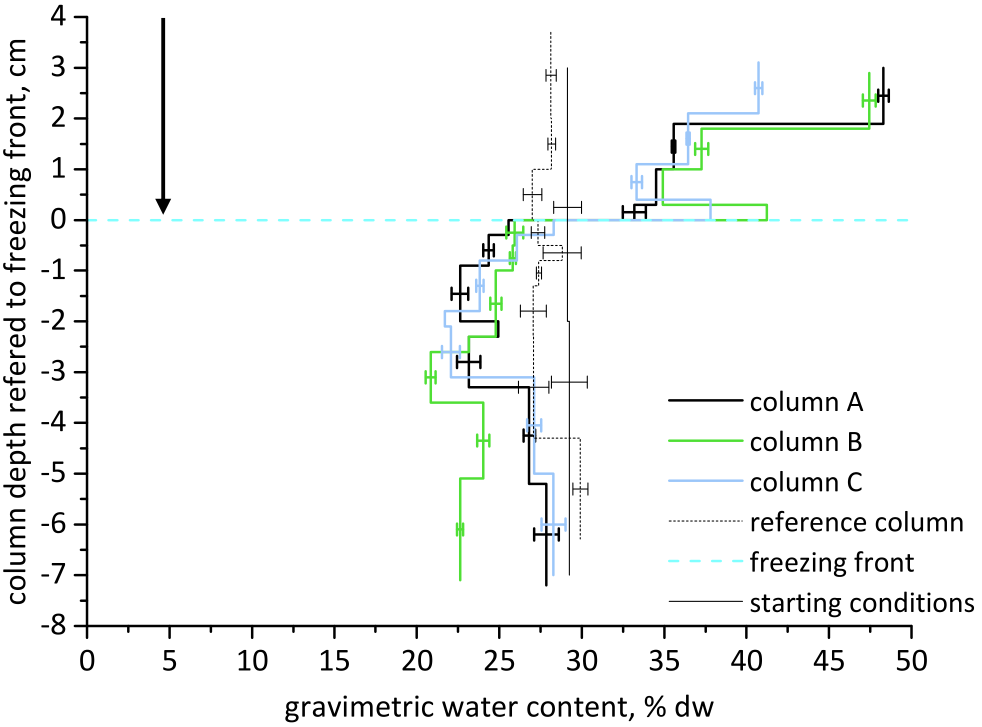

Figure 7.1 **Gravimetric water content for three experimental columns, reference column and starting conditions of the experiment *Uftpo*. Error bars display standard error reflecting n=3. Arrow marks freezing direction and frozen zone.**

The water distributions in the experimental columns of the experiment with sand, freezing from the top, ^{14}C-anthracene and the paraffin-based crude oil Ekofisk (*Sftao*) are shown in Figure 7.2. Similar observations as in the experiment with silt loam were made. The water distribution within the reference column varied with a standard error of 0.5 % g^{-1} dw. Its average lay about 1 % g^{-1} dw above the starting conditions of the material, that is why most of the water contents within the reference column differ significantly from the initial water content of the soil material. Water contents in the experimental columns differed all significantly from the initial water content of the material. Within the frozen soil they were significantly higher and in the unfrozen, lower part of the columns they were significantly lower than the starting conditions. Water contents in the frozen column part all exceed the maximum water holding capacity of the soil material (18.34 % dw). For all three experimental columns the maximum water content was found right above the freezing front within the frozen zone. In column C it accounted with 28.20 % dw for 298 % of the initial water content of the material at the beginning of the experiment. Therefore it may be assumed that ice segregation and water movement towards the freezing front took place in the sandy material. The maximum water content in column C is about 5 % g^{-1} dw higher than the maximum water contents in columns A and B. This difference might be explained by the slightly different temperature course (see Figure 5.6). Lowest water contents were found in the unfrozen bottom parts of the columns. Water contents in the bottom soil layers ranged around the wilting point (water content of 1.41 % dw) of the sand with values of 1.29 % dw, 1.72 % dw and 1.52 % dw for columns A-C, respectively. That indicates that cryosuction generated pore pressures of 1.5 MPa. Water contents directly beneath the freezing front in the unfrozen part of the columns were a little bit higher, but still at least 40 % below the initial water content. That means within the closed system the major part of the soil water had already migrated at the end of the experiment.

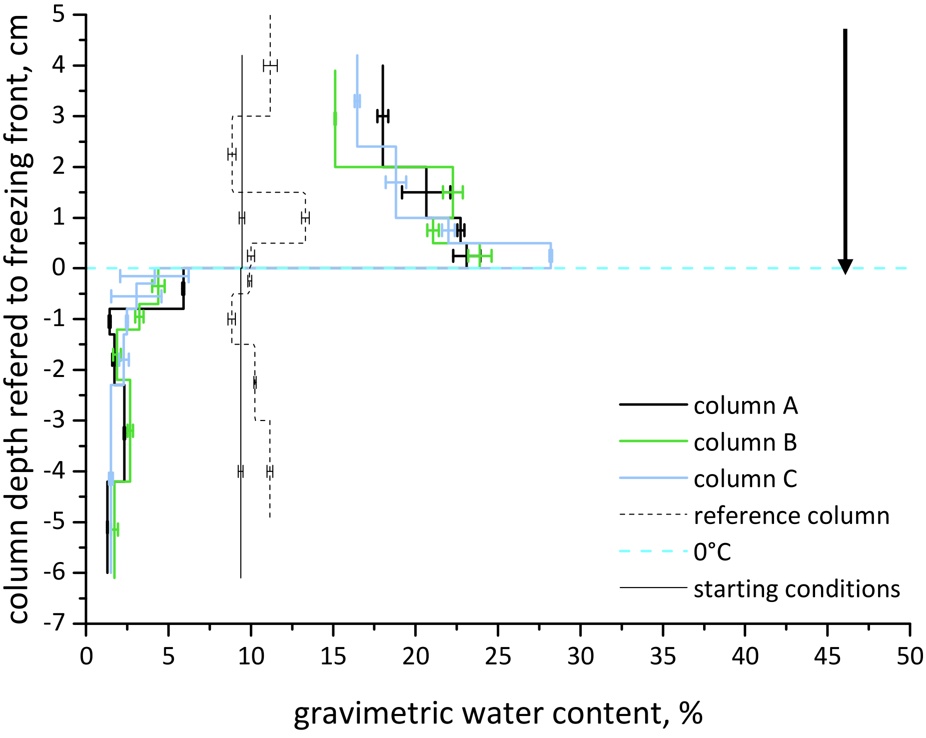

Figure 7.2 Gravimetric water content for three experimental columns, reference column and starting conditions of the experiment *Sftao*. Error bars display standard error reflecting n=3. Arrow marks freezing direction and frozen zone.

Differences between water above and beneath the freezing front in relation to the initial water content of the experiment with sand and silt loam were between 100 % and 255 % for sand and between 26 % and 52 % for silt loam. Additionally absolute values were higher for the silt loam than for the sand, due to different maximum water holding capacities.

7.1.2 DISTRIBUTION OF ^{14}C-ANTHRACENE AND ^{14}C-PYRENE DUE TO FREEZING

The redistribution of the ^{14}C-activity within the experimental columns was not as pronounced as the water distribution would suggest. Figure 7.3 shows the distribution of ^{14}C-activity for the experiment with silt loam, freezing from the top, ^{14}C-pyrene and crude oil (*Uftpo*) for each experimental column compared with the ^{14}C-activity of the reference column and the initial ^{14}C-activity of the material. The ^{14}C-activities within the reference column ranged between 96 % and 100 % in the contaminated part of the column in relation to the initial ^{14}C-activity of the material. In the contaminated parts of all three experimental columns ^{14}C-activities varied between 95 % and 101 % in relation to the starting conditions of the material. In column A the contamination level in the uppermost soil layer was significantly lower than the starting conditions, because variances were not equal. The following samples did not differ significantly from the starting conditions. The samples around the freezing front differed significantly from the starting conditions with a one-sided test, but compared to each other they did not show significant differences. Similar observations were made for the ^{14}C-activity in column C. The ^{14}C-activity in column B differed significantly from the starting conditions within the whole contaminated part, except for the uppermost soil sample.

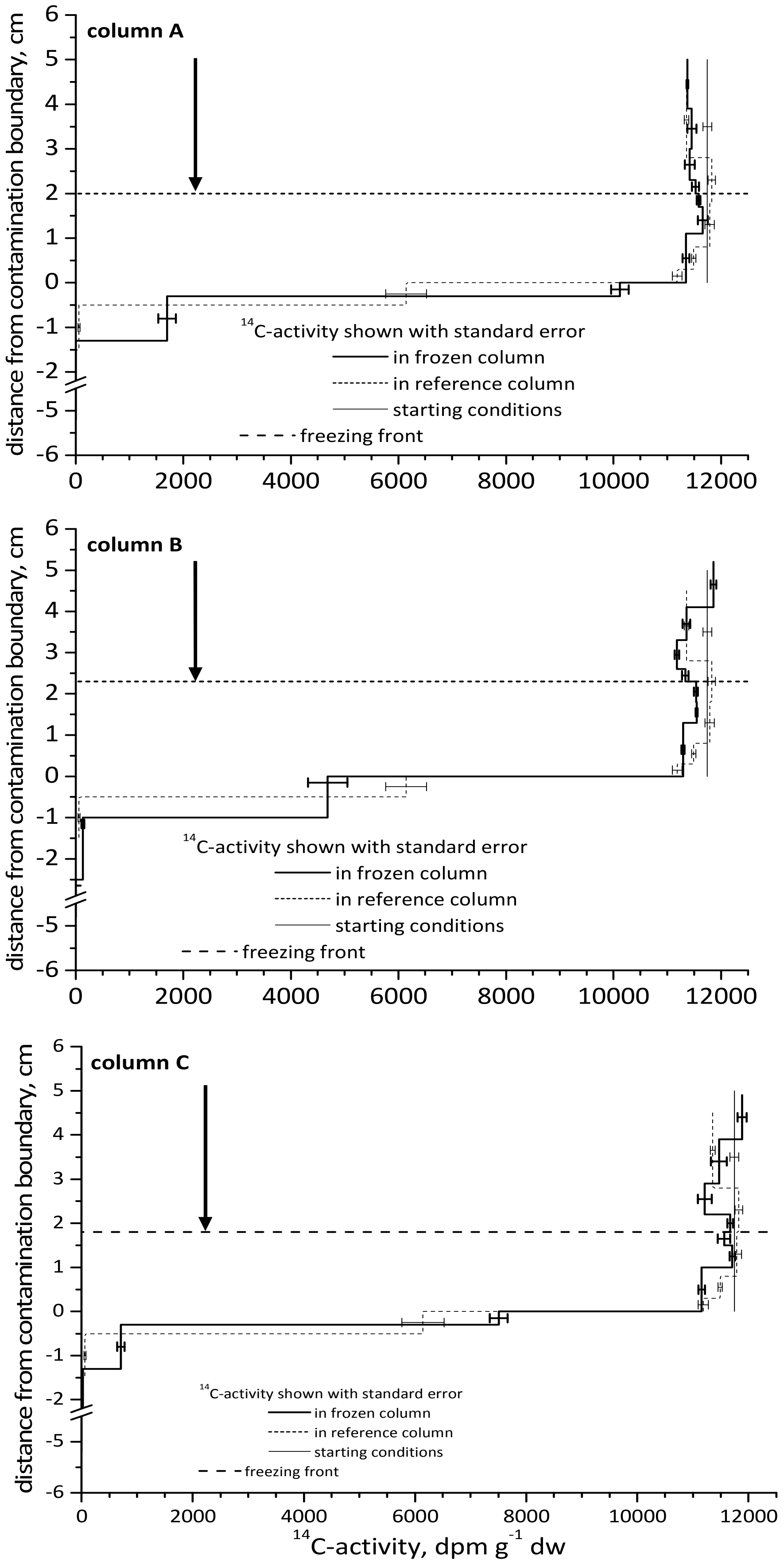

Figure 7.3 **Distribution of ^{14}C-activity in the three experimental columns (A-C) of experiment *Uftpo*. Arrow marks freezing direction. Standard error reflects n≥3.**

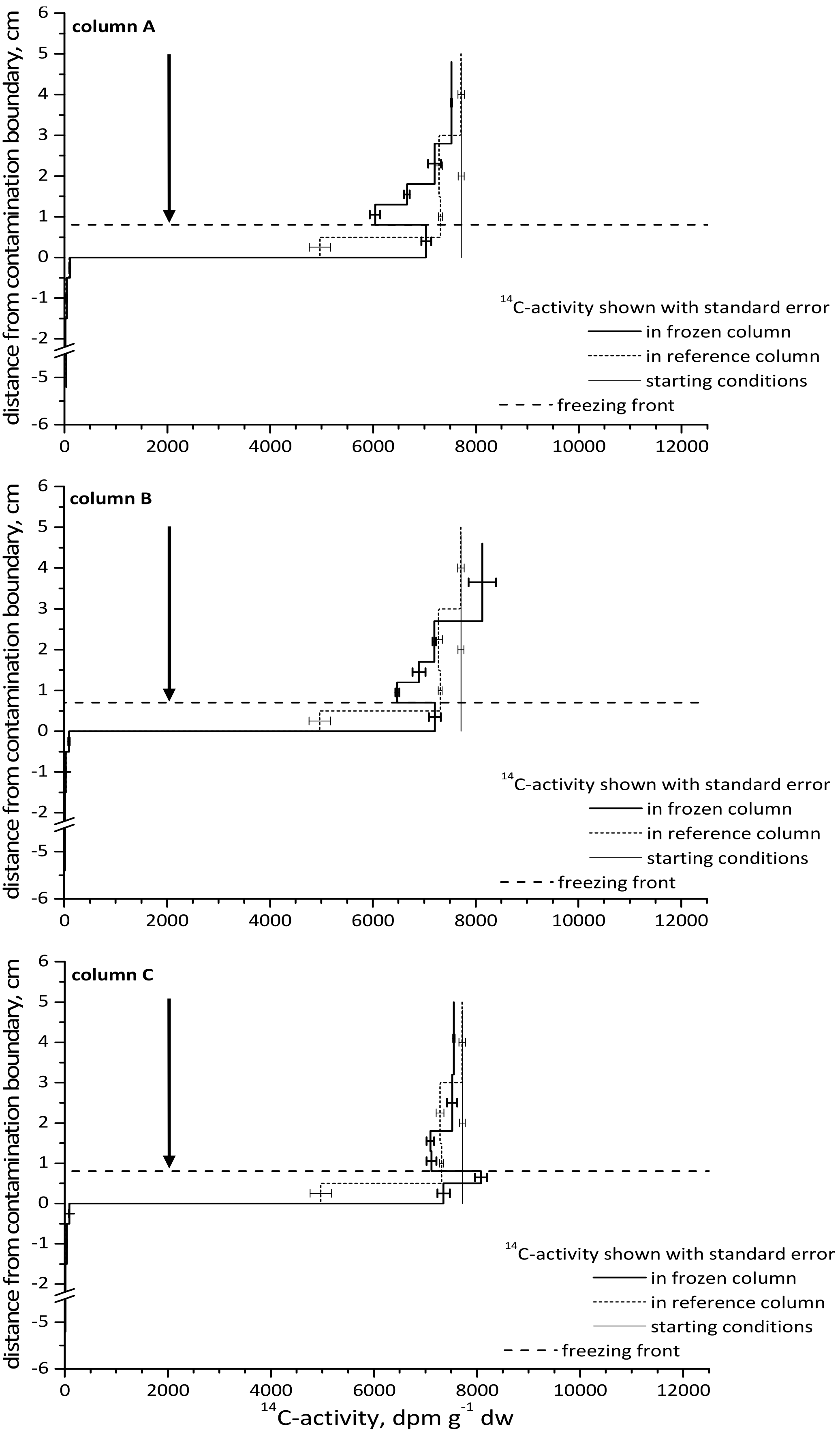

Figure 7.4 **Distribution of 14C-activity in the three experimental columns (A-C) of experiment Sftao. Arrow marks freezing direction. Standard error reflects n≥3.**

Furthermore the samples above and beneath the freezing front differed significantly compared to each other. That means, in column B the process of ^{14}C-pyrene migration from the frozen to the unfrozen part of the column in silt loam, has been proofed. However, the effect was very small and could not significantly be shown in the other two experimental columns. At the contamination boundary the difficulties of precise sampling were displayed again (see chapter 6.1). However, sampling of very thin sections of 0.3 cm caused a smoother step between the two parts. Due to this relation no assumptions concerning any migration from the contaminated to the uncontaminated part of the columns were made.

In the experiment with sand, freezing from the top, ^{14}C-anthracene and crude oil (*Sftao*) differences in ^{14}C-activity around the freezing front were more obvious (see Figure 7.4 and

Table A.9). The ^{14}C-activity in the reference column was equal to the starting conditions in the upper column part. It decreased in a smaller and a larger step towards the contamination boundary. As the larger decrease appeared just above the contamination boundary, it was most probably the result of uncontaminated material mixed into the sample during the sampling procedure (see chapter 6). Contamination boundaries within the experimental columns have been met very well in this experiment, as the contamination decreased to values of 100 dpm g^{-1} dw and less beneath the contamination boundary. In columns A and C the ^{14}C-activities in the uppermost, contaminated soil layers started off at the level of the initial contamination of the soil material. In column B ^{14}C-activities were slightly higher than the starting condition. Further towards the freezing front ^{14}C-activities decreased stepwise in columns A and B and increased below the freezing front with 16.5 % and 11.3 % of the value encountered within the last frozen soil layer of the column. In column C ^{14}C-activities within the frozen column part did not decrease as much as they did in the other two experimental columns. However, ^{14}C-activity increased below the freezing front with 13.5 % of the value found in the last frozen sample to reach 104.7 % of the initial ^{14}C-activity in this first unfrozen soil layer. These observations are evidence for the freezing induced redistribution of ^{14}C-anthracene from the frozen to the unfrozen part of the soil column during the experimental procedure.

With the paraffin-based crude oil Ekofisk present in soil, the formation of segregation ice leads to an enhanced downward migration within sand. For silt loam the process is slower and not as pronounced. In conjunction with the water distribution within the experimental columns it can be stated, that increased water contents, due to freezing induced water migration within the frozen soil zones led to lower contents of ^{14}C-activity.

7.1.3 EXTRACTABILITY OF ^{14}C-PAHs FROM SAND AND SILT LOAM WITH CRUDE OIL

To get an insight into the availability of ^{14}C-anthracene and ^{14}C-pyrene, extractable fractions with increasing power to extract the hydrophobic PAHs were determined. The extraction method used is described in chapter 3.2.4. Four different fractions were determined:

1. water extractable (blue)
2. methanol-water extractable (green)
3. ethyl acetate, first extraction step (red)
4. ethyl acetate, second extraction step (brown)

Extractability of ^{14}C-pyrene from silt loam with crude oil after a freezing process with segregated ice formation (*Uftpo*)

The results from the sequential extractions of the contaminated soil layers of the experiment with silt loam, freezing from the top, ^{14}C-pyrene and the paraffin-based crude oil Ekofisk (*Uftpo*) are displayed as stacked bars in Figure 7.5. The length of each bar displays the total extraction yield, which can be compared to the total amount of ^{14}C-activity determined by combustion. The latter are displayed as dots with standard error. The comparison revealed that the total extracted amount of ^{14}C-activity was always larger than 90 %, which means that less than 10 % of the ^{14}C-pyrene has been entrapped in the soil as non-extractable residues during the duration of the experiment. The mean of the total extracted ^{14}C-activity in the reference column was 95.9 % of the total ^{14}C-activity in the soil with a standard error of 1.4 %. The total extraction yields for the experimental columns were a little bit higher. They ranged between 97.2 % and 99.0 % of the total ^{14}C-activity in the soil with standard errors between 0.9 % and 1.1 %. The distribution of the non-extractable residues throughout the columns only showed an interesting distribution in column A, where 2.9 % to 4.9 % of non-extractable residues were formed in the upper, frozen part of the column, whereas no non-extractable residues could be determined in the unfrozen, lower soil layers. Maximum extraction yields were reached for the third extraction step, extraction with ethyl acetate (first step), with a mean of all experimental columns of 8143 dpm g^{-1} dw. This value is significantly higher than the amount of ^{14}C-activity extracted with the third extraction step from the contaminated soil samples of the reference column of 7626 dpm g^{-1} dw.

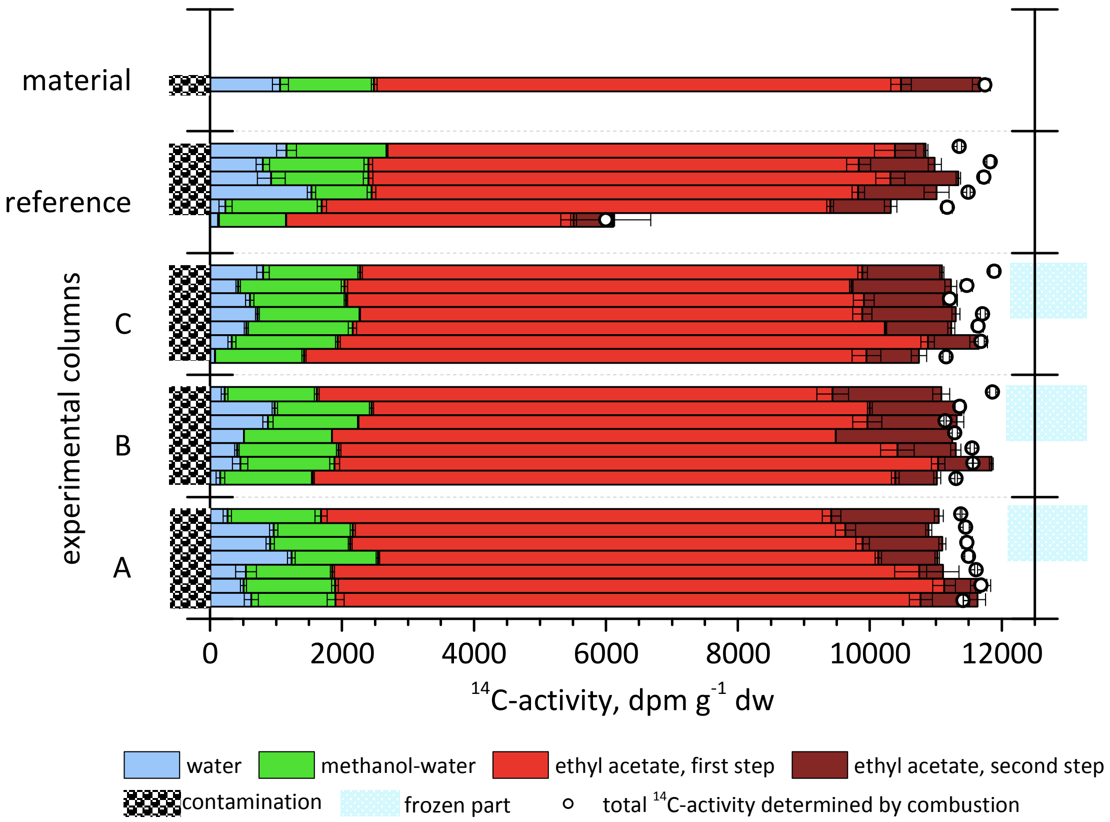

Figure 7.5 Summed ^{14}C-activity extraction yields of contaminated soil layers of the columns and material from the beginning of the Uftpo, water extraction (blue), methanol-water extraction (green) and two consecutive extractions with ethyl acetate (red and brown) were conducted sequentially. Dots display total ^{14}C-activity. Standard error reflects n≥3. Black and white rectangles on the left mark contaminated column parts at the beginning of the experiment. Light blue rectangles on the right mark frozen column parts.

The comparison of frozen and unfrozen parts of the experimental columns revealed that the extraction yields for the water extraction and the both ethyl acetate extractions differed significantly. Extraction values for the methanol-water fraction did not differ significantly between frozen and unfrozen column parts or compared to the reference column. The water extractable fraction was twice as large in the frozen column parts compared to the unfrozen column parts with a fraction of 5.4 % to 7.6 % of the total extraction yield (see Figure 7.6). For the first ethyl acetate extraction the relation was vice versa, the mean extracted ^{14}C-activity of the unfrozen parts of all experimental columns was 8.4 % higher than the extraction yield for this third extraction step from the frozen parts of the experimental columns. As the second ethyl acetate extraction yielded significantly higher amounts from the frozen soil layers, the effect for the overall ethyl acetate extraction yield was extenuated to a difference of 2.8 % or 483.8 dpm g $^{-1}$ dw. That means the observed trend for the redistribution of ^{14}C-activity in Figure 7.3 is proofed by the differences in extractability of ^{14}C-activities from frozen and unfrozen column parts. The ethyl acetate extractable fraction is enriched by 2.8 % in the unfrozen column parts compared to the frozen parts of the experimental columns. That the water extractable fraction is lower in the unfrozen column parts goes along with the water distribution within the experimental columns, with much higher water contents in the frozen column parts due to cryosuction.

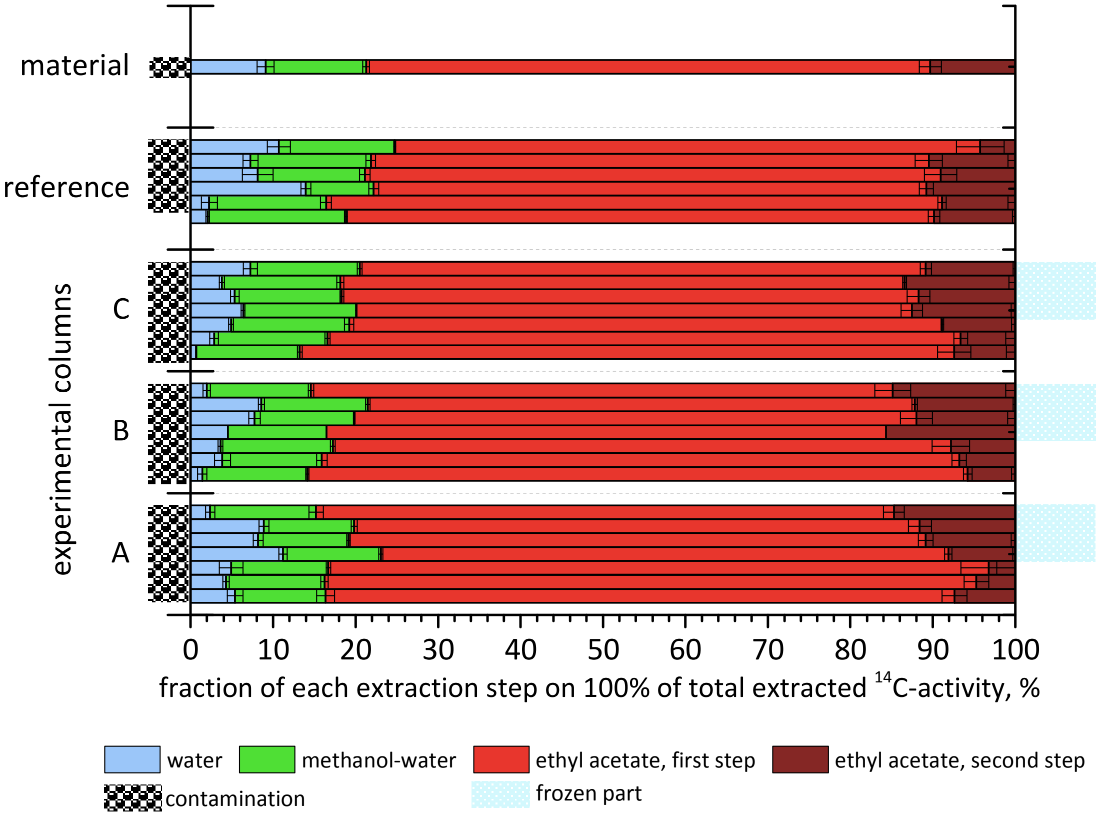

Figure 7.6 Fractions of the three sequential extractions for the *Uftpo* on the sum of extracted ^{14}C-activity, water (blue), methanol-water extraction (green) and two consecutive extractions with ethyl acetate (red and brown) were conducted sequentially. Standard error reflects n≥3. Black and white rectangles on the left mark contaminated column parts at the beginning of the experiment. Light blue rectangles on the right mark frozen column parts.

Extractability of ^{14}C-anthracene from sand with crude oil after a freezing process with segregated ice formation (*Sftao*)

The sequential extraction of the experiment with sand, freezing from the top, ^{14}C-anthracene and paraffin-based crude oil Ekofisk (*Sftao*) was conducted with three steps, including methanol-water extraction and two subsequent extractions with ethyl acetate. The water extractable fraction was determined using separate samples. To display results together, the values were subtracted from the values gained by the methanol-water extraction, as it can be assumed that all water extractable amounts are included in the methanol-water extractable amounts, if water extraction had not been conducted.

As in the experiments presented before, the sequential extraction of ^{14}C-activity was nearly exhausting. For the reference column the mean of the extracted sum for the upper three samples was 96.8 % of the total ^{14}C-activity in the soil with a standard error of 0.8 % (see Figure 7.7). That means only 3.2 % of the ^{14}C-activity remained in the soil as non-extractable residue. Total ^{14}C-activity extracted in the fourth sample (4.5 cm to 5 cm column depth) accounted only for 86.6 % of the ^{14}C-activity determined by combustion. But the latter also only reached 4969 dmp g^{-1} dw, which accounts for two thirds of the ^{14}C-activity found in the other samples of the reference column. This difference can be attributed to the difficulty to sample the reference column in slices with horizontal boundaries. Therefore it is very likely that uncontaminated material from the following, uncontaminated soil layer had been mixed in. The total extraction yields for the experimental columns were insignificantly lower than the mean of the upper three samples from the reference column. There was also no significant difference between non-extractable residues of frozen and unfrozen parts of the experimental columns. The water extractable fraction, which had been determined on separate samples, was even lower than the fraction of non-extractable residues, accounting for approximately 3 % of the total extraction yield. There were no significant differences between the results from the reference column and the experimental columns, nor between frozen and unfrozen column parts. However, the ^{14}C-activities extracted with methanol-water showed a distinct distribution pattern according to freezing. The methanol-water extractable fraction of the frozen column parts was with a mean of 1838 dpm g^{-1} dw significantly (27 %) lower than the mean of this fraction extracted from the unfrozen column parts (2525 dpm g^{-1} dw). In the reference column 2269 dpm g^{-1} dw were extracted with methanol-water. This accounts for 31.5 % (standard error 1.8 %) of the total extraction yield in the reference column, whereas only 25 % (standard error 0.6 %) were gained from the frozen column parts and 36.7 % (standard error 1.4 %) from the unfrozen column parts (see Figure 7.8). The values of ^{14}C-activity extracted by the first ethyl acetate extraction did only differ significantly between frozen and unfrozen part of columns C, with values of the frozen part being lower than in the unfrozen column part. However, the fractions on the total extracted amount of ^{14}C-activity did also not differ significantly. Values and fractions for the second ethyl acetate extraction step differed significantly between frozen and unfrozen column parts for all three experimental columns. The fraction extracted from the frozen column parts had a mean of 7.3 % of total extracted ^{14}C-activity, whereas the fraction within the unfrozen column parts only accounted for 1.1 % of the total extracted ^{14}C-activity. This fact led to a significant difference between frozen column parts and the reference columns for the sum of extracted ^{14}C-activity with ethyl acetate first and second step. However, the difference between frozen and unfrozen column parts is still not significant.

That fraction and values for the ethyl acetate extractable fraction of ^{14}C-activity in frozen and unfrozen column parts did not differ significantly. This observation revealed that for the ethyl acetate extractable ^{14}C-fraction no partitioning took place due to the migration processes. The latter obviously took place because total ^{14}C-activities differed considerably (see Figure 7.4 and Figure 7.7).

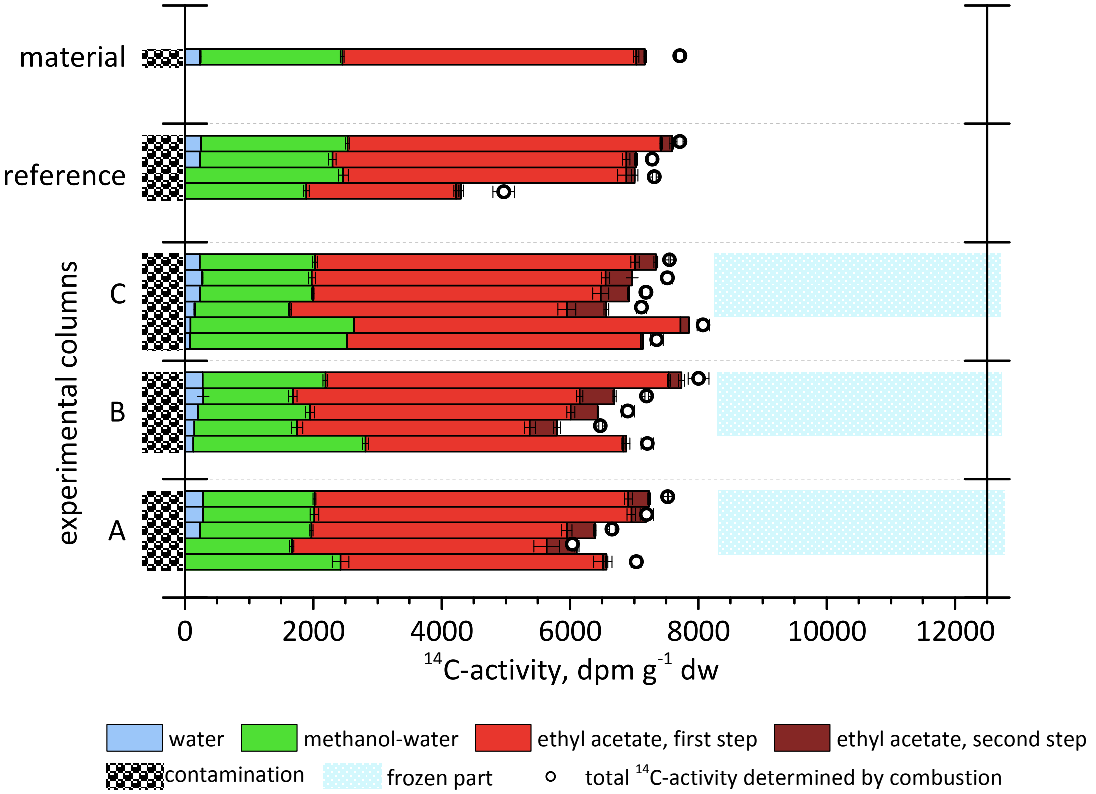

Figure 7.7 Summed ^{14}C-activity extraction yields of contaminated soil layers of the experiment *Sftao*, methanol-water extraction (green) and two consecutive extractions with ethyl acetate (red and brown) were conducted sequentially. Water extraction (blue) has been conducted separately. Water extractable fraction was not determined for all soil layers (see Table A.13). Dots display total ^{14}C-activity. Standard error reflects n≥3. Black and white rectangles on the left mark contaminated column parts at the beginning of the experiment. Light blue rectangles on the right mark frozen column parts.

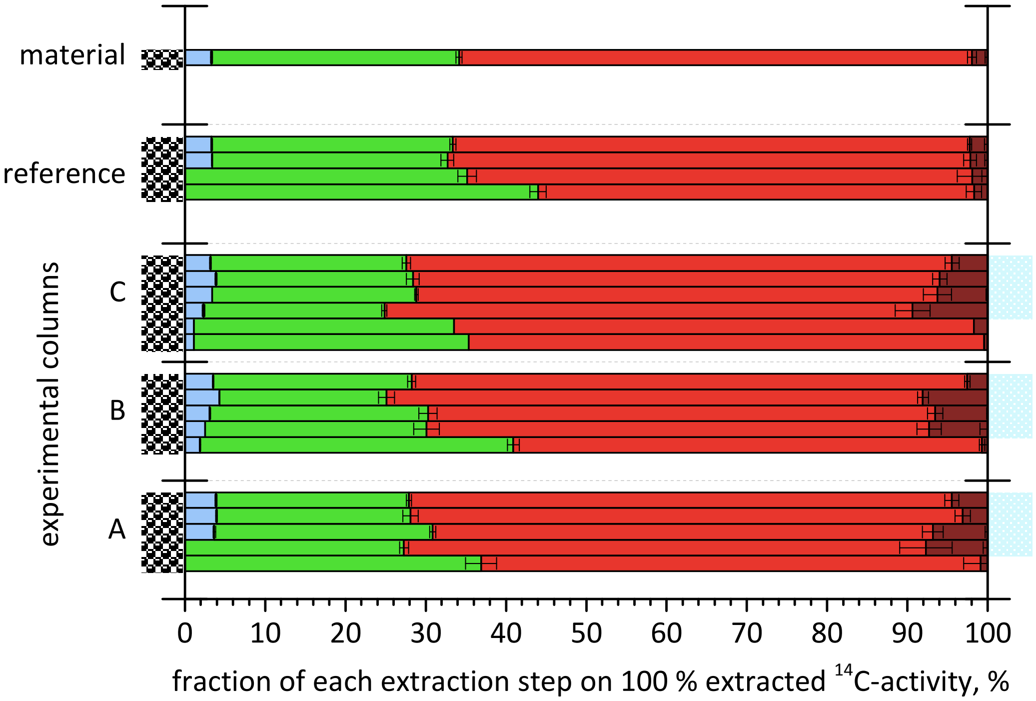

Figure 7.8 Fractions of the three sequential extractions for the experiment *Sftao* on 100 % of the extracted ^{14}C-activity.

7.2 COMPARISION OF EXTRACTABILITIES OF PAHs WITH AND WITHOUT CRUDE OIL

Availability and mobility of PAHs in soils are controlled by the physicochemical properties of all chemicals and soil constituents present (see chapter 2.3.1). The following extraction results are displayed in comparison to show the influence of crude oil, texture and PAH properties on the extractability of the ^{14}C-labeled PAHs in the freezing experiments.

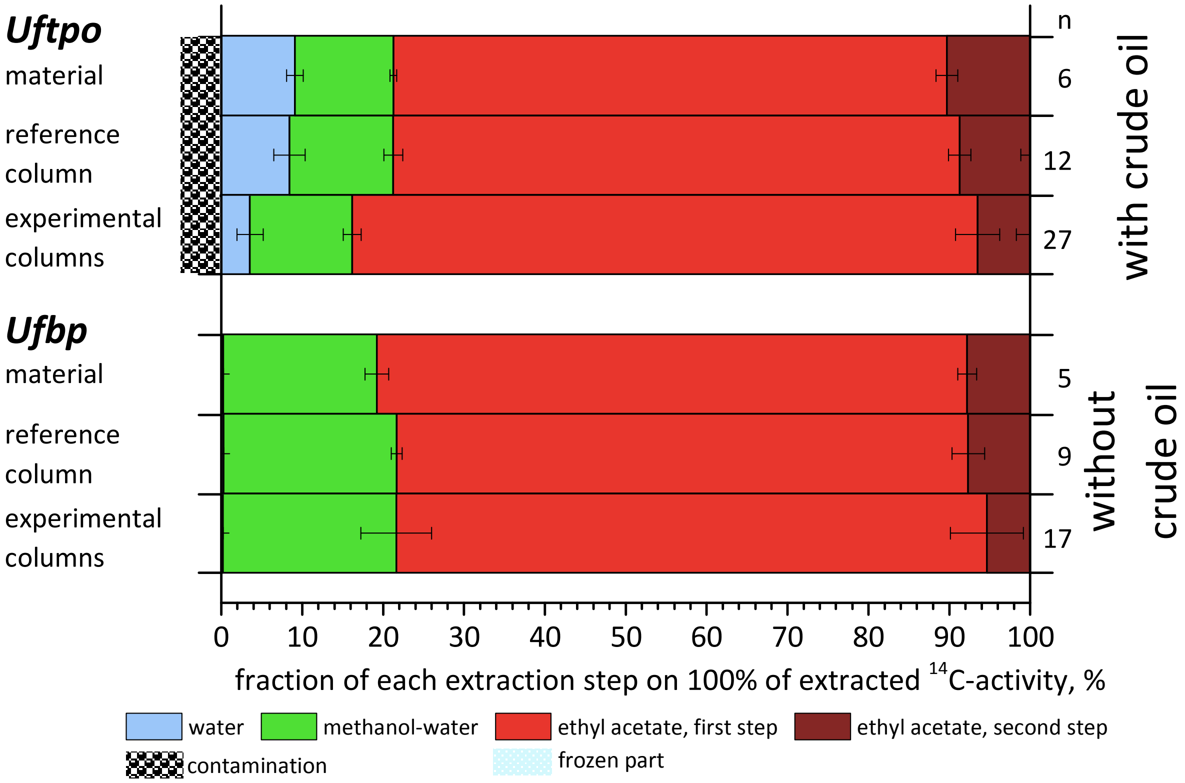

Figure 7.9 Comparison of means of extractable fractions from silt loam, in unfrozen experimental column parts, the reference column and the material at the beginning of the experiment contaminated with ^{14}C-pyrene with (*Uftpo*) and without (*Ufbp*) crude oil present in the soil. Standard error reflects n≥5 (according n is given on right hand side). Four fractions are given: water extractable (blue), methanol-water extractable (green), ethyl acetate extractable first and second step (red and brown).

In Figure 7.9 the influence of crude oil present in the soil system can be seen. To compare results from the two different experimental approaches with freezing from the top (*Uftpo*) and freezing from the bottom (*Ufbp*) only the means of the unfrozen samples are displayed. Furthermore the mean of the samples from the reference column and the mean of the samples taken before filling the columns are displayed for each experiment. On the right hand side the number of samples that make the mean of each group is shown. The most obvious differences between the extraction results of the two experiments were the amounts of water extractable and the amounts of methanol-water extractable ^{14}C-activity. In the experiment without crude oil present (*Ufbp*), the water extractable fraction does not exceed 0.3 % of the total extracted amount of ^{14}C-activity. In the experiment with ^{14}C-pyrene and crude oil

(*Uftpo*) 2.1 % up to 10.1 % of the extractable ^{14}C-activity could be extracted with the water extraction step. On the other hand the extraction with methanol-water had a much higher extraction yield in the experiment without crude oil present (*Ufbp*). Therefore the sum of the two first extraction steps with water and methanol-water did not differ significantly for the two experiments. The extraction yields for the two ethyl acetate extraction steps did not differ significantly between the two experiments, too. The observed differences showed, that in the presence of crude oil a higher fraction of pyrene is available for the weak solvent water.

The second comparison deals with different soil materials and their influence on the extractability of anthracene (see Figure 7.10). It is obvious that the methanol-water extractable fraction was significantly smaller in the silt loam (*Uftao*) than in the sand (*Sftao*). But it can also be seen that differences between frozen and unfrozen parts within an experiment were larger than differences between textures. The first ethyl acetate extraction step revealed no significant differences between the groups of sand and silt loam. The second ethyl acetate extraction step did, but here as before, the influence of freezing was much more pronounced. An interesting observation is, that the second ethyl acetate extraction was significantly higher in the means of the frozen soil parts than in the other three groups, corresponding to the small fraction of methanol-water extaction. However, the sum of the two ethyl acetate extraction steps differed significantly between the two soil materials for the frozen soil samples (8 % difference), the samples from the reference column (12 %) and the material from the beginning of the experiments (8 %). It was always higher in silt than in sand. The comparison of the unfrozen samples from the experimental columns also revealed that more ^{14}C-activity could be extracted from the silt, but the difference only accounted for 6 % of the total extracted ^{14}C-activtiy. Therefore it was only one sided significant. The comparison of the extractability of ^{14}C-activity from sand and silt loam contaminated with ^{14}C-anthracene showed that in sand the ^{14}C-activity was more easily available by a weak solvent, such as methanol-water. But also the influence of the freezing process on the extractability, which has already been presented in chapter 7.1.2 can be seen very clearly in Figure 7.10.

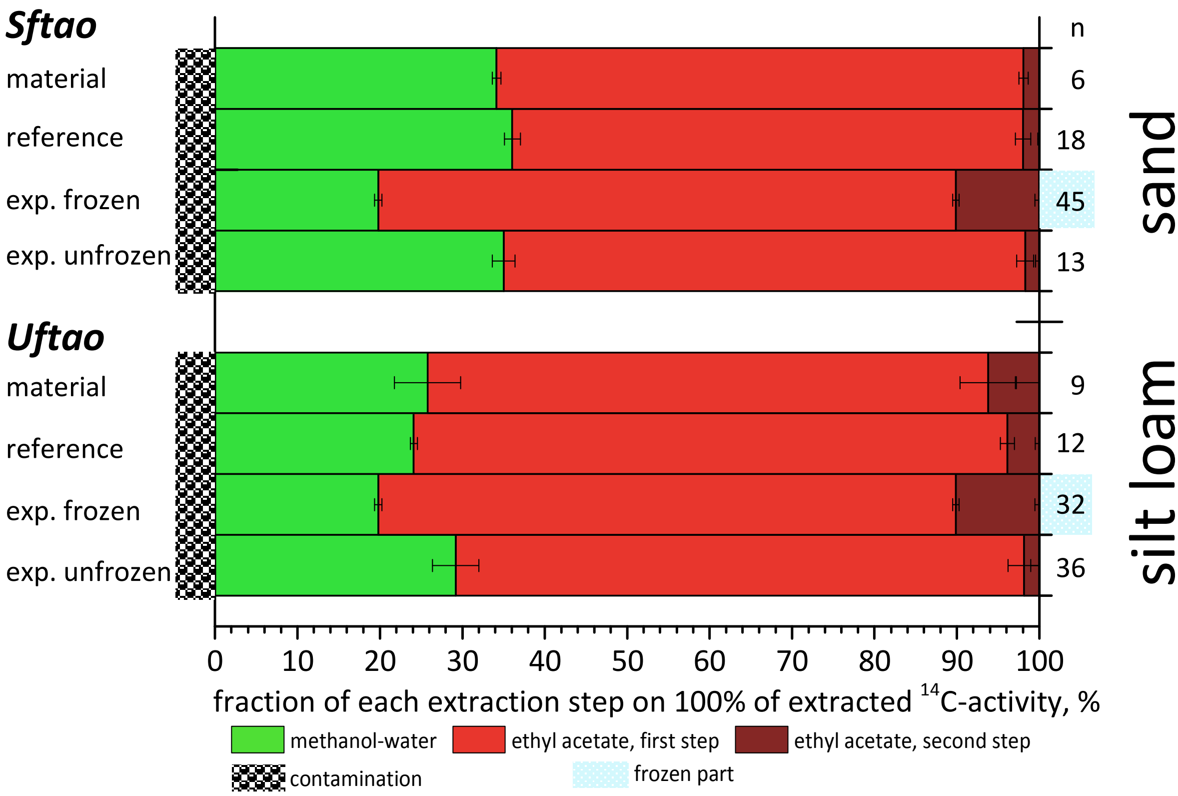

Figure 7.10 Comparison of means of extractable fractions from silt loam (Uftao) and sand (Sftao), in frozen and unfrozen experimental column parts, the reference column and the material at the beginning of the experiment contaminated with ^{14}C-anthracene and crude oil. Standard error reflects n≥6 (according n is given on right hand side). Three fractions are given: methanol-water extractable (green), ethyl acetate extractable first and second step (red and brown). Black and white rectangles on the left mark oil contaminated materials. Light blue rectangles on the right mark mean of frozen columns.

The third comparison is shown in Figure 7.11. It illustrates the impact of the freezing process in oil contaminated silt loam on ^{14}C-anthracene and ^{14}C-pyrene, respectively. The methanol-water extractable fraction was significantly higher for the ^{14}C-activity in the experiment with ^{14}C-anthracene, except for the means of the frozen soil samples. But it was again observed that the fraction extracted with the second ethyl acetate step was largest in the frozen soil samples for both PAHs. With the first ethyl acetate extraction step a significant lower fraction of ^{14}C-activity from the experiment with anthracene (68.9 %) was extracted than from the experiment with pyrene (77.3 %). Extractability in frozen column parts was also significantly different, but with the higher amount extracted of the samples from the experiment with anthracene (70.0 %) than from the one with pyrene (68.9 %). The means of the sums of the both ethyl acetate extraction steps did not differ significantly for frozen soil samples, whereas they differed significantly for the other three groups, with the values for anthracene being smaller than the ones for pyrene.

In summary that means that pyrene is less extractable in silt loam with crude oil present than anthracene in silt loam with crude oil. That would be expected according to the octanol-water partitioning coefficient and the organic carbon partitioning coefficient (see Table 2.3). This result underlines furthermore that the partitioning coefficients are more meaningful for the estimation of the behavior of PAHs in soils than the water solubility or fugacity ratio. The latter both would have suggested a better extractability for pyrene than for anthracene.

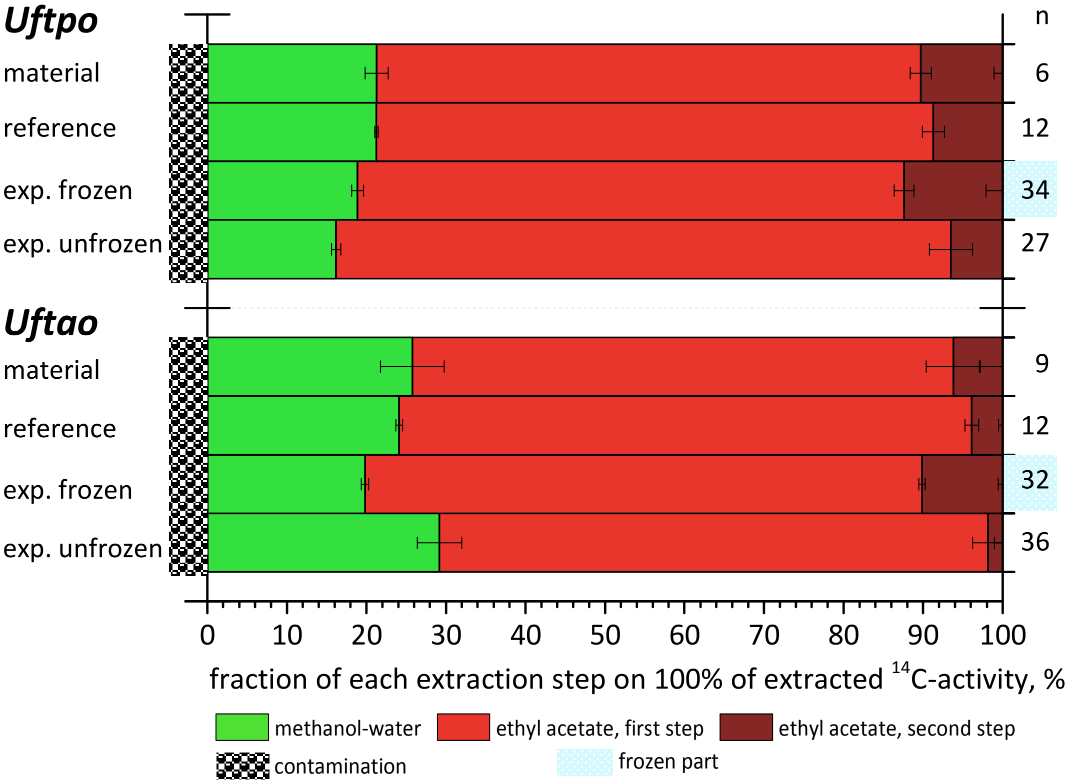

Figure 7.11 **Comparison of means of extractable fractions from silt loam in frozen and unfrozen experimental column parts, the reference column and the material at the beginning of the experiment contaminated with crude oil and ^{14}C-anthracene (*Uftao*) or ^{14}C-pyrene (*Uftpo*). Standard error reflects n≥6 (according n is given on right hand side). Three fractions are given: methanol-water extractable (green), ethyl acetate extractable first and second step (red and brown). Black and white rectangles on the left mark oil contaminated materials. Light blue rectangles on the right mark mean of frozen columns.**

It has been shown that the three parameters crude oil, texture and PAH properties influenced extractabilities of ^{14}C-activity in different ways. Oil had mainly an impact on the water extractable fraction, whereas the influence of texture was not as pronounced as the influence of the freezing process. ^{14}C-activities in the experiment with anthracene were to a higher extent extractable by methanol-water.

7.3 RESULTS OF FREEZING EXPERIMENTS WITH NON-LABELED PAHs AND LARGE COLUMNS (SETUP 2)

The experimental setup with the 40 cm high laboratory columns was used to simulate the thickness of an active layer. All soil material was homogeneously contaminated with non-labeled PAHs and crude oil (see chapter 3.2.2). The decision came for non-labeled PAHs, due to the dimension of the soil columns and the associated amount of soil material, which was needed to be contaminated (*Sftabo*: 4858 g dw per column, *Pftabo*: 472 g dw per column). Furthermore a pre-incubation step was included into the procedure (see chapter 3.2.3) Doing so it was accepted that total contents of PAHs could not be determined, but only the extractable fraction, leaving the discrepancy of non-extractable residues between the adjusted PAH content during contamination and the extracted and analyzed content after the experiments. Furthermore it had to be dealt with the considerably higher variation coefficients for the extraction and analysis method of the non-labeled PAHs in comparison to the variation coefficients for the combustion of ^{14}C-labeled PAHs. Variation coefficients for the determination of non-labeled PAHs with Soxhlet extraction and GC-MS analysis may be up to a value of 10. In oil contaminated soils recovery rates that range between 50 % to 180 % are not unusual (Zemanek et al., 1997). Variation coefficients for ^{14}C-labeled PAHs are between 1.9 to 3 (Eschenbach, 1995).

The experiments included a pre-incubation step of 14 days, between the contamination of the soil material and the start of the freezing procedure, because many authors emphasize on the importance of contact time of contaminants and soil with respect to the contaminants extractability (Eschenbach et al., 1997; Karickhoff, 1980; Luthy et al., 1997). Due to the two mentioned facts (extraction procedure and pre-incubation), the extracted PAH levels of the starting conditions (at start of freezing procedure) may vary considerably from the applied amounts of PAHs. The decision for the materials to be used fell for sand and peat (see Table A.4 for details), because they were encountered in the West Siberian histic Cryosol described in chapter 4.1. The two materials sand and peat were contaminated with anthracene (258.06 mg kg^{-1} dw and 223.16 mg kg $^{-1}$), benzo[a]pyrene (12.9 mg kg^{-1} dw and 11.16 mg kg $^{-1}$ dw) and the naphthene-based crude oil Gryphon (5 % dw for both materials). The experiments should reveal, if considerable redistribution processes of the PAHs together with the present crude oil due to the freezing process take place. In comparison to the experiment *Sftao* the influence of the properties of the crude oil should be investigated.

Experiment with sand, freezing from the top, anthracen, benzo[a]pyrene and naphthene-based crude oil Gryphon (*Sftabo*)

The water distribution within the experimental columns after the freezing procedure shown in Figure 5.7 for experiment *Sftabo* is displayed in Figure 7.12. Water contents in the frozen zone were increased for the second soil layer in column A compared to the starting conditions (12.9 % dw). In column B water contents within the frozen part of the column did not exceed the initial water content, while the water contents in the reference column did. However, columns A and B showed significant lower water contents compared to the starting conditions in the lower, unfrozen part of the experimental columns, whereas the water content of the reference column ranged around the starting conditions. Maximum differences in water content accounted for 3.2 % dw. Compared to the differences in water content encountered in experiment *Sftao* it has to be stated that hardly any freezing induced water migration process was observed in the experiment *Sftabo*, even though cooling rates were less than 2.47°C day^{-1}.

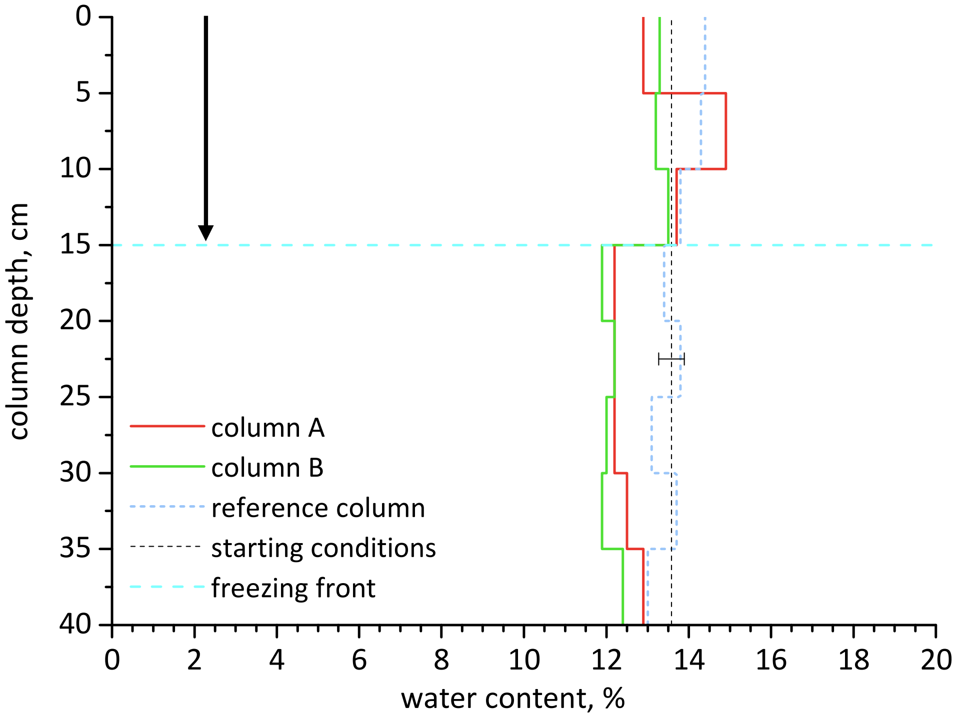

Figure 7.12 Water distribution in the experimental columns A and B and the reference column of experiment *Sftabo*, compared to the starting conditions. Arrow marks frozen part of the column and freezing direction.

The distribution of the solvent extractable fraction of the 3-ring PAH anthracene after the experimental approach shown in Figure 5.7 is displayed in Figure 7.13 (*Sftabo*). The experiment was conducted with sand and freezing from the top. The soil material was contaminated with anthracen, benzo[a]pyrene and the naphthene-based crude oil Gryphon. The indicated standard error and the course of the anthracene distribution in the reference column, which would be expected to show little variations, revealed that redistribution effects could only be detected, if they would exceed the described variations. However, as described above analytics with non-labeled PAHs usually have to admit variation coefficients around 10. Large variability could also be observed in the experimental columns (see Figure 7.13). No general trend could be observed. Overall the comparison of the mean of all samples of each column revealed that extracted anthracene content was significantly lower in the reference column, compared to the means of the experimental columns.

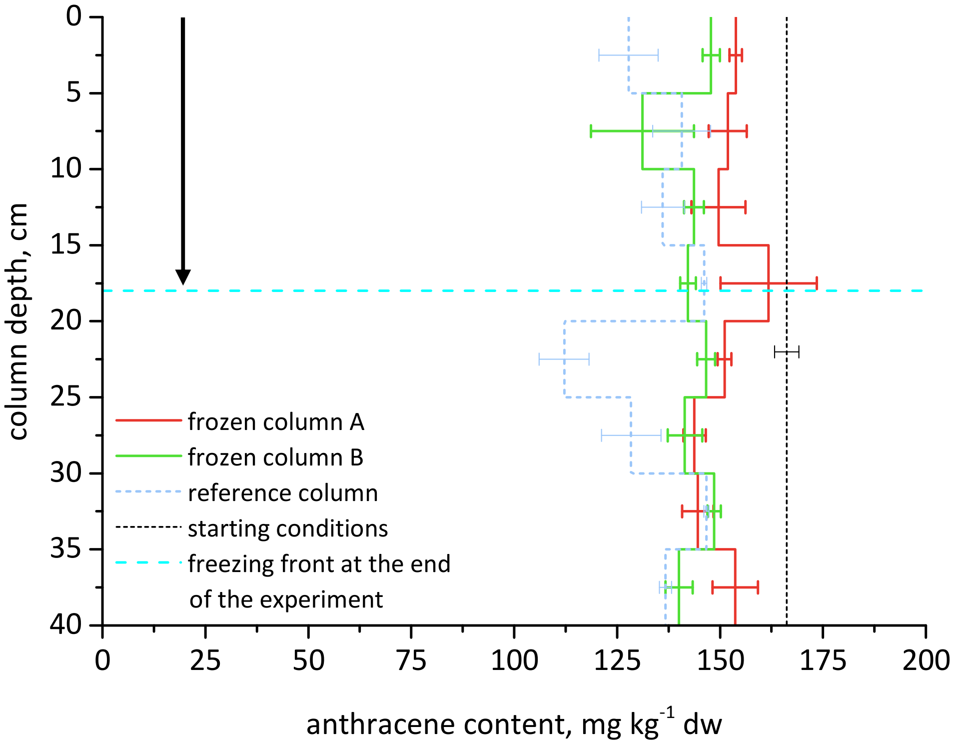

Figure 7.13 **Distribution of solvent extracted anthracene in the experiment Sftabo in the experimental columns, the reference column and the starting conditions. Standard error reflects n≥3. Arrow marks frozen part of the column and freezing direction.**

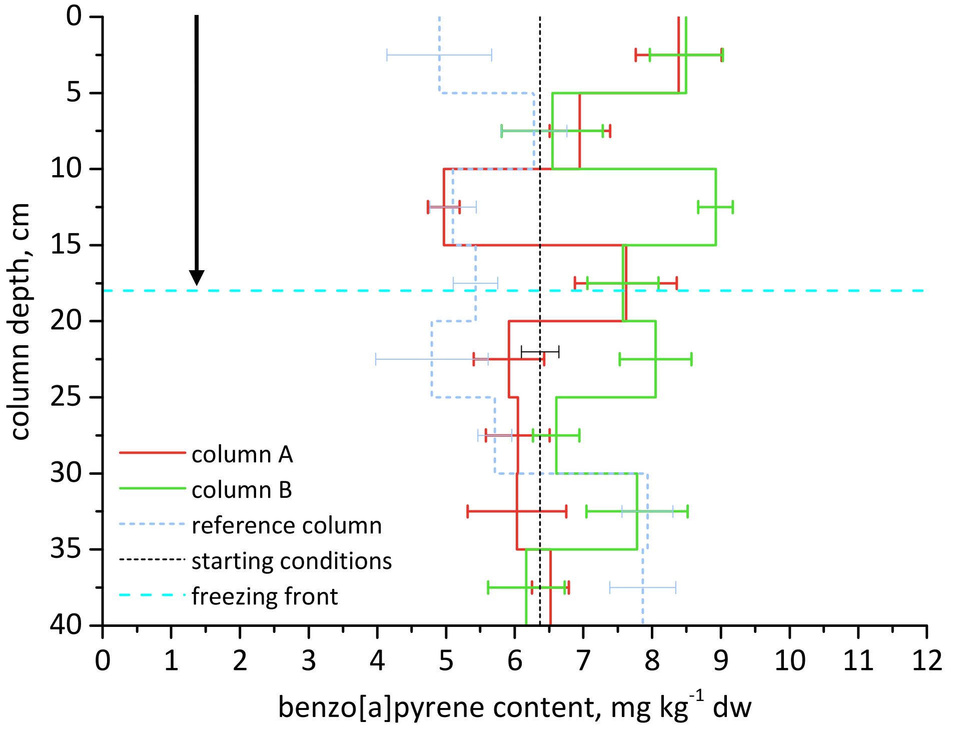

Figure 7.14 **Distribution of solvent extracted benzo[a]pyrene in the Sftabo in the experimental columns, the reference column and the starting conditions. Standard error reflects n≥3. Arrow marks frozen part of the column and freezing direction.**

That could be an indication for different processes in the reference column than in the experimental, frozen columns. Additionally the mean of column A was significantly higher than the mean of column B. The reference column showed the lowest absolute contents extracted with 112 mg kg^{-1} dw between 20 and 25 cm column depth. All extracted anthracene contents were significantly lower than the starting conditions.

The distribution of extracted benzo[a]pyrene within the experimental columns (A and B) and the reference column of the experiment with sand, freezing from the top, crude oil and two PAHs (Sftabo) is displayed in Figure 7.14. Data ranged around the starting conditions with a variability of about 30 %. Besides, the picture was similar to that of the anthracene distribution, determined by extraction. Generally, decreases and increases of extracted benzo[a]pyrene content were parallel to decreases and increases of extracted anthracene content. However, there were no significant differences between the means of the three columns. The lowest benzo[a]pyrene content was also found in the layer between 20 and 25 cm of the reference column. It is hypothesized that these data were outliers, which could not be removed due to the not normally distributed data of the reference column.

In summary it has to be admitted that freezing induced water migration could not be displayed well with the constantly low freezing rates. Therefore it is very likely that no significant effects on contaminant distribution were observed.

Experiment with peat, freezing from the top, anthracene, benzo[a]pyrene and napthene-based crude oil Gryphon (*Pftabo*)

In the experiment with peat, freezing from the top and anthracene, benzo[a]pyrene and naphthene-based crude oil Gryphon as contaminants (*Pftabo*) the most obvious features were the low total contents of extracted anthracene and benzo[a]pyrene at the end of the experiment, compared to the starting conditions (see Figure 7.15 and Figure 7.16). However, the displayed starting conditions were already very low, in comparison to the PAHs addition at the beginning of the experiment. That can be explained by the fact that the analyzed amounts displayed only hexan-extractable fractions of the peat material. Only 14.6 % of the initially added anthracene and 3.3 % of the added benzo[a]pyrene were extractable right after contamination. Again the importance of log K_{oc} can be taken from these results. Standard errors for the starting conditions, after the two weeks preincubation time were quite high, as can be seen in Figure 7.15 and Figure 7.16. After the experiment less than 50 % of the anthracene that was detected at the start of the experiment could be extracted from the upper 25 cm of the columns. In the experimental column A the extracted anthracene content triples below 25 cm column depth. In the reference column a similar behaviour can be observed below 30 cm. In column B highest extracted anthracene contents were reached between 5 and 15 cm column depth. Below, extracted anthracene content decreased to reach its minimum in the bottom layer of the soil column.

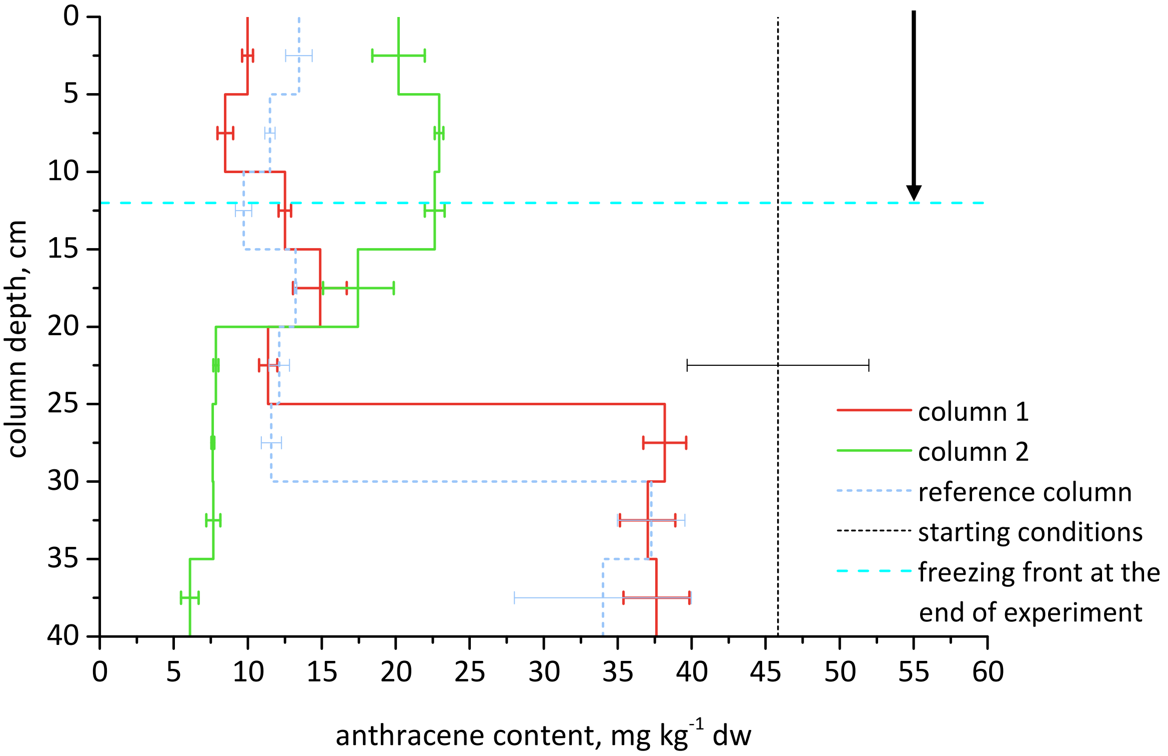

Figure 7.15 **Distribution of solvent extracted anthracene in the experiment with peat (*Pftabo*) within the experimental columns, in the reference column and the starting conditions. Standard error reflects n≥3. Arrow marks frozen part of the column and freezing direction.**

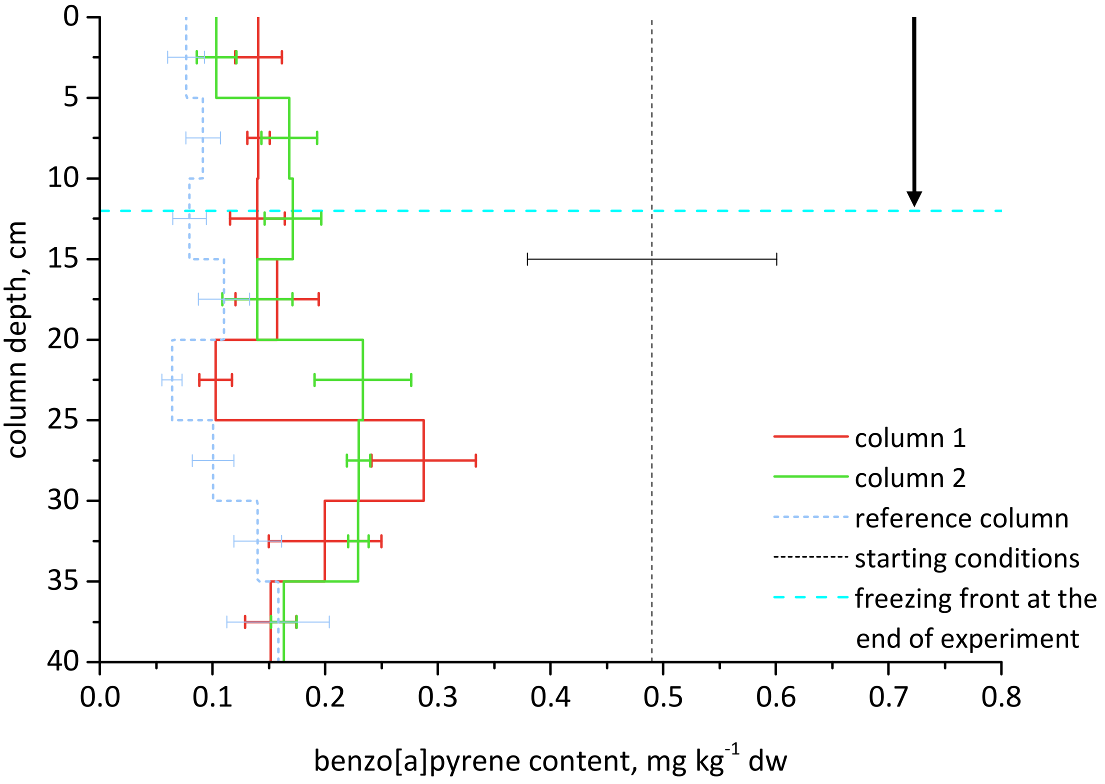

Figure 7.16 **Distribution of solvent extracted benzo[a]pyrene in the experiment with peat (*Pftabo*) in the experimental columns, the reference column and the starting conditions. Standard error reflects n≥3. Arrow marks freezing direction.**

The extracted benzo[a]pyrene content followed a similar trend as the extracted anthracene in column A with a maximum between 25 cm and 30 cm column depth. Although the increase was not as pronounced like it was for the anthracene content and benzo[a]pyrene content decrease directly beneath. In column B on the other hand the benzo[a]pyrene distribution followed almost an opposite trend compared to the anthracene distribution. The mean benzo[a]pyrene content of the reference column was significantly lower than the mean benzo[a]pyrene content of columns A and B. A trend according to the freezing front could not be distinguished. Exept one sample, all samples showed benzo[a]pyrene contents less than 50 % of the starting conditions. In comparison to the extraction yields of the experiment with sand, only about a twentieth part of the benzo[a]pyrene could be extracted from the peat material.

The presented results for sand and peat could not verify the hypothesis that PAHs in conjunction with crude oil gather ahead a freezing front. This was mainly due to the freezing procedure used, which did not induce water migration and accumulation next to the freezing front to a significant extend.

Another factor was the use of the naphthene-based crude oil Gryphon. It may be supposed that it consolidated in the upper column parts, as its pour point is at -3°C (see Table 3.1) and the experimental columns were cooled to less than -3°C within the upper 12.3 cm (see Table 5.2 and Table 5.3). With respect to the results and the observed standard errors, it has to be stated that the use of non-labeled PAHs was not in favor of the processes to be investigated and also the pre-incubation involved another parameter, whose influence cannot finally be estimated.

8. RESULTS ON THE IN-SITU DISTRIBUTION OF PAHS AND TPHS IN A PERMAFROST-AFFECTED SOIL

To get an insight into the behaviour and distribution of PAHs and TPHs under in-situ conditions a spill site in an else pristine area was investigated. The site was sampled twice within two years and anaylses of the properties and the organic contaminants are presented in this chapter. Table A.4 gives an overview of the soil properties. Further details of the site, the samples and the methods used for investigation are given in chapter 4.3.

8.1 PETROLEUM HYDROCARBON DISTRIBUTION 2009 AND 2011

About five and a half years after the diesel spill occurred, undisturbed 40 cm long soil cores were taken. In the laboratory the cylindrical, frozen samples were cut according to soil properties and layering over depth. The water content and the total petroleum hydrocarbon (TPH) content of the samples from the year 2009 are shown in Figure 8.1. TPHs are displayed as a sum parameter of the content of C_{10} to C_{40}. The water content was quite high throughout the whole profile, with a maximum of 167 % dw between 11.5 cm to 14 cm soil depth leaping from the decreasing trend in the upper part of the profile. The water content reached its minimum level of 65 % dw within the investigated soil profile between 14 cm and 16 cm soil depths. From this point downwards the water content increased until 160 % dw in the bottom soil layer.

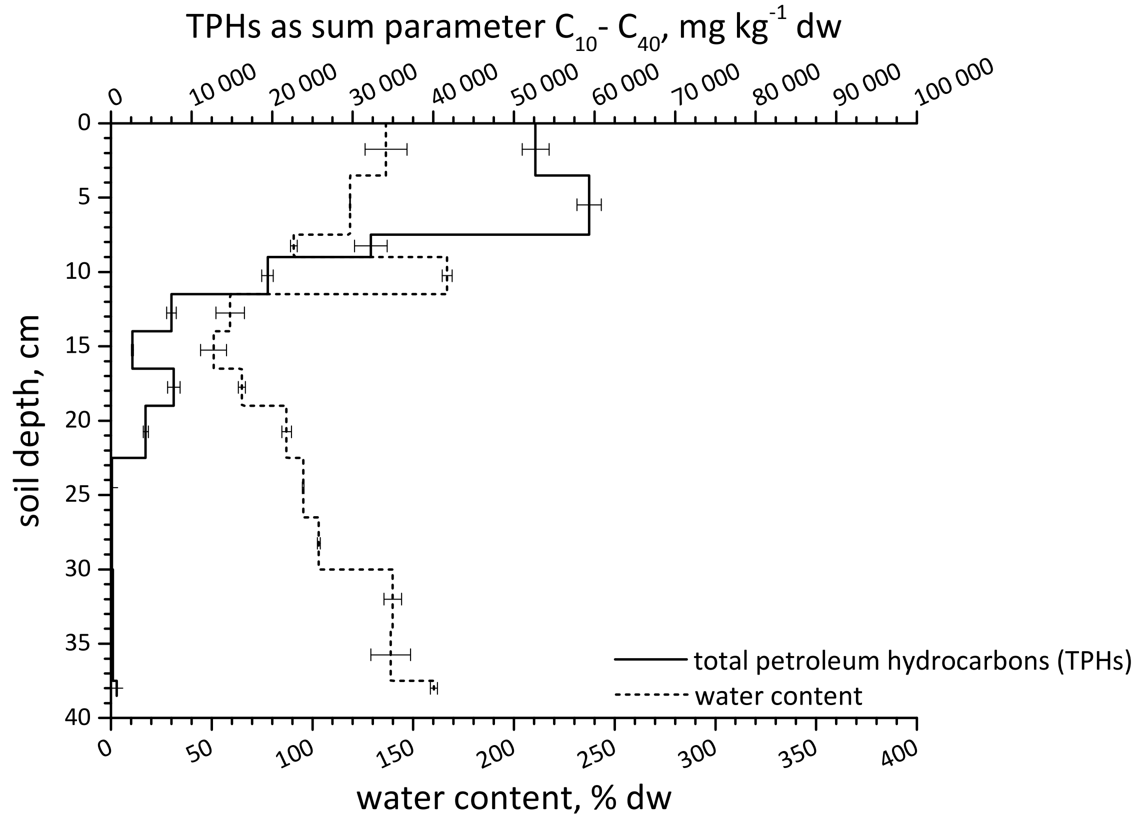

Figure 8.1 Distribution of TPH sum parameter (C10 – C40, grey line) and water (dashed, light grey line) within the contaminated soil profile in Northern Siberia at the sampling in 2009. Standard error reflects n≥3.

The maximum for the TPHs was with 60000 mg kg^{-1} dw in the second soil subsample between 3.5 cm and 7.0 cm. Below the TPH content decreased until 2680 mg kg^{-1} dw in the soil sample between 14.5 cm and 16.5 cm. The sample between 16.5 cm and 19.0 cm soil depth had with 7280 mg kg^{-1} dw a nearly threefold TPH content compared to the samples above and below it.

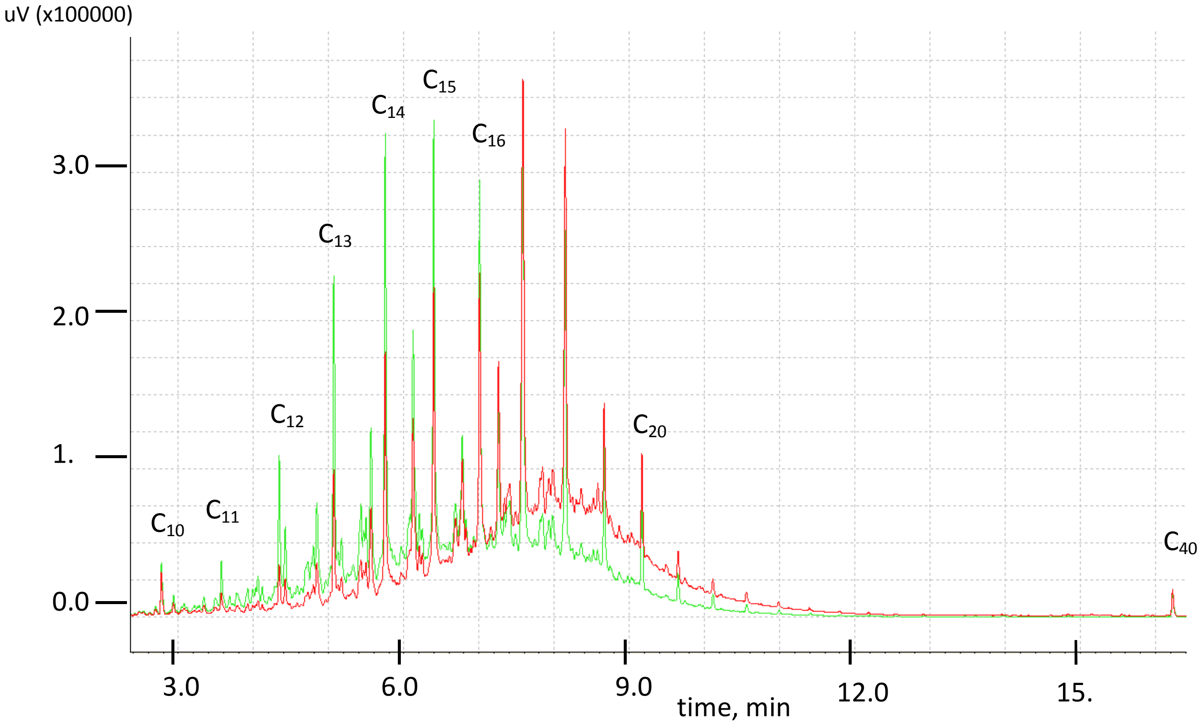

Figure 8.2 GC-FID Chromatograms of the first two samples from the diesel spill site in Northern Siberia from the year 2009. Red displays total petroleum hydrocarbons (TPHs) from the surface layer, green displays TPHs in the second soil layer (3,5 - 7,0 cm).

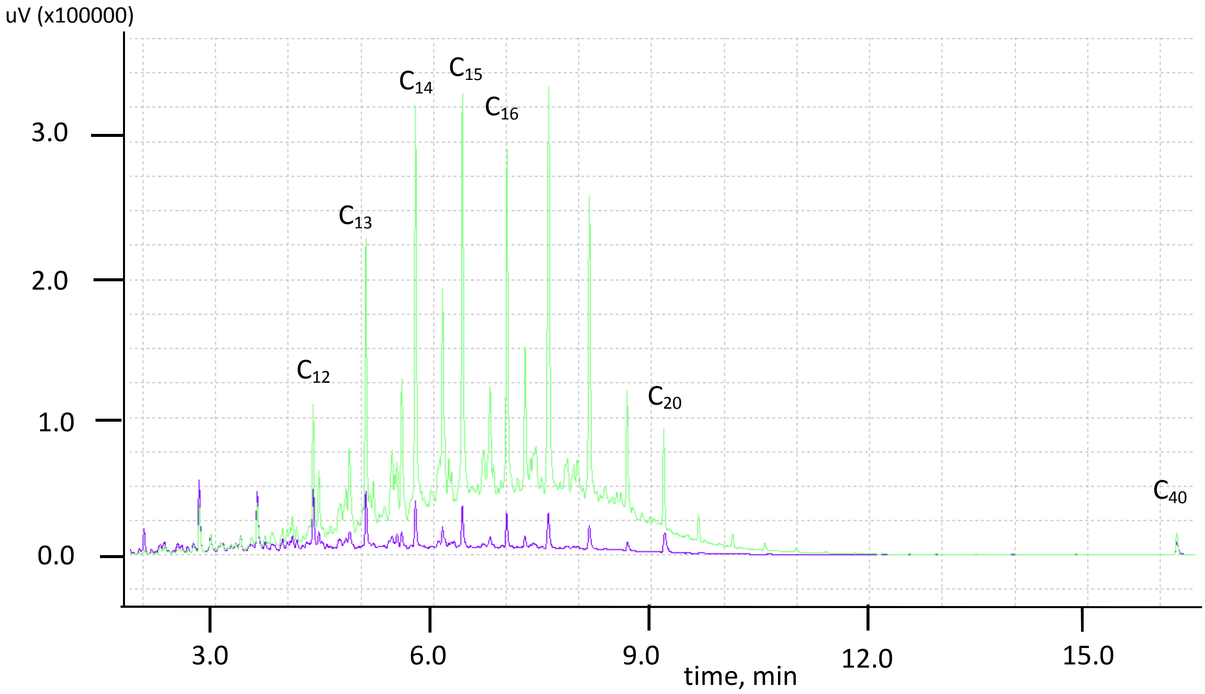

Figure 8.3 GC-FID Chromatograms of the second (3,5 – 7,0 cm) and the seventh (16,5 – 19 cm) soil layers of the soil core taken 2009. Green displays the analysis of the second soil layer and purple the ones for the seventh soil layer.

For a better interpretation of the different TPH contents some chromatograms are compared. In Figure 8.2 the PH chromatograms of the first two soil layers can be seen. It is obvious that in the second soil layer (green) the amounts for the hydrocarbons with shorter chains (C_{10} to C_{16}) were higher than in the surface soil layer (red). The comparison of the second and the seventh soil layer (Figure 8.3) revealed that even though the seventh layer has just a tenth amount of TPHs of the second soil layer, the amounts of C_{10} and C_{11} were higher there.

In Figure 8.4 the analyzed TPH content and water content of the samples from the year 2011 are shown. The maximum water content was found in the surface soil sample with 395 % dw. Further down the soil profile it decreased to 227 % dw between 9.5 cm and 12 cm soil depth. Then an increase of the water content of 66 % dw was observed, which was followed by a decrease by 182 % dw. The minimum water content of 75 % dw was reached in the soil layer between 17 cm and 19.5 cm. Below 19.5 cm it increased by 38 % dw and fluctuated further downwards around 115 % dw. The fairly high water content in the bottom layer of the soil core may be partially explained by melt water that occurred during sampling.

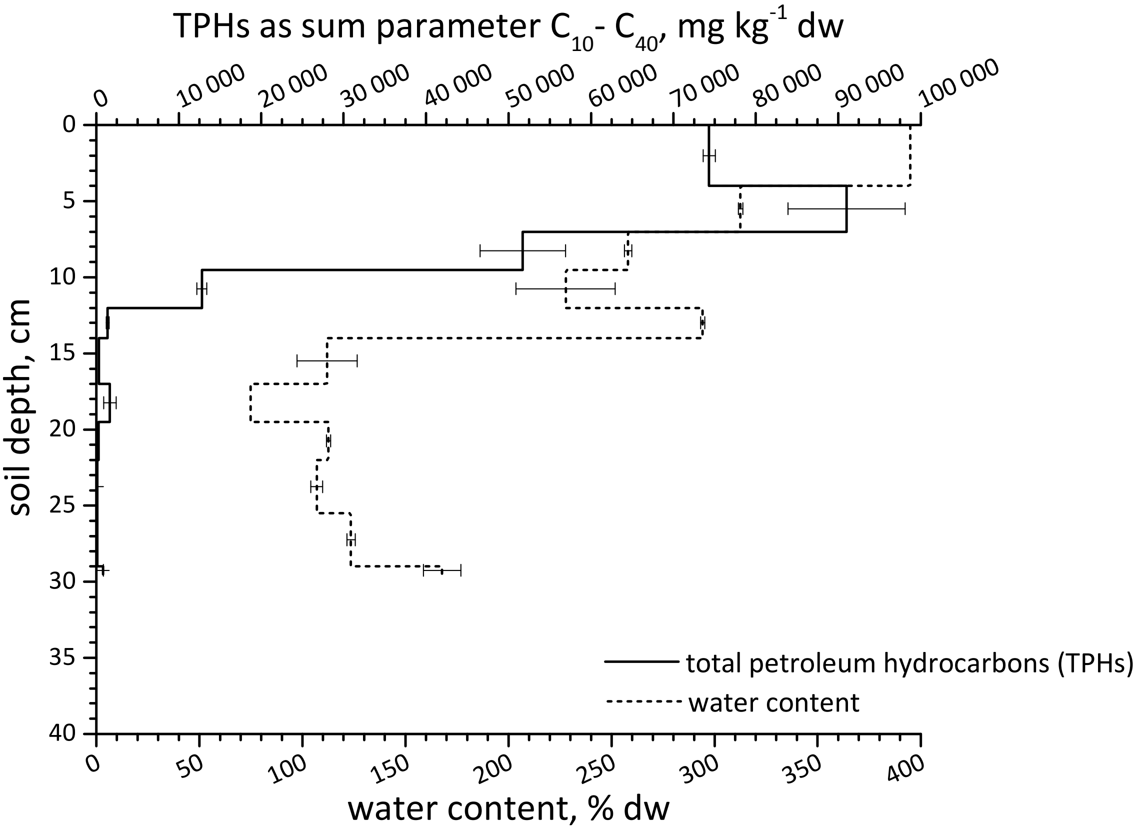

Figure 8.4 Distribution of TPH sum parameter (C10 – C40, grey line) and water (dashed, light grey line) within the contaminated soil profile in Northern Siberia at the sampling in 2011. Standard error reflects n≥3.

The TPH content in the soil core taken in 2011 had its maximum of 96660 mg kg^{-1} dw in the second soil layer between 4 cm and 7 cm. Downwards the soil core a steep decrease of TPH content was observed until a depth of 17 cm, where it was with

269 mg kg^{-1} dw close to zero. The soil layer from 17 cm to 19.5 cm shows a small increase in TPH content. Anyway in comparison to the minimum TPH content the increase made up 170 % of that minimum.

The comparison of the chromatograms of the first two soil layers of the soil profile from the year 2011 (see Figure 8.5) revealed that the amounts of the single petroleum hydrocarbons was not only higher for C_{10} to C_{16} but to C_{20}. This comparison confirmed the partitioning of the crude oil in the soil with time.

Comparing the results from 2009 and 2011 the most obvious differences could be seen in the absolute TPH contents and water contents. The water content in different soil depths is in all samples 9 % to 70 % lower for the samples from 2009 compared to the samples of 2011. Absolute TPH contents were much lower in the samples from 2009, too. A further difference is the absolute length of the soil cores taken. Both samples were taken at the end of August, but in 2009 the permafrost table was at 38.5 cm soil depth and in 2011 at 29.5 cm soil depth.

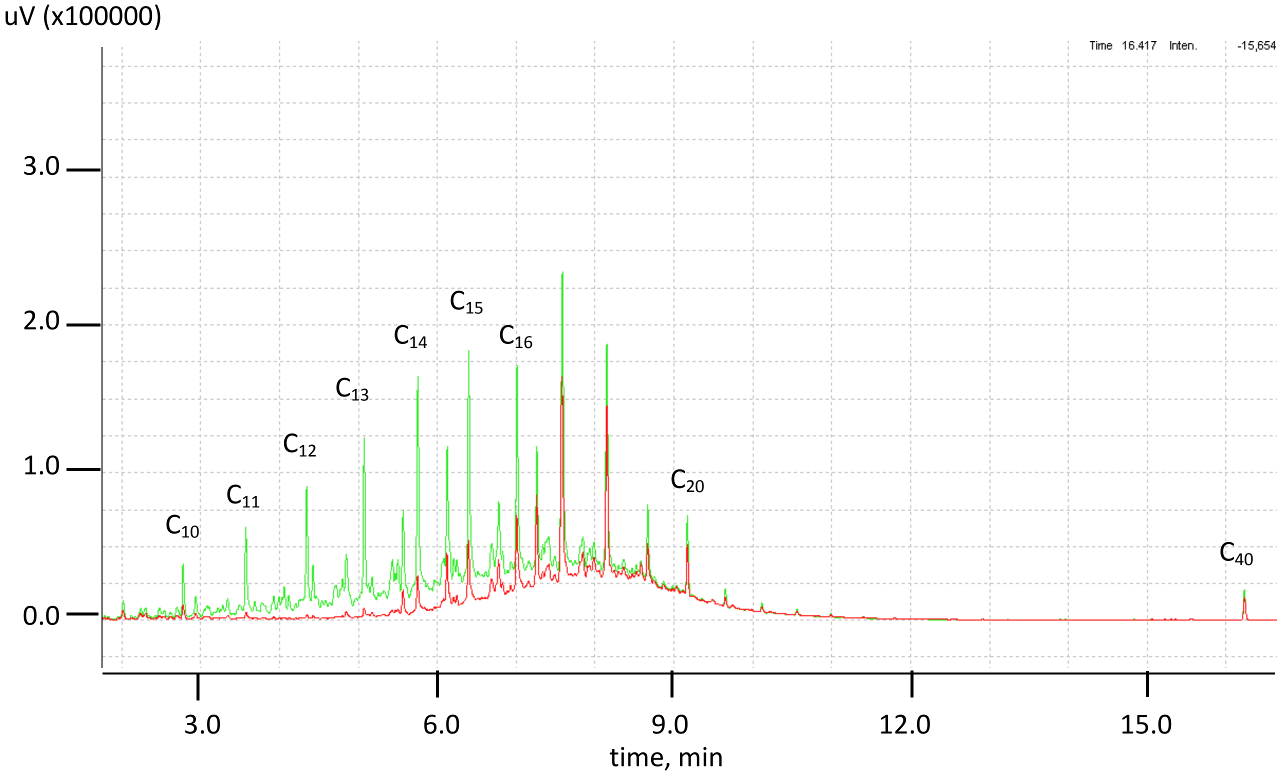

Figure 8.5 GC-FID Chromatograms of the TPH distribution in the first and the second soil layer of the soil profile sampled in 2011. Red shows the TPH distribution for the surface layer and green the TPH distribution for the second soil layer from 4 to 7 cm.

In general it was observed that the water content and TPH content showed similar trends for both soil profiles, even if a comparison of the absolute data between the two profiles was not possible. Both TPH content profiles showed an increase between 16 cm and 19 cm soil depth, even though the absolute contents differed by one order of magnitude. Furthermore the samples from 2009 and 2011 have in common that the water content increased within the lower part of the soil profile. PAH distribution and partitioning

The PAH distributions between the two soil cores differ, like the TPH courses did. Furthermore the sum parameter for the 16 EPA PAHs cannot undoubtedly be determined within the upper parts of the soil cores due to the high amounts of organic material within these soil parts. Further down in the soil profiles the sum of the 16 EPA PAHs and the TPH contents showed a similar course. Lowest detected PAH contents in the bottom layers of the soil cores still exceeded the natural background level, which is given with 4.8 µg kg^{-1} (Knoche et al., 1995).

Within the soil core taken in 2009 the 3-ring PAHs could not distinguished from the signals of the organic matter of the soil. Therefore they were not determined (see Table A.14). This circumstance results in an underestimation of the sums of the 16 EPA PAH in this part of the soil core (see Figure 8.6). The maximum value of the sum of the 16 EPA PAHs was found between 16.5 cm and 19 cm, together with the slight increase in TPH content in the otherwise decreasing TPH content curve. Furthermore the PAH curve showed the same pattern of increasing and decreasing values, as the TPH curve. Further downwards within the soil profile PAH contents were comparatively low, but with 66.5 µg kg^{-1} dw and 75.6 µg kg^{-1} dw they still exceeded the background level by more than factor ten.

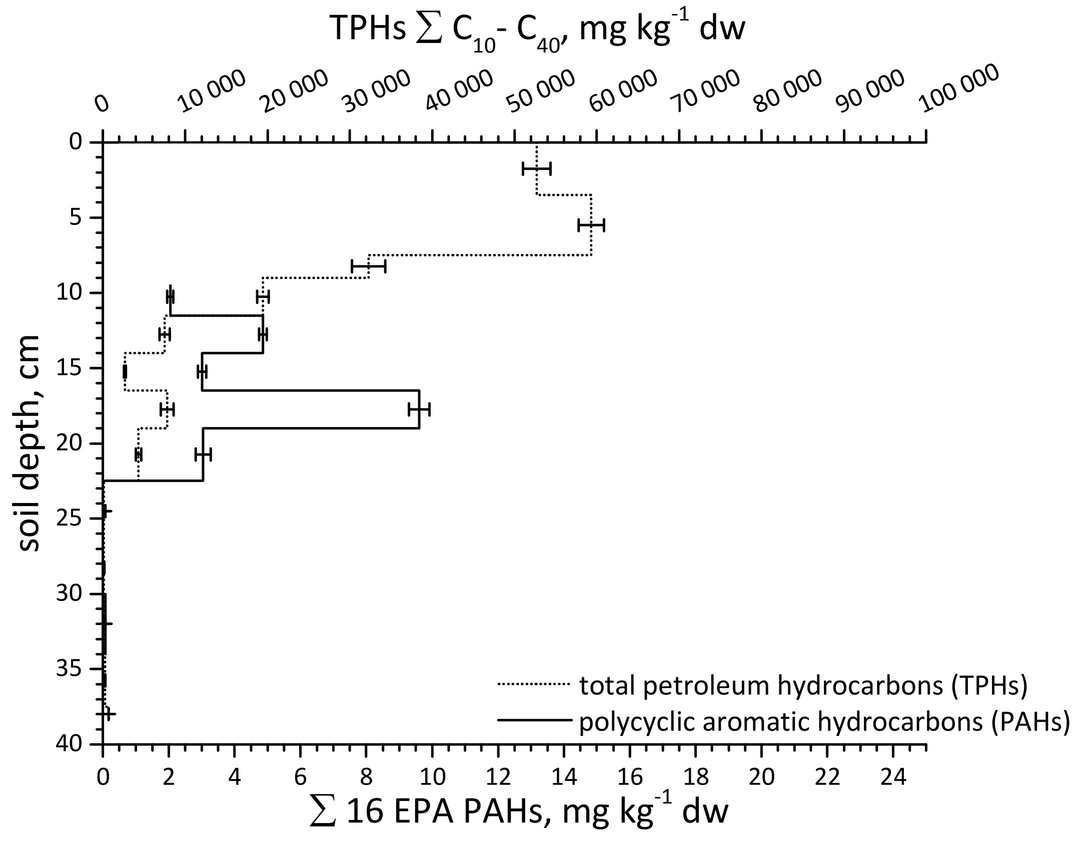

Figure 8.6 Distribution of TPHs and of Σ16 EPA PAHs in the soil samples taken 2009. Standard error reflects n≥3.

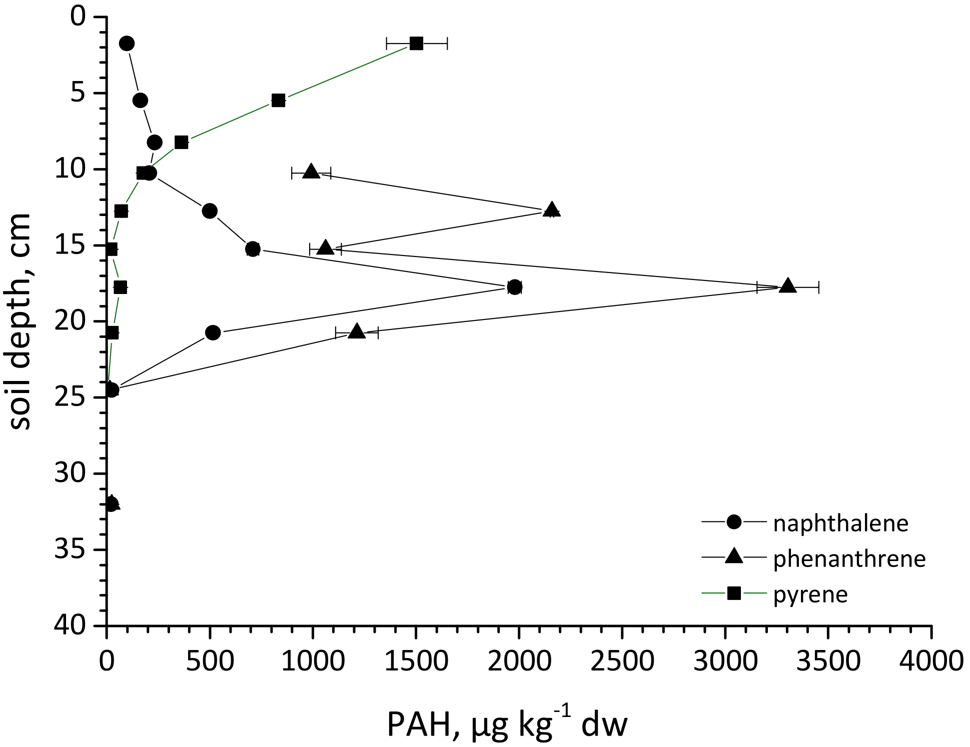

Figure 8.7 Distribution of single PAHs with different number of fused rings throughout the soil core taken at the contaminated site in Northern Siberia in 2009, standard error reflects n≥3.

As PAHs behave very differently according to their chemical structure the distribution of three single PAHs within the soil profile is shown in Figure 8.7. Naphthalene (dots), phenanthrene (triangles) and pyrene (rectangles) were chosen as examples. Naphthalene started off with low levels, with respect to a contaminated site, of 100 to 200 µg kg^{-1} dw within the first 10 cm of the soil profile. Further downwards an increase up to 1980 µg kg^{-1} dw was observed. However, below 19 cm soil depth the naphthalene content declined as steeply as the sum parameter of the 16 EPA PAHs and ended up at 20.8 µg kg^{-1} dw in the soil layer between 30 cm and 34 cm depth. The content for the 3-ring PAH phenanthrene was not determined in the upper 9.5 cm of the soil core, due to analytical difficulties described before. Beneath 9.5 cm soil depth the value for phenanthrene was determined with 992 µg kg^{-1} dw. From that point on it increased to reach 3304 µg kg^{-1} dw between 16.5 cm and 19.0 cm soil depth, which was the depth, where the TPH content had a local maximum.

The distribution of the 4-ring PAH pyrene differed distinctly from the distribution of the other two PAHs presented. Pyrene content had its maximum in the surface soil layer at 1500 µg kg^{-1} dw. Downward the soil profile the pyrene content decreased rapidly and reached 20.3 µg kg^{-1} dw in the soil layer between 14 cm and 16.5 cm. In the soil layer between 16.5 cm and 19 cm, where naphthalene and phenanthrene had their maximum contents, also a slight increase up to 68 µg kg^{-1} dw could be observed. The three PAHs presented have distinct partitioning coefficients for organic carbon (log K_{oc}) and distinct water solubility and fugacity ratio (see Table 2.3). Pyrene with its high organic carbon partitioning coefficient was adsorbed to a higher extent by the organic matter in the upper soil layers or other petroleum hydrocarbon components of the diesel oil, spilled at the site than naphthalene and phenanthrene, respectively. That this distribution is representative for the other 4-ring PAHs as well, can be taken from Figure 8.8. The contents for the single PAHs is shown for the surface soil layer and the soil layer between 16.5 cm and 19.0 cm soil depth, which held the maximum of the sum of the 16 EPA PAHs analyzed. Due to missing data for 3-ring PAHs in the surface soil layer, it cannot be stated that the 4-ring PAHs determined the sum of PAH present in this soil layer. But this statement could be made for the 3-ring PAHs in the soil layer between 16.5 cm and 19.0 cm soil depth. The depletion of naphthalene in the surface soil layer may also be an effect of volatilization. The higher molecular weight PAHs could only be analyzed in the surface soil layer, whereas their values were below the detection limit below 16.5 cm soil depth.

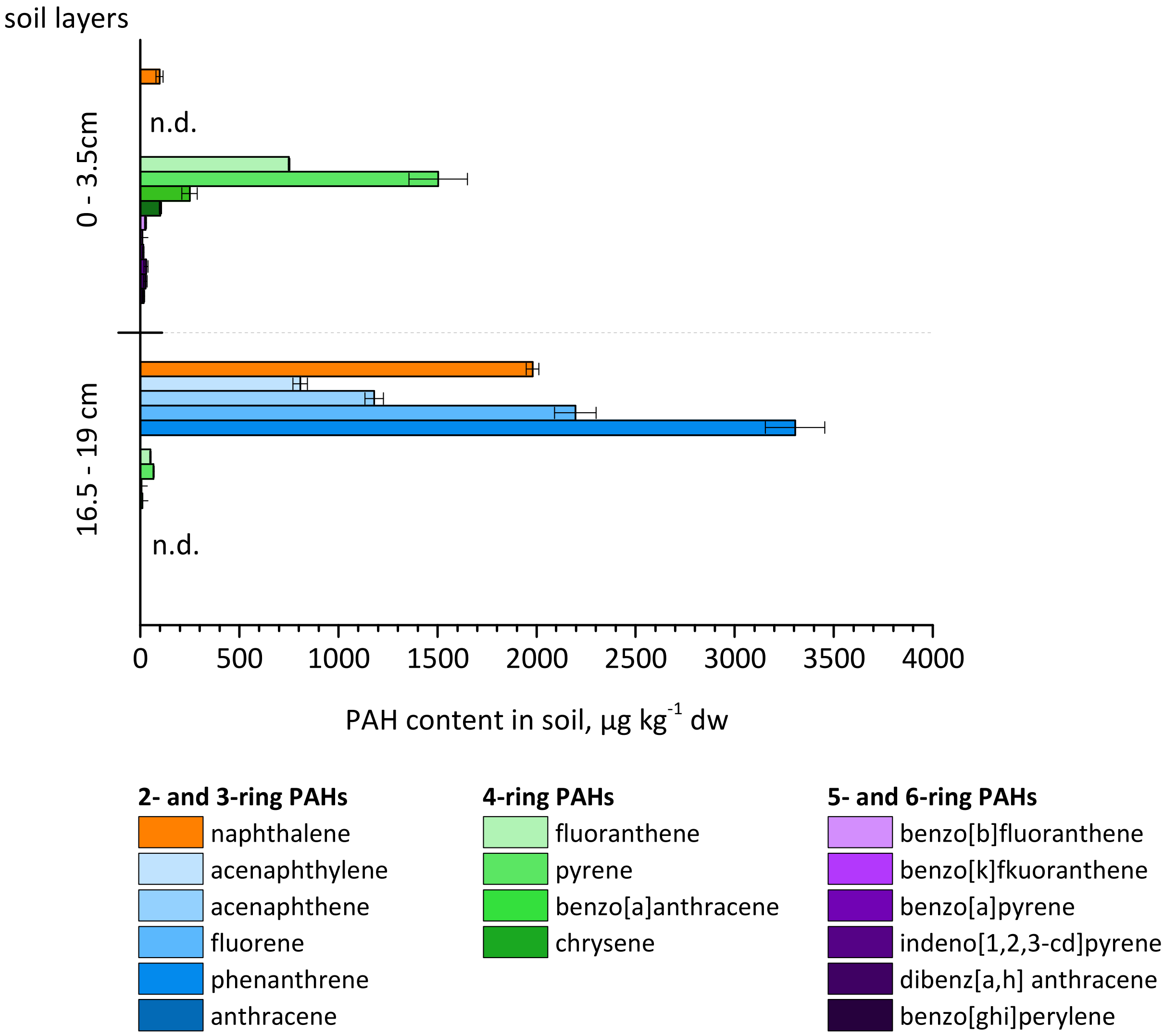

Figure 8.8 Contents of 16 EPA-PAHs in two soil depth (0 – 3.5 cm and 16.5 – 19.0 cm) of a diesel and lubricant oil contaminated soil in Northern Siberia, soil samples taken 2009.

The analysis of the TPH and PAH contents over depth revealed that a downward transport of both groups of compounds took place within the (at least) three years that passed by since the contaminants entered the soil. Furthermore a partitioning of both contaminant groups was observed, with a relative increase in higher molecular weight compounds in the upper two soil layers. Maximum contents of the analyzed TPH and PAH were found in different soil depth, even though the distribution patterns were similar.

In the soil samples taken in 2011 the course of the PAH distribution almost followed the course of the TPH distribution, except in the upper 7 cm of the soil, where organic carbon contents were fairly high (see Figure 8.9). The maximum value for the sum of the 16 EPA PAHs was found directly beneath the soil part with the most probably underestimated PAH values from 7 cm to 9.5 cm soil depth. It almost doubled the value of the PAH maximum determined in the soil core from 2009. The values of the single PAHs analyzed revealed that phenanthrene accounted for 52 % of the maximum of the Σ16 EPA PAHs (see Figure A.3 and Table A.15).

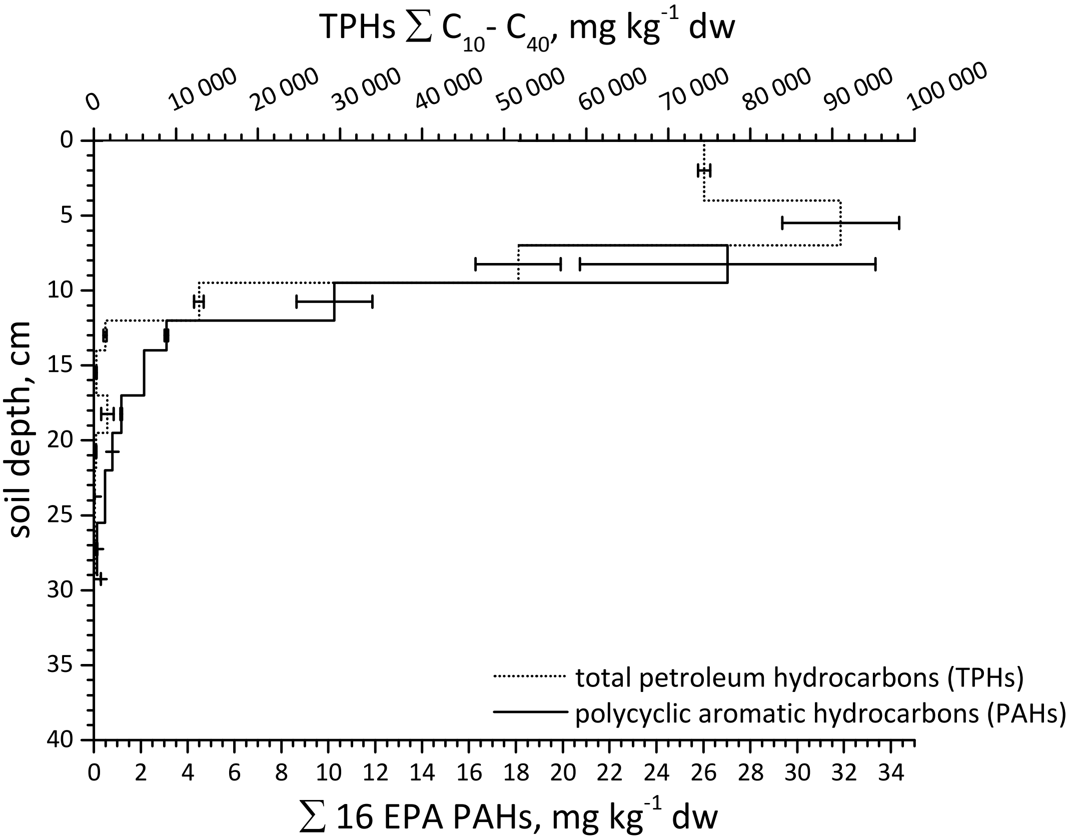

Figure 8.9 Distribution of TPHs and of Σ16 EPA PAHs in the soil samples taken 2011. Standard error reflects n≥3.

The distribution of naphthalene in the soil samples of 2011 was similar to that in the samples from 2009, but the maximum value in 2011 only made up two thirds of the maximum naphthalene content found in the soil core of 2009. The TPH maximum was found in the soil layer above the PAH maximum. Beneath 9.5 cm soil depth PAH contents decreased until the bottom of the soil core at 29 cm. The lowest value for the sum of the 16 EPA PAHs was 139.3 µg kg^{-1} dw, which far exceeds background level. The maximum for the 4-ring PAH pyrene was found in the second soil layer together with the TPH maximum content, whereas the maximum content of pyrene had been detected in the surface soil layer in 2009. Furthermore the value of the pyrene maximum only reached half of the maximum pyrene value found in the soil core from 2009.

In summary it can be said that PAH migrated through the soil, as they were detected at levels far above the background level. Furthermore the single substances partitioned, due to their physical and chemical properties. The PAH distribution pattern was similar to the TPH distribution pattern, but maxima for both contaminant groups were detected in different soil layers, which may be due to the fact that the 3-ring PAH phenanthrene was the main compound analyzed, but it could not be determined in the upper soil layers because of matrix effects that masked the values of most of the 3-ring PAHs in the upper soil layers.

9. DISCUSSION

Organic contaminants in soils pose a threat to the soil functions. Only little is known about the interaction of vulnerable freezing grounds and organic contaminants. To get an understanding of single processes taking place in soils contaminated with PAHs and TPHs laboratory studies were conducted. The first part of the studies presented here deals with the methodological implementation to bring the natural occurring freezing process with its accessory phenomena on a laboratory bench scale. On that basis the behavior of PAHs in freezing soils with and without crude oil present was studied in laboratory column experiments. In a second part the distribution of PAHs and TPHs in a permafrost-affected soil in Northern Siberia was analyzed. In conjunction with published data on the topic the influencing factors and processes of the fate of TPHs and PAHs in permafrost-affected soils are discussed.

9.1 SIMULATION OF THE FREEZING PROCESS IN LABORATORY EXPERIMENTS

The aim was to develop an experimental setup that allows the simulation of natural occurring freezing processes in soils contaminated with PAHs and TPHs. Having this target and the suggestions given in chapter 2.2.2 in mind two experimental setups were developed (see Figure 3.2 and Figure 3.3). Setup 1 with three parallel run columns and a reference column, all with a height of 10 cm and a volume of 385 cm^3 was invented to decode single processes taking place in contaminated freezing soils with ^{14}C-labeled chemicals. Studies on both, the influence of the freezing process on organic contaminants (Chuvilin et al., 2001; Konrad & Seto, 1991), as well as studies on the behavior of contaminants in soils in general (Wehrer & Totsche, 2005; Weigand et al., 1999) were carried out with columns of this magnitude. Working with ^{14}C-labeled chemicals includes the need of specific laboratory equipment and safety precautions, but it provides the possibility of recovery rates around 100 % with low standard errors. To get closer to real dimensions of the active layer and therefore involve more parameters to the system Setup 2 with two parallel run columns and a reference column, all with a height of 40 cm and a volume of 2776 cm^3 was invented. Due to the large amount of contaminated soil material needed to conduct the experiments, it was decided to use non-labeled contaminants for environmental protection reasons on the expense of recovery rate and low standard error of analysis.

For the **construction of the experimental setup** best column and insulation materials were defined. From Table 5.1 it can be taken that PVDF is the material that meets the requirements of high chemical resistance, low thermal conductivity and high material stability best. It was chosen for the construction of the columns for setup 1. As PVDF could not be provided in the dimensions of experimental setup 2, it was decided to use Plexiglas® for the column construction, due to its low thermal conductivity. The outer part of the soil samples was refused for analysis of organic contaminants to avoid influences of the column material on the results. Like in preliminary experiments by Barnes and Wolfe (2008) it has been shown that the tightness of the system at the bottom of the columns may not be assured by contact pressure only. Therefore a stainless steel lid was invented at the bottom parts of the experimental columns of setup 1. This improvement could ensure that columns were hermetically sealed, but decreased the heat flux from the cooling head to the soil. The cooling head at the top of the experimental columns had direct contact to the soil, to have nominal control over the cooling front within the soil column. An air-filled headspace, as suggest by Chuvilin et al. (2001), to account for expansion processes during freezing, proved to be disadvantageous. The low heat conductivity of air (0.0262 W $m^{-1} \cdot K^{-1}$) led to insufficient cooling within the soil. Hence, the position of the freezing front could not be controlled properly. Both experimental setups employed closed systems, to minimize input parameters. During sampling soil specimen were examined for side wall effects. As no preferential path ways were observed and soil material was still homogeneously distributed it can be stated that side wall effects did not occur. To control the thermal heat flux into the columns insulation material was mounted. Styrodur® and Armaflex® proofed to be the best choice, due to low heat conductivity. According to mounting Armaflex® showed the best properties. The 13 mm thick polyethylene cellular plastic insulation was too thin on the one hand and not flexible enough to be mounted tightly to the system on the other hand. Therefore freezing of half of the experimental columns was not achieved. The replacement of the polyethylene cellular plastic insulation by 35 mm Armaflex® could reduce thermal heat flux and more than half of the experimental column height could be subjected to controlled freezing. Tubes from cooling machine to experimental columns and back were also insulated with Armaflex®. Concerning the tubes, tube lengths and the device used to split the tube of the incoming cooling liquid to the three tubes running to the individual cooling heads of experimental setup 1 proofed to be of importance. In running three experimental columns parallel, reproducibility as suggested by Biggar and Neufeld (1996) should be gained. In the preliminary experiment *Ufb* temperatures between the three experimental columns varied with a maximum of 2.8°C. Different lengths of the tubes from the cooling machine to the cooling heads of the columns were identified as a factor for different soil temperatures inside the columns and therefore tube lengths were adjusted, to equal lengths. However, as could be seen in Figure 5.5 and Figure 5.6 temperature profiles of the three columns still did not run parallel during the whole time the experiment lasted. Especially column C showed retarded temperature decreases. The problem has been solved by mounting valves for the manual regulation of cooling liquid flux for each column. Therefore the temperatures in the three columns could be individually adjusted, resulting in parallel temperature profiles during the major part of the experiments. Soil and contaminant parameters were chosen according to relevance in permafrost-affected areas.

For the **determination of a freezing procedure** that simulates natural occurring freezing processes best, main emphasis lay on the use of naturally occurring freezing rates, lowest absolute temperatures in the experimental columns and the generation of freezing induced water migration with subsequent formation of segregation ice.

The water migration and ice formation process provide evidence for the simulation of a naturally occurring freezing process within an active layer. This was an important goal, as the impact of the freezing process on the fate of PAHs in soils should be investigated. Invented experimental procedures are given in chapter 5.2. The decision to work with cooling rates lower than 4°C day^{-1} based on the observations in Arctic soils, where cooling rates up to 3.1°C day^{-1} (Siberia) and between 0.05°C day^{-1} to 0.5°C day^{-1} (Canada) were observed (see chapter2.2.1). Furthermore Konrad and McCammon (1990) and Konrad and Seto (1991) determined threshold rates of cooling for the rejection of solved organic contaminants from segregation ice of 2.95 ± 0.25°C day^{-1} and 4 ± 1°C day^{-1}, respectively. Most pronounced influence of cooling and ice formation on soluble organic contaminant distribution was observed at cooling rates below 0.1°C day^{-1} (Konrad & McCammon, 1990). Different experimental procedures have been used to simulate the low naturally occurring cooling rates and investigate the impact of cryosuction, freezing induced water migration and segregated ice formation on the fate of PAHs or other contaminants in different soil materials. As mentioned before for research questions emphasizing on the investigation of single processes experimental setup 1 together with ^{14}C-labeled chemicals should be used. At the beginning of an experiment the columns have to be cooled down very rapidly, to prevent soil water migration before the actual freezing process started, because soil water already starts to migrate upon a thermal gradient within the soil (Grant & Hillel, 2005). It was necessary to prevent water migration before the process of ice segregation takes place within the column, because the experimental setup is constructed as closed systems. That means the amount of water available for the processes within the system is set.

The effect of too slow cooling at the beginning, especially for experiments with freezing from the bottom and the resulting water distribution can be seen in the water content distribution of the experiment with silt and freezing from the bottom (*Ufb*) (see Figure 5.3). Even though water contents differed significantly between frozen and unfrozen column parts, implying that a freezing induced water migration process took place, the water contents in the soil layer next to the freezing front, only showed slight increases in water content compared to the starting conditions. But the maximum absolute water content would have been expected in this soil layer, if the process of cryosuction and formation of segregation ice would have taken place in a considerable way. As maximum water contents were found in the frozen soil layer between 7 cm and 8 cm column depth, it may be assumed that the water migration process was most pronounced, when the freezing front was situated at this depth. The low input cooling rate and the maximum water content of up to 40.79 % dw in this soil layer lead also to the assumption that the propagation of the freezing front was retained for a certain time at that depth, because the water supply with subsequent freezing of the water resulted in the release of sufficient latent heat to cancel the incoming cooling energy out. However, on the propagation of the freezing front most of the water in the system was kept in frozen state in the lower part of the soil columns. Therefore it was not available anymore for the process of cryosuction and ice formatin, when the freezing front reached its final position within the soil columns. A second reason for the marginal differences between water contents found beneath and above the freezing front may be the short duration of the experiment. The experiment only lasted 96 hours. Water contents in the unfrozen zone of the experimental columns were still between 9.22 % dw and 23.05 % dw, which is fairly above the wilting point of the silt loam of 5.4 % dw. As the wilting point is defined as the soil water potential of 1.5 MPa and Williams and Smith (1991) stated that already temperature differences of 1°C m^{-1} may induce soil water gradients with a hydraulic potential of 1.2 MPa m^{-1} it is hypothesized that the freezing induced water migration was not finished by the end of the experiment. It is furthermore hypothesized that with prolonged experiment duration the water contents in the frozen layer next to the freezing front would have been higher and water contents in the unfrozen zone would have been lower than analyzed.

Abrupt temperature decrease on the other hand, as in experiment *Ufba* (see Figure A.1Figure 5.1) also did not lead to the desired effect of considerable segregation ice formation at the final freezing front, which would be displayed by maximum water contents within the experimental columns. Maximum water contents were also found in the lower, frozen parts of the experimental columns (see Figure 6.1). An adjustment of the freezing scenario in experiment *Ufbp,* with a cooling of 20.0 °C day^{-1} within the first 18 hours of the experiment, followed by a cooling rate of 3.5°C within the next 67 hours and constant input cooling temperatures for the last 64 hours of the experiment, resulted in the intended maximum water content at or close to the final freezing front (see Figure 6.2). Cryosuction and freezing induced water migration could also be displayed by the fact that even though input temperatures decreased between 36 and 96 hours after the experiment started the temperatures in the experimental columns remained constant. That means sufficient water arrives at the freezing front that the released latent heat from the phase transition from water to ice equals the input cooling energy out, resulting in a delay of freezing front propagation. In turn these results determine that a freezing rate of 3.5°C day $^{-1}$ may induce freezing induced water migration and ice segregation in silt loam with an initial water content of 26 % dw, if the soil columns have been partially frozen before. The phenomenon that TDR signals and to a small extend also temperatures (0.04°C – 0.28°C) oscillate during the last 64 hours of the experiment, even though input cooling rate is 0°C may be explained by small differences in ambient room temperature (0.6°C). If the oscillation also induced freezing front movements, these may explain the fact, that the maximum water contents in columns B and C were found 1 cm and 2 cm beneath the freezing front within the frozen column part (see Figure 5.4). Another interesting observation was that temperatures started to fall with high cooling rates, when the input cooling rate had been brought down from 20°C day^{-1} to 3.5 °C day $^{-1}$. This pattern might be a phenomenon of thermal impedance, as cooling input was too high before, but the effect has not been described in the literature yet.

Water contents within the whole frozen column part of experimental columns in experiment *Ufbp* were still elevated. This pattern may not finally be solved, as the freezing front always needs some time to propagate to its final position and during this time freezing induced water migration towards the freezing front takes place. In summary the specific water distribution pattern within the experimental columns with freezing from the bottom is mainly a result of:

- closed system condition
- water contents below water saturation level
- input cooling temperatures and cooling program

Konrad and Seto (1991) employed an open system setup with soils at water saturation level for their experiments with freezing from the bottom. With the open system setup, the process of water migration towards the freezing front and formation of segregated ice is not limited by the water content and therefore is just a function of freezing rate and experiment duration. Therefore K+S observed the formation of segregation ice, resulting in a visible 0.15 cm thick ice lens. It has to be admitted that the formation of segregation ice can be simulated best with an open system setup and water saturated soil material. Nevertheless the specific cooling program used in experiment *Ufbp* could simulate freezing induced water migration and to some extend ice formation at the freezing front at maximum water holding capacity of 60 % in a closed system.

All temperature courses for setup 1 with 2-wire pt 100 temperature probes show the distinct pattern of the freezing process at absolute temperatures above 0°C. That fact does not mean that the equilibrium freezing point was above 0°C, but displays a systematic measurement error. Firstly 2-wire probes are more susceptible to outside temperatures and the influence of the cable length on the measured temperature than 4-wire probes. Secondly the temperature probes measure the temperature over their total lengths. The probes at 3 cm column depths only extended 1 cm into the column and their main part rested in the insulation. They could not be inserted further into the column, because they should not disturb the measurement of the TDR probes. The systematic error accounted for at least 0.3°C. That was the temperature at the end of experiment *Uftpo*. During sampling it was observed that the temperature probes were located within the frozen part of the columns. That means temperatures at the end of the experiment must have been at least 0°C and were more likely lower, considering that the equilibrium freezing point is nearly always depressed in soil solutions(Yershov, 1998) and the presence of oil also rather leads to a depression of the equilibrium freezing point of the soil (Grechishchev et al., 2001). As the freezing process was also detected by the almost vertical decrease of the TDR signal, due to ice formation and the along going change in electric conductivity the measurement error may be determined by the initiation of this event. This was observed in the three experimental columns and the different experiments between 2.56°C and 3.51°C. Therefore the value of the over estimation of temperatures in the experiments with setup 1 is approximated to be within this range. Temperature courses with 4-wire pt100 temperature probes showed the effect around 0°C (see Figure 5.7 and Figure 5.9). Therefore the equilibrium freezing point for peat at 480 % dw water content was determined with -1.03°C and the one for sand with 13.6 % dw water content with -0.08°C. Furthermore it has been observed that temperatures fell below 0°C at 1.1 cm column depth with a time lag of only 40 minutes (accounting for 1.5 % difference) even though water contents differed extremely and input cooling rates were equal. But the time to reach the equilibrium freezing point differed considerably and was twelve times longer in peat than in sand. That means cooling of the soil at temperatures above 0°C is only slightly retarded due to higher water contents and different heat conductivities of the materials (sand: 1.8 W $m^{-1} \cdot K^{-1}$, peat: 0.5 W $m^{-1} \cdot K^{-1}$). However, the phase transition from water to ice at temperatures below 0°C and the along going release of latent heat, cause an increased impact of water content on soil temperatures and freezing front propagation.

For the experiments conducted with freezing from the top and oil contaminated soil materials the temperature probes at 3 cm column depth were within the frozen parts of the soil columns during the second half of the experiments (see Figure 5.5 and Figure 5.6). That means the freezing front passed the probes, thus the specific temperature and electric conductivity patterns of the freezing process were recorded. The temperature course with the specific temperature drop, followed by a short increase, due to latent heat release (Williams & Smith, 1991) is displayed best in the in column C of the experiment with silt loam (see Figure 5.5). The temperature in column C did not run parallel with the other two experimental columns and only a decrease of input temperature of from -5.0°C to -5.5°C and a manual adjustment of the cooling liquid flow led to the propagation of the freezing front below 3 cm column depth. However, as temperatures within the column equilibrated just above 0°C (actual temperature, not measured) the temperature drop until the probable equilibrium freezing point and the following temperature increase could be seen more clearly than in the other two experimental columns. The TDR signal displays the freezing induced water migration towards the freezing front, during the time, when temperatures probably were below 0°C with an increase and the ice formation with the almost vertical decease. This differing cooling procedure in column C compared to the other two experimental columns A and B of experiment *Uftpo* also led to a different water distribution within the experimental columns. Maximum water contents were found in the top soil layer of the experimental columns. Therefore it may be hypothesized that that the major amount of water migrated within the first half of the experiment. However, maximum water content in column C is considerably lower than the ones in columns A and B. That may be an indication that cryosuction was not as strong as in columns A and B, because the temperature gradient within the column was not as high as in the other two experimental columns. Therefore less water migrated. As temperature profiles ran parallel during the second half of the experiment, columns B and C both show a considerable increase of water content just above the freezing front, in the frozen part of the column, with column B having the highest water content in this soil layer. Column A does not show this pattern, even though temperature course did not differ from the ones of the other two columns. But the TDR signal course did. The almost vertical decrease, determining the phase transition from water to ice is not displayed. TDR signal even increased at the end of the experiment. This pattern might be explained by the location of the freezing front throughout the second half of the experiment directly at 3 cm column depth, were the TDR and temperature probes were installed. The steel rods probably disturbed the formation of segregation ice. The observations reveal that it is important to monitor the cooling and freezing of the experimental columns with both, temperature and TDR probes. Furthermore it can be seen, that a well reproduced freezing process and freezing front propagation, like observed in column C, results in the simulation of freezing induced water migration and segregation ice formation. However, it does not necessarily mean that freezing induced water migration and segregation ice formation are simulated in the best way.

In the experiment with crude oil and sand it is obvious that TDR signals in column A and B plotted a water increase in 3 cm column depth, 42 hours after the experiment had started. That was exactly the time, when input cooling rate was set to 0°C. From that point onwards temperatures fell with an increased cooling rate in columns A and B. In column C temperatures started to equilibrate and were only brought back to the course of the other two columns after manual adjustment of the cooling liquid flow. Indeed TDR signals in all columns decreased after the described event, but the almost vertical drop, which displays the formation of ice, could not be observed. Only upon decrease of input temperature by 0.2°C from -5°C to -5.2°C, temperature and TDR signals showed short and steep decreases, which indicated the propagation of the freezing front. After 96 hours of the experiment, the input cooling rate had been set from 0°C day^{-1} to 0.15°C day^{-1}, which resulted in a maximum cooling rate within the soil columns of 0,006°C day^{-1}. The resulting water distributions in the experimental columns reveal that with this procedure cryosuction was strongest, because the sand (with 5.61 % clay and 2.43 % silt) was dehydrated in the lower unfrozen part of the columns until water contents (1.29 % dw – 1.72 % dw) at wilting point level (1.41 % dw). That indicates furthermore that pore pressures up to 1.5 MPa were induced by cryosuction. Furthermore, the freezing procedure used led to maximum water contents, which reached saturation level, in the frozen soil adjacent to the freezing front. Water contents within the whole frozen column part were significantly higher compared to the reference column and the starting conditions. As this freezing procedure had not been used in an experiment with silt loam, it cannot finally be stated that the use of very low cooling rates during the last 42 hours of the experiment was the responsible factor for the distinct water distribution within the experimental columns. Texture might have played a role, too. The sand has also been used in a freezing experiment with setup 2 (see Figure 5.7 and Figure 7.12). Temperatures in the soil columns equilibrated at 4°C at the beginning of the experiment. Afterwards the soil was cooled with cooling rates between 2.47°C day^{-1} and 0.53°C day $^{-1}$, according to column depth. The water redistribution within the sand after this procedure changed only marginally, but at least with a significant difference between the water contents above and beneath the freezing front, which was the indication that freezing induced water migration had taken place. These observations confirmed that segregation potential depends on rate of cooling besides the soil characteristics (see chapter 2.1). As rate of cooling is the product of temperature gradient and rate of freezing front advance (Konrad, 1989), it is obvious that the temperature gradient between freezing front and warm end of the column together with the input cooling rate determine the formation of segregation ice within the experimental columns. This relation could be observed in experiment *Sftao*. The temperature gradient between the lower end of the columns (temperature probes at 6.5 cm column depth) and the finally determined freezing front in each column was largest for column C (2.17°C cm^{-1}), followed by the temperature gradient of column B (1.91°C cm^{-1}) and column A (1.80°C cm^{-1}). Hence the maximum water contents in the frozen zone adjacent to the freezing front was observed in column C, followed by the ones of column B and column A (see Figure 7.2).

The impact of water saturation level, experiment duration and freezing procedure on the formation of segregation ice in a closed system can be seen in results obtained by Chuvilin et al. (2001), who investigated a sand (1 % clay, 4 % silt) and two different clay loams at water saturation (see Table 2.1). For sand they hardly observed any differences in water content throughout the experimental column (see Figure 2.13a, left). Largest water redistribution effects were observed for the silt loam with highest silt and clay contents. These observations go along with the fact that water migration in soils depends on capillarity. Explanations for the water distribution pattern in the sand are the short experiment duration and the water content at saturation level. The latter assumption is supported with results from freeze-thaw studies conducted by Viklander and Eigenbrod (2000), who observed a drastic increase in hydraulic conductivity with several freeze-thaw cycles in sandy loam (clay 7 %, silt 35 %) for medium water contents, whereas hardly any changes were observed for soil samples with water contents at saturation level.

The **freezing process in the different soil materials** sand (*Sftabo*) and peat (*Pftabo*) with distinct water contents (13.6 % dw and 480 % dw, respecitvely) resulted in different temperatures throughout the soil columns after 144 hours experiment duration. While temperatures at 1.1 cm column depth only varied by 0.22°C, the difference between sand and peat at 12.3 cm column depth was 1.51°C (see Table 5.2 and Table 5.3). Compared soil layers were all frozen. The temperatures in peat at 12.3 cm column depth reached the temperature level of the sand at 144 hours experiment duration 19 hours and 10 minutes later. This difference is assumed to be due to different water contents and heat capacity of the material. The temperatures in sand and peat at 1.1 cm column depth hardly vary. This can be described by the value of -10°C on the one hand, because at that temperature hardly any liquid water is present any more (Andersland & Ladanyi, 1994). On the other hand the sum of heat capacity was approximated by the phase transition from water (0.02 $W\ m^{-1} \cdot K^{-1}$) to ice (2.2 $W\ m^{-1} \cdot K^{-1}$, Hillel (2003)) so that only the differences in heat capacity of the two materials carry weight.

In summary it can be stated that with a closed system setup freezing induced water migration and accumulation may be simulated if the following is considered:

- freezing initiated from one side, moderately heating from the other side, resulting in temperature gradients between the freezing front and the warm end of the column around 2°C, with this procedure the position of the freezing front can be controlled best
- experimental columns should be brought to a homogeneous low temperature (e.g. the temperature from heating side) at the beginning (e.g. by being placed in a climate chamber)
- freezing procedure during the experiments should be divided into two phases, a first one with high freezing rates, for a fast propagation of the freezing front until its final position, and a second one, with very low freezing rates (in experiment Sftao a freezing rate of 0.006°C day^{-1} in the soil resulted in good simulation of the processes), apart from these two cooling steps, even small temperature changes should be avoided
- the larger the used soil volume is, the more water is available for the process of freezing induced water migration and accumulation
- to assure reproducibility the flow velocity of the cooling liquid through the cooling heads should be measured and adapted on demand
- 4-wire temperature sensors should be used and inserted completely into the soil

The simulation of the formation of segregated ice is only possible in open system approaches.

9.2 BEHAVIOR OF POLYCYCLIC AROMATIC HYDROCARBONS IN FREEZING SOIL MATERIALS – DISCUSSION OF RESULTS FROM LABORATORY STUDIES

Two main ways for PAHs to enter the environment are atmospheric deposition and as compound of oil and oil products (see chapter 2.3.1). The fate of PAHs in freezing soils, such as permafrost-affected soils, is not well investigated yet. Only a few studies on the behavior of PAHs in freezing soils exist (Aislabie et al., 1999; Curtosi et al., 2007; Zhao et al., 2013). Therefore the present studies should reveal if the freezing induced water migration influences the behavior of different PAHs in silt loam, which is a soil material common for permafrost-affected soils. Furthermore the behavior of PAHs in oil contaminated, freezing soils and the influence of the formation of segregation ice on the contaminant distribution should be investigated. Furthermore partitioning effects were investigated, using a sequential extraction procedure.

Does freezing induced water migration have an impact on PAH behavior in silt loam?

To answer the question if freezing induced water migration influences the distribution of PAHs in soils, column experiments were conducted and two different ^{14}C-labeled PAHs, anthracene and pyrene, were investigated (see chapter 6). Silt loam was used, because it is common in Cryosols and Gleysols, which are abundant in Northwestern Siberia as explained in chapter 4 (Jones et al., 2010). The Western Siberian Basin is an area with increasing exploration activities and simultaneously an increasing threat for the environment of hazardous compounds, like PAHs. Experimental approaches used to simulate the freezing induced water migration employed a freezing from the bottom procedure with slightly differing cooling rates at the beginning of the experiments and different experiment duration (see Figure 5.1). In both experiments freezing induced water migration was observed, as water contents in unfrozen column parts were significantly lower than at the beginning of the experiment, whereas water contents in frozen column parts exceeded the initial water contents (see chapter 9.1).

The resulting distribution of ^{14}C-activity in the experiment with ^{14}C-anthracene (*Ufba*) was not equal for the three parallel run experimental columns. Whereas considerable amount of ^{14}C-activity were found beneath the former contamination boundary in column B, supporting the hypothesis that the freezing induced water migration enhanced anthracene mobility, the values for ^{14}C-activity in the other two columns only exceeded slightly the detection limit. Furthermore the aforementioned methodological weaknesses of the sampling procedure question the significance of the observed effect (see chapter 9.1). There are three main factors that might give an explanation for the differences of ^{14}C-activity of the experimental columns:

- different water distribution patterns around the freezing front
- different distances between freezing front and contamination boundary
- influence of sampling procedure on analyzed values of ^{14}C-activity

A possible scenario, which led to the increased ^{14}C-activities may have been as follows. Columns B and C of experiment Ufba were frozen from the bottom just above the temperature and TDR measurement devices (3 cm column depth) after 36 hours experiment duration (see Figure A.1). In column A measured temperatures between 36 and 88 hours of the experiment, which represented a static temperature state, were higher than in the other two columns. After this phase of static state temperatures input cooling temperature had been reduced. In turn the freezing fronts in the three experimental columns returned to their finally identified positions in 3.8 cm, 3.2 cm and 3.9 cm column depth in columns A, B and C, respectively. That means, as temperature devices were at 3 cm column depth, at least 0.2 cm and 0.9 cm of soil in columns B and C, respectively were frozen for 52 hours during the experiment, before they thawed at the end of the experiment. The water distributions throughout the experimental columns support this interpretation because the courses of columns A and C show large decreasing steps at 0.5 cm and 1.0 cm above the freezing front (see Figure 9.1). The position of the freezing fronts in these column depths in an earlier state of the experiment is a coherent explanation for the accumulation of the water in these soil layers. Furthermore, the last temperature level of the experiment, which produced the final freezing fronts, only lasted 25 hours. This time was not sufficient for all the water, which had accumulated in the upper soil layers before, to migrate to the newly established freezing front. In column B the large step in water content decrease is found only 0.8 cm above the freezing front detected at the end of the experiment. But the TDR signals, which are a measure of the volumetric water content (see Figure A.1) revealed that increase in water content at 3 cm column depth for the last 25 hours was higher in column B, compared to columns A and C. As all columns were constructed with the same density and soil material, it may be assumed that more water migrated in column B. It may be assumed that anthracene migrated with the water, because the water extractable fraction in the former uncontaminated soil layer in column B was about four fold compared to the water extraction yields of the contaminated parts of the columns (see Table A.6). Additionally the results from the sequential extractions in columns A and C revealed that the ^{14}C -activity found below the initially contaminated part of the columns had a 10 % increased methanol-water extractable fraction compared to the contaminated column parts, even though total amounts of ^{14}C -activity were relatively low (see Table A.13). Therefore it can be concluded that ^{14}C -activity migrated with the water and therefore the water extractable and the methanol-water extractable fraction in the former uncontaminated parts were higher than in the contaminated soil layers. Furthermore, no ^{14}C -activity had been detected below the contamination boundary in the reference column. Thus it has been proved that, to a small extend though, that freezing induced anthracene mobilization, especially of the weakly associated fraction.

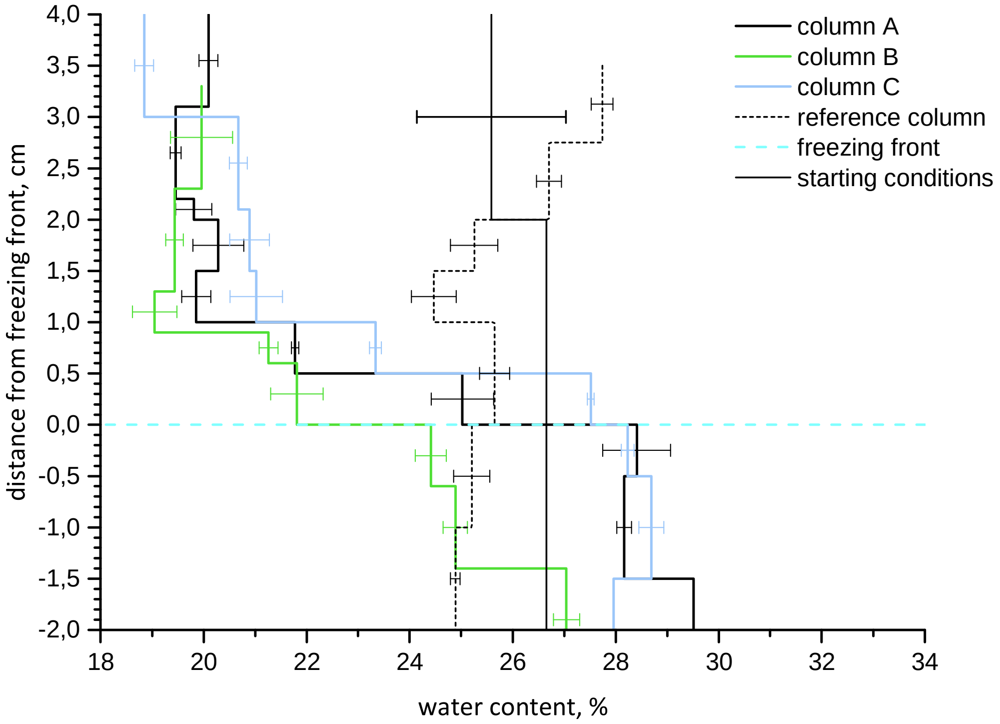

Figure 9.1 Detail of Figure 6.1 water content distribution at the end of experiment with silt loam, freezing from the bottom and ^{14}C-anthracene (*Ufba*), standard error reflects n≥3 (see Table A.6).

A factor for an enhanced contaminant migration in the described experiment could have been the formation of voids in the parts of the columns that were frozen during 36 to 88 hours, due to ice formation and subsequent thawing, as described by Yershov (1998). As this part of the column is closest to the contaminant boundary in column B, the higher amounts of ^{14}C-activity in this column compared to the other two columns may be explained.

The results obtained in the experiment with ^{14}C-pyrene were not as significant as the ones presented before, because the fairly high amounts of ^{14}C-activity found below the contamination boundary were also detected in the first uncontaminated soil layer in the reference column. However, increased experiment duration (47 hours), better simulation of the freezing process according to freezing induced water migration and higher water solubility of pyrene compared to anthracene would have been in favor for a migration process compared to experiment *Ufba* (see chapters 6.1 and 9.1 and Table 2.3). But the comparison of the methanol-water extractable fractions of the two PAHs may explain the differences. This fraction accounted only for 19.2 % of the total extracted amount of ^{14}C-activity in the experiment with ^{14}C-pyrene (*Ufbp,* see Figure A.2), compared to 40.0 % in the experiment with ^{14}C-anthracene (*Ufba*, see Figure 6.6). This goes along with the chemical properties of the two PAHs, which would suggest a higher amount of pyrene to be adsorbed by the organic phases present in the soil, due to its higher log K_{oc} (see Table 2.3). That means, that solution in water and volatilization did not influence the pyrene and anthracene migration in the silt loam under investigation to a considerable extend, because solubility in water and fugacity ratio are much higher for pyrene than for anthracene (see Table 2.3). The role DOC played as a carrier for PAH transport in the presented experiments cannot be estimated. However, due to the PAH properties and general sorption characteristics (see chapter 0) it may be hypothezised that it was a sorbent for the ^{14}C-labeled anthracene. Another assumption is that freezing induced water migration enhances partitioning of extractable fractions for single PAHs and the partitioning of the group of PAHs according to their log K_{oc}. PAH distribution patterns observed by Curtosi et al. (2007) in Antractic soils near Jubany station, would support such an interpretation (see Figure 2.10), if downward water migration in summer from the warm soil surface towards permafrost is assumed.

Which influence has an additional organic phase, such as crude oil, on the PAH behavior in soil?

PAHs do not only enter soils via atmospheric deposition, but as main component of crude oil, too. Crude oil is a mixture of hydrophobic compounds and its presence may change the behavior of PAHs in the soil considerably (Walter et al., 2000; Zemanek et al., 1997). As both contain mainly hydrophobic compounds, they competed for sorption sites. The oil phase may also block surfaces and smaller sized fissures with sorption places, resulting in an increased amount of easily, water extractable PAHs. On the other hand the crude oil itself represents a sorption site for the PAHs (see Table 2.4). The presence of the paraffin-based crude oil Ekofisk in silt loam (*Uftpo*, unfrozen samples) resulted in ten to 30-fold higher ^{14}C-extraction yields than in silt loam without oil (*Ufbp*) (see Figure 7.9). That observation goes along with results from Zemanek et al. (1997), who found water solubility increased for PAHs with average water solubility lower than that of phenanthrene (all higher molecular weight PAHs and some 3-ring PAHs, like anthracene) in oil contaminated soil materials. However, they also state that the water soluble content is negligible compared to the PAH contents associated with the present oil phase and the one in soil organic matter. But with respect to microbial degradation water solubility is an important factor. It may therefore be hypothesized that enhanced water solubility leads to enhanced biodegradation with time. The next extraction step, done with methanol-water yielded also significantly different results for the two experimental approaches (*Ufbp* and *Uftpo*), but in the contrary. Extraction yields of samples from experiment *Ufbp* were significantly higher than the ones obtained from the experiment with crude oil (*Uftpo*). The sum of both extraction steps did not differ significantly between the experimental approach with crude oil and without it. These observations lead to the hypothesis that crude oil hindered the PAHs to reach the weakly and polar sorption sites, thus increasing the water extractable fraction. On the other hand the ethyl acetate extractable fraction did not differ between the two experiments. This relation may be interpreted in two ways. Either the presence of crude oil did not influence the adsorption of pyrene to surfaces and soil particles from where it could be extracted with ethyl acetate. Or, the other possibility is, that the crude oil occupied sorption sites, but acted as sorption surface on the same level, therefore causing no significant difference between the fractions extracted from samples with and without crude oil. Due to its hydrophobic nature and the findings from Zemanek et al. (1997), the latter scenario is the more probable one.

For ^{14}C-anthracene the relation between extractabilities and the presence of crude oil was different (see Table A.13). Water extractabilities were low for both experimental approaches. However, extracted fractions of oil contaminated soil samples (*Uftao*) doubled the ones from the experiment without oil (*Ufba*). This goes along with the "solubility enhancement factor" (ESF) of water solubility of PAHs in oil contaminated soils determined by (Zemanek et al., 1997), which was 1.79 for pyrene and only 1.05 for anthracene. The much more striking difference was the extractability with methanol-water mixture. In the experiment with oil only 24 % to 30 % of the extractable ^{14}C-activity was extracted by methanol-water, whereas the fraction accounted for 40.0 % to 50 % of the extracted ^{14}C-activity in the experiment with ^{14}C-anthracene only (*Ufba*). That means the addition of the paraffin-based crude oil Ekofisk decreased the more easily extractable fraction of ^{14}C-anthracene by 10 % to 20 %. This goes along with the observations of Walter et al. (2000) and Zemanek et al. (1997), who found high concentrations of PAHs associated with the present oil phase. Zemanek et al. (1997) determined the fractions of anthracene in a creosote oil contaminated soil for oil phase, soil organic matter and water with 87.4 %, 12.4 % and 0.0017 %, respectively, which means that the behavior of the oil determines the behavior of the anthracene. This fact leads to the following question:

Do freezing induced water migration and ice formation influence the distribution of PAHs in soil materials contaminated with crude oil?

The effect of freezing or the formation of pore ice on oil distribution in contaminated soil has been studied by several authors (Barnes & Wolfe, 2008; Biggar & Neufeld, 1996; Chuvilin et al., 2001; Grechishchev et al., 2001) and is in parts presented in chapters 2.2.2 and 2.4.

Chuvilin et al. (2001) showed in closed column experiments that in a saturated sand contaminated with 6.2 % crude oil, the oil content decreased in the upper, frozen part of the column and increased beneath the final freezing front in the unfrozen part of the column within 24 hours experiment duration (see Figure 2.13 a). The increase in oil content below the freezing front accounted for approximately 15 % of the initial oil content. They explain this distinct distribution by expulsion of the oil out of the soil pores from the frozen zone into the unfrozen soil zone. Niven and Singh (2008) observed the formation of small LNAPL ganglia (singlets) due to a forwarding freezing front in a glass bead cell, which were finally entrapped in the forming ice. After thaw an increased number of independent ganglia (singlets) were observed. That means freezing led to a dispersion of the investigated crude oil and LNAPL, respectively in the investigated medium and therefore increased the amount of contaminated soil.

The distribution of ^{14}C-anthracene in sand contaminated with oil and subjected to a freezing process, led to decreased ^{14}C-activities in the frozen part of the experimental columns (see Figure 7.4). The simultaneously observed water content distribution, which runs exactly the opposite may give an explanation (see Figure 7.2). Additionally, an increase of ^{14}C-activity forward the slowly advancing freezing front (freezing rate 0.006°C day-1) of 11.3 % to 16.5 % compared to the ^{14}C-activity found in the last frozen soil layer was observed. In column C (see Figure 7.4) the ^{14}C-activity below the freezing front not only increased compared to the soil layer within the frozen part, but even exceeded the starting conditions with 5 %. These results imply that anthracene distribution in water unsaturated sand contaminated with paraffin-based crude oil subjected to a freezing process experiences a significant redistribution process. The results from the sequential extractions revealed furthermore that the anthracene had been partitioned due to its extractability. The methanol-water extractable fraction, which represents the weakly associated PAHs, was significantly increased in the unfrozen soil layers, compared to the frozen column parts. The water extractable fraction on the other hand was significantly higher in the frozen soil layers. In comparison with the extraction yields of soil samples from the reference column, it is observed that the methanol-water extractable fraction is depleted in the frozen column parts. This provides evidence of the migration of the methanol-water extractable fraction of ^{14}C-activity, which represents ^{14}C- anthracene. The ethyl acetate fraction on the other hand did not differ significantly between frozen und unfrozen column parts. This is interesting, because the PAH fraction extracted with ethyl acetate represents the PAH fraction associated to the hydrophobic sorbents within the soil, such as organic carbon and in the present case, crude oil. As stated before, it is expected that a high amount of PAHs will be associated to the oil in the soil (Zemanek et al., 1997)). With respect to the similar values of ethyl acetate extractable ^{14}C-activity in the frozen and unfrozen column parts it may be hypothesized, that the crude oil fractions associated with anthracene did not change their distribution pattern due to the freezing process and therefore also the distribution of the ^{14}C-anthracene fraction associated to the oil was not influenced by the freezing induced water migration. As the TPH contents could not be determined in the experiments employing ^{14}C-labeled PAHs, this consideration is only hypothetical. That would mean that the process supposed by Yershov (1998) and Chuvilin et al. (2001) of a push out effect ahead a freezing front on compounds in soil pores of coarse grained soils, did not occur in the experiment with sand, anthracene and crude oil (*Sftao*). The oil content of 0.5 % dw supports this hypothesis, because this contamination level is far below the residual saturation for oil of 14 % to 35 % in this soil material (Fetter, 1999). However, the water content seems to be a very important aspect in this issue. As Chuvilin et al. (2001) used saturated water conditions for their experiments there is no available pore space right from the beginning of the freezing experiment. The present studies were conducted using unsaturated conditions and low oil contents. That means that air filled pore spaces were present in the system. However, as the freezing induced water migration led to water saturated conditions in the frozen soil layer next to the freezing front (see fig. 7.2) with volumetric water contents around 43 vol% it can be assumed that pore spaces within this layer were filled with ice. That assumption only gives the possibility for the process of oil to be pushed out of soil pores with pore ice formation it does not explain the partitioning of the different extraction fractions of ^{14}C-anthracene. The latter might be explained by the process of solute exclusion ahead a freezing front, described for 1-propanol by Konrad and Seto (1991). In the present case it is not assumed that anthracene is in solution to such a great extent, but it may be hypothesized that the methanol-water extractable PAHs are associated to compounds in suspension or emulsion in the soil water. The very slow freezing process therefore led to the effect Konrad and Seto (1991) observed, namely that particles and fluids within the soil solution were excluded from ice formation and therefore gathered in the unfrozen soil next to the freezing front.

In the silt loam contaminated with crude oil and ^{14}C-pyrene (*Uftpo*) and ^{14}C-anthracene (*Uftao*), respectively no such significant effects could be observed like in the sand. This has several reasons. The first to be mentioned are the soil properties. The different texture does not only imply a different capacity in meso- and micro-pore structure and different k_f-values but also goes along with a variation in carbon content of 1.2 % (see Table A.4). As organic carbon provides sorption sites for PAHs, it might be assumed that more sorption sites are available in the silt loam than in the sand. Furthermore several authors described a relation between the silt fraction and PAH concentrations in natural soils (Krauss & Wilcke, 2005). Amongst others this relation was led back to high organic matter contents in this grain size fraction (see chapter 2.3.1). That means PAHs in silt loam should not be as easily available as in sand. But the presence of the crude oil as important sorption site for PAHs has also to be taken into account. As crude oil contents in all experiments with ^{14}C-labeled PAHs were similar it may be assumed that the methanol-water extractable fraction of the ^{14}C-activity is not significantly controlled by the paraffin-based oil present, because it varied considerably between the experiments. Extraction results support this assumption, because the methanol-water extractable fraction of ^{14}C-activity in experiments with ^{14}C-anthracene was significantly lower in silt loam than in sand and in turn the fraction of the ethyl acetate extraction was significantly higher in silt loam than in sand (see Figure 7.10). These observation and the total amounts of ^{14}C-activity used in the two experiments (see Table 3.5), which were higher in silt loam than in sand, may furthermore lead to the assumption that redistribution of anthracene starts at lower anthracene-levels in sand than in silt loam.

Another important factor, which may be responsible for differing results between the experiments with sand and silt loam is the freezing process. As the processes of cryosuction, freezing induced water migration and subsequent ice formation appear especially at low freezing rates (see chapter 2.1.) it has to be admitted that the freezing scenario in the sand was more in favor for these processes to appear than the freezing scenarios used in the experiment with silt loam. The reason was the very low freezing rate used during the second half of the experiment with sand (*Sftao*), compared to steady state conditions in the experiments with silt loam (*Uftao, Uftpo*). The low freezing rate implies a higher temperature gradient between warmer end of the experimental columns and freezing front. This leads to stronger cryosuction effects (see chapter 9.1). Furthermore Konrad and McCammon (1990) observed the process of solute exclusion for up to 90 % of the solutes at freezing rates below 0.1°C day^{-1}. If the process of particle and liquid exclusion ahead the freezing front was the process controlling the increased ^{14}C-activity ahead the freezing front, the freezing scenario used in the experiment with sand would have favored the process to a higher extend than the freezing scenarios used in the experiments with silt loam.

Finally it can be stated that PAH redistribution processes have been observed in oil contaminated sand. In oil contaminated silt loam trends indicate redistribution processes. It is hypothesized that these processes were mainly due to the formation of fairly pure ice at low freezing rates, than on the impact of ice formation on the oil (expulsion process), which was present in the soil. Upon the results obtained from the experiments it may be hypothesized that the following parameters determine the effect size of the PAH redistribution in freezing soils:

- freezing scenario (very low freezing rate)
- texture
- PAH properties
- water content and water available for the freezing induced water migration process

As even for soil chemical and physical properties there is no consensus yet, if effects of freezing accumulate or attenuate with the number of freeze-thaw cycles (Henry, 2007) it cannot be stated if the observed trends of PAH migration would be intensified with several freeze-thaw cycles.

Does oil content beneath the residual saturation level influence freezing induced water migration in freezing soils?

It has been shown, that water and its content in the soil is a very important parameter, determining the course of processes in conjunction with freezing. An oil phase present in the soil competes for pore space with the soil water. Therefore the water content influences the retention of oil, which is decreased with increasing water content (Fine et al., 1997). Crude oil present in soil below residual saturation level cannot migrate as discrete phase through the soil, but oil droplets dispersed in water may still migrate (Fetter, 1999). In the experiments with silt loam *Uftpo* and *Uftpa* local water content maxima were observed just below the freezing front in some experimental columns (see Figure 7.1). This observation may indicate, that water migration from the uncontaminated part was hindered by the presence of the oil and therefore a slight accumulation of migrating water just below the contamination boundary could be observed.

How do oil content and properties influence processes of PAH redistribution with respect to the freezing process?

The experiments with ^{14}C-labeled PAHs were conducted at oil contents in the soils of 0.5 % dw. The oil expulsion effect described by Chuvilin et al. (2001) in sandy material did most probably not take place in the experiments with the low oil contents. An experiment with sand, freezing from the top, two PAHs (anthracene and benzo[a]pyrene) and the naphthene based crude oil Gryphon (*Sftabo*), which is a medium viscous oil with a higher density than the paraffin-based Ekofisk (see Table 3.1) was conducted at a similar oil contamination level as the experiment of Chuvilin et al. (2001). Experimental setup 2 and non-labeled contaminants with a pre-incubation procedure were used. However, neither water contents nor anthracene or benzo[a]pyrene distributions revealed a significant influence of the freezing process on their distribution within the 40 cm high soil columns. The naphthene-based crude oil Gryphon at this high contamination level may have consolidated the soil, resulting in decreased permeability, which affected water distribution. (White et al., 2000) observed such consolidations of permafrost-affected soils already at oil contents of 1 % dw and determined them to influence the thermal and the hydraulic properties of the investigated soils significantly.

However, also the differing freezing scenario used, with a constant cooling rate, probably had an influence on the results obtained. Even though the cooling rates in the soil were always lower than the threshold rate of cooling determined by (Konrad & McCammon, 1990) and (Konrad & Seto, 1991) with 2.95 ± 0.25°C day^{-1} and 4 ± 1°C day^{-1}, respectively for solute exclusion from forming ice, no significant water distributions could be detected in the experiment with sand and experimental setup 2 (see Figure 7.12, Figure 7.13 and Figure 7.14). In contrast to the experiments cited the present study involved crude oil and PAHs, two hydrophobic organic compounds. The statement of (Grechishchev et al., 2001) that oil pollution reduces ice segregation and frost heave, which implies that less water redistribution takes place within these soils, may contribute to the explanation why the low cooling rates could not induce considerable water accumulation at the freezing front. However, compared to the experiments with experimental setup 1, the experiment with sand and setup 2 missed a nearly steady state phase or a phase of very low freezing rate (<0.1°C day^{-1}) during the second half of the experiment. This cooling scenario had been proved to induce considerable water migration processes, even in crude oil contaminated soils.

Also the use of non-labeled PAHs with the accompanying low recovery rates and high variation coefficients were not in favour to detect any small scale processes that would have taken place due to the freezing process. The pre-incubation time of the contaminated material, which was invented to consider the aging effect of PAHs in soils, increased the standard error of the starting conditions further. But it could be shown that the freezing process in the experimental columns resulted in significantly higher anthracene contents than were observed in the reference column. This may be an indication for a higher degree of microbial degradation of anthracene within the reference column.

The results of experiment *Sftabo* were similar to the results obtained by Biggar and Neufeld (1996), who observed oil distribution patterns without relation to the freezing process conducted, contaminant although their recommendations for experiment improvement have been considered.

The same experimental approach conducted with peat material (*Pftabo*) led to insignificant PAH distribution patterns within the experimental columns, too. Besides the reasons given for the experiment with sand already, the very high organic carbon content (53.1 %) led to increased PAH sorption. The extraction yields form the peat material for anthracene and benzo(a)pyrene reached only one fifth and one sixteenth of the values from the sandy material, respectively. These observations indicate that very high organic carbon contents may lead to decreased sorption of PAHs on a crude oil phase present, because equal crude oil contents were used in both experiments.

In all the experiment with sand, freezing from the top, naphthene-based crude oil Gryphon, anthracene and benzo[a]pyrene pointed out the importance of freezing scenario and contaminant properties and contact time, besides the influencing soil properties. Furthermore the choice of extraction and analysis method, with the very high variance, was not appropriate to the expected effect size.

Does the freezing process in contaminated soil materials intensify the formation of non-extractable residues (neR)?

The results presented from sequential, not matrix destroying extractions in chapters 6 and 7 revealed that fraction of non-extractable residues was low for all experiments, never accounting for more than 10 % of the total amount of ^{14}C-activity. Neither significant differences between non-extractable residues of frozen and of unfrozen column parts, nor between soil samples from experimental and from reference column were observed. In all it is hypothesized that the contact times of contaminants with 96 to 165 hours were not sufficient for the formation of non-extractable residues. Furthermore low organic carbon contents, the soil materials used and possibly also the oil in the soil system were not in favor for the formation of these strong bonds between PAHs and soil constituents.

An interesting observation was, that the second ethyl acetate extraction step showed a significant relation to the freezing procedure and the resulting ^{14}C-activity in experiments with crude oil present. The fraction of this extraction step was significantly higher in the unfrozen parts of the experimental columns.

This fourth extraction step had actually been invented to attenuate effects of aggregation during the extraction procedure and to make sure that the whole ethyl acetate fraction had been extracted. A hypothesis for the relationship may be the formation of aggregates due to dehydration (Yershov) of the unfrozen column parts during the experimental procedure. However, this hypothesis has to be assured by further studies on extraction behavior.

9.3 IN-SITU INVESTIGATIONS OF PAH AND TPH DISTRIBUTION IN PERMAFROST-AFFECTED SOILS

Organic contaminants that enter permafrost-affected soils are a threat to soil functions and water quality. Accidental releases of crude oil cannot be prevented completely and their appearance will probably increase, as exploration activities are increasing (see chapter 1.1.1). However, there are not many studies on the behavior of crude oil compounds, such as total petroleum hydrocarbons (TPHs) and polycyclic aromatic hydrocarbons (PAHs), in permafrost-affected soils. The latter were mainly investigated in Antarctica as trace elements originating from exhaust emissions and incomplete garbage combustion processes (Curtosi et al., 2007; Prus et al., 2015). Aislabie et al. (1999) investigated PAH distributions at oil spill sites situated around the Antarctic research station “Scott Base”. The spills occurred at former drum storage sites or where generators had been running. Other investigations on the behavior of oil in permafrost-affected soils were conducted in Alaska and Canada (Biggar et al., 1998; McCarthy et al., 2004), including an experimental spill in Alaska which should simulate an actual crude oil spill from a functioning pipeline (Collins et al., 1993; Johnson et al., 1980). The problem of environmental pollution has also been identified in Russia. Permafrost-affected soils cover approximately 55 % of Russia’s territory, which displays the importance of knowledge about the significant properties of the soils influenced by seasonal freezing and thawing. Researchers from Moscow University developed a soil map of Russia, giving the relative tolerance towards pollution with technogenic hydrocarbons (Gennadiev & Pikovskii, 2007) and several papers dealing with the influence of crude oil on freezing soils were published (Chuvilin et al., 2001; Grechishchev et al., 2001). Results from in-situ investigations were published in Russian language (Zykov et al., 2005; Zykov et al., 2008). Though the threat has been recognized, there are still many open questions upon the behavior of the organic contaminants in seasonally freezing ground. The present study dealt with a small diesel and lubricant oil spill at a former generator site with drum storage aside in Northern Siberia.

To investigate a contaminated site, firstly main properties of the soil, like grain size distribution, water/ice content and carbon content have to be determined and all knowledge about the site available has to be gathered. As each contamination site represents a unique interaction of the soil and contaminants present, the knowledge of as many factors as possible simplifies assessment and probably remediation. However, for the site under investigation, it is not known which amount of contaminants entered the ground, nor over which period of time. Details about the site and the soil properties are given in chapter 4.3 and Table A.4. Questions driving the investigations were:

- if the two groups of contaminants, TPHs and PAHs, had reached the transient layer yet
- if a considerable partitioning between the single substances of the two contaminant groups takes place

- which influence the supra-permafrost water table has on the migration behaviour of the contaminants
- and the identification of the main factors controlling the contaminant distribution in permafrost-affected soils, especially within the active layer

The active layer of permafrost-affected soils is characterized by changing thermal state and the along going transition of the soil water between the physical condition solid and liquid. The latter influences the hydraulic conductivity of the soil considerably. Johnson et al. (1980) could show at the experimental spill site “Caribou Poker Creek” in Alaska, that a crude oil spill of equal intensity affects a much larger surface area, when the spill happens in winter, compared to a summer spill (see Figure 2.11), because the frozen surface supported lateral movement of the contaminants. They observed furthermore that the main lateral movement of the oil took place within the first 14 days after the summer spill and within the first 172 days after the oil spill conducted in winter (chapter 2.4). Further expansion of the oil 15 years after contamination had only been observed to minor extend and was attributed to extreme weather events, like extraordinary heavy rain storms (Collins et al., 1994).

The contaminated surface area at the spill site in Northern Siberia accounts approximately for 5 m^2 (see Figure 4.5). It is not known, if the oil entered the soil during summer or winter. As the generator was running at a scientific measurement site, which could only be reached during the summer months, it may be hypothesized that the oil entered the soil during the winter months, when anybody could recognize the leakage. Another aspect is that the spill did not happen as a certain event, but most probably continuously, which implies that soil conditions varied over the time during which the oil entered the ground.

The surface area affected by oil contamination plays an important role, because the oil darkens the color of the soil. Balks et al. (2002) observed increased surface temperatures as a consequence. This in turn may lead to increased active layer depth and subsidence of the soil. At the experimental oil spill site in Alaska thaw depth had significantly increased at the winter and the summer spill site 15 years after the spills occurred. But while active layer thickness nearly tripled from 50 cm to 120 cm beneath the blackened soil surface of the winter spill, it only increased by 30 cm beneath the summer spill area (see fig. Figure 9.2, Collins et al. (1993)). Subsidence was larger beneath the winter spill site as well. Whether active layer thickness at the diesel spill site in Northern Siberia has increased after the spill occurred cannot be assessed yet. Maximum thaw depths for a polygonal rim of the area ranged from 42 cm to 56 cm between the years 2002 and 2011 (Boike et al., 2013). The soil cores were taken at the beginning of august in the years 2009 and 2011. The whole unfrozen soil part was sampled, which accounted for 34 cm in 2009 and 29 cm in 2011. As these depths were considerably smaller than the maximum thaw depth observed for the undisturbed soil, it may be hypothesized that maximum thaw depth had not been reached at the contaminated site, when samples were taken.

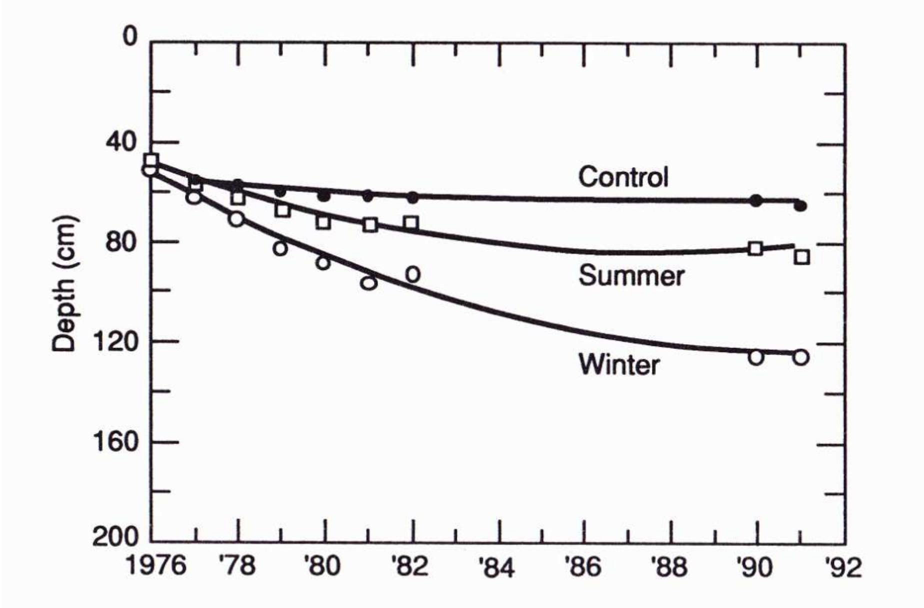

Figure 9.2 **Average thaw depth at winter and summer experimental spill site "Caribou Poker Creek", Alaska and the uncontaminated control, figure taken from (Collins et al., 1993)**

PAHs have been detected until the bottom layers of the investigated soil cores. The PAH contents exceeded arctic background levels (4.8 µg kg^{-1} dw, Knoche et al. (1995)), but were with 66 µg kg^{-1} dw and 139 µg kg^{-1} dw still below the global background level of 328 µg kg^{-1} dw (Nam et al., 2008). TPHs were also encountered until the bottom layers of the two soil cores. Lowest values were just above the detection limit of 100 mg kg $^{-1}$. That means the pristine soil has been contaminated over the total sampling depth, but in the bottom soil layers until 34 cm and 29 cm depth contaminant levels were comparably low, until five years after the contamination occurred. If deeper parts of the transient layer were reached by the contaminants, like it has been observed by (Curtosi et al., 2007) has to be determined by further analyses of samples from greater depth. However, it is hypothesized that PAH and TPH contents below the investigated soil depth do not increase again, as the bottom parts of the soil were water saturated.

The reason for the spill, the generator and the oil drums, have been removed. Therefore it may be stated that for the present no further contamination of the soil surface will occur. Further migration processes are also determined by the amount of oil spilled (see chapter 2.3.2). As stated before the total amount is not clear, but it may be estimated that it does not exceed 200 l, as this is the volume of an average oil drum. The maximum amounts of TPHs encountered within the two soil cores taken, were 4.56 % and 7.43 %, respectively. These amounts are within the approximately 9 % residual saturation within the vadose zone given by (Biggar & Neufeld, 1996; Iwakun et al., 2010; Schwille, 1984). Whether this kind of dispersion of the oil within the soil shall be assessed as remediation effort or as increased threat is a contentious issue. While Gennadiev and Pikovskii (2007) give dispersion as one of the two factors controlling "self-purification" of soils, Barnes and Chuvilin (2009), Børresen et al.

(2003) and McCarthy et al. (2004) rather judge the process as increased threat to soils.

Besides the expansion of the contamination the present studies focused on the distribution patterns of TPHs and PAHs over soil depth. Maximum TPH contents were found in the second soil layer of the two soil cores, respectively. Further down the soil profiles TPH contents decreased and showed a local maximum between 16.5 cm and 19.5 cm soil depth, which was much more pronounced in the soil core taken in 2009. The differences between the compositions of the sum parameter of TPHs of the two upper soil layers in both soil cores shown in Figure 8.1 and Figure 8.4 can be explained by several interacting processes. Firstly the relative depletion of the light hydrocarbons C10 to C16 within the surface soil layer may be the result of the continuous fractionation taking place, when a mixture of organic compounds, such as diesel oil enters the ground (Tang et al., 2012). The preferential migration of light compounds, due to their disposition for the partitioning to water and soil compartments leads to the relative increase of the higher hydrocarbons C_{17} to C_{20} in the surface soil layer. Secondly volatilization plays a role within the surface soil layer, especially for the light hydrocarbons, which may partition to the atmosphere. To which extend microbial degradation processes were involved in the differing compositions of TPHs over depth needs further study. Regarding the literature (Børresen et al., 2007; Rike et al., 2001) and the conditions needed by the micro-organisms (e.g. water availability, amount of hydrocarbons present) to degrade the hydrocarbons, it can only be stated that contact time of oil and soil under the present climatic conditions was relatively short. However, microbial degradation has been detected in oil contaminated, permafrost-affected soils even until temperatures of -6°C (Rike et al., 2005), which implied that not temperatures but water availability was the limiting factor. With respect to the finding of Siciliano et al. (2008) it can be assumed that hydrocarbons themselves enhance microbial degradation in some permafrost-affected soils, as they are an additional carbon source on the one hand and they increase liquid water content in frozen state of sandy loam and to a smaller extend in clay loam. The comparison of the composition of hydrocarbons of the two TPH maxima determined in the soil core from 2009 revealed a relative increase in low molecular weight hydrocarbons in the lower soil layer compared to the composition of the second soil layer with the TPH maximum. This fact leads to the assumption that the TPH migration process was selective and led to significant TPH partitioning over depth.

The TPH content over depth varies much between the two profiles, from the two years. This fact illustrates the small scale variability of soils and the statement of Berkowitz et al. (2008) that vertical migration of contaminants in soils is highly non-uniform. This applies especially to permafrost-affected soils, as cryopedogenic processes often lead to a destruction of the usually horizontal layering in the soil ((Jones et al., 2010)(see chapter 2). The soil samples of the upper 10 cm from 2009 contained only two thirds of the TPH content of the ones from 2011. Possible explanations may be the distance to the source (position of the generator) a different time (season) of entry of the LNAPL onto and into the soil or different migration patterns (e.g. preferential flow path ways). The latter is supported by the fact that further down the profile the TPH contents were higher in the samples from 2009. Anyway the differences imply that interpretations according to time between the results of the two sampling years cannot be made.

Aislabie et al. (1999) observed increased carbon contents and lowered pH in the surface soil layers of hydrocarbon contaminated Antarctic soils. As possible explanation for the lowered pH they give the accumulation of acidic microbial metabolites derived from hydrocarbon degradation processes. The pH values at the diesel spill site in Northern Siberia were elevated compared to pH values measured at the same location some years before (Kutzbach, 2006). But except for the surface soil layer the pH values were higher in the soil samples from 2009 than in the ones from 2011. As stated by (Aislabie et al., 1999), this may be an effect of microbial interaction with the contaminants present, which had more time to occur in the samples from 2011 than in the ones from 2009.

The PAH distribution within the investigated diesel spill in Northern Siberia mainly followed the TPH distribution (see Figure 8.6 and Figure 8.9). Low PAH levels within the upper soil layers do not display the absolute PAH contents, because most of the three ring PAHs were masked by the high TPH and organic matter contents in these soil layers (see Figure 8.8). That means the baseline of the chromatogram from the gas chromatograph is at a very high level, which PAH peaks did not exceed. Therefore they could not be determined with the mass spectrometer. Compared to other samples, where the three ring PAHs could be determined, it can be stated that the sum of the 16 EPA PAHs could not have exceeded 4 mg kg $^{-1}$ in the zones of uncertainty. Therefore it can be stated, that the absolute maximum for the sum of the 16 EPA PAHs in the soil core from 2009 was between 16.5 cm and 19.0 cm soil depth, which was the soil layer, where also the local maximum of TPHs had been encountered. A partitioning of the sum parameter revealed that 98.2 % of this maximum was made of 2- and 3-ring PAHs, which have water solubility larger than 1.1 mg l^{-1} (see Figure 8.8). Together with the observation that the 4-ring PAHs had their maxima in the upper soil layers, it may be assumed that the migration of low molecular weight PAHs to depth was favored under the present conditions and led to a considerable partitioning of the group of PAHs. Studies of PAH contents over soil depth in else pristine soils from Antarctica, near Jubany station, also revealed maximum PAH contents in the lower soil layers, with the absolute maximum being within the transient layer in the upper part of the perennial frozen ground (Curtosi et al., 2007). The authors hypothesized that the significant PAH distribution pattern was generated by freezing induced particle sieving. But this process, induced by washout of aggregates and small particles and freezing induced upward movement of coarse grained soil particles, is said to be low for fine grained soils with low ice content (<25 %)(Yershov, 1998). The water content for the investigated soils near Jubany station was only 10 % and the soil was classified as silt loam between 20 cm and

100 cm soil depth. Furthermore it is not clear, if the texture data Curtosi et al. (2007) used for their explanation are relevant for the investigated contaminant profiles. Upon the observation of partitioning made at the spill site in Northern Siberia, freezing induced, solute facilitated PAH migration in conjunction with adsorption of the PAHs to DOC, submicron particles and, if present, oil drops dispersed in the soil solution is suggested as transport mechanism. This transport could take place during the summer thaw period. Then permafrost constitutes the colder side of the active layer, which implies that cryosuction induces water migration from the upper part of the soil downwards to the permafrost table. This migrating water may carry the contaminants. The process runs conversely during freeze-back in autumn, but the latter is still shorter than the period of thawed state of the active layer and it has to run against the gravitational force.

The water content with respect to the creation of saturated or unsaturated conditions within the soil also influences the contaminant distribution within the soil profile. Even if TPHs were found until the lowest sampling depth, maximum contents were detected in the upper, organic dominated, soil layers. Collins et al. (1993) made similar observations at the aforementioned experimental spill site “Caribou Poker Creek” in Alaska, 15 years, after the oil entered the soil. The authors found TPHs mostly in the organic layers of the soil (see Figure 2.12). In conjunction with their observations of the soil water content they concluded that the TPHs only entered the mineral soil, where it was not water saturated. They stated that water saturation upon the permafrost table during the summer thaw period acts like a barrier for deeper LNAPL migration. However, that does not mean that single compounds of the oil phase in the soil do not migrate further, even in the saturated zone (see Figure 2.8).

The investigated samples from Northern Siberia had generally very high water contents, which often exceeded the average water saturation level for Historthels (Staff, 2014) of this region (75 % dw to 100 % dw; Boike et al. (2013); Kutzbach (2006); Sanders et al. (2010)). An explanation for the high water content is that samples were taken in summer in thawed state. It further indicates that the active layer is probably ice rich in frozen state. It is striking that both profiles showed a horizon with very high water content below the upper three and four soil horizons, respectively (see Figure 8.1 and Figure 8.2). In these upper horizons the highest TPH contents were found. It seems as if the high water contents impeded the TPH penetration into the soil. On the other hand, upward migration of water during freeze-back in autumn may be impeded by the presence of the TPHs, creating an ice lens below the soil horizons with the highest TPH contents. The possibility of this scenario is supported by the statement from Grechishchev et al. (2001), that alternate layers of ice and oil may form in cyclically freezing and thawing oil contaminated soils.

In general these observations lead to the conclusion that water content plays a decisive role concerning the vertical contaminant migration. It may be hypothesized that the vertical migration of contaminants is enhanced by low supra-permafrost water levels, or water levels at greater depth, which may go along with an increased active layer depth, because water migrates further down within the soil profile. On the other hand, high precipitation rates may increase contaminant migration, as they enhance the dissolved organic matter fraction and increase the flow of drainage water through highly porous soils (Curtosi et al., 2007). With respect to the predicted increase in precipitation for the northern latitudes in the last IPCC report (Bindoff et al., 2013), a scenario of high supra-permafrost water table is more probable. This would also increase ice content at the upper end of the transient layer, which would rather lessen the influence of increasing ambient temperatures. Therefore the difference in active layer thickness and contaminant migration to greater depth is difficult to predict. However, at contaminated sites the presence of taliks has to be taken into account. The connection of supra-permafrost waters to a talik may cause increased migration and contamination of larger soil areas and waters. Curtosi et al. (2007) stated that the influence of climate change would rather increase PAH mobilization and lead to unpredictable damages to Potter Cove basin at “25 de Mayo Island” in Antarctica.

In summary the answers to the questions posed at the beginning of this chapter concerning the investigated oil spill in Northern Siberia may be the following. The two groups of contaminants, TPHs and PAHs, were analyzed in all samples taken. As it may be hypothesized that the sampled depth from the beginning of august is not the maximum thaw depth that may be reached, the statement concerning the transient layer must remain vague. However, as TPH and PAH contents below 22 cm soil depth were comparatively low and the oil spill was only three and five years old, when it was sampled, it may be hypothesized, that contents of TPHs and PAHs did not exceed these levels in greater depth. To ensure this hypothesis further sampling has to take place.

The migration of contaminants that took place until the sampling went along with a considerable partitioning between the single substances of the two groups. Leaving higher molecular weight compounds in the upper soil layers and showing enrichment in lower molecular weight compounds in the soil layers between 16.5 cm and 19.5 cm. This soil layer of relative enrichment in TPHs and PAHs is situated just above the supra-permafrost water table, which implies that the latter at least attenuates further downward migration of the contaminants. However, it does not impede it, as contaminants have been found below it, albeit at low contents.

The main factors controlling this migration and accumulation were identified to be:

- water content and supra-permafrost water table and with respect to freezing the freezing induced water migration process, as well as the process of ice formation
- organic matter content
- soil texture
- contaminant content and composition

10. CONCLUSION AND OUTLOOK

The present studies focused on two groups of organic contaminants that belong to the main constituents of crude oil, namely total petroleum hydrocarbons (TPHs, sum parameter of C_{10} to C_{40}) and polycyclic aromatic hydrocarbons (PAHs, single substances and sum of 16 EPA PAHs). Their distribution in permafrost-affected soils and the influence of the freezing process on the distinct contaminant distribution has been studied.

To investigate the impact of the freezing process on the behavior of PAHs in abundant arctic soil materials, experimental setups and procedures have been developed. It has been shown that it is possible to simulate a naturally occurring freezing process in the vadose zone of the soil with a closed column setup with a two-phase cooling scenario. The first phase of cooling employs high cooling rates up to 20°C day^{-1} and the second phase uses either a constant cooling input or cooling rates smaller than 0.01°C day^{-1}. With the described procedure it was possible to control the location of the freezing front and induce the process of cryosuction, which results in water migration towards the freezing front. However, the formation of segregation ice or the simulation of several freeze-thaw cycles can only be simulated well using an open system approach, because in a closed system set up the water available for the freezing induced water migration and accumulation processes is limited. In an experiment with sand (*Sftao*) it has been shown that nearly all water available for the migration process had migrated during the second phase of cooling (see chapter 7.1). This was enough to increase the water content from the maximum water holding capacity to water saturated conditions at the freezing front, but for ice lens formation the amount of available water was insufficient. If thawing and a subsequent, second freezing process would be simulated in the closed system the occurring water redistribution processes would not correspond to natural occurring processes and would therefore not be adequate to simulate the latter and their impact. Furthermore, it has been seen that constant parameters (cooling input) were more important than the achievement of a certain freezing depth for the interpretation and comparison of results from different experiments with varying soil or contaminant parameters. The results also showed that interpretation was easier for homogeneously contaminated soils compared to those with a boundary between contaminated and clean soil. Even though the contamination boundary could be identified well with the quartz sand marks, the cutting as sampling procedure could not assure the exact relocation of the boundary between contaminated and uncontaminated column parts. One important parameter for water and contaminant migration processes, namely soil structure, has not been regarded in the present study, because columns were packed with homogenized soil material. The latter has the advantage of reproducibility and minimization of sidewall flow and avoids the described difficulties generated by a contamination boundary. All of which may represent problems for undisturbed soil monoliths. However, it is recommended to give the use of undisturbed soil samples from Arctic sites a try with the experimental approach of the two phase freezing process and the experimental setup 1 with three parallel run columns.

The investigations on the impact of freezing induced water migration on the behavior of PAHs in silt loam showed trends according to the freezing procedure. Where migration has been observed, it was mainly related to the weakly associated fraction of the PAHs (methanol-water extractable fraction). This fraction was twice as large for the 3-ring PAH anthracene (40 %) as for pyrene (19.2 %). This goes along with log K_{OC} values (see Table 2.3), which is lower for anthracene than for pyrene, indicating that pyrene has a higher affinity to the organic carbon of the soil and is therefore less mobile. This observation points out that water solubility and fugacity ratio did not play a decisive role for the PAH migration, induced by cryosuction, because these two parameters are higher for pyrene. In basic approach it has been seen that freezing induced water migration enhances PAH migration. The influence increases with decreasing log K_{OC} and is therefore different for different PAHs. For further studies homogeneously contaminated soil columns should be used to avoid the uncertainties that arose from the sampling procedure. If the observed trends can be confirmed, evidence for PAH partitioning induced by cryosuction and freezing induced water migration would be provided. Further investigations should determine the carrier which is responsible for the PAH migration within the methanol-water extractable fraction.

For PAHs that appear in conjunction with crude oil the influence of the freezing induced water accumulation and ice formation at the freezing front have been investigated. It could be shown that PAHs gather in front of the freezing front in the unfrozen soil, especially in sandy soil material (see Figure 7.4). Again the methanol-water extractable fraction was the one that was mainly responsible for the increase in PAH content. The observations support the interpretation that particles and solutes in the soil solution are excluded from the forming ice if the freezing process is slow enough. As the ethyl-acetate extractable fraction of the PAH, which is supposed to extract PAHs associated to crude oil did not change around the freezing front, it is assumed that the process of oil expulsion out of the soil pores, described by Chuvilin et al. (2001) has not taken place. However, the assumption should be verified by further investigation including the analysis of the TPH distribution. The main reasons for the different processes observed by Chuvilin et al. (2001) and in the present studiy are supposed to be water and oil content, which were both considerably lower in the experiments conducted. For the PAH migration generated by freezing induced water migration and accumulation the influence of texture seems to be less than the influence of the PAH properties, namely log K_{OC} (see Figure 7.10). The availability of PAHs was not significantly influenced by the freezing process of the experiments itself, as the comparisons of experimental columns and reference column showed. The amount of non-extractable residues was very low for all analyzed materials and was also not altered significantly due to the freezing process. However, as experimental times were comparatively short and mostly did not include pre-incubation times, it is suggested to conduct further experiments, which also include freeze-thaw cycles. It is hypothesized that differences in availability of PAHs develop with increasing time and number of freeze-thaw cycles compared to unfrozen equivalents.

The experimental results, data from the literature and the analysis of the diesel contaminated site in Northern Siberia lead to the assumption that PAH in oil contaminated soils get more dispersed within the soil due to the freezing process. Maximum PAH contents were encountered between 16.5 cm and 19.0 cm soil depth, and between 7 cm and 9.5 cm and were mainly formed of 3-ring PAHs. Compared to the surface soil layers they were relatively depleted in high molecular weight PAHs (which contain 4 rings and more). These observations have also been made by Curtosi et al. (2007). To assess the extent of partitioning, extracts should be cleaned employing activated columns. However, silica columns tested in these studies did not show satisfactory results, therefore further methodological development has to be done. PAH maxima go along with relative TPH maxima, albeit absolute TPH maxima were found in the second soil layer of both sampling years. TPHs also experienced partitioning during migration, but from the present investigations it cannot be stated whether the partitioning processes were controlled by freezing or freezing induced water migration and accumulation.

The supra-permafrost water table in the two sampling years was encountered in 19 cm and 19.5 cm soil depth, respectively. Below both, PAH and TPH contents decreased steeply and ranged at very low levels. It is very likely that the contaminants did not reach the transient layer in higher amounts yet. The elevation of PAHs and TPHs just above the supra-permafrost water table implies that contaminant migration is at least attenuated by supra-permafrost water. However, it is not impeded, as PAHs and TPHs were detected below it. It may be hypothesized that especially PAHs would gather in the upper part of the transient layer with time. This hypothesis goes along with the in situ observations of Børresen et al. (2003) and Curtosi et al. (2007). The observation at the experimental spill site “Caribou Poker Creek” in Alaska suggest that the influence of supra-permafrost water is bigger at sites with high oil contamination level and thick organic surface soil layers, because hardly any contaminants were encountered there beneath the supra-permafrost water table within the mineral soil, even after 15 years. In all, for process understanding and with respect to relevance more investigations on organic soils are needed. The present study identified water content and freezing scenario, organic matter content and contaminant properties and content, as well as soil texture as the main factors influencing the fate of PAHs and TPHs in permafrost-affected soils.

The formation of micro-fissures in oil contaminated, freezing soils and the formation of small ganglia have often been described in the literature (Barnes & Biggar, 2008; Biggar & Neufeld, 1996; White & Coutard, 1999). However, it is not clear, if the often accompanying dispersion effect of the oil compounds in permafrost-affected soils should be assessed positively or negatively. A main factor for this assessment is the rate of biodegradation and how it is influenced by the already observed effects. In-situ investigations on this issue should be conducted at Caribou Poker Creek, Alaska, because the boundary conditions at this site are better known than at accidental spill sites.

In summary it can be said that the migration behavior of the organic contaminant groups PAHs and TPHs in permafrost-affected soils is influenced by the seasonally freezing processes and the freezing induced water migration. However, water content, texture and contaminant properties determine the magnitude of the impact freezing has on contaminant behavior in permafrost-affected soils.

Ambient temperatures, as well as precipitation rates in the Arctic are predicted to alter with climate change (Bindoff et al., 2013). The effects of such changes are not yet fully understood. On the one hand increased temperatures would favor an increase in active layer depth with the formation of taliks. Furthermore the temperature gradient within the active layer would be increased, supra-permafrost water table could be lowered and the probability of the connection of supra-permafrost waters with surface waters or groundwater is increased. The mentioned factors could enhance the migration of contaminants to depth and to other compartments of the environment.

On the other hand the increased precipitation rates could favor higher supra-permafrost water tables and increased ice content in the transient layer. Upon this effect the influence of changing ambient temperatures would be abated and active layer depth would not or hardly increase for a certain time. But it cannot be stated that organic contaminant migration is limited by increased precipitation rates, because high precipitation rates could increase the dissolved organic matter fraction and increase the drainage flow within the active layer at slopes. In all it can be stated that freezing dynamics and hydrodynamics will be altered due to the predicted climatic changes. As they have been shown to have a main impact on organic contaminant redistribution in soil, their interaction and effect in conjunction with organic contaminants should be investigated.

REFERENCES

Abdul, A.S. (1988): Migration of Petroleum Products Through Sandy Hydrogeologic Systems. Ground Water Monitoring & Remediation 8(4): 73-73.

ACIA (2004): Impacts of a Warming Arctic: Arctic Climate Impact Assessment., Cambrigde, p. 140.

Aislabie, J., Balks M., Astori N., Stevenson G., Symons R. (1999): Polycyclic aromatic hydrocarbons in fuel-oil contaminated soils, Antarctica. Chemosphere 39(13): 2201-2207.

Aislabie, J.M., Balks M.R., Foght J.M., Waterhouse E.J. (2004): Hydrocarbon Spills on Antarctic Soils: Effects and Management. Environmental Science & Technology 38(5): 1265-1274.

AMAP (2002): Persistent Organic Pollutants in the Arctic. Oslo, Norway, p. 310.

Andersland, O.B., Ladanyi B. (1994): An Introduction to Frozen Ground Engineering. Chapman & Hall, New York

APSC (2013): Transalaska pipeline system - the facts. In: company Aps (ed). vol 15.01., Anchorage.

Atlas, R., Bragg J. (2009): Bioremediation of marine oil spills: when and when not – the Exxon Valdez experience. Microbial Biotechnology 2(2): 213-221.

Bachmann, J., Horton R., T. R., van der Ploeg R.R. (2001): Comparison of the thermal properties of four wettable and four water-repellent soils. Soil Science Society of America Journal 65: 1675-1679.

Balks, M.R., PAETZOLD R.F., KIMBLE J.M., AISLABIE J., CAMPBELL I.B. (2002): Effects of hydrocarbon spills on the temperature and moisture regimes of Cryosols in the Ross Sea region. Antarctic Science 14(04): 319-326.

Banwart, S. (2011): Save our soils. Nature 474(7350): 151-152.

Barnes, D.L., Biggar K.W. (2008): Movement of petroleum through freezing and frozen soils. In: Filler DM, Snape I & Barnes DL (eds) Bioremediation of Petroleum Hydrocarbons in Cold Regions. Cambridge University Press, Cambridge, p. 273.

Barnes, D.L., Chuvilin E.M. (2009): Migration of Petroleum in Permafrost-Affected Regions. In: Margesin R (ed) Permafrost Soils. Soil Biology. Springer, p. 263-278.

Barnes, D.L., Filler D.M. (2003): Spill evaluation of petroleum products in freezing ground. Polar Record 39(04): 385-390.

Barnes, D.L., Wolfe S.M. (2008): Influence of Ice on the Infiltration of Petroleum into Frozen Coarse-grained Soil. Petroleum Science and Technology 26(7): 856-867.

Barnes, D.L., Wolfe S.M., Filler D.M. (2004): Equilibrium distribution of petroleum hydrocarbons in freezing ground. Polar Record 40(03): 245-251.

Bauw, D.H., de Wilde P.G.M., Rood G.A., Aalbers T.G. (1991): A standard leaching test, including solid phase extraction, for the determination of PAH leachability from waste materials. Chemosphere 22(8): 713-722.

BBodSchG (1998): Gesetz zum Schutz vor schädlichen Bodenveränderungen und zur Sanierung von Altlasten (Bundes-Bodenschutzgesetz - BBodSchG) § 2, 3, Bundesministerium für Umwelt N, Bau und Reaktorsicherheit, Berlin.

Bergknut, M. (2006): Characterization of PAH-contaminated soils focusing on availability, chemical composition and biological effects. In: Chemistry, Environmental Chemistry. Umeå, Umeå. p 58.

Bergström, L. (2000): Leaching of agrochemicals in field lysimeters - a method to test mobility of chemicals in soil. In: Cornejo J, Jamet P & F. L (eds) Pesticide/Soil interactions: Some current research methods. . INRA, Paris, p. 279-287.

Berkowitz, B., Dror I., Yaron B. (2008): Contaminant Geochemistry. Springer-Verlag, Berlin, Heidelbergp. 412.

Biggar, K.W., Haidar S., Nahir M., Jarrett P.M. (1998): Site Investigations of Fuel Spill Migration into Permafrost. Journal of Cold Regions Engineering 12(2): 84-104.

Biggar, K.W., Neufeld J.C.R. Vertical Migration of Diesel into Silty Sand Subject to Cyclic Freeze-Thaw. In: ASCE/CSCE Cold Regions Engeneering Conference. Fairbanks, Alaska. 1996.

Bindoff, N.L., Stott P.A., AchutaRAo K.M., Allen M.R., Gillett N., Gutzler D., Hansingo K., Hegerl G., Hu Y., Jain S., Mokhov I.I., Overland J., Perlwitz J., Sebbari R., Zhang X. (2013): Detection and Attribution of Climate Change: from Global to Regional. . In: Stocker TF, Qin D, Plattner G-K, Tignor M, Allen SK, Boschung J, Nauels A, Xia Y, Bex V & Midgley PM (eds) The Physical Science Basis. Contribution of Working Group I to the Fifth Assessment Report of the Intergovernmental Panel on Climate Change. Cambridge University Press, Cambridge (U.K.), New York (USA),

Bird, J.K., Charpentier R.R., Gautier D.L.C.P.C., Houseknecht D.W., Klett T.R., Pitman J.K., Moore T.E., Schenk C.J., Tennyson M.E., Wandrey C.J. (2008): Circum-Arctic Resource Appraisal: Estimates of Undiscovered Oil and Gas North of the Arctic Circle. U.S. Geological Survey, p. 4.

Birkel, U. (2000): Transformation organischer Schadstoffe und abiotische Bildung von Huminstoffen in Böden durch oberflächeninduzierte Reaktionen an Tonmineralen. In: Mathematisch-Naturwissenschaftliche Fakultät. Georg-August-Universität, Göttingen. p 205.

Blanchard, D., Fremond M. Cryogenic suction in soils. In: Proceedings of the Third International Symposium on Ground Freezing. Hanover, New Hampshire. 1982. vol 1. p 233-238.

Blume, H.-P., Brümmer G.W., Horn R., Kandeler E., Kögel-Knabner I., Kretzschmar R., Stahr K., Wilke B.-M. (2010): Scheffer/Schachtschabel: Lehrbuch der Bodenkunde. Springer, Berlin

Boike, J. (2014): Controlling factors of refreezing times, e-mail to Zschocke A.

Boike, J., Kattenstroth B., Abramova K., Bornemann N., Chetverova A., Fedorova I., Fröb K., Grigoriev M., Gräber M., Kutzbach L., Langer M., Minke M., Muster S., Piel K., Pfeiffer E.M., Stoof G., Westermann S., Wischnewski K., Wille C., Hubberten H.W. (2013): Baseline characteristics of climate, permafrost and land cover from a new permafrost observatory in the Lena River Delta, Siberia (1998-2011). Biogeosciences 10(3): 2105-2128.

Bojes, H.K., Pope P.G. (2007): Characterization of EPA's 16 priority pollutant polycyclic aromatic hydrocarbons (PAHs) in tank bottom solids and associated contaminated soils at oil exploration and production sites in Texas. Regulatory Toxicology and Pharmacology 47(3): 288-295.

Børresen, M., Breedveld G.D., Rike A.G. (2003): Assessment of the biodegradation potential of hydrocarbons in contaminated soil from a permafrost site. Cold Regions Science and Technology 37(2): 137-149.

Børresen, M.H., Barnes D.L., Rike A.G. (2007): Repeated freeze-thaw cycles and their effects on mineralization of hexadecane and phenanthrene in cold climate soils. Cold Regions Science and Technology 49(3): 215-225.

Braddock, J.F., McCarthy K.A. (1996): Hydrologic and Mircobiological Factors Affecting Persistence and Migration of Petroleum Hydrocarbons Spilled in a Continuous- Permafrost Region. Environmental Science and Technology 30: 2626-2633.

Braddock, J.F., Ruth M.L., Catterall P.H., Walworth J.L., McCarthy K.A. (1997): Enhancement and Inhibition of Microbial Activity in Hydrocarbon-Contaminated Arctic Soils: Implications for Nutrient-Amended Bioremediation. Environmental Science & Technology 31(7): 2078-2084.

Bromly, M., Hinz C., Aylmore L.A.G. (2007): Relation of dispersivity to properties of homogeneous saturated repacked soil columns. European Journal of Soil Science 58(1): 293-301.

Brost, E.J., deVaull G.E. (2000): Non-Aqueous Phase Liquid (NAPL) Mobility Limits in Soil. American Petroleum Institute 9: 10.

Busche, U., Hirner A.V. (1997): Mobilisierbarkeit von hydrophoben organischen Schadstoffen in belasteten Böden und Abfällen. Teil II: Mobilisierbarkeit von PAK, PCB und Phenolen durch reale Wässer. Acta hydrochimica hydrobiologica 25(5): 248-252.

Caravaca, F., Roldán A. (2003): Assessing changes in physical and biological properties in a soil contaminated by oil sludges under semiarid Mediterranean conditions. Geoderma 117(1–2): 53-61.

CEC, C.o.t.E.C. (2006): Proposal for a Directive of the European Parliament and the Council establishing a framework for the protection of soil and amending Directive 2004/35/EC 2006/0086 (COD), COM(2006) 232 final, Brussels, p. 30.

Chang, W., Akbari A., Snelgrove J., Frigon D., Ghoshal S. (2013): Biodegradation of petroleum hydrocarbons in contaminated clayey soils from a sub-arctic site: The role of aggregate size and microstructure. Chemosphere 91(11): 1620-1626.

Chiou, C.T. (2002): Partition and Adsorption of Organic Contaminants in Evironmental Systems. Wiley & Sons, New Jersey,

Chuvilin, E.M. (1999): Migration of ions of chemical elements in freezing and frozen soils. Polar Record 35(192): 59-66.

Chuvilin, E.M., Miklyaeva E.S. (2003): An experimental investigation of the influence of salinity and cryogenic structure on the dispersion of oil and oil products in frozen soils. Cold Regions Science and Technology 37(2): 89-95.

Chuvilin, E.M., Naletova N.S., Miklyaeva E.C., Kozlova E.V., Instanes A. (2001): Factors affecting spreadability and transportation of oil in regions of frozen ground. Polar Record 37(202): 229-238.

Collins, C.M., Racine C.H., Walsh M.E. (1993): Fate and Effects of Crude Oil Spilled on Subarctic Permafrost Terrain in Interior Alaska. CRREL, Hanover, p. 20.

Collins, C.M., Racine C.H., Walsh M.E. (1994): The Physical, Chemical, and Biological Effects of Crude Oil Spills after 15 Years on a Black Spruce Forest, Interior Alaska. Arctic 47(2): 164 - 175.

Cooper, T.G. (1981): Biochemische Arbeitsmethoden. de Gruyter, Berlin

Cornelissen, G., Gustafsson Ö., Bucheli T.D., Jonker M.T.O., Koelmans A.A., van Noort P.C.M. (2005): Extensive Sorption of Organic Compounds to Black Carbon, Coal, and Kerogen in Sediments and Soils: Mechanisms and Consequences for Distribution, Bioaccumulation, and Biodegradation. Environmental Science & Technology 39(18): 6881-6895.

Cornelissen, G., van Noort P.C.M., Parsons J.R., Govers H.A.J. (1997): Temperature Dependence of Slow Adsorption and Desorption Kinetics of Organic Compounds in Sediments. Environmental Science & Technology 31(2): 454-460.

Curtosi, A., Pelletier E., Vodopivez C.L., Mac Cormack W.P. (2007): Polycyclic aromatic hydrocarbons in soil and surface marine sediment near Jubany Station (Antarctica). Role of permafrost as a low-permeability barrier. Science of The Total Environment 383(1-3): 193-204.

Das, N., Chandran P. (2010): Microbial Degradation of Petroleum Hydrocarbon Contaminants: An Overview. Biotechnology Research International 2011:

Delle Site, A. (2001): Factors Affecting Sorption of Organic Compounds in Natural Sorbent/Water Systems and Sorption Coefficients for Selected Pollutants. A Review. Journal of Physical and Chemical Reference Data 30(1): 187-439.

Desler, C., Johannessen C., Rasmussen L.J. (2009): Repair of DNA damage induced by anthanthrene, a polycyclic aromatic hydrocarbon (PAH) without bay or fjord regions. Chemico-Biological Interactions 177(3): 212-217.

DIN10390 (2005): Bestimmung des pH. In: e.V. DIfN (ed) Bodenbeschaffenheit. Beuth Verlag, Berlin,

DIN10694 (1995): Bestimmung von organischem Kohlenstoff und Gesamtkohlenstoff nach trockener Verbrennung (Elementaranalyse) In: e.V. DIfN (ed) Bodenbeschaffenheit. Beuth Verlag, Berlin,

DIN11260 (2011): Bestimmung der effektiven Kationenaustauschkapazität und der Basensättigung unter Verwendung von Bariumchloridlösung. In: e.V. DIfN (ed) Bodenbeschaffenheit. Beuth Verlag, Berlin,

DIN11274 (1998): Bestimmung des Wasserrückhaltevermögens - Laborverfahren. In: e.V. DIfN (ed) Bodenbeschaffenheit. Beuth Verlag, Berlin,

DIN11277 (1998): Bestimmung der Partikelgrößenverteilung in Mineralböden - Verfahren mittels Siebung und Sedimentation. In: e.V. DIfN (ed) Bodenbeschaffenheit. Beuth Verlag, Berlin,

DIN11465 (1996): Bestimmung des Trockenrückstandes und des Wassergehalts auf Grundlage der Masse – Gravimetrisches Verfahren. In: e.V. DIfN (ed) Bodenbeschaffenheit. Beuth Verlag, Berlin,

DIN13878 (1998): Bestimmung des Gesamt-Stickstoffs durch trockene Verbrennung (Elementaranalyse). In: e.V. DIfN (ed) Bodenbeschaffenheit. Beuth Verlag, Berlin,

DIN18287 (2006): Bestimmung der polyzyklischen aromatischen Kohlenwasserstoffe (PAK) - Gaschromatographische Verfahren mit massenspektrometrischem Nachweis (GC-MS). In: e.V. DIfN (ed) Bodenbeschaffenheit. Beuth Verlag, Berlin,

Ehlers, J. (1987): Erläuterungen zu Blatt Nr. 2525 Harburg. In: Hamburg GL (ed) Geologische Karte von Hamburg 1:25000. Hamburg,

Ensinger (2011): Tecaflon PVDF. In: sheet td (ed). Ensinger GmbH, Nufringen.

Ensinger (2012): Tecaflon PTFE. In: sheet td (ed). Ensinger GmbH, Nufringen.

Eschenbach, A. (1995): Einfluss von *Pleurotus ostreatus*, Kompost, *Sphingomonas paucimobilis* und der Kontaminationsdauer auf den Verbleib und Abbau ^{14}C-markierter polycyclischer aromatischer Kohlenwasserstoffe (PAK) in Altlastböden. In: Technische Universität. Hamburg-Harburg. p 198.

Eschenbach, A., Kästner M., Bierl R., Schaefer G., Mahro B. (1994): Evaluation of a new, effective method to extract polycyclic aromatic hydrocarbons from soil samples. Chemosphere 28(4): 683-692.

Eschenbach, A., Kästner M., Wienberg R., Mahro B. (1995): Microbial PAH Degradation in Soil Material from a Contaminated Site — Mass Balance Experiments with Pleurotus Ostreatus and Different ^{14}C-PAH. In: Brink WJ, Bosman R & Arendt F (eds) Contaminated Soil ’95. Soil & Environment. Springer Netherlands, p. 377-378.

Eschenbach, A., Mescher H., Wienberg R., Mahro B. (2001): Humification of PAH and TNT During Bioremediation — Evaluation of Long Term Risk and Sustainability. In: Stegmann R, Brunner G, Calmano W & Matz G (eds) Treatment of Contaminated Soil. Springer Berlin Heidelberg, p. 271-291.

Eschenbach, A., Oing K. (2013): Gutachten - Erarbeitung eines gestuften Extraktionsverfahrens zur Bewertung gebundener Rückstände. University of Hamburg, Hamburg, p. 99.

Eschenbach, A., Wienberg R., Mahro B. (1997): Bildung und Langzeitstabilität von nicht-extrahierbaren PAK-Rückständen im Boden. Altlasten Spektrum 6: 292-297.

Eschenbach, A., Wienberg R., Mahro B. (1998): Fate and Stability of Nonextractable Residues of [14C]PAH in Contaminated Soils under Environmental Stress Conditions. Environmental Science & Technology 32(17): 2585-2590.

Evonik (2014): Eigenschaften von Plexiglas®. In. vol 24.03.2014. Evonik Industries AG, Darmstadt.

Fetter, C.W. (1999): Contaminant hydrology. Macmillan Publishing Company, p. 458.

Filler, D.M., van Stempvoort D., Leigh M.B. (2009): Remediation of frozen ground contaminated with petroleum hydrocarbons: Feasibility and Limits. In: Margesin R (ed) Permafrost Soils. Springer, Berlin, Heidelberg, p. 348.

Fine, P., Graber E.R., Yaron B. (1997): Soil interactions with petroleum hydrocarbons: Abiotic processes. Soil Technology 10(2): 133-153.

Flerchinger, G.N., Lehrsch G.A., McCool D.K. (2005): Freezing and Thawing, Processes. In: Hillel D (ed) Encyclopedia of Soils in the Environment. Elsevier, Oxford, p. 104-110.

Fourie, W., Shur Y. (2008): Freezing and frozen soils. In: Filler DMS, I.; & Barnes, Dave L. (ed) Bioremediation of Petroleum Hydrocarbons in Cold Regions. Cambridge University Press, Cambridge, p. 273.

French, H.M. (2007): The Periglacial Environment. Wiley, Chichester

Funderburg, S.W., Moore B.E., Sorber C.A., Sagik B.P. (1979): Method of soil column preparation for the evaluation of viral transport. Appl Environ Microbiol 38(1): 102-107.

Gan, S., Lau E.V., Ng H.K. (2009): Remediation of soils contaminated with polycyclic aromatic hydrocarbons (PAHs). Journal of Hazardous Materials 172(2-3): 532-549.

Gennadiev, A.N., Pikovskii Y.I. (2007): The maps of soil tolerance toward pollution with oil products and polycyclic aromatic hydrocarbons: Methodological aspects. Eurasian Soil Science 40(1): 70-81.

Godagnone, R.E. (1997): Península Potter (Isla 25 de Mayo) Antártida Argentina. Mapa detallado de suelos, escala 1:10000. Dirección Nacional del Antártico, Buenos Aires, p. 45.

Grant, S.A., Hillel D. (2005): HYDRAULIC PROPERTIES, TEMPERATURE EFFECTS. In: Encyclopedia of Soils in the Environment. Elsevier, Oxford, p. 207-211.

Grathwohl, P. (2007): Natürlicher Abbau und Rückhalt von Schadstoffen. In: Ingenieurgeochemie. Springer Berlin Heidelberg, p. 151-242.

Grechishchev, S.E., Instanes A., Sheshin J.B., Pavlov A.V., Grechishcheva O.V. (2001): Laboratory investigation of the freezing point of oil-polluted soils. Cold Regions Science and Technology 32(2-3): 183-189.

Haritash, A.K., Kaushik C.P. (2009): Biodegradation aspects of Polycyclic Aromatic Hydrocarbons (PAHs): A review. Journal of Hazardous Materials 169(1â€"3): 1-15.

Harlan, R.L. (1973): Analysis of coupled heat-fluid transport in partially frozen soil. American Geophysical Union 9(5): 1314-1323.

Hartmann, D.L., Klein Tank A.M.G., Rusticucci M., Alexander L.V., Brönnimann S., Charabi Y., Dentener F.J., Dlugokencky E.J., Easterling D.R., Kaplan A., Soden B.J., Thorne P.W., Wild M., Zhai P.M. (2013): Observations: Atmosphere and Surface. In: Stocker TF, Qin D, Plattner G-K, Tignor M, Allen SK, Boschung J, Nauels A, Xia Y, Bex V & Midgley PM (eds) Climate Change 2013: The Physical Science Basis. Contribution of Working Group I to the Fifth Assessment Report of the Intergovernmental Panel on Climate Change. Cambridge Univertiy Press, Cambridge (UK), New York (USA),

Henry, H.A.L. (2007): Soil freeze-thaw cycle experiments: Trends, methodological weaknesses and suggested improvements. Soil Biology and Biochemistry 39(5): 977-986.

Hillel, D. (2003): 1 - Soil Physics and Soil Physical Characteristics. In: Introduction to Environmental Soil Physics (First). Academic Press, Burlington, p. 3-17.

Hillel, D. (2005): THERMAL PROPERTIES AND PROCESSES. In: Encyclopedia of Soils in the Environment. Elsevier, Oxford, p. 156-163.

Hinzman, L., Bettez N., Bolton W.R., Chapin F.S., Dyurgerov M., Fastie C., Griffith B., Hollister R., Hope A., Huntington H., Jensen A., Jia G., Jorgenson T., Kane D., Klein D., Kofinas G., Lynch A., Lloyd A., McGuire A.D., Nelson F., Oechel W., Osterkamp T., Racine C., Romanovsky V., Stone R., Stow D., Sturm M., Tweedie C., Vourlitis G., Walker M., Walker D., Webber P., Welker J., Winker K., Yoshikawa K. (2005): Evidence and Implications of Recent Climate Change in Northern Alaska and Other Arctic Regions. Climatic Change 72(3): 251-298.

Horn, R., Bachmann J., Peth S. (2014): Hartge/Horn: Einführung in die Bodenphysik. Schweizerbart, p. 372.

Howsam, M., Jones K.C. (1998): Sources of PAHs in the Environment. In: Neilson AH (ed) PAHs and Related Compounds. The Handbook of Environmental Chemistry. Springer, Berlin, p. 137-174.

Hulscher, T.E.M., Cornelissen G. (1996): Effect of temperature on sorption equilibrium and sorption kinetics of organic micropollutants - a review. Chemosphere 32(4): 609-626.

Hutchinson, T.C., Freedman W. (1978): Effects of experimental crude oil spills on subarctic boreal forest vegetation near Norman Wells, N.W.T., Canada. Canadian Journal of Botany 56(19): 2424-2433.

Hwang, S., Ramirez N., Cutright T.J., Ju L.K. (2003): The Role of Soil Properties in Pyrene Sorption and Desorption. Water, Air, and Soil Pollution 143(1-4): 65-80.

Inubushi, K., Brookes P.C., Jenkinson D.S. (1991): Soil microbial biomass C, N and ninhydrin-N in aerobic and anaerobic soils measured by the fumigation-extraction method. Soil Biology and Biochemistry 23(8): 737-741.

Ireson, A.M., van der Kamp G., Ferguson G., Nachshon U., Wheater H.S. (2013): Hydrogeological processes in seasonally frozen northern latitudes: understanding, gaps and challenges. Hydrogeology Journal 21(1): 53-66.

IUSS Working Group WRB (2014): World Reference Base for soil resources 2014. FAO, Rome, p. 128.

Iwakun, O., Biggar K., Sego D. (2010): Influence of cyclic freeze-thaw on the mobilization of LNAPL and soluble oil in a porous media. Cold Regions Science and Technology 64(1): 9-18.

Jarsjö, J., Destouni G., Yaron B. (1994): Retention and volatilisation of kerosene: Laboratory experiments on glacial and post-glacial soils. Journal of Contaminant Hydrology 17(2): 167-185.

Jepsen, S.M., Adams E.E., Priscu J.C. (2006): Fuel movement along grain boundaries in ice. Cold Regions Science and Technology 45(3): 158-165.

Johnsen, A., Karlson U. (2007): Diffuse PAH contamination of surface soils: environmental occurrence, bioavailability, and microbial degradation. Applied Microbiology and Biotechnology 76(3): 533-543.

Johnsen, A.R., Wick L.Y., Harms H. (2005): Principles of microbial PAH-degradation in soil. Environmental Pollution 133(1): 71-84.

Johnson, L.A., Sparrow E.B., Jenkins T.F., Collins C.M., Davenport C.V., McFadden T.T. (1980): The fate and effects of crude oil spilled on subarctic permafrost terrain in interior Alaska. CRREL, Hanover, p. 67.

Jones, A., Stolbovoy C., Tarnocai C., Broll G., Spaargaren O., Montanarella L. (Eds) (2010): Soil Atlas of the Northern Circumpolar Region. Publications Office of the European Union, Luxembourg.

Jorgenson, M.T., Romanovsky V., Harden J., Shur Y., O'Donnell J., Schuur E.A.G., Kanevskiy M., Marchenko S. (2010): Resilience and vulnerability of permafrost to climate changeThis article is one of a selection of papers from The Dynamics of Change in Alaskaâ€™s Boreal Forests: Resilience and Vulnerability in Response to Climate Warming. Canadian Journal of Forest Research 40(7): 1219-1236.

Karickhoff, S.W. (1980): Sorption kinetics of hydrophobic pollutants in natural sediments. In: Baker RA (ed) Contaminants and Sediments: Analysis, Chemistry, Biology. Ann Arbor Science, Michigan, p. 193-205.

Karickhoff, S.W. (1981): Semi-empirical estimation of sorption of hydrophobic pollutants on natural sediments and soils. Chemosphere 10(8): 833-846.

Karttunen, V., Myllynen P., Prochazka G., Pelkonen O., Segerbäck D., Vähäkangas K. (2010): Placental transfer and DNA binding of benzo(a)pyrene in human placental perfusion. Toxicology Letters 197(2): 75-81.

Knoblauch, C., Beer C., Sosnin A., Wagner D., Pfeiffer E.-M. (2013): Predicting long-term carbon mineralization and trace gas production from thawing permafrost of Northeast Siberia. Global Change Biology 19(4): 1160-1172.

Knoche, H., Klein W., Kördel W., Wahle K., Hund K., Müller J., Klein W. (1995): Literaturstudie zur Ableitung von Bodengrenzwerten für polyzyklische aromatische Kohlenwasserstoffe (PAK). Umweltbundesamt, Berlin,

Kögel-Knabner, I., Totsche K.U. (1998): Influence of dissolved and colloidal phase humic substances on the transport of hydrophobic organic contaminants in soils. Physics and Chemistry of The Earth 23(2): 179-185.

Konrad, J.M. (1989): Influence of cooling rate on the temperature of ice lens formation in silt loams. Cold Regions Science and Technology 16(1): 25-36.

Konrad, J.M., McCammon A.W. (1990): Solute partitioning in freezing soils. Canadian Geotechnical Journal 27(6): 726-736.

Konrad, J.M., Morgenstern N.R. (1980): A mechanistic theory of ice lens formation in fine-grained soils. Canadian Geotechnical Journal 17: 473-486.

Konrad, J.M., Morgenstern N.R. FRost susceptibility of soils in terms of their segregation potential. In: Fourth International Conference on Permafrost. U.S. National Academy Press, Washington, D.C., Fairbanks, Alaska. 1983. U.S. National Academy Press, Washington, D.C., p 660-665.

Konrad, J.M., Seto J.T.C. (1991): Freezing of a silt loam contaminated with an organic solvent. Journal of Contaminant Hydrology 8(3-4): 335-355.

Kozlowski, T. (2009): Some factors affecting supercooling and the equilibrium freezing point in soil-water systems. Cold Regions Science and Technology 59(1): 25-33.

Krauss, M., Wilcke W. (2002): Sorption Strength of Persistent Organic Pollutants in Particle-size Fractions of Urban Soils. Soil Sci. Soc. Am. J. 66(2): 430-437.

Krauss, M., Wilcke W. (2005): Persistent organic pollutants in soil density fractions: distribution and sorption strength. Chemosphere 59(10): 1507-1515.

Krauss, M., Wilcke W., Zech W. (2000): Polycyclic aromatic hydrocarbons and polychlorinated biphenyls in forest soils: depth distribution as indicator of different fate. Environmental Pollution 110(1): 79-88.

Kurylyk, B.L., Watanabe K. (2013): The mathematical representation of freezing and thawing processes in variably-saturated, non-deformable soils. Advances in Water Resources 60(0): 160-177.

Kutzbach, L. (2006): The Exchange of Energy, Water and Carbon Dioxide between Wet Arctic Tundra and the Atmosphere at the Lena River Delta, Northern Siberia. In: Geowissenschaften. Universität Hamburg, Hamburg.

Kutzbach, L., Zubrzycki S., Knoblauch C., Fiencke C., Pfeiffer E.M. (2014): Permafrostbeeinflusste Böden (Kryosole) im Klimawandel. In: Lozán JL, Graßl H, Piepenburg D & Notz D (eds) Warnsignal Klima: die Polarregionen. Wissenschaftliche Auswertungen, Hamburg, p. 376.

Lane, W.F., Loehr R.C. (1992): Estimating the equilibrium aqueous concentrations of polynuclear aromatic hydrocarbons in complex mixtures. Environmental Science & Technology 26(5): 983-990.

Lange, G. (2015): Permafrost - die große Unbekannte im Klimawandel. Spektrum der Wissenschaft 3/2015: 78-89.

Lee, L.S., Hagwall M., Delfino J.J., Rao P.S.C. (1992): Partitioning of polycyclic aromatic hydrocarbons from diesel fuel into water. Environmental Science & Technology 26(11): 2104-2110.

Lewis, J., Sjoestrom J. (2010): Optimizing the experimental design of soil columns in saturated and unsaturated transport experiments. Journal of Contaminant Hydrology 115(1-4): 1-13.

Luthy, R.G., Aiken G.R., Brusseau M.L., Cunningham S.D., Gschwend P.M., Pignatello J.J., Reinhard M., Traina S.J., Weber W.J., Westall J.C. (1997): Sequestration of Hydrophobic Organic Contaminants by Geosorbents. Environmental Science & Technology 31(12): 3341-3347.

Mackay, D., Callcott D. (1998): Partitioning and Physical Chemical Properties of PAHs. In: Neilson AH (ed) The Handbook of Environmental Chemistry Vol. 3 Part I. Springer-Verlag, Berlin Heidelberg,

Madsen, E.L. (2003): Report on bioavailability of chemical wastes with respect to potential for soil bioremediation. US Environmental Protection Agency, Washington, p. 122.

Mahro, B., Kästner M. (1993): Der mikrobielle Abbau polyzyklischer aromatischer Kohlenwasserstoffe (PAK) in Böden und Sedimenten: Mineralisierung, Metabolitenbildung und Entstehung gebundener Rückstände. BioEngineering 9: 50-58.

Maliszewska-Kordybach, B. (2005): Dissipation of Polycyclic Aromatic Hydrocarbons in Freshly Contaminated Soils – The Effect of Soil Physicochemical Properties and Aging. Water, Air, and Soil Pollution 168(1-4): 113-128.

Margesin, R., Labbé D., Schinner F., Greer C.W., Whyte L.G. (2003): Characterization of Hydrocarbon-Degrading Microbial Populations in Contaminated and Pristine Alpine Soils. Appl Environ Microbiol 69(6): 3085-3092.

Marschner, B. (1998): DOM-enhanced mobilization of benzo(a)pyrene in a contaminated soil under different chemical conditions. Physics and Chemistry of The Earth 23(2): 199-203.

Marschner, B., Winkler R., JÖdemann D. (2005): Factors controlling the partitioning of pyrene to dissolved organic matter extracted from different soils. European Journal of Soil Science 56(3): 299-306.

Matmon, D., Hayden N.J. (2003): Pore space analysis of NAPL distribution in sand–clay media. Advances in Water Resources 26(7): 773-785.

Matzner, E., Hübner D., Thomas W. (1981): Content and storage of polycyclic aromatic hydrocarbons in two forested ecosystems in northern Germany. Zeitschrift für Pflanzenernährung und Bodenkunde 144(3): 283-288.

McCarthy, J.F., Zachara J.M. (1989): Subsurface transport of contaminants. Environmental Science & Technology 23(5): 496-502.

McCarthy, K., Walker L., Vigoren L. (2004): Subsurface fate of spilled petroleum hydrocarbons in continuous permafrost. Cold Regions Science and Technology 38(1): 43-54.

McCauley, C.A., White D.M., Lilly M.R., Nyman D.M. (2002): A comparison of hydraulic conductivities, permeabilities and infiltration rates in frozen and unfrozen soils. Cold Regions Science and Technology 34(2): 117-125.

McRoberts, E.C., Morgenstern N.R. (1975): Pore Water Expulsion during Freezing. Canadian Geotechnical Journal 12(1): 130-141.

Müller-Lupp, W. (2002): Gefrier- und Tauprozesse im sibirischen Permafrost; Untersuchungsmethoden und oekologische Bedeutung. In: Berichte zur Polar- und Meeresforschung, AWI. Christian-Albrechts Universität, Kiel, Bremerhaven. p 145.

Müller, S., Wilcke W., Kanchanakool N., Zech W. (2000): Polycyclic aromatic hydrocarbons (pahs) and polychlorinated biphenyls (pcbs) in particle-size separates of urban soils in bangkok, thailand. Soil Science 165(5): 412-419.

Nakano, Y. (1999): Water expulsion during soil freezing described by a mathematical model called M1. Cold Regions Science and Technology 29(1): 9-30.

Nam, J.J., Sweetman A.J., Jones K.C. (2009): Polynuclear aromatic hydrocarbons (PAHs) in global background soils. Journal of Environmental Monitoring 11(1): 45-48.

Nam, J.J., Thomas G.O., Jaward F.M., Steinnes E., Gustafsson O., Jones K.C. (2008): PAHs in background soils from Western Europe: Influence of atmospheric deposition and soil organic matter. Chemosphere 70(9): 1596-1602.

Niven, R.K., Singh K. (2008): Mobilization and Rupture of LNAPL Ganglia during Freeze-Thaw: Two-Dimensional Cell Experiments. Environmental Science & Technology 42(15): 5467-5472.

Northcott, G.L., Jones K.C. (2001): Partitioning, Extractability, and Formation of Nonextractable PAH Residues in Soil. 1. Compound Differences in Aging and Sequestration. Environmental Science & Technology 35(6): 1103-1110.

Ostroumov, V., Hoover R., Ostroumova N., Van Vliet-LanoÃ« B., Siegert C., Sorokovikov V. (2001): Redistribution of soluble components during ice segregation in freezing ground. Cold Regions Science and Technology 32(2â€“3): 175-182.

Othman, M.A., Benson C.H. (1993): Effect of freeze–thaw on the hydraulic conductivity and morphology of compacted clay. Canadian Geotechnical Journal 30(2): 236-246.

Oztas, T., Fayetorbay F. (2003): Effect of freezing and thawing processes on soil aggregate stability. CATENA 52(1): 1-8.

Penner, E. Soil moisture redistribution by ice lensing in freezing soils. In: 17th annual meeting of the Canadian Society of Soil Science. Lethbridge, Alberta. 1972. p 44-62.

Pernot, A., Ouvrard S., Leglize P., Faure P. (2013): Protective role of fine silts for PAH in a former industrial soil. Environmental Pollution 179(0): 81-87.

Peters, C.A., Mukherji S., Knightes C.D., Weber W.J. (1997): Phase Stability of Multicomponent NAPLs Containing PAHs. Environmental Science & Technology 31(9): 2540-2546.

Pignatello, J.J., Xing B. (1995): Mechanisms of Slow Sorption of Organic Chemicals to Natural Particles. Environmental Science & Technology 30(1): 1-11.

Prus, W., Fabiańska M.J., Łabno R. (2015): Geochemical markers of soil anthropogenic contaminants in polar scientific stations nearby (Antarctica, King George Island). Science of The Total Environment 518–519(0): 266-279.

Qi, J., Ma W., Song C. (2008): Influence of freeze-thaw on engineering properties of a silty soil. Cold Regions Science and Technology 53(3): 397-404.

Qi, J., Vermeer P.A., Cheng G. (2006): A review of the influence of freeze-thaw cycles on soil geotechnical properties. Permafrost and Periglacial Processes 17(3): 245-252.

Raber, B., Kögel-Knabner I., Stein C., Klem D. (1998): Partitioning of polycyclic aromatic hydrocarbons to dissolved organic matter from different soils. Chemosphere 36(1): 79-97.

Raisbeck, J.M., Mohtadi M.F. (1974): The environmental impacts of oil spills on land in the arctic regions. Water, Air, and Soil Pollution 3: 195-208.

Revill, A.T., Snape I., Lucieer A., Guille D. (2007): Constraints on transport and weathering of petroleum contamination at Casey Station, Antarctica. Cold Regions Science and Technology 48(2): 154-167.

Rike, A.G., Børresen M., Instanes A. (2001): Response of cold-adapted microbial populations in a permafrost profile to hydrocarbon contaminants. Polar Record 37(202): 239-248.

Rike, A.G., Haugen K.B., Børresen M., Engene B., Kolstad P. (2003): In situ biodegradation of petroleum hydrocarbons in frozen arctic soils. Cold Regions Science and Technology 37(2): 97-120.

Rike, A.G., Haugen K.B., Engene B. (2005): In situ biodegradation of hydrocarbons in arctic soil at sub-zero temperatures--field monitoring and theoretical simulation of the microbial activation temperature at a Spitsbergen contaminated site. Cold Regions Science and Technology 41(3): 189-209.

Rike, A.G., Schiewer S., Filler D.M. (2008): Temperature effects on bioremediation of petroleum contaminants in cold soils. In: Filler DM, Snape CE & Barnes DL (eds) Bioremediation of Petroleum Hydrocarbons in Cold Regions. Cambridge University Press, Cambridge, p. 273.

Ross, D.J. (1989): Estimation of soil microbial C by A fumigation-extraction procedure: Influence of soil moisture content. Soil Biology and Biochemistry 21(6): 767-772.

Rost, H., Loibner A.P., Hasinger M., Braun R., Szolar O.H.J. (2002): Behavior of PAHs during cold storage of historically contaminated soil samples. Chemosphere 49(10): 1239-1246.

Sanders, T., Fiencke C., Pfeiffer E.M. (2010): Small-scale variability of dissolved inorganic nitrogen (DIN), C/N ratios and ammonia oxidizing capacities in various permafrost affected soils of Samoylov Island, Lena River Delta, Northeast Siberia. Polarforschung 80(1): 23-35.

Schadt, C.W., Martin A.P., Lipson D.A., Schmidt S.K. (2003): Seasonal Dynamics of Previously Unknown Fungal Lineages in Tundra Soils. Science 301(5638): 1359-1361.

Schindler, D.W., Smol J.P. (2006): Cumulative Effects of Climate Warming and Other Human Activities on Freshwaters of Arctic and Subarctic North America. AMBIO: A Journal of the Human Environment 35(4): 160-168.

Schoen, R., Gaudet J.P., Bariac T. (1999): Preferential flow and solute transport in a large lysimeter, under controlled boundary conditions. Journal of Hydrology 215(1â€“4): 70-81.

Schwille, F. (1984): Migration of Organic Fluids Immiscible with Water in the Unsaturated Zone. In: Yaron B, Dagan G & Goldshmid J (eds) Pollutants in Porous Media. Ecological Studies, vol 47. Springer, Berlin, Heidelberg, New York, Tokyo, p. 296.

Serreze, M.C., Walsh J.E., Chapin F.S., III, Osterkamp T., Dyurgerov M., Romanovsky V., Oechel W.C., Morison J., Zhang T., Barry R.G. (2000): Observational Evidence of Recent Change in the Northern High-Latitude Environment. Climatic Change 46(1-2): 159-207.

Shur, Y., Hinkel K.M., Nelson F.E. (2005): The transient layer: implications for geocryology and climate-change science. Permafrost and Periglacial Processes 16(1): 5-17.

Siciliano, S.D., Schafer A.N., Forgeron M.A.M., Snape I. (2008): Hydrocarbon Contamination Increases the Liquid Water Content of Frozen Antarctic Soils. Environmental Science & Technology 42(22): 8324-8329.

Sims, R.C., Overcash M.R. (1983): Fate of polynuclear aromatic compounds (PNAs) in soil-plant systems. In: Residue Reviews. Residue Reviews. Springer New York, p. 1-68.

Singh, K., Niven R.K. (2013): Non-aqueous Phase Liquid Spills in Freezing and Thawing Soils: Critical Analysis of Pore-Scale Processes. Critical Reviews in Environmental Science and Technology 43(6): 551-597.

Skark, C., Kuhlmann B., Zullei-Seibert N. (2011): Verfeinerung und Validierung des Screenings nach trinkwasserrelevanten Chemikalien im Geltungsbereich der REACH-Verordnung. Institut für Wasserforschung GmbH im Auftrag des UBA, Schwerte, p. 75.

Sloan, C.E., van Everdingen R.O. (1988): Region 28: Permafrost region. In: America TGSo (ed) The geology of North America. p. 263-270.

Šmídová, K., Hofman J., Ite A.E., Semple K.T. (2012): Fate and bioavailability of 14C-pyrene and 14C-lindane in sterile natural and artificial soils and the influence of aging. Environmental Pollution 171(0): 93-98.

Snape, I., Acomb L., Barnes D.L., Brainbridge S., Eno R., Filler D.M., Plato N., Poland J.S., Raymond T.C., Rayner J.L., Riddle M.J., Rike A.G., Ruttler A., Schafer A.N., Siciliano S.D., Walworth J.L. (2008): Contaminations, regulation, and remediation: an introduction to bioremediation of petroleum hydrocarbons in cold regions. In: Filler DM, Snape I & Barnes DL (eds) Bioremediation of Petroleum Hydrocarbons in Cold Regions. Cambridge University Press, Cambridge, p. 273.

Spagnoli, G. (2012): Comparison between Casagrande and drop-cone methods to calculate liquid limit for pure clay. Canadian Journal of Soil Science 92(6): 859-864.

Sparrman, T., Öquist M., Klemedtsson L., Schleucher J., Nilsson M. (2004): Quantifying Unfrozen Water in Frozen Soil by High-Field 2H NMR. Environmental Science & Technology 38(20): 5420-5425.

Staff, S.S. (2014): Keys to Soil Taxonomy, 12th ed. USDA-Natural Resources Conservation Service, Washington, DCp. 360.

Stepanova, V.A., Pokrovsky O.S., Viers J., Mironycheva-Tokareva N.P., Kosykh N.P., Vishnyakova E.K. (2015): Elemental composition of peat profiles in western Siberia: Effect of the micro-landscape, latitude position and permafrost coverage. Applied Geochemistry 53(0): 53-70.

Tang, J., Lu X., Sun Q., Zhu W. (2012): Aging effect of petroleum hydrocarbons in soil under different attenuation conditions. Agriculture, Ecosystems & Environment 149(0): 109-117.

Tice, A.R., Anderson D.M., Banin A. (1976): The prediction of unfrozen water contents in frozen soils from liquid limit determinations.

Ting, W.T.E., Yuan S.Y., Wu S.D., Chang B.V. (2011): Biodegradation of phenanthrene and pyrene by Ganoderma lucidum. International Biodeterioration & Biodegradation 65(1): 238-242.

Tsibart, A.S., Gennadiev A.N. (2013): Polycyclic aromatic hydrocarbons in soils: Sources, behavior, and indication significance (a review). Eurasian Soil Science 46(7): 728-741.

Tumeo, M.A., Davidson B. (1993): Hydrocarbon exclusion from ground water during freezing. Journal of Environmental Engineering 119(4): 715-724.

Valentín, L., Nousiainen A., Mikkonen A. (2013): Introduction to Organic Contaminants in Soil: Concepts and Risks. In: Vicent T, Caminal G, Eljarrat E & Barceló D (eds) Emerging Organic Contaminants in Sludges. The Handbook of Environmental Chemistry. Springer Berlin Heidelberg, p. 1-29.

Viklander, P., Eigenbrod D. (2000): Stone movements and permeability changes in till caused by freezing and thawing. Cold Regions Science and Technology 31(2): 151-162.

Vogt, C., Richnow H. (2014): Bioremediation via in situ Microbial Degradation of Organic Pollutants. In: Schippers A, Glombitza F & Sand W (eds) Geobiotechnology II. Advances in Biochemical Engineering/Biotechnology. Springer Berlin Heidelberg, p. 123-146.

Wabbels, D., Teutsch G. (2008): Leitfaden Natürliche Schadstoffminderungsprozesse bei mineralölkontaminierten Standorten. KORA Themenverbund 1: Raffinerien, Tanklager, Kraftstoffe/Mineralöl, MTBE. ZAG Universität Tübingen, Tübingen

Wagner, D., Kobabe S., Pfeiffer E.-M., Hubberten H.W. (2003): Microbial controls on methane fluxes from a polygonal tundra of the Lena Delta, Siberia. Permafrost and Periglacial Processes 14(2): 173-185.

Walter, T., Ederer H.J., Först C., Stieglitz L. (2000): Sorption of selected polycyclic aromatic hydrocarbons on soils in oil-contaminated systems. Chemosphere 41(3): 387-397.

Walvoord, M.A., Striegl R.G. (2007): Increased groundwater to stream discharge from permafrost thawing in the Yukon River basin: Potential impacts on lateral export of carbon and nitrogen. Geophysical Research Letters 34(12): L12402.

Walvoord, M.A., Voss C.I., Wellman T.P. (2012): Influence of permafrost distribution on groundwater flow in the context of climate-driven permafrost thaw: Example from Yukon Flats Basin, Alaska, United States. Water Resources Research 48(7): W07524.

Washburn, A.L. (1979): Geocryology. Edward Arnold, Londonp. 406.

Wehrer, M., Totsche K.U. (2005): Determination of effective release rates of polycyclic aromatic hydrocarbons and dissolved organic carbon by column outflow experiments. European Journal of Soil Science 56(6): 803-813.

Weigand, H., Totsche K.U., Kögel-Knabner I., Annweiler E., Richnow H.H., Michaelis W. (1999): Desorption controlled mobility and intrinsic biodegradation of anthracene in unsaturated soil. Physics and Chemistry of the Earth, Part B: Hydrology, Oceans and Atmosphere 24(6): 549-555.

Weihermüller, L., Siemens J., Deurer M., Knoblauch S., Rupp H., Göttlein A., Pütz T. (2007): In Situ Soil Water Extraction: A Review. J. Environ. Qual. 36(6): 1735-1748.

Whelan, M.J., Coulon F., Hince G., Rayner J., McWatters R., Spedding T., Snape I. (2015): Fate and transport of petroleum hydrocarbons in engineered biopiles in polar regions. Chemosphere (0):

White, P.A., Claxton L.D. (2004): Mutagens in contaminated soil: a review. Mutation Research/Reviews in Mutation Research 567(2–3): 227-345.

White, T.L., Coutard J.P. (1999): Modification of silt microstructure by hydrocarbon contamination in freezing ground. Polar Record 35(192): 41-50.

White, T.L., Williams P.J. (1999): The influence of soil microstructure on hydraulic properties of hydrocarbon-contaminated freezing ground. Polar Record 35(192): 25-32.

White, T.L., Williams P.J., Marchand Y., Rees W.G. (2000): Microstructural alteration in permafrost-affected soils due to hydrocarbon contamination: implications for subsurface transport Contaminants in freezing Ground (Collected Proceedings of 2nd International Conference, Part I): 7 - 21.

Wiggert, D.C., Andersland O.B., Davies S.H. (1997): Movement of liquid contaminants in partially saturated frozen granular soils. Cold Regions Science and Technology 25(2): 111-117.

Wilcke, W. (2000): SYNOPSIS Polycyclic Aromatic Hydrocarbons (PAHs) in Soil — a Review. Journal of Plant Nutrition and Soil Science 163(3): 229-248.

Williams, P.J. (1976): Volume change in frozen soils. In: N. Janbu FJ, B. Kjaernsli (ed) Laurits Bjerrum memorial volume. Norwegian Geotechnical Institute, Oslo, p. 233 - 346.

Williams, P.J., Smith M.W. (1991): The frozen earth: Fundamentals in Geocryology. Cambridge University Press, Cambridgep. 306.

Wilson, J.L., Conrad S.H., Mason W.R., Peplinski W., Hagan E. (1990): Laboratory investigation of residual liquid organics from spills, leaks, and the disposal of hazardous wastes in groundwater. Department of Geoscience & Geophysical Research Center, New Mexico Institute of Mining and Technology, Oklahoma, p. 287.

Woo, M.-k. (2012): Permafrost Hydrology. Springer, Berlin, Heidelbergp. 563.

Xue, W., Warshawsky D. (2005): Metabolic activation of polycyclic and heterocyclic aromatic hydrocarbons and DNA damage: A review. Toxicology and Applied Pharmacology 206(1): 73-93.

Yang, Y., Ratté D., Smets B.F., Pignatello J.J., Grasso D. (2001): Mobilization of soil organic matter by complexing agents and implications for polycyclic aromatic hydrocarbon desorption. Chemosphere 43(8): 1013-1021.

Yaron, B., Dror I., Berkowitz B. (2012): Soil-Subsurface Change: Chemical Pollutant Impacts. Springer, Berlin, Heidelberg

Yershov, E.D. (1998): General Geocryology. Cambridge University Press, Cambridgep. 580.

Zemanek, M.G., Pollard S.J.T., Kenefick S.L., Hrudey S.E. (1997): Multi-phase partitioning and co-solvent effects for polynuclear aromatic hydrocarbons (pah) in authentic petroleum- and creosote-contaminated soils. Environmental Pollution 98(2): 239-252.

Zhang, T., Heginbottom J.A., Barry R.G., Brown J. (2000): Further statistics on the distribution of permafrost and ground ice in the Northern Hemisphere 1. Polar Geography 24(2): 126-131.

Zhang, Y., Zhu S., Xiao R., Wang J., Li F. (2008): Vertical transport of polycyclic aromatic hydrocarbons in different particle-size fractions of sandy soils. Environmental Geology 53(6): 1165-1172.

Zhao, Q., Li P., Stagnitti F., Ye J., Dong D., Zhang Y., Li P. (2009): Effects of aging and freeze-thawing on extractability of pyrene in soil. Chemosphere 76(4): 447-452.

Zhao, Q., Xing B., Tai P., Li H., Song L., Zhang L., Li P. (2013): Effect of freeze-thawing cycles on soil aging behavior of individually spiked phenanthrene and pyrene at different concentrations. Science of The Total Environment 444(0): 311-319.

Zhe, L., Zeng F., Xue N., Li F. (2012): Occurrence and distribution of polycyclic aromatic hydrocarbons in organo-mineral particles of alluvial sandy soil profiles at a petroleum-contaminated site. Science of The Total Environment 433(0): 50-57.

Zhu, J., Sykes J.F. (2000): The influence of NAPL dissolution characteristics on field-scale contaminant transport in subsurface. Journal of Contaminant Hydrology 41(1–2): 133-154.

Zubrzycki, S., Kutzbach L., Pfeiffer E.M. (2014): Permafrost-affected soils and their carbon pools with a focus on the Russian Arctic. Solid Earth 5(2): 595-609.

Zykov, I.D., Chuvilin E.M., Motenko R.G., Roman L.T., Shevchenko L.V., Zhuravlev I.I., Anisimova I.V., Kozlova E.V., Nefed'eva I.A., Volochev S.S., Miklyaeva E.S., Ershov E.D. (2005): Crude oil infiltration in frozen soils and transformation of their properties caused by pollution [Proniknovenie nefti v merzlye grunty i izmenenie ikh svoistv] (Russian). Russian Federationp. 45-52.

Zykov, Y.D., Koshurnikov A.V., Anisimova I.V., Mironova T.E., Kane D.L., Hinkel K.M. (2008): The oil pollution influence of frozen soils on their geophysical characteristics. Ninth international conference on Permafrost; extended abstracts: 367-368.

A. APPENDIX

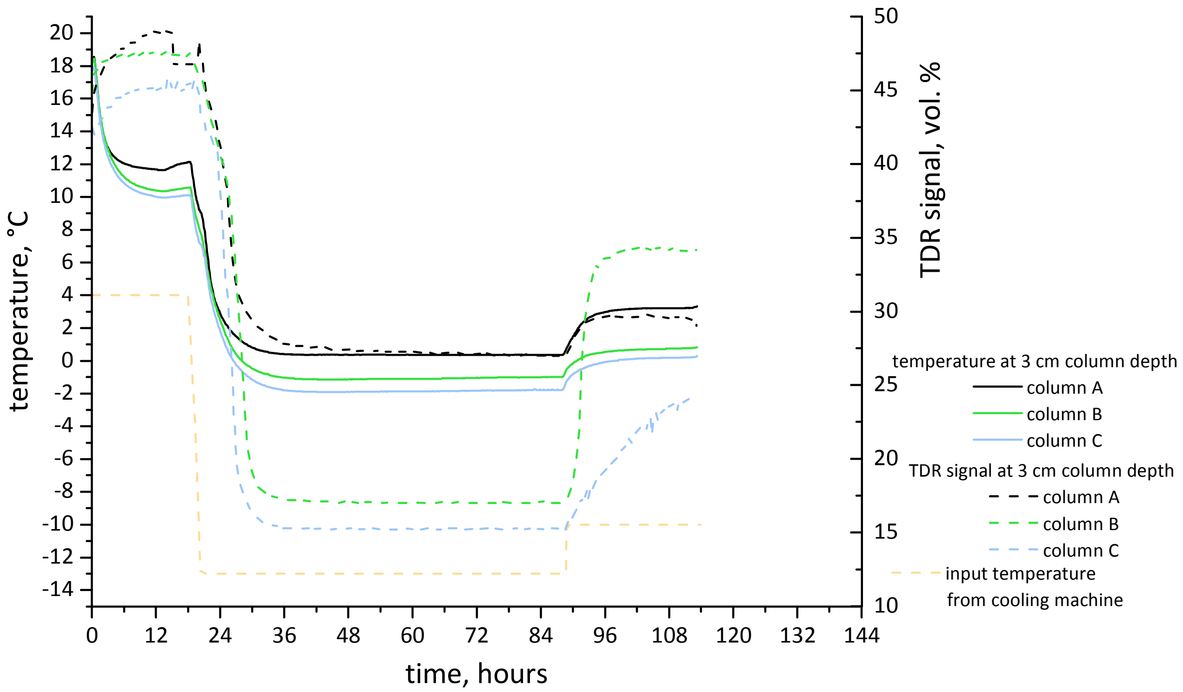

Figure A.1 TDR (lines) and temperature (dashed lines) profiles for three experimental columns of the experiment with silt loam and freezing from the bottom (*Ufba*)

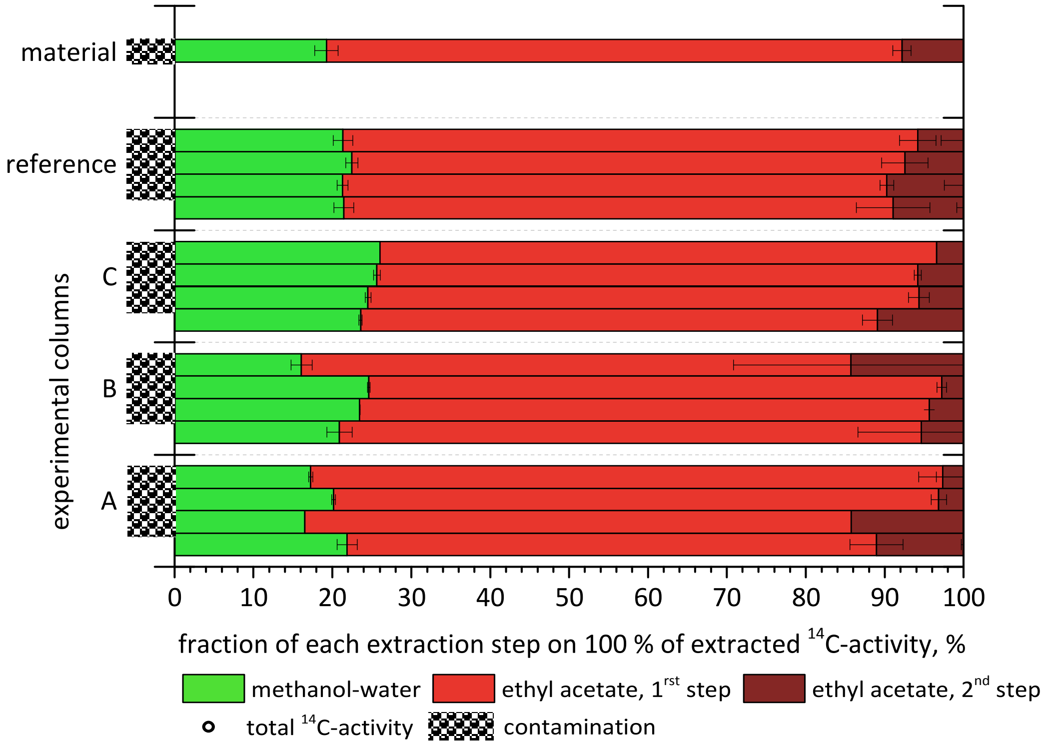

Figure A.2 Fractions of the three sequential extractions for the experiment with ^{14}C-pyrene (*Ufbp*) on the sum of extracted ^{14}C-activity, methanol-water extraction (green) and two consecutive extractions with ethyl acetate (red and brown) were conducted sequentially. Standard error reflects n≥3. Black and white rectangle marks contaminated column parts at the beginning of the experiment.

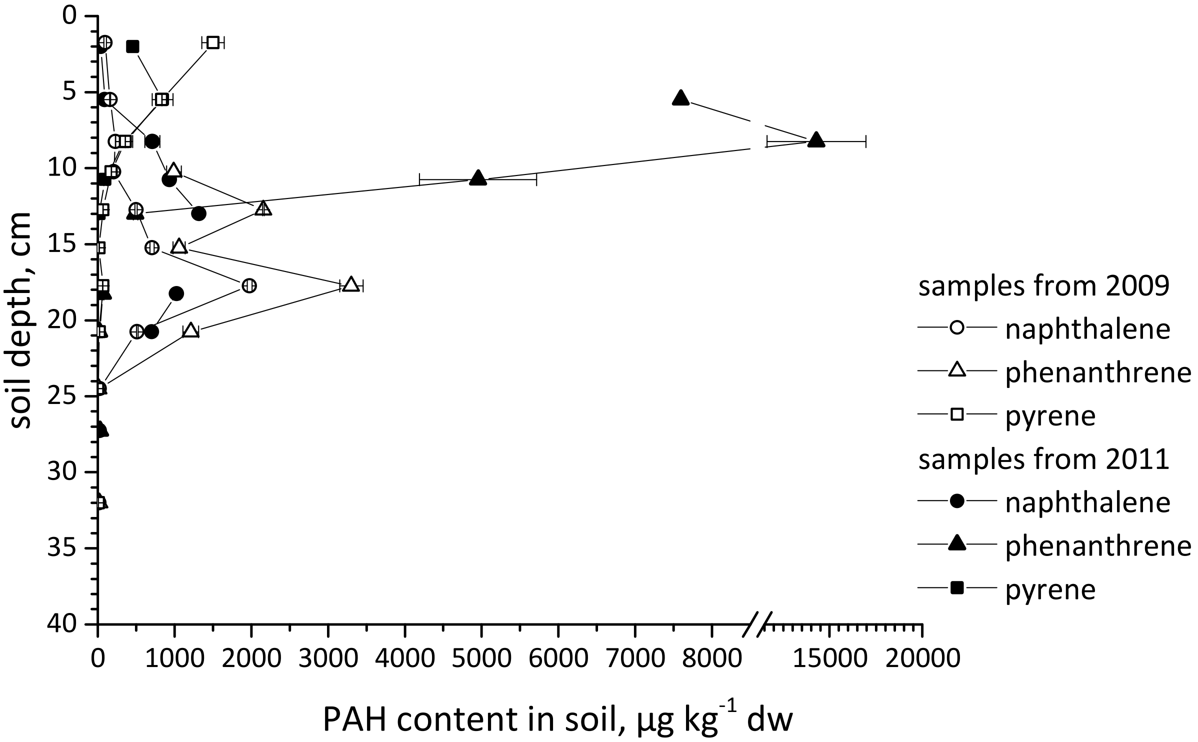

Figure A.3 **Distribution of single PAHs with different number of fused rings throughout the soil cores taken at the contaminated site in Northern Siberia in 2009 and 2011, standard error reflects n≥3**

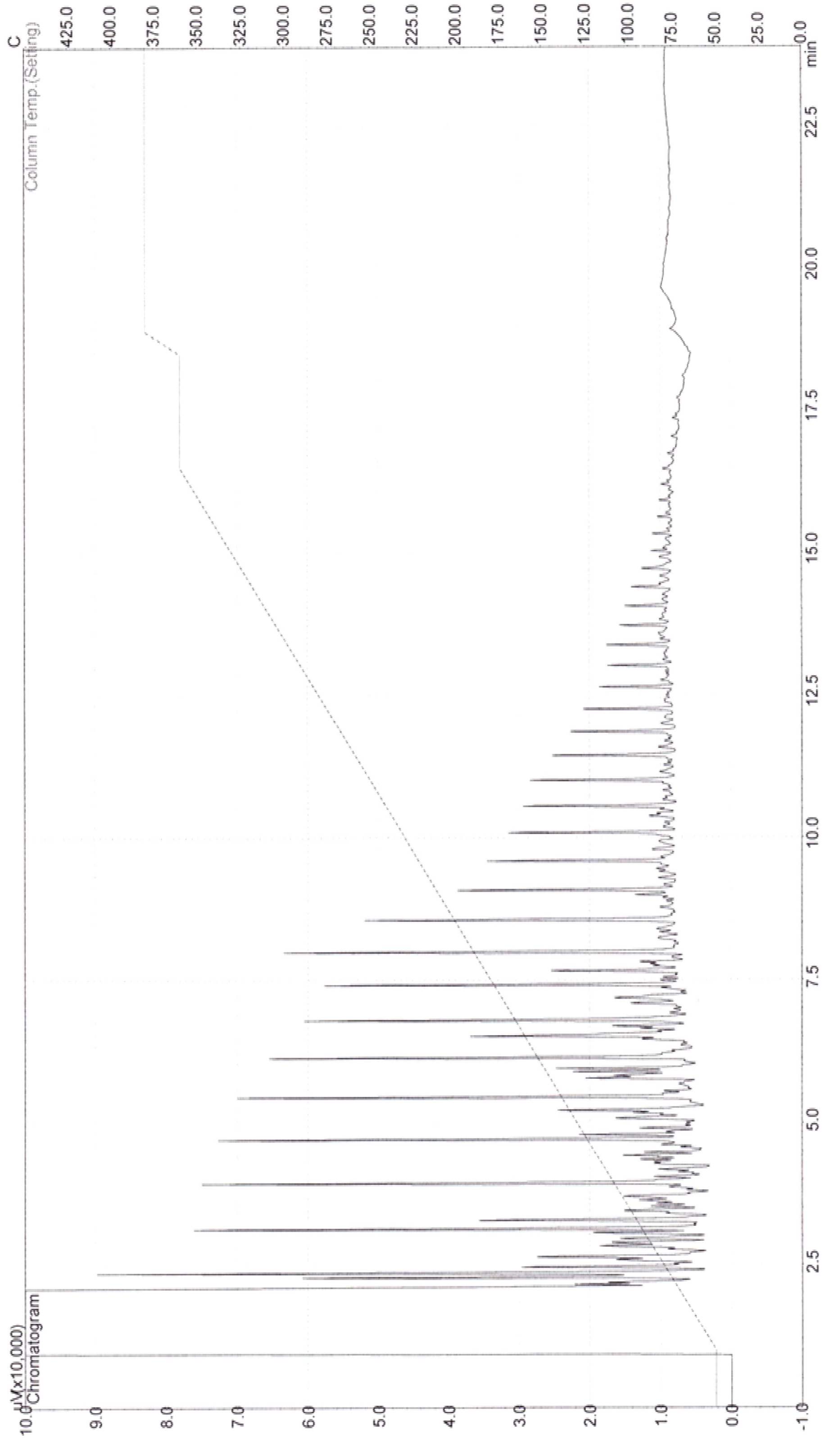

Figure A.4 **Chromatogram of Ekofisk - paraffin- based crude oil from North Sea, Royal Dutch Shell plc**

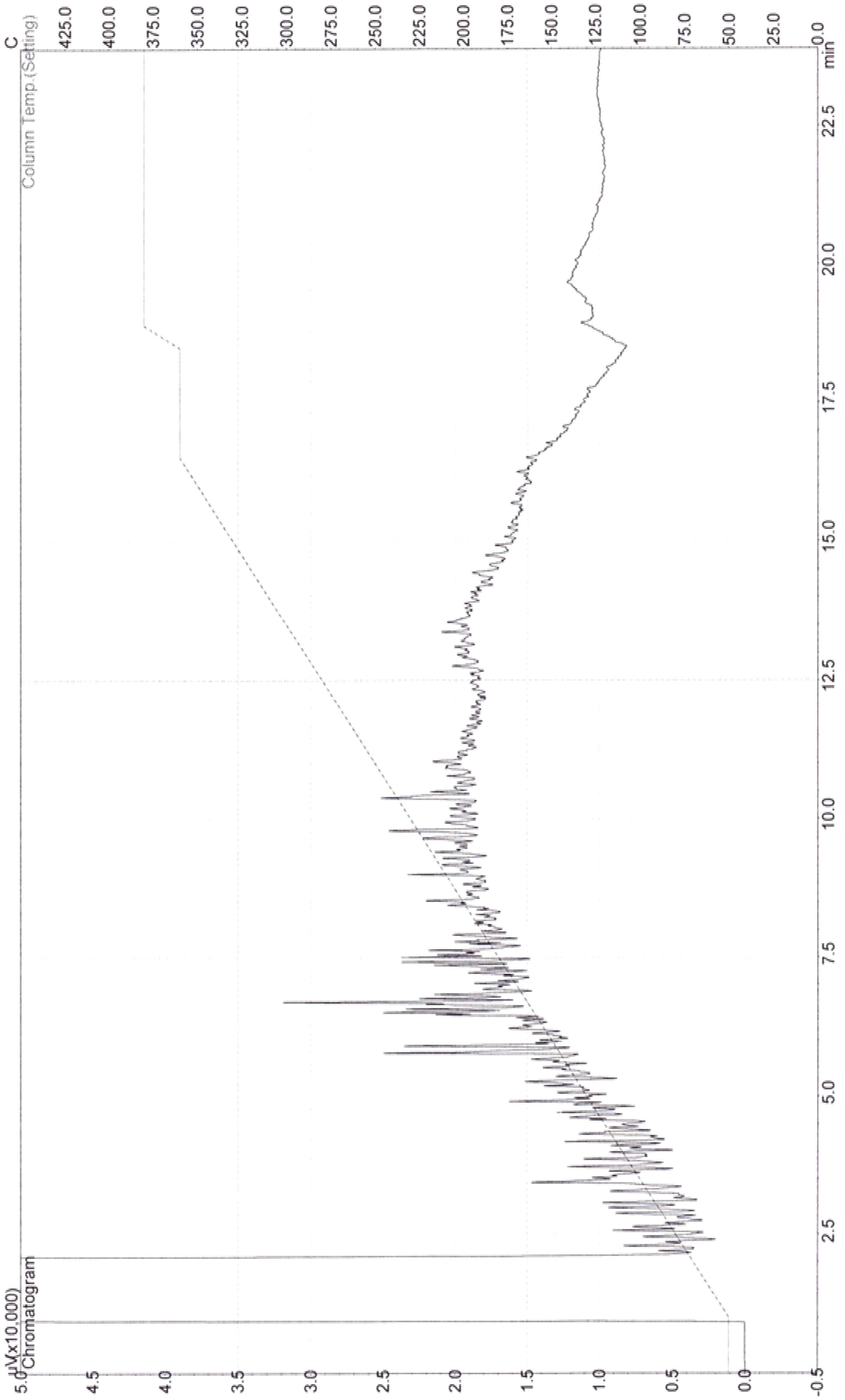

Figure A.5 Chromatogram of Gryphon – naphthene based crude oil from North Sea, Royal Dutch Shell plc

Table A.1 Parameters for measurement of ^{14}C-activity with Wallac 1409 β-scintillation counter

Parameter	adjustment
measurement time, s	300
precision	1
counting mode	decays per minute (dpm)
low count reject	no
number of labels	single
isotopes and library	C14, Wallac library
quench	SQPE
vial type	diffuse
cocktail	xylene

Table A.2 Parameters of GC-FID analysis

GC-type	Shimadzu 2010
detector	FID
auto-sampler	AOC 20i
injection technique	Splitless 1 min
injection temperature	350°C
injection volume	1.0 µl
column	SGE HT5
gas carrier	He
temperature program	50°C hold 1 min 25.3°C min^{-1} heating until 380°C 380°C hold for 10 min
detection limit	15 mg L^{-1}

Table A.3 Parameters of GC-MS analysis

GC type	Agilent Technologies 5975 C
MS type	Agilent Technologies 7890 A
auto-sampler	CTC Analysis auto-sampler
temperature program	50°C hold 1 min 25°C min^{-1} heating until 200°C 8 °C min^{-1} heating until 316°C 316°C hold 11,5 min
	Split/splittless
column type	HP-5MS 5 % Phenyl Methyl Silox
column length	30 m
column inner diameter	250 µm
film thickness	0,12µm
carrier gas	Helium
temperature transfer line to MS	280°C
temperature MS source	250°C
temperature MS quadropol	180°C
EM voltage	1059
EM voltage after 13.4 min	+94
EM voltage after 22 min	-94

Table A.4 **Properties of Siberian soils, equivalent soil materials and in-situ contaminated soil; the profiles from Siberia displayed the whole active layer thickness at time of sampling. Parameters were analyzed according to the methods given in Table 3.4. Densities marked with a star are taken from (Kutzbach, 2006)**

soil type ***WRB*** **Soil taxonomy**	**soil horizon**	**soil depth**	**texture according to soil tax**	**Munsell color**	**carbon content**	**pH**	**clay**	**silt**	**sand**	**bulk density**	**remarks**
unit		cm			%		$g\,g^{-1}$	$g\,g^{-1}$	$g\,g^{-1}$	$g\,cm^{-3}$	
Turbic Cryosol (reductaquic) Typic Aquiturbel	Oe	0…8	silt loam		19.36	6.2				1.53	
	Bbga A	8…26	silt loam		1.02	6.2	18.72	75.18	3.97	1.47	
	A Bgjj	26…55	silt loam		1.05	5.9	17.88	79.25	3.03	1.59	cryomethamorphic, relictic structures of soil ice
	Bgjj	55…79	loam		0.25	6.0	23.15	75.35	2.27		Field observation: higher density than horizon A Bgjj
Histic Cryosol (arenic, thixotropic) Typic Historthel	Oi	0…16	peat		48.45	4.3	14.29	40.46	45.29		
	Oe	16…21	Peat		48.67	4.1					
	Oa	21…28	Peat		41.83	3.5					
	Ah	28…33			0.62	4.5				1.76	thixotropy
	Bg 1	33…50	loam		0.24	4.5	23.6	49.1	27.3	1.80	hydromorphic
	Bg 2	50…70	loam								
U silt material			silt loam	10 YR6/4	1.36	4.8	10.84	79.73	9.43	1.51	density used in experimental setup, 24.78% base saturation
S sand material			sand		0.16	4.1	5.61	2.43	92.0	1.62…1.75	densities varied between experiments, 10.23% base saturation
P peat material			peat	10 YR2/1	53.1	3.0	n.d.	n.d.	n.d.	0.17	density used for experimental construction

soil type ***WRB*** **Soil taxonomy**	**soil horizon**	**soil depth**	**texture according to soil tax**	**Munsell color**	**carbon content**	**pH**	**clay**	**silt**	**sand**	**bulk density**	**remarks**
unit		cm			%		g g^{-1}	g g^{-1}	g g^{-1}	g cm^{-3}	
Soil profile 2009 *Turbic histic Cryosol* Typic Historthel	Oi1	0…3.5		10 YR5/3	14.8	4.8				0.1*	
		3.5…7.5			12.0	6.7					
	transition Oi1 to Oi2	7.5…9.0	sandy loam		8.4	7.0					
	Oi2	9.0…11.5		10 YR4/2	7.0	7.4				0.65*	
		11.5…14.0			5.1	6.5					
	Bgjj	14.0…16.5	loamy sand	10 YR 3/1	4.1	6.7	4.42	16.15	79.45		
		16.5…19.0	sandy loam		4.8	6.5	7.33	29.82	62.9		
		19.0…22.5	sandy loam		6.1	6.5	7.55	36.92	55.55		
		22.5…26.5	sandy loam		3.4	6.4	7.66	37.92	55.05		
		26.5…34.0			2.9	6.3					
		34.0…37.5			2.4	6.3					
Soil profile 2011 *Turbic, histic Cryosol* Typic Historthel	Oi1	0…4.0		10 YR5/3	17.2	7.4				0.1*	
		4.0…7.0			17.1	6.1					
		7.0…9.5			14.8	5.8					
		9.5…12.0			11.5	5.9					
	Oi2	12.0…14.0		10 YR4/2	13.2	5.6				0.65*	
		14.0…17.0			6.0	5.8					
	Bgjj	17.0…19.5		10 YR 3/1	5.8	5.9					
		19.5…22.0			3.8	5.8					
		22.0…25.5			6.1	6.1					
		25.5…29.0			4.5	5.8					

Table A.5 Properties of the three materials used in the experiments concerning their interaction with water

Parameter	silt loam	sand	peat
maximum water holding capacity in %	47.23	18.34	731.7
water content in experiments % (60% WHK_{max})	26.1…29.2	9.4…13.6	480.0
kf-value	$8.39\cdot 10^{-8}$	$7.9 \cdot 10^{-5}$	$9.98 \cdot 10^{-7}$

Table A.6 Analyses of water content and ^{14}C-activity of experiment *Ufba*

sample ID	n	contamination	freezing	sample thickness cm	column depth cm	water content % dw	standard error wc % dw	stud. T-test wc	^{14}C-activity dpm g^{-1} dw	std error ^{14}C-act. dpm g^{-1} dw	stud. T-test ^{14}C-act.
A 7	3	y	n	0.9	0.9	20.10	0.18	s.	21936.9	288.0	n.s.
A 6	6	y	n	0.9	1.8	19.46	0.10	s.	15291.8	845.3	s.
A 5	3	n	n	0.2	2.0	19.81	0.35	s.	515.1	69.7	n.s.
A 4	2	n	n	0.5	2.5	20.29	0.49	s.	115.6		
A 3	5	n	n	0.5	3.0	19.86	0.28	s.	77.3	28.2	
A 2	3	n	n	0.5	3.5	21.78	0.07	s.	112.3	5.4	
A 1	3	n	n	0.5	4.0	25.02	0.60	n.s.	132.5	4.5	
A 8	5	n	y	0.5	4.5	28.41	0.66	o.s.	141.1	57.4	
A 9	3	n	y	1.0	5.5	28.16	0.14	s.	95.1	5.7	
A 10	5	n	y	1.5	7.0	29.51	0.14	s.	143.6	60.4	
A 11	3	n	y	1.5	8.5	28.81	0.02	s.	102.1	3.8	
A 12	5	n	y	1.5	10.0	31.79	0.15	s.	64.8	22.1	
B 5	6	y	n	1.0	1.0	19.96	0.60	s.	21901.3	531.3	n.s.
B 4	6	y	n	1.0	2.0	19.44	0.17	s.	17655.7	953.9	s.
B 3	4	n	n	0.3	2.3	19.05	0.43	s.	3427.8*	74.8	s.
B 2	3	n	n	0.3	2.7	21.26	0.18	s.	1711.3	182.1	s.
B 1	5	n	n	0.5	3.2	21.81	0.51	s.	57.0	15.6	
B 6	4	n	y	0.5	3.9	24.41	0.30	s.	106.4*	49.8	
B 7	5	n	y	0.5	4.7	24.89	0.24	s.	47.1	13.6	
B 8	5	n	y	1.0	5.7	27.04	0.25	o.s.	74.3	34.1	
B 9	6	n	y	1.5	7.2	28.64	0.34	s.	310.9	35.5	
B 10	5	n	y	1.5	8.7	28.14	0.35	o.s.	157.2	81.3	

B 11	5	n	y	1.5	10.2	33.68	0.15	s.	147.2	62.0	
C 6	5	y	n	1.0	1.0	18.85	0.18	s.	18977.2*	251.4	s.
C 5	6	y	n	0.9	1.9	20.67	0.18	s.	15410.1	771.9	s.
C 4	5	n	n	0.6	2.5	20.89	0.39	s.	402.9	33.0	s.
C 3	6	n	n	0.5	3.1	21.02	0.51	s.	43.4	11.7	n.s.
C 1	5	n	n	0.5	3.6	23.34	0.12	s.	156.5*	76.6	
C 2	6	n	n	0.5	4.1	27.52	0.06	n.s.	33.9	6.9	
C 7	5	n	y	0.5	4.6	28.23	0.12	s.	135.3*	93.3	
C 8	5	n	y	1.0	5.6	28.69	0.24	s.	91.2	42.9	
C 9	5	n	y	1.5	7.1	27.96	0.52	n.s.	72.7	30.7	
C 10	5	n	y	1.5	8.6	28.55	0.26	s.	102.0	37.9	
C 11	3	n	y	1.5	10.1	28.98	0.28	s.	72.4	6.0	
ref 4	6	y	n	0.8	0.8	27.74	0.21	n.s.	22492.5	610.3	n.s.
ref 3	6	y	n	0.8	1.5	26.70	0.24	n.s.	20619.1	757.6	o.s.
ref 1	3	y	n	0.5	2.0	25.25	0.46	n.s.	5795.2	149.4	s.
ref 2	4	n	n	0.5	2.5	24.47	0.43	s.	147.8*	29.5	
ref 5	4	n	n	1.0	3.5	25.65	0.29	n.s.	113.2*	66.9	
ref 6	3	n	n	1.0	4.5	25.21	0.35	n.s.	115.0	5.8	
ref 7	5	n	n	1.0	5.5	24.89	0.09	s.	75.7	34.7	
ref 8	3	n	n	1.0	6.5	24.72	0.33	o.s.	105.5	5.7	
ref 9	5	n	n	1.0	7.7	24.48	0.16	s.	68.3	25.1	
ref 10	3	n	n	1.0	8.7	24.39	0.14	s.	82.4	2.7	
ref 11	3	n	n	1.5	10.2	24.41	0.17	s.	80.7	4.8	
cont start	27	y	n			26.23	0.46		22099.5	434.1	
un cont start	7	n	n			26.66	0.50		11.1	2.5	

Table A.7 Analyses of water content and ^{14}C-activity of experiment *Ufbp*

sample ID	**n**	**contamination**	**freezing**	**sample thickness** cm	**column depth** cm	**water content** % dw	**standard error wc** % dw	**stud. T-test wc**	**^{14}C-activity** dpm g^{-1} dw	**std error ^{14}C-act.** dpm g^{-1} dw	**stud. T-test ^{14}C-act.**
A 5	3	y	n	1.2	1.2	17.46	1.27	s.	24526.8	139.7	n.s.
A 4	3	y	n	0.5	1.7	16.03	0.16	s.	20479.5	166.0	s.
A 3	6	y	n	0.4	2.1	17.28	0.10	s.	8240.6	305.8	s.
A 2	6	n	n	0.7	2.8	19.04	0.13	s.	830.2	87.5	s.
A 1	3	n	n	0.6	3.4	22.10	0.37	s.	27.9	3.5	n.s.
A 6	3	n	y	0.5	3.9	32.90	0.39	s.	68.0	16.3	
A 7	3	n	y	0.4	4.3	31.40	0.25	s.	24.7	13.1	

A 8	3	n	y	1	5.3	30.59	0.47	s.	2.7	1.2	
A 9	3	n	y	1.5	6.8	29.97	0.31	s.	2.9	2.9	
A 10	3	n	y	1.5	8.3	29.22	0.35	s.	1.7	1.7	
A 11	3	n	y	2	10.3	28.79	0.21	s.	0.0	0.0	
B 5	3	y	n	0.7	0.8	17.11	0.08	s.	24321.3	204.1	n.s.
B 4	3	y	n	0.5	1.3	18.35	0.06	s.	24106.0	317.7	n.s.
B 3	6	y	n	0.5	1.8	19.25	0.12	s.	21808.0	360.8	s.
B 2	3	n	n	0.5	2.3	18.71	0.21	s.	3704.6	91.7	s.
B 1	3	n	n	0.6	2.9	20.46	0.16	s.	31.4	7.5	n.s.
B 6	3	n	y	0.5	3.4	22.53	0.37	s.	41.0	0.2	n.s.
B 7	3	n	y	0.5	4	26.89	0.14	n.s.	0.0	0.0	
B 8	3	n	y	1	5	30.85	0.25	s.	0.4	0.4	
B 9	3	n	y	1.5	6.5	30.31	0.65	s.	3.7	2.8	
B 10	3	n	y	1.7	8.2	29.89	0.27	s.	1.4	1.4	
B 11	3	n	y	2.1	10.3	30.31	0.29	s.	4.5	3.1	
C 5	6	y	n	0.9	1.2	16.25	0.10	s.	24361.4	95.6	n.s.
C 4	3	y	n	0.5	1.7	17.05	0.28	s.	24492.4	195.5	n.s.
C 3	3	y	n	0.5	2.2	16.92	0.66	s.	18153.6	322.7	s.
C 2	5	n	n	0.3	2.5	19.75	0.37	s.	3588.5	105.2	s.
C 1	3	n	n	0.3	2.8	24.81	0.10	s.	5.6	4.2	n.s.
C 6	3	n	y	0.5	3.3	24.71	0.18	s.	7.6	3.9	n.s.
C 7	3	n	y	0.5	3.8	21.71	0.04	s.	19.5	9.6	
C 8	3	n	y	1	4.8	26.14	0.35	n.s.	7.3	1.1	
C 9	3	n	y	1.5	6.3	29.53	0.22	s.	6.1	2.4	
C 10	3	n	y	1.8	8.1	29.08	0.24	s.	1.7	1.7	
C 11	3	n	y	2.2	10.3	29.76	0.10	s.	10.5	2.6	
ref 3	3	y	n	0.8	1.1	27.55	0.09	s.	23971.8	250.9	n.s.
ref 2	3	y	n	0.5	1.6	26.81	0.38	n.s.	24155.5	298.2	n.s.
ref 1	2	y	n	0.5	2.1	27.51	0.18	s.	21977.3		
ref 4	5	n	n	0.5	2.6	25.12	0.26	s.	3393.2*	47.4	o.s.
ref 5	3	n	n	0.5	3.1	24.22	0.25	s.	37.6	30.0	n.s.
ref 6	3	n	n	1	4.1	24.68	0.21	s.	27.6	20.0	
ref 7	3	n	n	1.2	5.3	24.74	0.40	s.	18.9	9.8	
ref 8	3	n	n	1.5	6.8	24.88	0.45	s.	12.0	6.2	
ref 9	3	n	n	1.5	8.3	24.33	0.25	s.	5.8	2.9	
ref 10	3	n	n	2	10.3	25.22	0.16	o.s.	6.0	3.1	
cont. start	12	y	n		10.3	26.19	0.21		24220.0	83.8	
uncont. start	12	n	n		10.3	26.11	0.20		10.5	2.7	

Table A.8 **Analyses of water content and ^{14}C-activity of experiment *Uftao***

sample ID	n	contamination	freezing	sample thickness cm	column depth cm	water content % dw	standard error wc % dw	stud. T-test wc	^{14}C-activity dpm g^{-1} dw	std error ^{14}C-act. dpm g^{-1} dw	stud. T-test ^{14}C-act.
A 11	3	y	y	1.1	0	48.85	0.32	s.	23507.3	300.0	n.s.
A 10	3	y	y	1	1.1	36.91	0.67	s.	22040.9	737.0	n.s.
A 9	3	y	y	0.5	2.1	37.62	0.22	s.	21699.7	1190.2	o.s.
A 8	3	y	y	0.5	2.6	34.85	0.77	s.	22786.6	516.4	n.s.
A 1	3	y	n	0.25	2.85	25.88	0.23	n.s.	22281.7	603.0	n.s.
A 2	3	y	n	0.5	3.1	21.87	0.22	s.	23241.4	155.1	n.s.
A 3	3	y	n	1	3.6	19.70	0.40	s.	22318.6	250.8	n.s.
A 4	3	y	n	0.5	4.6	20.33	0.12	s.	20344.0	148.6	s.
A 5	3	n	n	0.5	5.1	20.16	0.31	s.	5649.2	683.8	s.
A 6	3	n	n	1.5	5.6	20.81	0.24	s.	144.0	44.0	
A 7	3	n	n	3	7.1	19.98	0.21	s.	39.2	6.8	
B 8	3	y	y	0.6	0	36.95	0.68	s.	23387.2	198.3	n.s.
B 11	3	y	y	2.1	0.6	35.14	0.55	s.	24054.4	91.4	o.s.
B 10	3	y	y	0.5	2.7	35.70	0.66	s.	23622.2	172.7	n.s.
B 9	3	y	y	0.5	3.2	35.94	0.34	s.	23547.4	210.5	n.s.
B 1	3	y	n	0.4	3.7	24.72	0.70	s.	22814.3	114.6	n.s.
B 3	3	y	n	0.5	4.1	22.49	0.45	s.	22911.6	624.1	n.s.
B 4	3	y	n	1	4.6	19.21	1.16	s.	15934.9	120.8	s.
B 5	3	n	n	0.5	5.6	19.39	0.16	s.	333.7	42.9	s.
B 6	3	n	n	2	6.1	21.42	0.23	s.	68.0	2.9	
B 7	3	n	n	2	8.1	21.25	0.53	s.	63.8	11.5	
C 11	3	y	y	1	0	39.24	0.33	s.	23185.1	276.2	n.s.
C 10	3	y	y	1.3	1	37.82	0.08	s.	22281.8	670.1	n.s.
C 9	3	y	y	1.1	2.3	44.47	0.39	s.	22610.3	134.6	n.s.
C 1	5	y	n	0.5	3.4	23.78	0.18	s.	22923.8*	182.7	n.s.
C 2	6	y	n	0.5	3.9	20.30	0.48	s.	22190.7	561.3	n.s.
C 3		y	n	1	4.4	20.41	0.22	s.	19164.8	261.3	s.
C 5	3	y	n	1	5.4	20.17	0.28	n.s.	18440.3	209.5	s.
C 7	3	n	n	1.9	6.4	19.63	0.39	s.	22.7	1.4	n.s.
C 8	3	n	n	1.9	8.3	19.38	0.29	s.	71.7	4.3	
ref 1	3	y	n	1	0	24.99	1.35	s.	22519.7	180.4	n.s.
ref 2	3	y	n	1	1	25.54	0.35	o.s.	21256.9	1418.8	n.s.
ref 3	3	y	n	1	2	26.15	0.34	n.s.	21649.5	183.9	s.
ref 4	3	y	n	1	3	26.33	0.12	n.s.	19254.6	1140.6	s.
ref 6	3	y	n	1	4	25.10	0.45	s.	18193.5	383.6	s.
ref 8	3	y	n	1.5	5	27.17	0.44	s.	11420.3	465.7	s.
ref 9	3	n	n	2	6.5	26.23	0.01	n.s.	46.3	1.6	n.s.
ref 10	3	n	n	2	8.5	25.00	0.05	o.s.	29.8	4.0	
cont start	24					26.89	0.23		23002.3	204.1	

un cont start	18					26.27	0.28		72.2	3.4	

Table A.9 **Analyses of water content and ^{14}C-activity of experiment *Sftao***

sample ID	n	contamination	freezing	sample thickness cm	column depth cm	water content % dw	standard error wc % dw	stud. T-test wc	^{14}C-activity dpm g^{-1} dw	std error ^{14}C-act. dpm g^{-1} dw	stud.T-test ^{14}C-act.
A 9	3	y	y	2	2	18.01	0.32	s.	7522.7	12.8	n.s.
A 8	3	y	y	1	3	20.65	1.47	s.	7196.4	124.7	s.
A 7	3	y	y	0.5	3.5	22.74	0.20	s.	6659.2	56.8	s.
A 6	3	y	y	0.5	4	15.41	7.72	s.	6038.2	100.8	s.
A 1	3	y	n	0.8	4.8	5.90	0.06	s.	7033.8	95.9	s.
A 2	3	n	n	0.5	5.3	1.43	0.06	s.	105.2	8.1	s.
A 3	3	n	n	1	6.3	1.72	0.12	s.	47.4	7.8	
A 4	3	n	n	1.9	8.2	2.33	0.03	s.	21.3	6.2	
A 5	3	n	n	1.8	10	1.29	0.02	s.	38.5	12.0	
B 9	3	y	y	1.9	1.9	15.12	0.05	s.	8130.7	266.6	s.
B 8	3	y	y	1	2.9	22.26	0.61	s.	7196.6	34.5	s.
B 7	3	y	y	0.5	3.4	21.06	0.35	s.	6898.8	125.9	s.
B 6	3	y	y	0.5	3.9	23.90	0.71	s.	6475.4	36.3	s.
B 1	3	y	n	0.7	4.6	4.39	0.38	s.	7207.6	117.0	s.
B 2	3	n	n	0.5	5.1	3.24	0.27	s.	92.2	8.8	s.
B 3	3	n	n	1	6.1	1.88	0.24	s.	24.3	2.0	
B 4	3	n	n	2	8.1	2.68	0.16	s.	11.6	1.3	
B 5	3	n	n	1.9	10	1.72	0.21	s.	11.0	5.7	
C 9	3	y	y	1.8	1.8	16.46	0.15	s.	7551.1	14.5	n.s.
C 8	3	y	y	1.4	3.2	18.80	0.63	s.	7516.7	95.8	n.s.
C 7	3	y	y	0.5	3.7	21.97	0.39	s.	7094.6	71.9	s.
C 6	3	y	y	0.5	4.2	28.20	0.08	s.	7115.7	94.8	s.
C 2	3	y	n	0.3	4.5	4.16	2.08	s.	8075.8	118.2	s.
C 1	3	y	n	0.5	5	3.05	1.53	s.	7350.4	121.3	s.
C 3	3	n	n	0.5	5.5	2.49	0.07	s.	90.7	2.1	s.
C 4	3	n	n	1	6.5	2.29	0.30	s.	38.0	3.5	
C 5	2	n	n	3.7	10.2	1.52	0.11	s.	16.3*		
ref 8	3	y	n	2	2	11.18	0.42	s.	7713.0	61.1	n.s.
ref 7	3	y	n	1.5	3.5	8.86	0.25	n.s.	7279.9	75.6	s.
ref 6	3	y	n	1	4.5	13.31	0.24	s.	7312.9	38.2	s.
ref 5	3	y	n	0.5	5	10.00	0.21	s.	4969.0	206.9	s.
ref 4	3	n	n	0.5	5.5	9.93	0.12	n.s.	92.6	6.1	s.
ref 3	3	n	n	1	6.5	8.84	0.23	n.s.	32.6	3.6	
ref 2	3	n	n	1.5	8	10.25	0.08	s.	10.3	2.8	

ref 1	3	n	n	2	10	11.15	0.18	s.	12.1	3.2	
cont start	18	y	n			9.46	0.16		7714.2	56.8	
wc start	15	n	n			9.38	0.15		6.6	1.6	

Table A.10 **Analyses of water content and ^{14}C-activity of experiment *Uftpo***

sample ID	n	contamination	freezing	sample thickness cm	column depth cm	water content % dw	standard error wc % dw	stud. T-test wc	^{14}C-activity dpm g^{-1} dw	std error ^{14}C-act. dpm g^{-1} dw	stud. T-test ^{14}C-act.
A 12	3	y	y	1.1	10.2	48.30	0.33	s.	11372.4	14.77	s.
A 11	2	y	y	0.9	9.1	35.57	0.10	s.	11455.8	81.85	n.s.
A 10	3	y	y	0.7	8.2	34.51	0.75	s.	11418.2	96.07	n.s.
A 9	3	y	y	0.3	7.5	33.19	0.70	o.s.	11524.4	65.70	o.s.
A 2	3	y	n	0.3	7.2	25.56	0.85	n.s.	11582.3	35.01	s.
A 3	3	y	n	0.6	6.9	24.35	0.33	s.	11660.3	90.67	n.s.
A 4	3	y	n	1.1	6.3	22.62	0.51	s.	11347.3	65.91	s.
A 5	3	n	n	0.3	5.2	24.93	0.07	n.s.	10118.6	162.71	s.
A 6	6	n	n	1	4.9	23.15	0.71	s.	1701.3	165.82	s.
A 7	3	n	n	1.9	3.9	26.82	0.35	n.s.	1.6	0.37	
A 8	3	n	n	2	2	27.85	0.75	n.s.	0.5	0.36	
B 11	3	y	y	1.3	1.3	47.43	0.39	s.	11858.8	55.83	n.s.
B 10	3	y	y	0.8	2.1	37.28	0.40	s.	11354.5	72.37	o.s.
B 9	3	y	y	0.7	2.8	34.93	0.17	s.	11180.3	43.27	s.
B 8	3	y	y	0.3	3.1	41.22			11334.1	59.07	s.
B 1	3	y	n	0.5	3.6	25.93	0.50	n.s.	11534.2	35.04	s.
B 2	3	y	n	0.5	4.1	25.83	0.18	n.s.	11542.9	19.12	s.
B 3	3	y	n	1.3	5.4	24.79	0.33	o.s.	11291.5	25.43	s.
B 4	3	n	n	0.3	5.7	23.15	0.11	s.	4686.0	365.95	s.
B 5	6	n	n	1	6.7	20.83	0.30	s.	134.5	26.89	s.
B 6	3	n	n	1.5	8.2	24.03	0.37	s.	1.9	0.38	
B 7	3	n	n	1.8	10	22.62	0.18	s.	0.0		
C 11	3	y	y	1	10.1	40.73	0.23	s.	11886.2	79.69	n.s.
C 10	2	y	y	1	9.1	36.45	0.10	s.	11467.9*	143.82	n.s.
C 9	3	y	y	0.7	8.1	33.34	0.32	o.s.	11212.4	127.87	s.
C 1	3	y	y	0.4	7.4	37.82	0.25	s.	11672.1	50.46	n.s.
C 2	3	y	n	0.3	7	28.30	0.36	n.s.	11559.3	112.87	n.s.
C 3	3	y	n	0.5	6.7	26.06			11705.3	48.25	n.s.
C 4	3	y	n	1	6.2	23.82	0.22	s.	11158.0	61.27	s.
C 5	3	n	n	0.3	5.2	21.70	0.08	s.	7507.4	163.44	n.s.
C 6	6	n	n	1	4.9	22.06	0.54	s.	706.9	67.18	s.
C 7	3	n	n	1.9	3.9	27.11	0.44	n.s.	22.9	7.98	
C 8	3	n	n	2	2	28.29	0.72	n.s.	1.5	1.29	

ref 9	3	y	n	1.7	10	28.14	0.32	n.s.	11355.8	41.97	s.
ref 8	3	y	n	1	8.3	28.18	0.23	n.s.	11826.8	68.57	n.s.
ref 7	3	y	n	1	7.3	27.02	0.56	n.s.	11787.7	87.71	n.s.
ref 6	3	y	n	0.5	6.3	27.35	0.42	n.s.	11491.4	35.36	s.
ref 5	3	y	n	0.3	5.8	28.82	1.15	n.s.	11183.2	92.03	s.
ref 4	6	n	n	0.5	5.5	27.40	0.16	n.s.	6142.6	380.34	s.
ref 3	3	n	n	1	5	27.06	0.78	n.s.	61.0	18.95	s.
ref 2	3	n	n	2	4	27.08	0.92	n.s.	0.7	0.70	
ref 1	3	n	n	2	2	29.92	0.46	n.s.	0.0	0.00	
cont start	18	y	n			29.14	0.84		11743.3	81.1	
wc start	12	n	n			29.25	1.08		12.5	4.5	

Table A.11 Analyses of water content and Σ 16 EPA PAHs of experiment *Sftabo*

	sample ID	lower boundary	upper boundary	water content	anthracene	std error Ant	benzo[a] pyrene	std error Bap
material after contamination				12.18	152.97	2.06	7.24	0.10
material after preincubation				13.60	166.18	2.91	6.37	0.27
sand	A 13	5	0	12.91	153.69	5.51	6.52	0.27
	A 14	10	5	12.50	144.58	3.80	6.03	0.72
	A 15	15	10	12.16	143.78	2.76	6.05	0.46
	A 16	20	15	12.20	151.11	1.63	5.92	0.51
	A 17	25	20	12.15	161.82	11.69	7.62	0.74
	A 18	30	25	13.70	149.62	6.53	4.97	0.23
	A 19	35	30	14.85	151.87	4.67	6.95	0.44
	A 20	40	35	12.87	153.81	1.49	8.39	0.63
sand	B 21	5	0	12.41	140.04	3.26	6.17	0.56
	B 22	10	5	11.90	148.59	1.67	7.78	0.74
	B 23	15	10	11.98	141.43	4.18	6.60	0.34
	B 24	20	15	12.22	146.63	2.16	8.05	0.52
	B 25	25	20	11.93	142.20	1.88	7.57	0.52
	B 26	30	25	13.46	143.67	2.44	8.92	0.25
	B 27	35	30	13.21	131.17	12.51	6.55	0.74
	B 28	40	35	13.29	147.83	2.10	8.50	0.53
sand	C 29	5	0	13.02	136.75	1.44	7.86	0.48
	C 30	10	5	13.66	146.66	0.62	7.93	0.37
	C 31	15	10	13.11	128.40	7.21	5.71	0.25
	C 32	20	15	13.84	112.13	6.09	4.79	0.82
	C 33	25	20	13.41	146.13	0.63	5.43	0.32
	C 34	30	25	13.79	136.10	5.19	5.10	0.34
	C 35	35	30	14.29	140.72	7.03	6.28	0.48
	C 36	40	35	14.36	127.79	7.18	4.90	0.76

Table A.12 Analyses of water content and Σ 16 EPA PAHs of experiment *Pftabo*

	sample ID	lower boundary	upper boundary	water content	anthracene	std error Ant	benzo[a] pyrene	std error Bap
material after contamination					32.59	7.21	0.37	0.08
material after preincubation					45.84	6.15	0.49	0.11
peat	A 13	5	0		37.61	2.22	0.15	0.02
	A 14	10	5		37.02	1.87	0.20	0.05
	A 15	15	10		38.17	1.44	0.29	0.05
	A 16	20	15		11.38	0.63	0.10	0.01
	A 17	25	20		14.88	1.82	0.16	0.04
	A 18	30	25		12.50	0.41	0.14	0.02
	A 19	35	30		8.47	0.53	0.14	0.01
	A 20	40	35		9.99	0.37	0.14	0.02
peat	B 21	5	0		11.41	0.65	0.13	0.03
	B 22	10	5		58.05	1.49	0.65	0.11
	B 23	15	10		66.80	5.58	0.78	0.07
	B 24	20	15		77.44	6.24	0.93	0.11
	B 25	25	20		17.46	2.39	0.14	0.03
	B 26	30	25		22.64	0.67	0.17	0.02
	B 27	35	30		22.93	0.28	0.17	0.02
	B 28	40	35		20.20	1.78	0.10	0.02
peat	ref 29	5	0		33.99	5.98	0.16	0.05
	ref 30	10	5		37.26	2.28	0.14	0.02
	ref 31	15	10		11.59	0.67	0.10	0.02
	ref 32	20	15		12.12	0.70	0.06	0.01
	ref 33	25	20		13.24	0.09	0.11	0.02
	ref 34	30	25		9.72	0.55	0.08	0.01
	ref 35	35	30		11.50	0.34	0.09	0.02
	ref 36	40	35		13.46	0.89	0.08	0.02

Table A.13 Sequential extraction yields for all four extraction steps in dpm g^{-1} dw, total extraction yields and determined, non-extractable residues for experiments *Ufba*, *Ufbp, Uftao, Uftpo* and *Sftao*. For experiments *Ufba*, *Uftao* and *Sftao* only Ex2 to Ex4 were extracted sequentially, water extraction was conducted on different samples. n.a. = not analyzed, n.d. = not determined

name	sample ID	n	cont	freeze	Ex 1 water	Ex 1 standard error	Ex 2 methanol-water	Ex 2 standard error	Ex3 ethyl acetate first	Ex 3 standard error	Ex 4 ethyl acetate second	E x4 standard error	total extraction yield	total Ex standard error	neR
					dpm g^{-1} dw										
Ufba	A 7	3	y	n	n.a.		9096.8	112.9	12349.2	194.4	757.0	54.0	22202.9	61.5	n.d.
	A 6	3	y	n	n.a.		6560.5	205.0	8991.0	247.9	617.0	122.9	16168.5	323.5	n.d.
	A 5	3	n	n	n.a.		157.6	10.5	136.9	17.9	18.7	6.6	313.2	23.7	201.9
	B 5	3	y	n	263.1	5.1	6688.4	583.8	13956.6	452.3	727.6	286.3	21372.6	394.3	528.7
	B 4	3	y	n	239.1	9.2	6897.0	440.2	11277.2	139.6	130.0	64.9	18304.1	470.7	n.d.
	B 3	2	n	n	n.a.		1885.0		2849.8		0.0		4734.8		n.d.
	B 2	3	n	n	23.9	2.8	137.1	15.5	196.4	15.9	14.7	7.3	348.2	22.3	1363.2
	C 6	3	y	n	n.a.		8584.2	307.4	11618.1	489.0	1374.9	83.1	21577.2	356.1	n.d.
	C 5	3	y	n	n.a.		7096.6	203.6	9402.1	137.5	712.0	17.1	17210.7	336.2	n.d.
	C 4	3	n	n	n.a.		158.3	12.2	157.9	26.7	6.4	5.9	322.6	36.8	80.3
	ref 4	3	y	n	n.a.		8498.9	71.1	12618.5	129.8	1166.4	19.2	22283.8	179.1	208.6
	ref 3	3	y	n	n.a.		8253.8	92.4	11115.6	265.1	1163.2	81.1	20532.5	120.4	86.6
	ref 1	3	y	n	81.5	5.2	2228.6	64.0	2865.4	97.8	209.3	13.0	5303.2	144.2	491.9
	ref 2	3	n	n	5.2	0.9	20.8	3.2	8.8	3.9	0.0	1.3	29.6	2.9	118.2
	material	6	y	n	n.a.		8554.3	44.5	12286.1	23.4	1082.3	12.4	21922.7	12.3	176.9
Ufbp	A 5	3	y	n	61.1	13.0	3921.2	59.7	18494.7	704.5	607.6	806.9	23084.6	372.1	1454.0
	A 4	3	y	n	44.0	4.2	4391.2	57.2	16857.4	213.1	694.5	107.2	21987.1	241.2	2027.3
	A 3	1	y	n	22.5	0.0	1456.4	0.0	6204.9	0.0	1274.6	0.0	8958.4	0.0	n.d.
	A 2	3	n	n	11.0	5.5	144.2	9.0	476.3	23.9	78.5	2.1	709.9	28.3	67.4
	B 5	2	y	n	49.1	4.2	3651.0	304.7	16013.7	3417.3	3287.4	0.0	23001.1		1340.6
	B 4	3	y	n	54.0	4.9	5829.7	33.8	17354.1	145.1	716.1	244.7	23899.8	166.8	245.0
	B 3	3	y	n	62.3	2.4	4892.5	10.7	15258.5	4.6	980.7	60.1	21131.8	53.3	571.6

	B 2	3	n	n	23.8	2.8	673.8	53.7	2463.4	267.2	203.3	56.1	3340.4	365.3	384.2
	C 5	3	y	n	56.1	3.1	6134.6	0.0	16798.5	0.0	873.7	0.0	23806.9	0.0	740.4
	C 4	3	y	n	61.1	5.7	5959.8	98.8	16091.4	105.9	1427.3	62.9	23478.6	165.1	1013.8
	C 3	3	y	n	40.8		4181.3	63.2	12021.6	231.3	1017.0	72.9	17219.9	219.0	933.8
	C 2	3	n	n	18.6		789.0	6.6	2244.1	65.3	392.9	100.2	3426.0	39.7	18.2
	ref 3	3	n	n	77.9	4.5	4932.6	291.0	17107.7	539.8	1364.0	668.3	23482.2	843.9	532.2
	ref 2	3	n	n	67.2	6.9	5170.6	181.4	16359.9	682.2	1737.8	64.8	23335.5	540.9	861.6
	ref 1	3	n	n	71.0	1.7	4568.1	151.6	15033.2	191.5	2118.1	533.3	21790.4	217.9	133.4
	ref 4	3	n	n	16.1	2.6	788.7	46.7	2611.1	175.1	335.1	32.1	3751.0	249.7	n.d.
	mean	5	y	n	63.8	6.1	4374.5	339.0	16824.4	268.9	1802.0	73.9	23064.8	191.2	1155.2
Uftao	A 11	3	y	y	501.4	20.9	3370.9	75.3	15394.1	262.0	3470.0	130.5	22235.0	314.9	1272.2
	A 10	3	y	y	956.2	52.9	4759.7	125.2	15498.1	45.4	2240.0	46.1	22497.8	85.2	n.d.
	A 9	1	y	y	n.a.		5624.5		15526.1		1613.0		22763.6		n.d.
	A 1	3	y	n	1028.4	32.4	6244.8	106.7	14938.7	139.6	1007.5	182.6	22191.0	310.2	90.6
	A 2	5	y	n	562.6	0.6	5271.3	105.8	16112.5	302.5	925.3	171.1	22309.1	276.1	932.3
	A 3	3	y	n	n.a.		5219.4	131.5	15317.5	699.9	966.1	554.4	21503.0	285.7	815.7
	A 4	4	y	n	394.1	2.4	4934.0	68.9	14949.1	125.9	458.3	4.5	20341.5	168.6	2.5
	A 5	3	n	n	n.a.		2115.9	0.0	3780.3	0.0	138.7	28.9	6034.9	289.8	n.d.
	A 7	3	n	n	n.a.		58.8	20.5	79.8	86.8	-15.6	14.0	123.0	92.1	0.0
	B 8	5	y	y	654.6	39.6	4762.6	79.6	15942.2	227.4	1869.2	189.7	22574.0	198.2	813.2
	B 11	3	y	y	1126.5	17.8	4811.2	185.3	15574.5	37.7	2028.5	190.3	22414.2	35.9	1640.2
	B 10	3	y	y	851.4	0.0	5141.3	166.9	15151.2	114.4	1512.8	117.2	21805.3	234.0	1816.8
	B 9	1	y	y	n.a.		1454.4		5029.0		539.2		7022.6		16524.8
	B 1	2	y	n	533.2		5909.0		15350.1		513.6		21772.7		1041.6
	B 3	3	y	n	435.7	21.8	5705.2	20.9	15048.5	182.3	24.1	157.4	20777.8	75.7	2133.7
	C 11	3	y	y	739.9	26.8	4320.0	48.6	14960.3	398.0	2541.3	63.7	21821.6	377.8	1363.5
	C 10	3	y	y	1003.4	62.5	4359.6	33.6	15741.3	55.3	2268.6	46.3	22369.5	87.8	0.0
	C 9	3	y	y	1101.6	50.8	3739.2	29.8	15951.5	584.0	1992.0	799.1	21682.7	458.0	927.6
	C 1	4	y	n	901.0	47.0	4975.4	125.0	15789.9	141.5	1415.7	157.6	22181.0	265.4	742.8
	C 2	3	y	n	449.4	27.5	4840.6	37.6	17082.0	308.5	831.6	500.2	22754.1	262.0	n.d.

	C 3	3	y	n	367.2	7.6	4744.6	41.4	13828.9	302.6	413.0	138.8	18986.5	161.3	178.3
	C 5	3	n	n	n.a.		3114.0	26.5	6967.9	87.0	199.1	76.2	10281.0	120.4	8159.3
	ref 1	3	y	n	1282.9	49.8	4998.6	71.0	15507.9	560.9	912.5	37.6	21419.1	539.8	1100.7
	ref 2	3	y	n	1000.5	28.3	5197.1	161.7	15167.9	61.1	1004.4	288.1	21369.3	404.3	n.d.
	ref 3	3	y	n	940.9	55.6	4792.9	136.6	15463.8	832.1	386.2	277.0	20642.9	446.1	1006.6
	ref 4	3	y	n	975.5	46.1	5018.2	101.7	13696.8	257.4	932.3	81.2	19647.3	433.9	n.d.
	ref 6	3	n	n	730.6	112.9	4361.6	35.8	11796.8	235.5	938.2	127.3	17096.6	138.4	1096.9
	ref 8	3	n	n	n.a.		3363.8	188.9	7634.7	465.2	544.2	60.4	11542.6	702.3	n.d.
	material	3	y	n	n.a.		5872.5	914.6	15484.9	776.6	1410.5	669.0	22767.9	441.1	234.4
Uftpo	A 12	3	y	y	263.0	62.0	1418.5	93.4	7737.9	141.4	1626.3	71.4	11045.6	89.6	334.9
	A 11	3	y	y	966.6	65.3	1195.8	38.5	7466.6	152.5	1261.3	44.1	10890.2	86.0	565.6
	A 10	3	y	y	910.2	65.7	1214.1	25.5	7766.3	100.4	1208.0	55.3	11098.6	25.1	373.3
	A 9	3	y	y	1234.2	56.5	1310.8	28.4	7581.9	49.6	895.9	34.9	11022.9	77.4	474.8
	A 2	3	y	n	544.7	157.5	1310.0	30.3	8891.2	371.3	361.4	247.0	11107.4	274.6	503.3
	A 3	3	y	n	505.0	46.3	1391.5	51.3	9228.9	174.0	553.0	152.3	11678.4	49.6	8.8
	A 4	3	y	n	626.2	108.7	1277.9	128.3	8867.8	176.6	858.9	119.9	11630.8	249.2	n.d.
	B 11	3	y	y	219.2	50.5	1397.7	37.1	7818.3	240.9	1647.9	128.1	11083.1	124.6	775.7
	B 10	3	y	y	979.5	42.3	1467.4	32.3	7551.5	39.4	1390.5	31.4	11388.9	36.1	n.d.
	B 9	3	y	y	877.5	78.0	1366.8	9.9	7716.8	218.5	1355.4	106.3	11316.5	92.3	0.0
	B 8	1	y	y	509.7	0.0	1341.3	0.0	7632.6	0.0	1766.0	0.0	11249.6	11250.6	37.3
	B 1	3	y	n	407.8	34.1	1541.3	35.8	8468.8	256.2	883.9	78.0	11301.8	255.4	249.8
	B 2	3	y	n	455.9	114.2	1430.1	76.5	9148.0	103.5	806.6	31.1	11840.6	66.6	n.d.
	B 3	3	y	n	156.5	62.6	1403.0	21.3	8825.4	56.8	634.7	51.3	11019.5	75.2	287.7
	C 11	3	y	y	801.8	95.1	1472.7	30.0	7612.9	73.4	1204.2	29.4	11091.6	43.1	794.6
	C 10	3	y	y	426.8	32.5	1611.0	46.4	7682.0	26.5	1506.3	89.2	11226.1	77.8	241.9
	C 9	3	y	y	601.8	61.8	1456.8	27.9	7846.7	155.6	1316.7	104.2	11222.1	100.2	0.0
	C 1	3	y	y	718.8	26.5	1551.5	9.4	7614.4	145.7	1416.6	59.7	11301.3	100.6	408.4
	C 2	3	y	n	550.4	30.6	1608.5	63.9	8076.9	17.3	996.8	52.5	11232.6	79.2	411.7
	C 3	3	y	n	331.2	60.5	1604.4	35.4	8940.0	98.3	773.2	135.1	11648.8	114.2	38.5
	C 4	3	y	n	73.6	7.2	1347.6	33.0	8527.0	218.1	795.8	116.1	10743.9	81.1	414.1

	ref 9	3	y	n	1160.5	151.8	1523.6	13.5	7698.9	313.9	463.0	30.2	10846.0	244.1	509.8
	ref 8	3	y	n	797.9	100.3	1602.2	63.5	7429.4	180.3	1153.0	97.8	10982.5	134.6	844.3
	ref 7	3	y	n	926.5	210.4	1471.5	73.4	7915.5	221.3	1029.5	32.6	11343.0	123.6	388.0
	ref 6	3	y	n	1536.8	65.9	909.0	64.9	7377.8	95.5	1187.8	187.6	11011.4	311.0	480.1
	ref 5	3	y	n	233.1	99.3	1459.8	69.0	7706.5	52.1	916.6	95.0	10316.1	36.9	856.9
	ref 4	3	n	n	126.5	13.2	1024.6	9.9	4357.4	44.0	602.2	20.0	6110.7	44.6	n.d.
	material	6	y	n	1062.9	122.0	1423.3	46.7	7987.1	157.4	1204.2	125.4	11677.5	83.7	65.8
Sftao	A 9	3	y	y	280.4	9.5	1739.0	22.5	4890.8	63.2	322.1	20.1	7232.3		
	A 8	3	y	y	283.6	8.7	1734.6	67.3	4938.7	68.6	223.7	53.0	7180.5	140.2	15.9
	A 7	3	y	y	234.5	9.9	1736.5	25.6	3979.0	81.6	435.3	19.2	6385.4	54.4	273.8
	A 6	3	y	y	n.a.		1667.8	32.4	3969.0	199.1	468.7	33.3	6105.5	252.6	0.0
	A 1	3	y	n	n.a.		2424.9	128.6	4088.2	140.0	56.9	16.5	6570.0	24.5	463.8
	B 9	3	y	y	274.8	6.9	1912.3	38.4	5350.6	25.1	196.6	41.5	7734.3	77.3	270.3
	B 8	3	y	y	287.4	3.5	1393.8	66.7	4470.5	44.7	539.3	25.3	6691.0	55.5	505.6
	B 7	3	y	y	201.1	5.1	1747.9	73.1	4063.5	62.2	419.5	9.5	6432.0	67.2	466.8
	B 6	3	y	y	148.0	0.0	1596.7	92.0	3629.1	87.1	421.9	55.1	5795.6	82.5	679.7
	B 1	3	y	n	130.9	6.0	2683.6	49.6	4016.6	23.9	47.5	51.8	6878.6	28.5	329.0
	C 9	3	y	y	232.9	6.3	1792.6	37.6	4989.1	65.3	325.2	29.0	7339.8	75.3	211.3
	C 8	3	y	y	270.4	9.2	1709.3	54.9	4576.4	63.8	415.0	1.9	6971.1	108.9	545.6
	C 7	3	y	y	235.6	0.0	1757.7	15.2	4486.3	122.3	433.6	11.1	6913.2	120.4	273.5
	C 6	3	y	y	151.8	11.3	1480.4	22.2	4319.1	141.7	612.9	38.5	6564.2	160.1	551.6
	C 2	2	y	n	86.8	0.0	2547.7		5082.9		133.8		7851.3		224.5
	C 1	2	y	n	79.1	0.0	2445.2		4581.2		31.9		7137.4		213.0
	ref 8	3	y	n	252.3	8.4	2281.6	27.5	4884.1	19.5	169.8	30.9	7587.8	69.0	125.1
	ref 7	3	y	n	238.6	5.1	2060.6	56.3	4576.3	55.7	152.1	24.9	7027.6	18.4	252.3
	ref 6	3	y	n	n.a.		2465.0	79.7	4412.4	132.8	132.0	49.0	7009.4	96.9	303.5
	ref 5	3	y	n	n.a.		1892.8	42.9	2335.6	41.7	72.7	38.1	4301.0	45.9	667.9
	material	6	y	n	237.9	9.5	2212.2	27.8	4582.0	40.3	138.9	20.1	7170.9	34.8	543.4

Table A.14 GC-MS analysis of 16 single PAHs of the contaminated soil cores taken in Northern Siberia in 2009

soil depth cm	0 - 3.5		3.5 - 7.5		7.5 - 9.0		9.0 - 11.5		11.5 - 14.0		14.0 - 16.5		16.5 - 19.0		19.0 - 22.5		22.5 - 26.5		30.0 - 34.0	
PAH	µg kg^{-1} dw																			
Nap	97,9	18,1	163,2	3,6	233,0	1,2	206,3	6,3	500,1	12,8	708,9	27,5	1980,0	31,9	516,4	10,4	23,4	0,3	20,8	0,3
Any	n.d.		n.d.		n.d.		n.d.		426,8	1,5	189,2	4,6	806,8	36,4	273,4	30,6	n.d.		n.d.	
Ace	n.d.		n.d.		n.d.		n.d.		562,2	97,0	324,0	17,8	1179,9	46,9	249,4	8,9	1,2	1,2	n.d.	
Fln	n.d.		n.d.		n.d.		495,8	3,1	1054,4	46,9	679,1	10,6	2196,2	105,0	738,5	80,6	4,8	0,1	7,3	0,5
Phe	n.d.		n.d.		n.d.		992,3	95,0	2159,6	8,5	1060,9	77,4	3304,9	150,3	1214,0	103,6	15,0	0,1	24,7	0,5
Ant	n.d.		n.d.		n.d.		n.d.		n.d.		n.d.		n.d.		n.d.	0,0	n.d.		n.d.	
Fth	750,9	4,4	426,9	43,1	209,7	17,7	129,6	0,0	66,0	2,5	15,5	0,1	51,8	3,2	18,0	1,7	5,3	0,4	7,6	0,1
Pyr	1503,9	147,4	834,2	2,6	362,5	0,7	177,2	1,2	71,5	2,9	20,3	1,6	68,1	2,1	25,4	0,7	5,9	0,7	8,7	0,6
Baa	249,6	39,2	52,9	2,9	27,8	0,1	16,5	2,3	8,3	0,7	8,4	3,9	7,6	0,9	5,9	2,9	5,2	0,0	4,3	0,2
Chr	101,4	5,4	62,1	3,0	43,5	0,4	24,7	2,3	12,6	0,2	7,6	1,2	10,8	0,7	5,6	0,3	5,8	1,4	2,3	2,3
Bbf	26,3	4,0	13,3	0,5	n.d.		5,9	5,9	n.d.		n.d.		n.d.		n.d.		n.d.		n.d.	
Bkf	10,8	0,5	7,7	0,0	n.d.		3,0	3,0	n.d.		n.d.		n.d.		n.d.		n.d.		n.d.	
Bap	14,8	4,6	n.d.		n.d.		n.d.		n.d.		n.d.		n.d.		n.d.		n.d.		n.d.	
Ind	28,7	10,4	n.d.		n.d.		n.d.		n.d.		n.d.		n.d.		n.d.		n.d.		n.d.	
Dah	25,5	8,7	n.d.		n.d.		n.d.		n.d.		n.d.		n.d.		n.d.		n.d.		n.d.	
Ghi	16,4	5,9	n.d.		n.d.		n.d.		n.d.		n.d.		n.d.		n.d.		n.d.		n.d.	
sum	2826,2	229,0	1560,2	50,5	876,6	20,0	2051,4	92,0	4861,7	115,1	3013,8	125,3	9606,0	311,8	3046,6	221,9	66,5	3,8	75,7	1,7

Table A.15 **GC-MS analysis of 16 single PAHs of the contaminated soil cores taken in Northern Siberia in 2011**

soil depth cm	0 - 4.0		34.0 - 7.0		7.0 - 9.5		9.5 - 12.0		12.0 - 14.0		17.0 - 19.5		19.5 - 22.0		25.5 - 29.0	
PAH	µg kg^{-1} dw															
Nap	41,5	1,7	93,5	4,3	713,3	97,3	933,6	24,5	1318,5	34,2	1026,7	50,0	702,2	7,0	24,5	5,1
Any	n.d.		n.d.		1351,5	316,9	390,9	90,0	131,0	4,3	n.d.		n.d.		n.d.	
Ace	n.d.		n.d.		2934,1	1121,5	1097,5	289,8	281,7	16,2	n.d.		n.d.		n.d.	
Fln	n.d.		2796,7	540,7	7014,4	1930,6	2610,7	406,1	755,4	43,0	33,1	0,4	9,6	0,3	6,6	0,0
Phe	n.d.		7597,4	0,0	14288,8	2657,6	4954,1	763,8	492,5	31,3	71,5	6,1	25,5	0,6	33,0	0,4
Ant	n.d.		n.d.		n.d.		n.d.		n.d.		n.d.		n.d.		n.d.	
Fth	n.d.		308,0	14,9	262,8	69,1	80,1	18,9	17,3	1,1	5,1	0,5	5,2	0,1	7,2	0,0
Pyr	459,5	56,3	845,8	138,1	347,3	105,6	98,9	20,2	17,4	1,6	5,6	0,3	5,9	0,6	8,3	0,7
Baa	7,1	5,3	114,9	7,6	85,5	5,8	79,7	1,0	80,3	2,5	20,4	12,9	39,9	2,9	53,0	0,6
Chr	114,7	4,3	72,1	1,5	40,8	8,9	20,0	1,9	4,3	4,3	4,6	0,6	2,7	2,7	6,7	0,6
Bbf	19,5	5,0	15,8	1,7	n.d.		n.d.		n.d.		n.d.		n.d.		n.d.	
Bkf	16,4	2,2	11,5	0,5	n.d.		n.d.		n.d.		n.d.		n.d.		n.d.	
Bap	10,8	10,8	n.d.		n.d.		n.d.		n.d.		n.d.		n.d.		n.d.	
Ind	n.d.		n.d.		n.d.		n.d.		n.d.		n.d.		n.d.		n.d.	
Dah	n.d.		n.d.		n.d.		n.d.		n.d.		n.d.		n.d.		n.d.	
Ghi	n.d.		n.d.		n.d.		n.d.		n.d.		n.d.		n.d.		n.d.	
sum	669,4	63,0	8608,3	3643,3	27038,6	6313,3	10265,5	1616,2	3098,4	75,8	1166,9	32,2	791,0	0,9	139,3	7,3